ULTRASONIC PROPAGATION IN LIQUID ALLOY SYSTEMS

A Thesis submitted for the degree of Doctor of Philosophy in the Faculty of Science of the University of London by

Gerald Michael Bartlett Webber, B.Sc., A.R.C.S.

1969

ABSTRACT

An ultrasonic interferometer has been used to measure the sound velocity in liquid zinc, cadmium, mercury, indium, tin, lead and bismuth at temperatures up to 520°C. Experimental techniques and sound velocity measurements on various liquid metals are reviewed. The adiabatic and isothermal compressibilities, together with the ratio of the principal specific heats, are evaluated for eighteen liquid metals.

The results of sound velocity measurements as a function of temperature and concentration across the whole alloy system for mercury-zinc, mercury-cadmium, mercury-indium, mercury-tin, mercury-lead and mercury-bismuth alloys are presented. It is found that the addition of solute to mercury causes the adiabatic compressibility to decrease rapidly with concentration.

It is seen that the Bohm-Staver sound velocities are in fair agreement with experimental values for sound velocity in alkali metals. As the valency Z in the polyvalent group of metals increases, then the Bohm-Staver sound velocity becomes progressively larger than the experimental sound velocity. An empirical compressibility defined by $Z\ \beta_T^{(e\ell)}$ gives better agreement with experimental values for isothermal compressibility than does the free-electron compressibility $\beta_T^{(e\ell)}$. Various theoretical approaches to compressibility of metals are discussed. The semi-phenomenological model due to Ascarelli is found to

give good agreement with experimental compressibilities. Expressions for the free-electron compressibility and Bohm-Staver sound velocity for alloys are derived and compared with the present alloy results. The pseudo-potential approach and semi-phenomenological model for compressibility are also extended to liquid alloys.

Measurements of sound absorption in mercury are reported. The value for the ratio of bulk to shear viscosity is found to be 0.86 ± 0.3. Experimental values of η_B/η_s for various liquid metals are reviewed and it is seen that the values for this ratio evaluated from the dense-gas formulation are in reasonable agreement with experiment.

CONTENTS

1. REVIEW OF PREVIOUS EXPERIMENTAL WORK AND THEORY

1.1 Sound Propagation in Liquid Metallic Systems

The velocity of propagation of longitudinal waves c in an isotropic medium is given by

$$c^2 = \frac{1}{\rho}\left(\frac{1}{\beta_s} + \frac{4}{3}G\right), \tag{1.1}$$

where β_s is the adiabatic compressibility, G the shear modulus, and ρ the density. For acoustic measurements carried out at frequencies of several hundred MHz in liquids of fairly small viscosity, such as liquid metals, the effect of the shear modulus is neglected. This procedure is justifiable since the relaxation time for the shearing process is much shorter than the period of the applied stress. The sound velocity in a fluid is thus related to the adiabatic compressibility by

$$c^2 = \frac{1}{\rho\beta_s} \quad . \tag{1.2}$$

Now adiabatic and isothermal compressibilities are defined respectively by

$$\beta_s = -\frac{1}{\Omega}\left(\frac{\partial\Omega}{\partial p}\right)_s \tag{1.3}$$

and

$$\beta_T = -\frac{1}{\Omega}\left(\frac{\partial \Omega}{\partial p}\right)_T \quad . \tag{1.4}$$

Here, Ω is the volume of the system and p the applied pressure. It can also be shown thermodynamically that

$$\beta_T = \gamma \beta_S \quad , \tag{1.5}$$

where γ is the ratio of the principal specific heats. Few direct measurements of isothermal compressibility have been made on liquid metals and acoustic measurements make it possible to estimate β_T. The estimation of isothermal compressibilities of various liquid metals is discussed in Section 4.3.

1.2 Previous Experimental Work

Although sound propagation has been studied in many types of liquids and the results interpreted in terms of various theories for liquids, there has been comparatively little investigation of liquid metals. The first sound velocity measurements on liquid metals were made by Kleppa (1950) who investigated thirteen metals. From his results he calculated the adiabatic and isothermal compressibilities, the ratio of principal specific heats, and the Grüneisen constant.

His results showed that γ is slightly greater than unity, near the melting point, and there is a small increase in isothermal compressibility from the solid to the liquid state.

An early interest in liquid metals was the measurement of the sound velocity near the melting point. Yao and Kondic (1952) had found that the shear viscosities of tin, lead and zinc showed deviations from the Andrade equation near the melting point. This implied the existence of a relaxation time for tin of 10^{-7} sec, such that the liquid would present a more solid character to sound waves of a frequency greater than about 2 MHz. Acoustic measurements at 5 MHz made by Gordon (1959) with tin and Proffit and Carome (1962) with gallium, the metals cooled to a few degrees below their freezing points, did not show any change in the linear decrease of velocity with temperature. The temperature variation of velocity would be affected by the existence of a shear modulus due to incomplete relaxation at the frequency of the experiment. In verification of these acoustic measurements which indicated the absence of pre-solidification phenomena, later shear viscosity investigations have failed to support the reported deviations in viscosity.

More recently the interests have been in the investigation of high melting point metals, such as antimony, copper and silver, and in propagation of sound in liquid metals subject to external pressures. The latter investigations are important for the evaluation of equations

of state for liquids. Coppens et al. (1967) measured the sound velocity in sodium, mercury, indium, tin and bismuth as a function of pressure, whilst Davis and Gordon (1967) made measurements on mercury at pressures up to 15 Kbars. The sound propagation measurements made by the author were performed at atmospheric pressure only. Published sound velocity data are compiled and discussed in Sections 3.1C, 3.3 and 4.3; the various experimental techniques are discussed in Section 2.1.

A few sound velocity measurements have been made on liquid alloy systems. The investigators interpret the variation of sound velocity with composition and temperature in terms of structural changes in the alloy systems. For example, Hill and Ruoff (1965b) found an anomalous behaviour for the variation of sound velocity with temperature in liquid bismuth-cadmium entectic. The sound velocity increased with temperature in the temperature range 150 to 180°C and then decreased, and this behaviour was interpreted as being due to the presence of bonding between unlike atoms. In general the sound velocity varies smoothly with composition of the alloy system when at a fixed temperature. For liquid tin-lead alloys Gordon (1961) found that the sound velocity at a fixed temperature and at a fixed composition was smaller than the value given by the linear average of the two pure component values at the same temperature (see Fig. 4.18). The adiabatic compressibility was found to vary approximately linearly with composition. In contrast, Abowitz

and Gordon (1962a) found that although the variation of sound velocity with composition for sodium-potassium alloys was similar to that for tin-lead, (see Fig. 4.17) the adiabatic and isothermal compressibilities were up to about 4% greater than the weighted means of the compressibilities of the pure liquids.

The investigations of Golik et al. (1961) and Abowitz and Gordon (1963) have shown that the variation of adiabatic compressibility with composition for mercury alloys differs from the other alloy systems which have been studied so far. Abowitz and Gordon found that for the mercury alloy systems Hg-Zn, Hg-Cd, Hg-In, Hg-Tl, Hg-Sn, Hg-Pb and Hg-Bi the sound velocity increased with increasing content of solute, and the adiabatic compressibility decreased rapidly with the addition of a few atomic percent of solute. Apart from Hg-Tl which was investigated for concentrations up to about 40 at.% Tl, the other alloy systems were studied to only a few atomic percent. The variation of sound velocity with composition of Hg-Tl alloys is shown in Fig. 1.1. For this alloy system it is seen that the sound velocity at a fixed temperature and at a fixed composition is greater than the weighted means of the sound velocities of the pure components. In contrast to the mercury alloys which have already been mentioned Abowitz and Gordon (1963) found that for dilute Hg-K alloys the sound velocity decreases with addition of potassium and the adiabatic compressibility increases. These authors proposed that the variation of compressibility

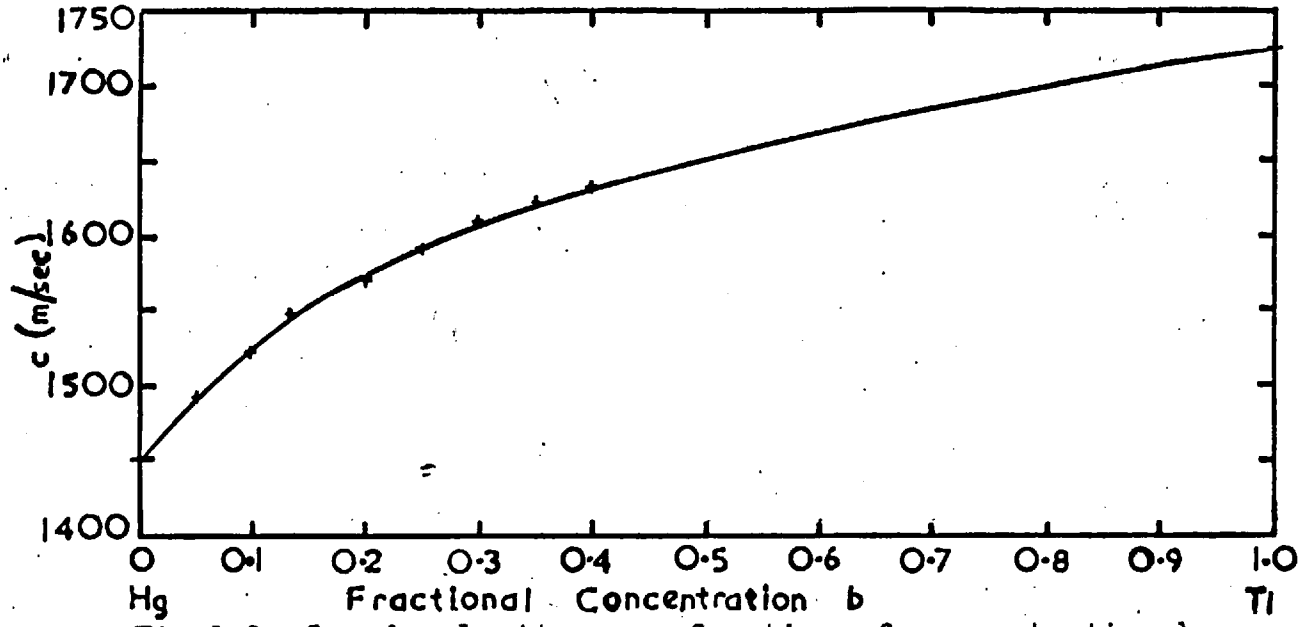

Fig.1.1. Sound velocity as a function of concentration b in the Hg-Tl alloy system. Sound velocity data shown in Table A.18.

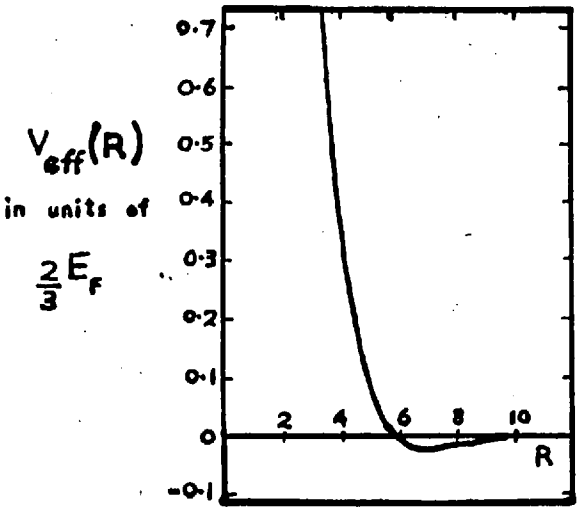

Fig. 1.2. Effective ion-ion interaction in sodium.

with composition in mercury alloys is due to an alteration of the structure of liquid mercury itself, which leads to increased Debye temperatures of the alloys.

Many physical and electrical properties have been measured on mercury alloys and in particular the electrical behaviour has attracted much interest. The present study gives the results of the measurements of sound velocity in six mercury alloy systems, studied over their entire range of concentration, and the sound velocities and compressibilities of pure metals and alloys are discussed from several theoretical approaches to these physical properties.

1.3 Various Theoretical Approaches to Sound Velocity and Compressibility of Metals

Several theoretical approaches have been used to interpret sound velocity measurements and these approaches are introduced and discussed below.

A. Hole Model due to Frenkel

If an equation of state for a material giving the volume as a function of temperature and pressure is known, than expressions for thermal expansion α_p and isothermal compressibility β_T can be calculated. In the simple model of liquid structure derived by Frenkel (1956) it is assumed that the thermal expansion and compressibility of the liquid

are determined by a certain concentration of "holes" each of definite volume. The work u required to form a hole of volume v by expanding the liquid against a constant pressure p is given by

$$u = u_o + pv,$$

and the number of holes N_H among the N atoms of a mole of liquid is assumed to be

$$N_H = N \exp(-u/k_B T).$$

Here k_B is the Boltzmann constant and T the absolute temperature. The assumption that all the thermal expansion of the liquid is due to hole formation gives

$$N_H v = \Omega - \Omega_o,$$

where Ω_o is the incompressible volume corresponding to a close-packed array of atoms. Hence the volume Ω is given by

$$\Omega = \Omega_o \left[1 + \frac{Nv}{\Omega_o} \exp\left(-\frac{u_o + pv}{k_B T}\right)\right]. \qquad (1.6)$$

This leads to β_T and α_p being expressed by

$$\beta_T = \frac{(\Omega - \Omega_o)v}{\Omega k_B T} \qquad (1.7)$$

and

$$\alpha_p = \frac{(\Omega - \Omega_o)u}{\Omega k_B T^2} \quad . \tag{1.8}$$

Gordon (1959) used measured data for Ω, β_T and α_p and solved equations (1.6), (1.7) and (1.8) to find u, Ω_o and v. He found two sets of solutions were obtained. Assuming that Ω_o is the same as the volume occupied by a close-packed array of atoms, Gordon took the first set of solutions which gave Ω_o closest to that corresponding to their Pauling radii for co-ordination number 12. Gordon computed u, Ω_o and v for sodium, mercury, tin and lead. Neither u or v could be compared directly with experiment, although their values were seen to be physically reasonable.

Pronin and Filippov (1963a,b) have treated this approach in more detail. In Pronin and Filippov (1963a) they considered the temperature variation of Ω_o for cadmium, tin, lead and bismuth and found that neither solution gave the expected constancy of Ω_o. However, since the free volume $\Omega - \Omega_o$ is physically expected to increase with temperature, they consider the second solution to be more appropriate. These authors assume that the variation of energy of hole formation with temperature (absolute) is represented by the power series

$$u = u_o' + AT + BT^2, \tag{1.9}$$

where u_o' is that part of the energy of hole formation which is independent of temperature (i.e. $u_o + pv$), and A and B are constants, and solve for u and v. They solve equation (1.9) in a different manner in Pronin and Filippov (1963b). There they choose Ω_o in such a way as to satisfy the condition that u_o' remains constant within the temperature range considered. Frenkel's equation [equation (1.6)] then assumes the following form

$$(\Omega - \Omega_o)^2 = \beta_T \Omega RT \exp\left(-\frac{\Omega \alpha_p T}{\Omega - \Omega_o}\right) \exp\left(-\frac{A + 2BT}{k_B}\right), \qquad (1.10)$$

where R is the gas constant. A plot of $(A + 2BT)/k_B$ versus T enables A and B to be determined. After this the constancy of u_o' is checked. Values of u were calculated for sodium, copper, silver, cadmium, mercury, tin, lead and bismuth and were compared with their latent heats of vapourisation L. The ratio Nu/L varied between 0.24 and unity. The authors concluded that metals with a low value of Nu/L (for example, tin) had a solution of equation (1.10) without a temperature correction over a wide temperature range, whilst metals with high values for this ratio (for example, cadmium) had no such solution.

Both Gordon (1959) and Pronin and Filippov (1963a) looked at the applicability of the distributed free volume theory of Eyring and Hirschfelder (1937) to sound velocity measurements. Since this theory gave poorer agreement with the Pauling radii for co-ordination number 12 and

gave Ω_o decreasing with increasing temperature, they concluded that this approach was not applicable to liquid metals. Hole models do not allow the sound velocity to be estimated accurately since u and v are not measured physical quantities and therefore this approach will not be discussed any further.

B. Hard-Sphere Model

Helfand et al. (1961) have shown that an equation of state for the rigid-sphere fluid can be presented in the form

$$\frac{p_h \Omega_A}{RT} = \frac{(1 + z + z^2)}{(1 - z)^3} , \tag{1.11}$$

where p_h is the pressure and Ω_A the molar volume. If σ is the rigid-sphere diameter of the atoms comprising the pure fluid, then the packing fraction z is given by

$$z = \frac{\pi \sigma^3 N_{av}}{6\Omega_A} , \tag{1.12}$$

where N_{av} is Avogadro's constant. The isothermal compressibility $\beta_T^{(h)}$ of the hard-sphere fluid can be calculated from equation (1.11) and is found to be

$$\beta_T^{(h)} = \frac{\Omega_A (1 - z)^4}{RT(1 + 2z)^2} . \tag{1.13}$$

Seemann and Klein (1965) estimated values of σ from X-ray data and the hard-sphere compressibilities of mercury and aluminium were compared with the experimental compressibilities. The computed $\beta_T^{(h)}$ for mercury was 3.06×10^{-12} cm^2/dyne as compared with the experimental value of 4.01×10^{-12} cm^2/dyne for the isothermal compressibility at 20°C, and the temperature dependence of $\beta_T^{(h)}$ was opposite to that found experimentally for β_T. For aluminium the computed $\beta_T^{(h)}$ was almost a quarter to a fifth of the experimental β_T. Values of σ calculated from equations (1.12) and (1.13) are smaller than experimental values and decrease with increasing temperature, contrary to the expected behaviour.

C. Pair Distribution Function Approach

The isothermal compressibility of a liquid composed of particles with spherically symmetric force fields can be represented in terms of the radial distribution function g(r), [see Egelstaff (1967)], by

$$\beta_T = \frac{\Omega}{Nk_BT}\left\{1 + \frac{4\pi N}{\Omega}\int_\Omega [g(r) - 1]r^2 dr\right\}, \qquad (1.14)$$

where N is the total number of particles in volume Ω. This is known as the "compressibility" equation. Here the average number of atoms at a distance between r and r + dr from a given atom is $4\pi r^2\, g(r)\frac{N}{\Omega}\, dr$. The value of the integral in equation (1.14) is close to -1.0 and thus β_T results from the small difference between the two terms. For

this reason theoretical and experimental results for g(r) lead to poor estimates of the compressibility.

A further equation of state, usually termed the "pressure" equation can be calculated within the framework of the canonical ensemble, and is given by

$$p = \frac{Nk_BT}{\Omega}\left[1 - \frac{2\pi N}{3\Omega k_BT}\int_\Omega r^3 \frac{du(r)}{dr} g(r)dr\right], \qquad (1.15)$$

where u(r) is the pair potential. Differentiation of equation (1.15) with respect to volume gives

$$\frac{1}{\beta_T} = \frac{Nk_BT}{\Omega} - \frac{4\pi N^2}{3\Omega^2}\int_\Omega r^3 \frac{du}{dr} g(r)dr + \frac{2\pi N^2}{3\Omega}\int_\Omega r^3 \frac{du}{dr}\left(\frac{\partial g}{\partial \Omega}\right)_T dr. \qquad (1.16)$$

Now since $p \approx 0$ at the triple point, then from equation (1.15) it is seen that

$$\frac{2\pi N}{3\Omega k_BT}\int_\Omega r^3 \frac{du}{dr} g(r)dr \approx 1. \qquad (1.17)$$

Hence, near the triple point,

$$\frac{1}{\beta_T} \approx \frac{-Nk_BT}{\Omega} + \frac{2\pi N^2}{3\Omega}\int_\Omega r^3 \frac{du(r)}{dr}\left(\frac{\partial g(r)}{\partial \Omega}\right)_T dr. \qquad (1.18)$$

Since typically $\beta_T^{-1} \sim 30\ Nk_BT/\Omega$ the numerical evaluation of the integral

term is seen to be important. Measurements of $(\frac{\partial g(r)}{\partial \Omega})_T$ are not available to test this approach.

D. Bohm-Staver Sound Velocity

Pines (1955) used the collective co-ordinate approach to derive the sound velocity, known as the Bohm-Staver velocity, in a metal. Ziman (1964) derives the same expression in the following manner. The metal is regarded as a lattice of positively charged ions immersed in a gas of conduction electrons. The electron cloud about each ion screens its electric field, so that at large atomic distances the Coulomb potential associated with a bare ion of valency Z is reduced by an exponential screening factor, such that

$$V(r) \approx (-Ze^2/r) \exp(-k_s r). \qquad (1.19)$$

The screening parameter k_s depends on the density of states at the Fermi surface, $N(E_F)$, and is defined by

$$k_s^2 = 4\pi e^2 N(E_F),$$

where e is the electron charge. If we consider a lattice of point positive ions of valency Z and of volume density n, then a long-wavelength vibration of these unscreened point charges gives rise to local volume

changes and polarisation fields. When an ion of mass M is displaced a distance $\underline{x}$ from its equilibrium position, its equation of motion is

$$M\,\ddot{\underline{x}} = -4\pi Z^2 e^2 n \underline{x}.$$

The plasma frequency ϕ (angular) of the ions would then be given by

$$\phi^2 = 4\pi Z^2 e^2 n/M.$$

Electron screening reduces the polarisation forces by the Hartree dielectric function $\varepsilon(q)$, which leads to the expression for the observed angular frequency ν_q of an excitation of wavenumber q,

$$\nu_q^2 = \phi^2/\varepsilon(q). \qquad (1.20)$$

Now in the long-wavelength limit, when $q \to 0$,

$$\varepsilon(q) \to 1 + \frac{4\pi e^2 N(E_F)}{q^2}.$$

The free-electron model gives the electron density of states $N(E_F)$ at the Fermi energy E_F as

$$N(E_F) = 3nZ/2E_F.$$

Therefore in the limit $q \to 0$, equation (1.20) becomes

$$\nu_q \to q[nZ^2/MN(E_F)]^{\frac{1}{2}}, \tag{1.21}$$

which shows that the frequency is proportional to the wavenumber as is observed acoustically at low frequencies. The longitudinal isothermal velocity $c^{(BS)}$ obtained from equation (1.21) is expressed by either of the equations

$$c^{(BS)} = [nZ^2/MN(E_F)]^{\frac{1}{2}} \tag{1.22}$$

or

$$c^{(BS)} = [Zm/3M]^{\frac{1}{2}} v_F, \tag{1.23}$$

where v_F is the Fermi velocity of the electrons of mass m. This expression is known as the Bohm-Staver sound velocity [see Bohm and Staver (1951)].

It follows from equation (1.23) that the isothermal compressibility $\beta_T^{(BS)}$ is given by

$$\begin{aligned} \beta_T^{(BS)} &= 3/2nZE_F \\ &= \gamma' \beta_s^{(BS)}, \end{aligned} \tag{1.24}$$

where $\beta_s^{(BS)}$ is the corresponding adiabatic compressibility. This calculation has been made at the temperature of absolute zero. At finite temperature it is necessary to know the ratio of principal specific

heats, γ', associated with the ion plasma model, which has not yet been evaluated theoretically.

Pines (1955) compared the values of $c^{(BS)}$ with experimental values of sound velocity for solid metals and found that there was fairly good agreement for the alkali metals. For polyvalent metals $c^{(BS)}$ was several times larger than experimental values. The Bohm-Staver sound velocity is compared with experimental values for sound velocity in liquid metals in Section 4.4.

E. Energy of Electron Gas Approach

The Bohm-Staver sound velocity can also be derived from the equation of state of a Fermi gas. At absolute zero of temperature the lowest-order approximation to the ground state energy for a non-interacting electron gas is due to the total kinetic energy of the electrons. The total energy E_o of NZ electrons in volume Ω is given simply by

$$E_o = \frac{3}{5} NZE_F .$$

Hence the pressure p at T = 0 is found from

$$\begin{aligned} p &= - \partial E_o / \partial \Omega \\ &= \frac{2}{5} \frac{NZE_F}{\Omega} . \end{aligned} \tag{1.25}$$

Differentiation of equation (1.25) with respect to volume gives the same expression for compressibility $\beta_T^{(e\ell)}$ as given by equation (1.24). $\beta_T^{(e\ell)}$ is known as the free-electron compressibility and may be written in terms of radius r_s (in Bohr units). r_s is defined by

$$\frac{4}{3}\pi r_s^3 a_o^3 = \frac{\Omega}{NZ}, \tag{1.26}$$

where a_o is the Bohr radius. In these atomic units $\hbar = 2m = e^2/2 = 1$ and therefore E_o(ryd) and $\beta_T^{(e\ell)}$ (Bohr units^3/ryd) are written respectively as

$$\begin{aligned} E_o/NZ &= 3/5\alpha^2 r_s^2 \\ &= 2.21/r_s^2 \end{aligned} \tag{1.27}$$

and

$$\begin{aligned} \beta_T^{(e\ell)} &= 2\pi\alpha^2 r_s^5 \\ &= 1.7 r_s^5 \end{aligned} , \tag{1.28}$$

where $\alpha^3 = (4/9\pi)$. It is seen that the free-electron compressibility is an increasing function of r_s. The experimental isothermal compressibility of various liquid metals is plotted as a function of r_s in Fig. (4.10), where it is seen that within each valency group with the exception of the pentavalent group, β_T increases with r_s.

Pines and Nozières (1966) have included the exchange and correlation energies in the calculation of the ground state energy of the electron

gas. When the exchange energy E_x is included, the ground state energy is given by

$$\frac{E}{NZ} = \frac{3}{5\alpha^2 r_s^2} - \frac{3}{2\pi\alpha r_s},$$

and simple calculation gives for the isothermal compressibility $\beta_T^{(ex)}$

$$\beta_T^{(ex)} = \frac{\beta_T^{(e\ell)}}{[1 - 0.166 r_s]}. \qquad (1.29)$$

This expression is similar to that derived by Harrison (1966). For the alkali metals with a large r_s, the inclusion of exchange energy drastically increases the theoretical compressibility.

The correlation energy E_c may be added and the form proposed by Pines and Nozières (1966) is used. There are several existing interpolation formulae for E_c which differ by about 10% over the relevant range of r_s. The ground state energy is now given by

$$\frac{E}{NZ} = \frac{3}{5\alpha^2 r_s^2} - \frac{3}{2\pi\alpha r_s} - (0.115 - 0.031\ \ell n r_s), \qquad (1.30)$$

and the corresponding isothermal compressibility $\beta_T^{(exc)}$ is found to be

$$\beta_T^{(exc)} = \frac{\beta_T^{(e\ell)}}{[1 - 0.166 r_s - 0.0042 r_s^2]}. \qquad (1.31)$$

The term in r_s^2, which comes from the correlation energy, has only a

slight influence on the compressibility compared to that arising from the exchange energy.

F. Pseudo-Potential Approach to Calculation of Total Energy

A calculation of the total energy based on perturbation theory was used by Ashcroft and Langreth (1967a) to estimate the compressibility of nearly-free electron metals. In addition to the usual kinetic, exchange and correlation energies, discussed previously, the energy of a solid contains terms resulting from the electron-ion and ion-ion interactions. Following the analysis due to Harrison (1966), if the direct interaction between ions centred at $\underline{r}_a$ and $\underline{r}_b$ is given by $V_d(|\underline{r}_a - \underline{r}_b|)$, then the contributions per ion, E_d, of the direct interaction to the total energy of the system of ions is simply

$$E_d = \frac{1}{2N} \sum_{\substack{a,b \\ a \neq b}} V_d(|\underline{r}_a - \underline{r}_b|). \tag{1.32}$$

The total energy of the electrons in the field of the ions can be obtained from second-order perturbation theory. The time-independent Schrödinger equation is

$$\left[-\frac{\hbar^2}{2m} + W(\underline{r})\right]\phi(\underline{r}) = E\phi(\underline{r}),$$

where the potential W is small. The zero-order equation is solved to

give the zero-order eigenstates $|\underline{k}\rangle = \Omega^{-\frac{1}{2}} e^{i\underline{k}.\underline{r}}$ and zero-order energies $E^{(o)} = \hbar^2k^2/2m$. The wavefunctions are normalised in a box of volume Ω. In the usual notation, the matrix elements of W may be written

$$\langle \underline{k} + \underline{q}|W|\underline{k}\rangle = \frac{1}{\Omega}\int_{\Omega} e^{-i(\underline{k}+\underline{q}).\underline{r}} W(\underline{r}) e^{i\underline{k}.\underline{r}} d^3r.$$

The zero-, first- and second-order contributions to the electron energy $E(\underline{k})$ are added respectively to give

$$E(\underline{k}) = \frac{\hbar^2k^2}{2m} + \langle \underline{k}|W|\underline{k}\rangle + \sum_{q}{}' \frac{\langle \underline{k} + \underline{q}|W|\underline{k}\rangle\langle \underline{k}|W|\underline{k} + \underline{q}\rangle}{\frac{\hbar^2}{2m}\left[k^2 - \left[\underline{k} + \underline{q}\right]^2\right]} . \quad (1.33)$$

The prime on the summation indicates that the $q = 0$ term is to be omitted.

Another important feature of the total pseudo-potential $W(\underline{r})$ is the assumption that $W(\underline{r})$ can be written as the sum of the superposition of individual ionic pseudo-potentials, such that

$$W(\underline{r}) = \sum_{a} w(\underline{r} - \underline{r}_a) .$$

Then it may be shown that the matrix element $\langle \underline{k} + \underline{q}|W|\underline{k}\rangle$ can be written in the form

$$\langle \underline{k} + \underline{q}|W|\underline{k}\rangle = S(\underline{q})\langle \underline{k} + \underline{q}|w|\underline{k}\rangle \quad , \quad (1.34)$$

where

$$S(\underline{q}) = \frac{1}{N} \sum_{a} e^{-i\underline{q}.\underline{r}_a} \tag{1.35}$$

and

$$\langle \underline{k} + \underline{q} | w | \underline{k} \rangle = \frac{N}{\Omega} \int_{\Omega} e^{-i(\underline{k}+\underline{q}).\underline{r}} \, w(r) \, e^{i\underline{k}.\underline{r}} \, d^3r.$$

Thus the matrix element is factorised into a structure factor $S(\underline{q})$, which depends only on the ion positions, and a form factor $\langle \underline{k} + \underline{q} | w | \underline{k} \rangle$ which depends only upon the individual ion potentials and is independent of the ion positions. The electron energy $E(\underline{k})$ may now be written

$$E(\underline{k}) = \frac{\hbar^2 k^2}{2m} + \langle \underline{k} | w | \underline{k} \rangle + {\sum_{q}}' \frac{S^*(\underline{q}) S(\underline{q}) \langle \underline{k} | w | \underline{k} + \underline{q} \rangle \langle \underline{k} + \underline{q} | w | \underline{k} \rangle}{\frac{\hbar^2}{2m} \left[k^2 - [\underline{k} + \underline{q}]^2 \right]} . \tag{1.36}$$

The total energy per ion $E_{e\ell}$ is obtained from

$$\begin{aligned} E_{e\ell} &= \frac{1}{N} \sum_{k<k_F} E(\underline{k}) \\ &= \frac{\Omega}{4\pi^3 N} \int E(\underline{k}) d^3k \\ &= \frac{3}{5} Z E_F + Z \, \overline{\langle \underline{k} | w | \underline{k} \rangle} \\ &\quad + {\sum_{q}}' S^*(\underline{q}) S(\underline{q}) \frac{\Omega}{4\pi^3 N} \int \frac{\langle \underline{k} | w | \underline{k} + \underline{q} \rangle \langle \underline{k} + \underline{q} | w | \underline{k} \rangle d^3k}{\frac{\hbar^2}{2m} \left[k^2 - [\underline{k} + \underline{q}]^2 \right]} . \end{aligned} \tag{1.37}$$

The first two terms depend upon the volume of the system but otherwise are independent of the details of the ion positions. The third term is known as the band-structure energy E_{bs}. It must be noticed that the electron-electron interaction $E_{e\ell-e\ell}$ has been counted twice in the average value $\overline{\langle \underline{k}|w|\underline{k}\rangle}$ of $\langle \underline{k}|w|\underline{k}\rangle$ and $E_{e\ell-e\ell}$ must be subtracted from the total energy $E_{e\ell}$ when calculating the total energy per ion of the metal.

It is now necessary to discuss the effect of the electron-electron interaction and screening. The electrons are assumed to interact with each ion through a local potential $w^{o}(\underline{r})$, which includes the Coulomb potential of the ion, and to interact with the other electrons through a Coulomb potential which may be determined from the charge density due to all electrons. The latter interaction is determined from a self-consistent-field treatment to give a potential $W^{1}(r)$. Then the total potential seen by the electrons is

$$W(\underline{r}) = W^{o}(\underline{r}) + W^{1}(\underline{r}) \qquad (1.38)$$

since

$$W^{o}(\underline{r}) = \sum_{a} w^{o}(\underline{r} - \underline{r}_{a}) \quad .$$

The oscillatory component of the electron density $n'(\underline{r})$ may be written in terms of its Fourier components n_{q}, such that

$$n'(\underline{r}) = \sum_{q}{}' n_q e^{i\underline{q}.\underline{r}}$$

and n_q is found to be given by

$$n_q = \frac{1}{2\pi^3} \int \frac{\langle \underline{k} + \underline{q} | W | \underline{k} \rangle \, d^3k}{\frac{\hbar^2}{2m} \left[k^2 - [\underline{k} + \underline{q}]^2 \right]} \quad . \tag{1.39}$$

Assuming that W is a local potential, then $\langle \underline{k} + \underline{q} | W | \underline{k} \rangle$ is independent of $\underline{k}$, and can therefore be taken outside the integral. Integration of equation (1.39) gives

$$n_q = \frac{-mk_F \langle \underline{k} + \underline{q} | W | \underline{k} \rangle}{2\pi^2 \hbar^2} \left(1 + \frac{1 - x^2}{2x} \ln \left| \frac{1 + x}{1 - x} \right| \right) , \tag{1.40}$$

where $x = q/2k_F$. If W_q^1 is the qth Fourier component of $W^1(r)$ such that

$$W^1(r) = \sum_{q}{}' W_q^1 e^{i\underline{q}.\underline{r}} ,$$

then using Poisson's equation gives

$$W_q^1 = \frac{4\pi e^2}{q^2} n_q \quad . \tag{1.41}$$

Since W_q^1 is defined by $\langle \underline{k} + \underline{q} | W^1 | \underline{k} \rangle$, then it follows from equations (1.38), (1.40) and (1.41) that

$$\langle \underline{k} + \underline{q} | W | \underline{k} \rangle = \frac{\langle \underline{k} + \underline{q} | W^{o} | \underline{k} \rangle}{\epsilon(q)} \quad , \tag{1.42}$$

where

$$\epsilon(q) = 1 + \frac{me^2}{2\pi\hbar^2 x^2 k_F} \left[1 + \frac{1 - x^2}{2x} \ln \left| \frac{1 + x}{1 - x} \right| \right] \quad . \tag{1.43}$$

Thus the screened potential $W(r)$ may be found from the unscreened potential by the dividing factor $\epsilon(q)$, which is called the static Hartree dielectric function.

As a further step in the calculation of the total energy it is necessary to consider the electron-electron interaction energy (per ion) E_{ee}, which is given by

$$\begin{aligned} E_{ee} &= \frac{1}{2N} \int_{\Omega} n(\underline{r}) W^{1}(\underline{r}) d^3 r \\ &= \frac{\Omega}{2N} \sum_{q} n_q^* W_q^1 \\ &= \frac{\Omega}{2N} \sum_{q}{}' n_q^* W_q^1 + \frac{\Omega}{2N} n_o W_o^1 \\ &= \frac{\Omega}{8\pi N e^2} \sum_{q}{}' q^2 W_q^{1*} W_q^1 + E_{su} \quad . \end{aligned} \tag{1.44}$$

Here E_{su} is the Coulomb self energy of a uniform negative charge distribution. It is also useful to split the energy term $Z \overline{\langle \underline{k} | w | \underline{k} \rangle}$, seen in equation (1.36), into three contributions. We write

$$w(r) = -\frac{Ze^2}{r} + w^o_{core}(r) + w^1(r) \ . \qquad (1.45)$$

The first term leads to the potential energy, E_e, of a uniform electron cloud in the Coulomb field of the ions; the second gives the potential energy, E_{ec}, of a uniform electron cloud in the field w^o_{core} of the ion; and the third term leads to a potential energy equal to twice the Coulomb self-energy, E_{su}, of the electron cloud. The total energy may be determined by adding all the terms discussed above, together with the electron exchange E_x and correlation energies E_c, in the following manner

$$E_{total\ (per\ ion)} = \frac{3}{5} ZE_F + ZE_x + ZE_c + E_{ec}$$

$$+ [E_d + E_e + E_{su}] + E_{bs} - [E_{e\ell} - E_{su}] \ . \qquad (1.46)$$

The term $[E_d + E_e + E_{su}]$ is known as the Fuchs energy E_{ii}. The last three energy terms in equation (1.46) may be added and simplified. Using the definitions of $\epsilon(q)$ given in equation (1.43) and the band-structure energy in equation (1.37), together with equations (1.38, 1.42, 1.44), we obtain

$$E_{BS} = E_{bs} - E_{e\ell} + E_{su}$$

$$= \frac{\Omega}{8\pi e^2 N} \sum_q{}' q^2 |w^o_q|^2 S^*(q) S(q) \left(\frac{1}{\epsilon(q)} - 1\right). \qquad (1.47)$$

Here w_q^o is the qth Fourier component of the interaction between an electron and a bare ion. Hence the total energy may be written

$$E_{\text{total (per electron)}} = \frac{3}{5} E_F + E_x + E_c + \frac{E_{ii}}{Z} + \frac{E_{ec}}{Z} + \frac{1}{Z} E_{BS} \quad . \qquad (1.48)$$

The pseudo-potential approach to the calculation of the total energy has been successful in determining crystal structure [see for example, Heine and Weaire (1966)], cohesive energy and compressibility. Ashcroft and Langreth (1967a) basically use the above energy expression to calculate the compressibility of simple solid metals. In order to obtain their energy equation it is necessary to redefine some of the terms. We first note that

$$NS^*(\underline{q})S(\underline{q}) = a(q) \qquad (1.49)$$

since

$$a(q) = \frac{1}{N} \left| \sum_i e^{i\underline{q}\cdot\underline{r}_i} \right|^2 . \qquad (1.50)$$

a(q) is the usual structure factor. We also define the qth. Fourier component of the bare ion potential V_q by

$$V_q = \frac{\Omega}{N} w_q^o \quad . \qquad (1.51)$$

The zeroth Fourier coefficient of the electron-ion potential is never

small and its contribution to the energy (per electron) may be written in the form $3A/4\pi r_s^3$, where

$$A = \frac{1}{Z} \lim_{q \to 0} \left(V_q + \frac{4\pi e^2 Z}{q^2} \right) . \tag{1.52}$$

The value of the Fuchs term E_{ii}/Z is then calculated as follows:-

$$\frac{E_{ii}}{Z} = \frac{1}{2NZ} \sum_{i \neq j} \sum_{q}' \frac{4\pi e^2 Z^2}{q^2} e^{i\underline{q}.(\underline{r}_i - \underline{r}_j)}$$

$$= \sum_{q}' \frac{2\pi e^2 Z}{q^2} \left[a(q) - 1 \right] . \tag{1.53}$$

Ashcroft and Langreth (1967a) evaluate the value of this term as $-1.792Z^{2/3}/r_s$ for hcp, fcc and bcc structures.

With the above definitions, the band-structure energy E_{BS}/Z (per electron) given in equation (1.47) is written in atomic units as

$$\frac{E_{BS}}{Z} = \frac{1}{16\pi Z\Omega} \sum_{q}' q^2 V_q^2 \left(\frac{1}{\varepsilon_q} - 1 \right) a(q) . \tag{1.54}$$

Contributions to E_{BS} occur at all non-zero reciprocal lattice vectors $\underline{q} = \underline{G}$. For a crystal the structure factor becomes

$$a(q) = N \delta_{\underline{q},\underline{G}} . \tag{1.55}$$

Ashcroft and Langreth write the Lindhard dielectric function ε_q in the form

$$\varepsilon_q = 1 + \frac{\lambda_L^2}{x^2} f(x), \tag{1.56}$$

where

$$f(x) = \frac{1}{2} + \frac{1 - x^2}{4x} \ln\left|\frac{1 + x}{1 - x}\right|, \tag{1.57}$$

$$\lambda_L^2 = [\pi a_o k_F]^{-1} = 0.166 r_s, \tag{1.58}$$

and

$$x = q/2k_F \quad . \tag{1.59}$$

The authors use the simple form of V_q proposed by Ashcroft (1966), where V_q is given by

$$V_q = \int e^{-i\underline{q}\cdot\underline{r}} V(r) d^3r$$

and

$$V(r) = 0 \qquad \text{for } r < r_c,$$
$$V(r) = -2Z/r \quad \text{for } r > r_c \quad . \tag{1.60}$$

Integration gives the form of V_q as

$$V_q = -\frac{8\pi Z}{q^2} \cos qr_c \quad . \tag{1.61}$$

V_q has the advantage of being in an analytical form and r_c can be chosen to give the best fit to Fermi surface or electrical resistivity data.

The band-structure energy per electron now takes the form

$$\frac{E_{BS}}{Z} = \frac{4\pi NZ}{\Omega} \sum_{g} \frac{\cos^2 g r_c}{g^2} \left(\frac{1}{\epsilon_g} - 1\right). \tag{1.62}$$

If we define

$$y = x r_c 2k_F = 3.84\, x r_c / r_s \ , \tag{1.63}$$

then using equations (1.56) to (1.59), equation (1.62) becomes

$$\frac{E_{BS}}{Z} = - \frac{4\pi NZ}{\Omega} \sum_{x} \frac{\cos^2 y \quad 0.166 r_s f(x)}{x^4 \left[1 + \dfrac{0.166 r_s f(x)}{x^2}\right]} \ . \tag{1.64}$$

By defining

$$G(r_s) = \sum_{x} \frac{f(x)}{x^4 \left[1 + \dfrac{0.166 r_s f(x)}{x^2}\right]} \ , \tag{1.65}$$

then the energy contribution due to band-structure may be written as

$$\frac{E_{BS}}{Z} \text{ (ryd/electron)} = -0.0338\, G(r_s) \cos^2 y. \tag{1.66}$$

When the Fuchs term, equation (1.53), and band-structure term, equation (1.66) are substituted into the total energy expression given by equation (1.48), it is found that the total energy of the solid

$E^{(AL,s)}$ can be written in the form proposed by Ashcroft and Langreth as

$$E^{(AL,s)} = \frac{2.21}{r_s^2} - \frac{0.916}{r_s} - (0.115 - 0.031 \ln r_s)$$

$$- \frac{1.792Z^{2/3}}{r_s} + \frac{3A}{4\pi r_s^3} - 0.0338\, G(r_s) \cos^2 y. \qquad (1.67)$$

The energy term $3A/4\pi r_s^3$ is large and if it is assumed that the zeroth Fourier component of the potential V_q given in equation (1.61) is accurate, it can be shown that

$$A = 4\pi r_c^2. \qquad (1.68)$$

Ashcroft and Langreth then found that the equilibrium condition $dE/dr_s = 0$ predicts values of r_s in fair agreement with observed densities. However for the calculation of binding energy $E_G^{(AL,s)}$ and isothermal compressibility $\beta_T^{(AL,s)}$ they used the more accurate procedure of eliminating A with the zero-pressure condition $dE/dr_s = 0$, and found that

$$\underset{\text{(ryd/electron)}}{E_G^{(AL,s)}} = \frac{0.737}{r_s^2} - \frac{2}{3}\left(\frac{0.916 + 1.792Z^{2/3}}{r_s}\right) - 0.105 + 0.031 \ln r_s$$

$$- 0.0338\, G(r_s)\left[\cos^2 y + \frac{Y}{3} \sin 2y\right], \qquad (1.69)$$

and

$$\frac{\beta_T^{(AL,s)}}{\beta_T^{(e\ell)}} = \frac{22.1}{[0.093r_s^2 + 2(0.916 + 1.792Z^{\frac{2}{3}})r_s - 4.42 - 0.0338r_s^2 G(r_s)\{2y(\sin 2y - y\cos 2y)\}]} \tag{1.70}$$

Here $\beta_T^{(e\ell)}$ is the free-electron compressibility, already discussed in Section 1.3E. The negligible contributions arising from the differentiation of $(\frac{1}{\varepsilon_q} - 1)$ are ignored.

Table 1.1 Comparison of Theoretical Compressibilities with Experiment for Solid Metals

Metal	$\beta_T/\beta_T^{(e\ell)}$	
	Theory	Experiment
Na	1.6	1.5
K	1.1	1.0
Rb	0.82	0.82
Cs	0.71	0.78
Zn	2.1	2.1
Al	3.5	3.9
Pb	3.2	3.5

With the exception of the band-structure contribution, the relative sizes of the various contributions to the binding energy and compressibility can be seen in equations (1.69)and (1.70). In order to estimate the size of the band-structure contribution it is sufficient to take $y \sim \pi/2$, and it can be shown that $G(r_s) \sim N_x/3x^6$, where N_x is the number of shortest reciprocal-lattice vectors. The values of r_s for various metals can be estimated from Fig. 4.10. It is clearly seen from the $G(r_s)$ term that the band-structure contribution to binding energy is very small. In the determination of compressibility, however, the term $G(r_s)$ due to band-structure is of the order of unity and therefore greatly influences $\beta_T^{(AL)}$. The band-structure contribution is of greatest importance in the polyvalent metals (more than 100% in aluminium) and is still fairly important for the alkali metals. The result of the calculation of $\beta_T^{(AL)}/\beta_T^{(e\ell)}$ for several simple metals is shown in Table 1.1, due to Ashcroft and Langreth (1967a). They conclude that the pseudo-potential method shows fairly good agreement with experiment, and the importance of the band-structure energy is clearly significant.

The application of the pseudo-potential approach to the calculation of compressibility, based on the Ashcroft and Langreth paper, is discussed for liquid metals in Section 4.4B.

G. Semi-Phenomenological Model due to Ascarelli

A fairly successful calculation of sound velocity and compressibility

of liquid metals has just been published by Ascarelli (1968). As a background to this model it is of interest to calculate the effective interatomic potential between ions. We have seen in Section 1.3F that the direct ion interaction E_d and band-structure energy E_{BS} depend upon both volume and structure. The band-structure energy may be considered as giving rise to an indirect interaction between ions in the following manner:-

$$E_{BS} = \sum_{\underline{q}}{}' S^*(\underline{q})S(\underline{q})F(q),$$

where

$$F(q) = \frac{\Omega q^2}{16\pi N} |w^o(q)|^2\left(\frac{1}{\varepsilon(q)} - 1\right). \tag{1.71}$$

Therefore, using the definitions of $S^*(\underline{q})$ and $S(\underline{q})$,

$$E_{BS} = \sum_{\underline{q}}{}' \sum_{i,j} F(q) \frac{1}{N^2} e^{-i\underline{q}.(\underline{r}_i - \underline{r}_j)}$$

$$= \sum_{\underline{q}}{}' \sum_{i \neq j} \frac{F(q)}{N^2} e^{-i\underline{q}.(\underline{r}_i - \underline{r}_j)} + \frac{1}{N} \sum_{\underline{q}}{}' F(q) \ . \tag{1.72}$$

The last term in equation (1.72) is independent of ionic arrangement, except through the total volume of the system. We can write the indirect interaction $V_{ind}(r)$ between the ions as

$$V_{ind}(r) = \frac{2}{N} \sum_{\underline{q}}{}' F(q) e_2^{i\underline{q}.\underline{r}}$$

$$= \frac{\Omega}{4\pi^3 N} \int F(q) e^{i\underline{q}.\underline{r}} \, d^3q. \tag{1.73}$$

The following definitions are made for simplification:-

$$q = 2k_F x \quad ,$$

$$R = 2k_F r \quad ,$$

$$\lambda_L^2 = \frac{3Z\pi e^2 N}{2E_F k_F^2 \Omega} \quad ,$$

and

$$(\tfrac{2}{3} E_F)U^o(x) = w^o(x) \quad . \tag{1.74}$$

The form of the bare potential $U^o(x)$, in units of $\frac{2}{3} E_F$, proposed by Ashcroft (1966) is

$$U^o(x) = - \frac{\lambda_L^2 \cos(2k_F x r_c)}{x^2} \quad . \tag{1.75}$$

Then $V_{ind}(R)$ is found from equation (1.73) by simple substitution to be

$$V_{ind}(R) = (\tfrac{2}{3} E_F)(\tfrac{3Z^2}{\pi}) \int \frac{x^2}{\lambda_L^2} |U^o(x)|^2 \, e^{i\underline{R}.\underline{x}} \, (\tfrac{1}{\varepsilon} - 1) d^3x \quad . \tag{1.76}$$

The direct interaction between a pair of ions is Z^2e^2/r and can be written in the form $6\pi Z^2 \lambda_L^2 (\frac{2}{3} E_F)/R$. This interaction together with the indirect interaction $V_{ind}(R)$ gives the effective interaction between ions, $V_{eff}(R)$, such that

$$V_{eff}(R) = \tfrac{2}{3} E_F \left[\frac{6\pi Z^2 \lambda_L^2}{R} + (\tfrac{3Z^2}{\pi}) \int \frac{x^2}{\lambda_L^2} |U^o(x)|^2 \, e^{i\underline{R}.\underline{x}} \, (\tfrac{1}{\varepsilon} - 1) d^3x \right] . \tag{1.77}$$

Ashcroft and Langreth (1967c) evaluate this expression for several metals and $V_{eff}(R)$, (in units of $\frac{2}{3} E_F$), which is shown for sodium in Fig. 1.2, is seen to exhibit a hard-core nature. It was found that the effective hard-sphere diameter σ gave a packing fraction z of 0.44 which was in good agreement with a value of 0.45 found by Ashcroft and Lekner (1966) to fit the structure curve a(q). The effective interaction between ions for alkali, noble and several polyvalent metals was seen to be hard-core in nature.

Ascarelli (1968) proposed that $V_{eff}(R)$ could be approximated by a simple hard-sphere potential $V_h(r)$, which has the form

$$V_h(r) = \infty \quad \text{for } r < \sigma$$
$$= 0 \quad \text{for } r > \sigma \ .$$

The semi-phenomenological model proposed by Ascarelli consists of hard-spheres immersed in a uniform background potential, which provides the cohesion that the hard-sphere gas otherwise lacks.

If we now look at the total energy expression given in equation (1.48) it is seen that the energy can be separated into two terms, such that

$$E^{(A)} = E_o^{(A)} + \frac{1}{2N} \sum_{\substack{i,j \\ (i \neq j)}} V_{eff}(r_{ij}) \ . \qquad (1.78)$$

Here $E_o^{(A)}$ depends upon volume alone and the second term depends upon both structure and volume. Thus Ascarelli proposes that to a good approximation

$$E^{(A)} = E_o^{(A)} + \frac{1}{2N} \sum_{\substack{i,j \\ (i \neq j)}} V_h(r_{ij}) \quad . \tag{1.79}$$

It is now necessary to consider the volume dependences of the interactions which contribute to $E_o^{(A)}$. If we compare $E_o^{(A)}$ with equation (1.48), we see that E_F depends upon $1/r_s^2$, whilst the energy terms E_x, E_e, and E_{su} depend upon $1/r_s$. The correlation energy E_c can be written as $0.284/r_s$ (ryd) to a good approximation. Ascarelli makes the further assumption that the ions can be considered as point ions since the volume of the Wigner-Seitz sphere is large with respect to the ionic core volume and therefore the positive repulsive term contained in the energy of the lowest state of the valence electrons can be neglected. Hence, with these assumptions, $E_o^{(A)}$ is made up of contributions depending upon $\Omega^{-2/3}$ and $\Omega^{-1/3}$. Thus the total energy $E^{(A)}$ of the system may be written

$$NE^{(A)} = \frac{3}{5} NZE_F - \frac{NB}{\Omega^{1/3}} \quad . \tag{1.80}$$

For simplicity, B is written in terms of a dimensionless constant C defined by

$$B = 3C(\Omega_m)^{1/3} k_B T_m \quad , \tag{1.81}$$

where Ω_m is the volume of the system at the melting point T_m. Hence the total energy $E^{(A)}$ of the system in this approximation is given by

$$\frac{NE^{(A)}}{k_B T} = \frac{3NZE_F}{5\,k_B T} - 3CN\,\frac{T_m}{T}\,\left(\frac{\Omega_m}{\Omega}\right)^{1/3} \quad . \tag{1.82}$$

In this model, the pressure of the system is the sum of the pressure derived from the above energy expression and the pressure p_h of a hard-sphere fluid, which has been defined previously in equation (1.11). The pressure of the system is therefore

$$\frac{p\Omega}{Nk_B T} = \frac{2ZE_F}{5k_B T} - C\left(\frac{\Omega_m}{\Omega}\right)^{1/3}\frac{T_m}{T} + \frac{p_h\Omega}{Nk_B T}$$

$$= \frac{2ZE_F}{5k_B T} - C\left(\frac{\Omega_m}{\Omega}\right)^{1/3}\frac{T_m}{T} + \frac{1 + z + z^2}{(1 - z)^3} \quad . \tag{1.83}$$

In order to calculate the sound velocity at the melting point it is assumed that all the simple metallic liquids have the same packing fraction $z = 0.45$ at the melting point. This value for z has been seen to yield a good fit to diffraction data. Thus $p_h\Omega/Nk_BT_m \sim 10$ is assumed to hold for all the simple liquid metals. The value of C can be determined by considering the pressure p of the system to be zero at the melting point and from equation (1.83) it is seen that

$$C = 10 + \frac{2Z\left[E_F\right]_m}{5k_B T_m} \quad , \tag{1.84}$$

where $[E_F]_m$ is the value of the Fermi energy at T_m.

The isothermal compressibility, $\beta_T^{(A)}$, and sound velocity, $c^{(A)}$, may be derived from equation (1.83) by simple differentiation with respect to volume, such that

$$\frac{1}{\beta_T^{(A)}} = \frac{Nk_BT}{\Omega}\left[\frac{(1+2z)^2}{(1-z)^4} + \frac{2ZE_F}{3k_BT} - c\left(\frac{\Omega_m}{\Omega}\right)^{1/3}\frac{4T_m}{3T}\right], \qquad (1.85)$$

and

$$\left[c^{(A)}\right]^2 = \frac{\gamma' k_BT}{M}\left|\frac{(1+2z)^2}{(1-z)^4} + \frac{2ZE_F}{3k_BT} - c\left(\frac{\Omega_m}{\Omega}\right)^{1/3}\frac{4T_m}{3T}\right|. \qquad (1.86)$$

Here M is the atomic mass and γ' is the value of the ratio of principal specific heats to be associated with this model. Ascarelli assumed $\gamma' = 1.15$ for simple metals at their melting point. It follows from equations (1.84) and (1.86) that at the melting point the sound velocity $\left[c^{(A)}\right]_m$ is given by

$$\left[c^{(A)}\right]_m^2 = \frac{\gamma' k_BT_m}{M}\left[27 + \frac{2Z[E_F]_m}{15k_BT_m}\right] . \qquad (1.87)$$

Ascarelli found that the values of $\left[c^{(A)}\right]_m$ calculated from equation (1.87) were in fairly good agreement with experiment. Those values of $\left[c^{(A)}\right]_m$ are compared with experiment in Section 4.4c and are discussed further there.

2. APPARATUS AND EXPERIMENTAL PROCEDURE

2.1 Review of Experimental Techniques

A variety of techniques have been employed for the measurement of sound velocity in liquid metals. Since quartz ceases to be piezoelectric at temperatures above 573°C, measurements above this temperature with the transducer in the furnace are not feasible. For these high temperatures a length of fused silica rod is often interposed between the specimen and quartz transducer, the latter being outside the furnace. The measuring techniques are grouped below into four classes.

A. Direct Pulse Methods

In these methods the velocity of propagation is determined by a direct measurement of the transit time for an ultrasonic pulse to traverse a known distance in the liquid. A short radio frequency pulse of 5 to 12 MHz is applied across a quartz transducer and a short train of waves (periodically repeated) is transmitted directly, or via a delay line, into the liquid. The ultrasonic pulses reflected from a plane parallel reflector re-excite the transducer and the electrical signal is amplified and displayed on an oscilloscope. Kleppa (1950) measured the transit time by counting the number of time markers between the pulses, and hence calculated the sound velocity from the known distance between the end of the delay line and reflector. The dissimilar shapes of the leading edges of the pulse echoes introduce

an error in the measurement of the transit time and Kleppa estimated that his velocity measurements were only accurate to 1%.

Several investigators [Polotskii et al. (1959), Pronin and Filippov (1963 a, b), and Plass (1963)] increased the accuracy of measurement by using the direct pulse method with a variable path length in the liquid. The use of a movable reflector makes it possible to exclude the errors associated with dissimilar pulse shapes, but the accuracy is again limited by the difficulty in measuring the time interval by the oscilloscope. The estimated errors in sound velocity range from 0.3% (Polotskii et al.) up to 3.5% (Pronin and Filippov).

B. Pulse Comparison Method

The time interval between two pulses which have travelled a known path length ℓ_1 in the liquid is compared with the propagation time of ultrasound in a reference liquid, usually mercury or distilled water, with a known sound velocity c_2. Gordon (1959) used the transducer in direct contact with the liquid metal and adjusted the length of a mercury delay line until the leading edges of the two sets of reflections were just in coincidence. The sound velocity c_1 in the liquid metal is then given by

$$c_1 = c_2 \ell_1 / \ell_2 \quad , \tag{2.1}$$

where ℓ_2 is the path length in the reference liquid. The oscilloscope is used essentially as a "null" indicator. The error in the sound velocity c_1 was estimated to be about 0.2%. The change of velocity with temperature could be measured with good precision (a few per cent) from the small displacement of either reflector. Hill and Ruoff (1965 a) used this method of measurement but had a stepped reflector to give the known path length.

C. Repetition Rate Method

The acoustic cell used by Coppens et al. (1967) consisted of a liquid-filled cylinder with parallel quartz transducers mounted at each end. An ultrasonic pulse from one transducer traverses the liquid and is received by the second, undergoing multiple reflections at each transducer. The pulse repetition rate was so adjusted that the signal from each pulse is received at the second transducer in phase with the echoes of the previous pulses, thus leading to a reinforcement of the signal. This superposition is observed only when the repetition rate f_r is adjusted so that

$$c = 2\ell f_r \quad , \tag{2.2}$$

where c is the velocity of sound in the liquid and ℓ is the length of the cylinder. Coppens et al. (1967) used a path length of 2 inches and estimated that their error in the sound velocity was 0.1%. This

technique was used to measure sound velocity as a function of temperature and pressure in various low melting point metals.

D. Phase Comparison

The phase between two ultrasonic pulses is made to fluctuate periodically by either changing the frequency or path length in the liquid. In the technique used by McSkimin (1959) the quartz transducer was in direct contact with the molten metal and the pulse width was adjusted so that overlap occurred between the first and second wavetrains which had traversed the liquid. The specimen length ℓ was fixed by the silica cell and no correction for expansion was needed. By changing the frequency of the ultrasound the received signal fluctuates and f_n is measured when phase opposition is produced. In this "out of phase" condition the sound velocity is given by

$$c = 2\ell f_n/n \quad , \tag{2.3}$$

in which f_n is any frequency for which the "out of phase" condition for echoes exists and n is the appropriate integer. By swinging the frequency f_n and noting the separation Δf between adjacent "out of phase" conditions, obtained by averaging over as wide a frequency span as possible, n can be calculated from

$$n = f_n/\Delta f \quad . \tag{2.4}$$

The absolute value of c at 232°C was determined by the above method with an error of 0.5%. The relative change of sound velocity with temperature was determined by changing the frequency f_n at a particular value of n so as to maintain the phase opposition. The frequency must be known accurately and the technique uses a gated amplifier in conjunction with a stable continuous wave oscillator.

Hubbard and Loomis (1928) varied the liquid path length by moving a reflector and used a continuous wave electrical interference method to detect the positions for standing waves. The impedance of the liquid varies through a cycle and results in a periodic swinging of the transmitter frequency applied to the quartz transducer. The transmitter frequency was "beat" against a constant frequency from a second oscillator. A vernier condenser in the transmitter circuit requires a cyclic variation in order to maintain the transmitter frequency f constant. Since a single transducer and reflector system was employed, successive positions are recorded from the micrometer corresponding to movements of a half-wavelength. The sound velocity is determined from

$$c = \lambda f \quad , \tag{2.5}$$

where λ is the wavelength of the sound.

Gitis and Mikhailov (1966a,b,c) used a pulsed acoustic interferometer

with electrical interference. The ultrasound transmitted through the liquid was detected by a second quartz transducer, amplified and added to a sinusoidal reference voltage. The mixed signal is zero when the two signals are equal in amplitude and opposite in phase. The second transducer was bonded to the delay line and its gradual displacement caused the interference pattern to vary periodically on moving through multiples of a sound wavelength. A knowledge of the frequency enabled the sound velocity to be computed.

Another type of pulsed acoustic interferometer depends upon varying the path length in the liquid [Jarzynski (1963)]. The path length is short and the pulse length is increased so as to produce an overlap of the pulses reflected from the interfaces between delay rod and liquid and between reflector rod and liquid. As the liquid path length is varied the pulses interfere and are periodically "out of phase". Measurements of the successive positions of constructive interference correspond to movements of half-wavelengths of sound in the liquid. Since the transmitter is pulsed it is necessary to measure the frequency by a beat technique. This technique was the one employed for the measurement of sound velocity in the present study. The results of sound velocity measurements on various liquid metals by numerous investigators is examined in Section 3.3.

The choice of the pulsed acoustic interferometer method for the measurement of sound velocity in liquid metals was guided by the

following considerations:

(a) since much difficulty is experienced in transmitting a satisfactory ultrasonic signal into the liquid metal due to the poor wettability with the quartz delay rod and also the sound absorption is such that the reflected pulse reduces, with distance, to the noise level, it is important to keep the path length fairly small;

(b) the results of previous investigations which employed the method of direct time measurement were seen to be of poor accuracy and inconsistent with one another. This method requires a fairly long path length in the liquid;

(c) the pulse comparison method requires a fairly long path length and requires a transmitter capable of giving a high amplitude R.F. pulse since the signal is applied simultaneously to two quartz transducers. For this reason the R.F. frequency usually employed is about 5 MHz;

(d) the repetition rate technique requires a fairly long liquid path length and also the quartz transducers to be in contact with the liquid metal, thus limiting the temperature range of the experiment;

(e) phase comparison techniques are capable of greater accuracy than the direct time delay measurements. A movable reflector was required for measurements of sound absorption, for which it was necessary to use a pulse method capable of operation in the frequency range 20 to 100 MH≠.

2.2 Explanation of Sound Velocity Technique

A block diagram of the apparatus used for sound velocity measurements is shown in Fig. 2.1. A 20 μsec radio frequency pulse from a modulated transmitter is applied to a 4 MHz X-cut quartz transducer. When operating at 68 MHz the crystal is resonating at its 17th harmonic. The ultrasonic pulse which is generated traverses the fused silica delay rod and is partly reflected at the interface between delay rod and metal and partly transmitted into the liquid metal. When the reflector rod immersed in the liquid metal is accurately aligned parallel to the transmitting surfaces, some of the ultrasonic pulse is reflected back towards the transducer, which reconverts the series of ultrasonic pulses into electrical pulses. After the signals are detected by the R.F. receiver, the I.F. of 7.5 MHz or the video pulse envelope is displayed on an oscilloscope. A typical pulse pattern is shown in Fig. 2.2a. Pulse 1 is the signal applied to the transducer and pulses 2, 4, 6 and 7 are the series of pulses due to reflections from the interface between delay rod and metal. Pulses 3 and 5 are due to reflections from the interface between metal and silica reflector. As the liquid path length is decreased pulses 2 and 3, 4 and 5 start to overlap. Movements of the reflector corresponding to changes in path length of the order of a wavelength cause the phase between the two pulses to change such that the pulses add or cancel. Figs. 2.2b,c,d show the effect of moving the rod from an "out of phase" condition

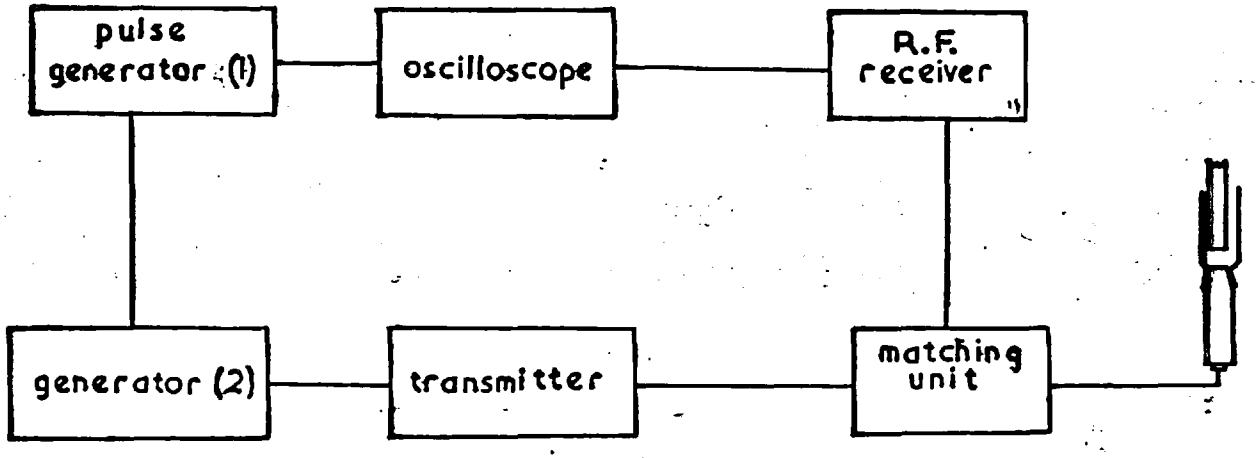

Fig.2.1. Block diagram of - sound velocity apparatus.

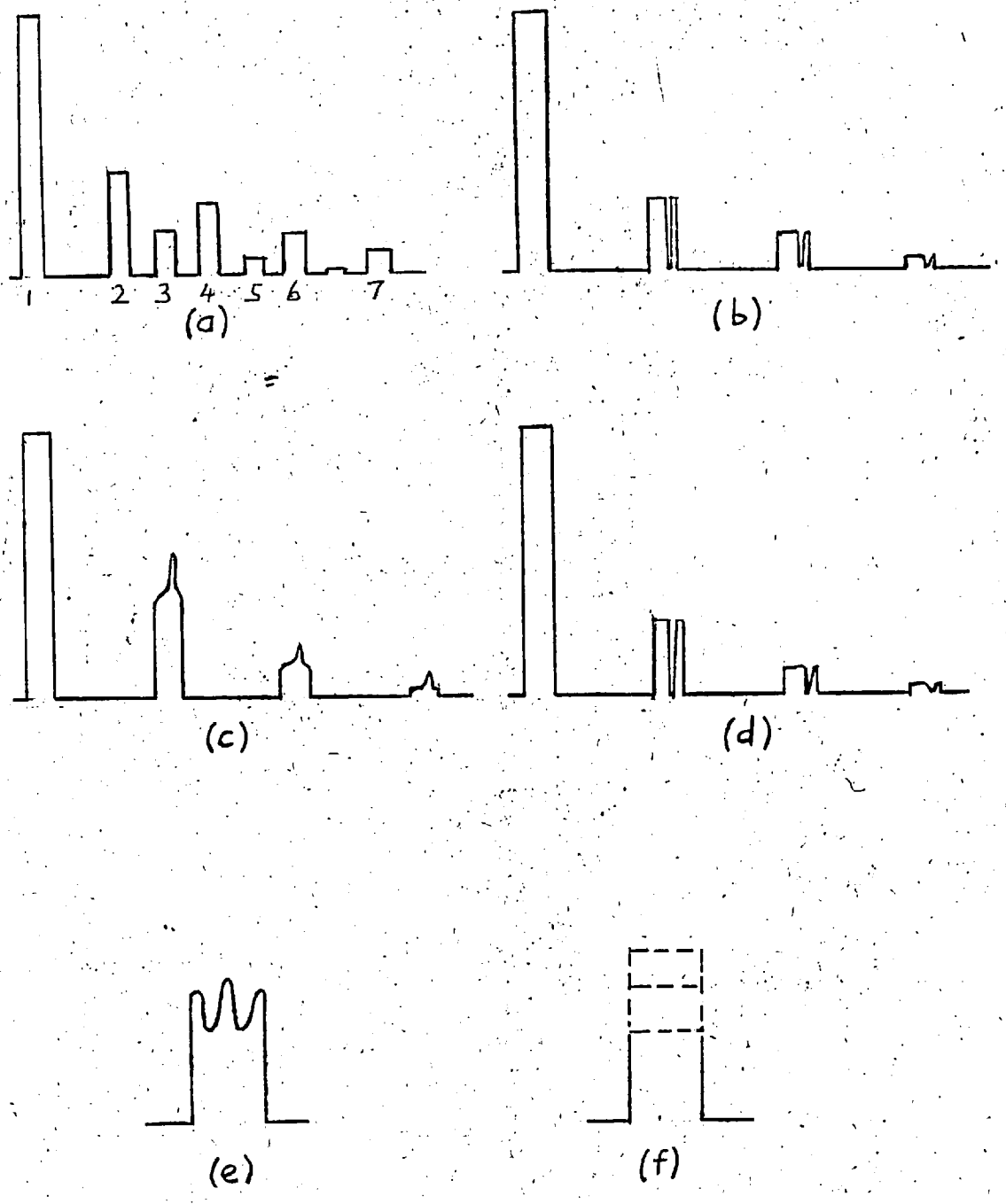

Fig. 2.2. Observed pulse patterns.

successively by a quarter- and a half-wavelength. A typical micrometer movement for a change of $\lambda/2$ is 1×10^{-3} cm.

A more precise measurement of wavelength λ is obtained by noting the micrometer positions of the first 10 minima (i.e. "out of phase" conditions) and then shifting by 50 to 100 minima and recording the next 10 minima positions. Since the number of minima has been counted an accurate value for λ is determined from the micrometer settings. The frequency of the sound wave is determined by mixing the transmitted signal with the continuous wave output of a Schomandl Frequency Synthesizer. The two R.F. signals beat together and the frequency corresponding to a zero beat (i.e. to a slow amplitude variation of the pulses) is recorded from the standard frequency generator. Fig. 2.2e shows the effect when the two frequencies are fairly close and in Fig. 2.2f when the frequencies are equal. The sound velocity is then simply given by λf at a given temperature. All the measurements are made at an ambient pressure of one atmosphere.

2.3 Description of the Electronic Apparatus

A block diagram of the electronic apparatus is shown in Fig. 2.1. The basic sections of the electronic apparatus had been constructed previously by Jarzynski (1961) and will only be briefly described here. The electronic circuits are reproduced in the Appendix for reference.

The repetition rate of the pulse generator is synchronised to that of the mains supply in order to avoid "jitter" of the observed pulses. The pulse generator provides a positive pulse to trigger the oscilloscope and a 50 volt pulse of 5 to 20 μsec duration. The latter pulse is amplified and triggers the modulator circuit so that a 500 volt negative pulse is applied to the cathode of the transmitter valve. The transmitter oscillates for the duration of the negative pulse and its frequency can be altered by means of the variable air-condenser. Frequencies of 12, 20, 68 and 92 MHz are obtained by inserting the appropriate inductance coil in the tank circuit of the oscillator. The R.F. receiver is a radar receiver type R. 1355, the units of which had been modified by Jarzynski to cover the frequency range 12 to 92 MHz. The author modified the receiver so that both the I.F. and video outputs can be displayed on an oscilloscope. An E.M.I. oscilloscope type W.M.2 is used, which has a band width of 0 to 20 MHz. When observing the intermediate frequency the I.F. strip of the first R.F. receiver is coupled to the I.F. amplifier strip of a second modified R. 1355 unit. The H.T. and filament current for the second unit are obtained from an external power supply. Details of the stabilised power supplies are given in Jarzynski (1961).

At resonance the equivalent circuit of the quartz transducer consists of a capacitance of about 25 pf in parallel with an equivalent

resistance of about 5 k. For efficient operation of the transducer it is necessary to tune out its capacity so that it does not act as a shunt for the R.F. signal. The matching unit consists of a tuned transformer (see Fig. A.5) and the variable capacitor is so chosen that, together with the capacity of the transducer, it can be tuned to resonance with the coil at the required frequency. The variable capacitor is adjusted until the received R.F. signal is maximum.

2.4 Fused Silica Cell

A diagram of the silica apparatus is shown in Fig. 2.3 and the silica cell can be seen in Plate 1. Fused silica was used since it is not chemically attacked by many liquid metals and it has an extremely low sound absorption at the high frequencies used. The choice of the dimensions of the delay rod was governed by the following factors:

(a) The size of container, which needed to be as small a diameter as possible, was influenced by the size of standard silica sockets available. Sufficient space inside the container was required for the reflector rod and thermocouple.

(b) The length of the delay rod had to be sufficient for the quartz transducer to be at room temperature outside the furnace.

(c) The length was chosen such that there was a suitably long time interval between pulses of ultrasound reflected within the delay rod.

This delay between the initial R.F. pulse applied across the transducer and reflected pulses allows time for the detector circuits to recover from being overloaded. The actual time interval was 54 μsec.

(d) It was decided to cover the frequency range from 20 to 100 MHz. Mason (1958) states that if the sound pulses are to be propagated as if the rod diameter were infinite, it is necessary for the ratio of rod diameter to sound wavelength to exceed the figure of 20. At 20 and 70 MHz this ratio is 80 and 280 respectively for a rod diameter of 24 mm.

(e) The radiating quartz may be regarded as a plane piston and the resulting polar diagram is similar to that due to optical diffraction at a circular aperture. The path length L over which the sound pulse radiates as a plane wave, known as the Fresnel region, is determined by

$$L = \frac{R^2}{\lambda} = \frac{R^2 f}{c} \quad , \tag{2.6}$$

where R is the radius of the transducer and λ is the wavelength of sound in the medium. In the present apparatus the transducer is bonded on to fused silica, in which the velocity of sound c is 5970 m/sec at room temperature. At a frequency f of 70 MHz the wavelength λ is 8.5×10^{-3} cm. For a transducer of radius 0.7 cm, L is about 57 cm.

Fig. 2.3. Silica cell.

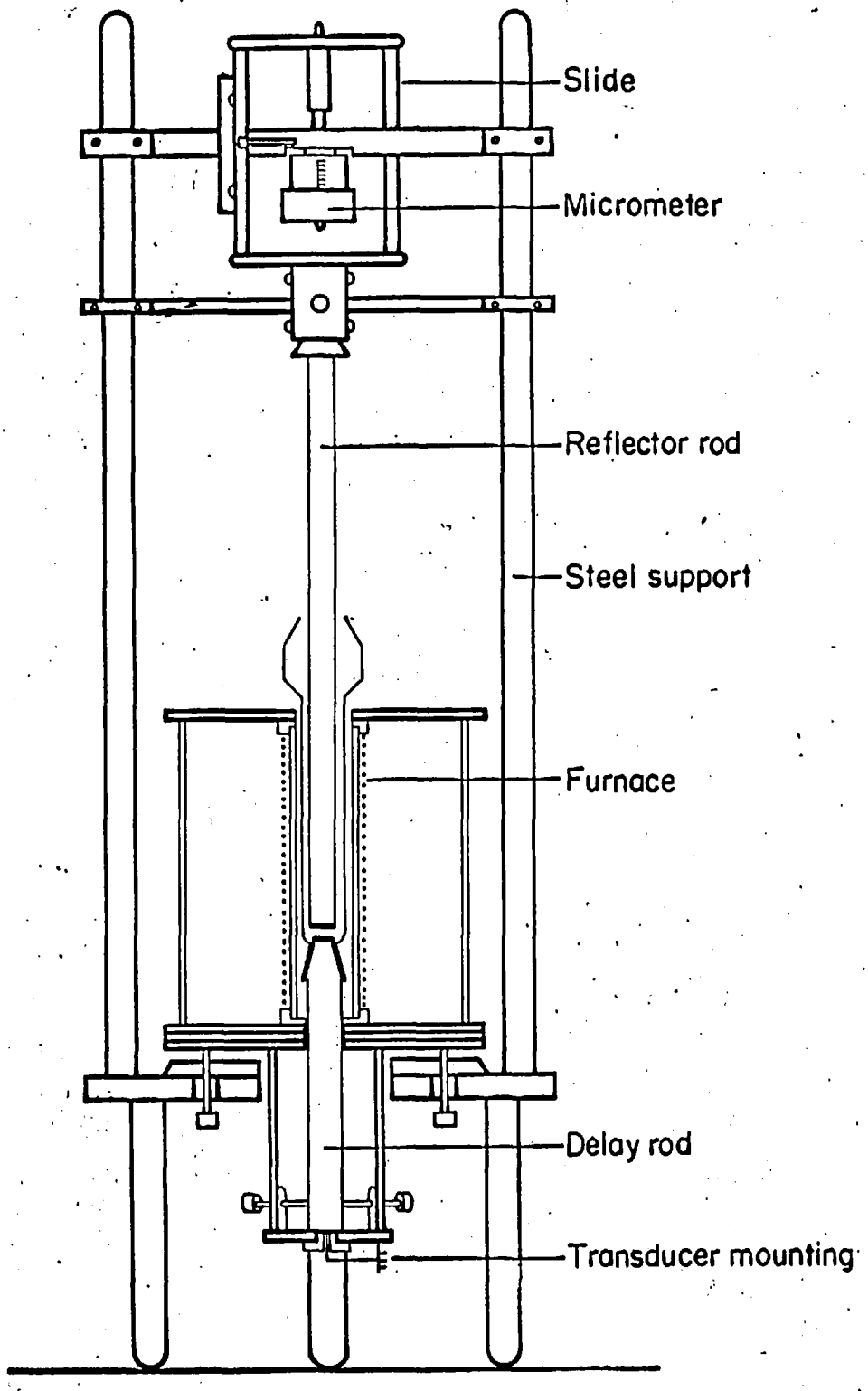

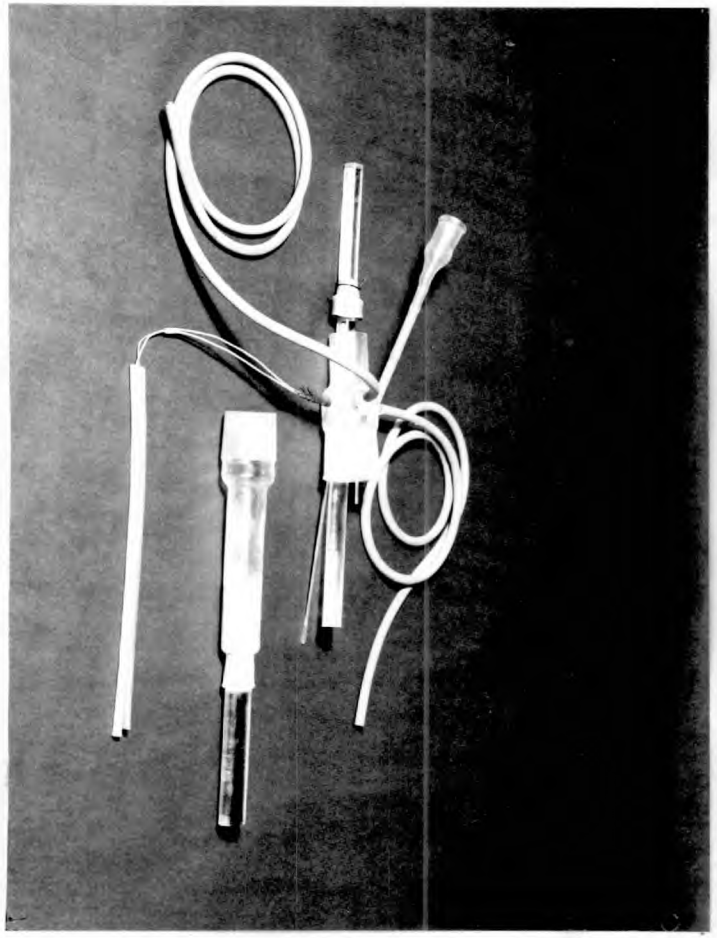

Plate 1. Silica cell.

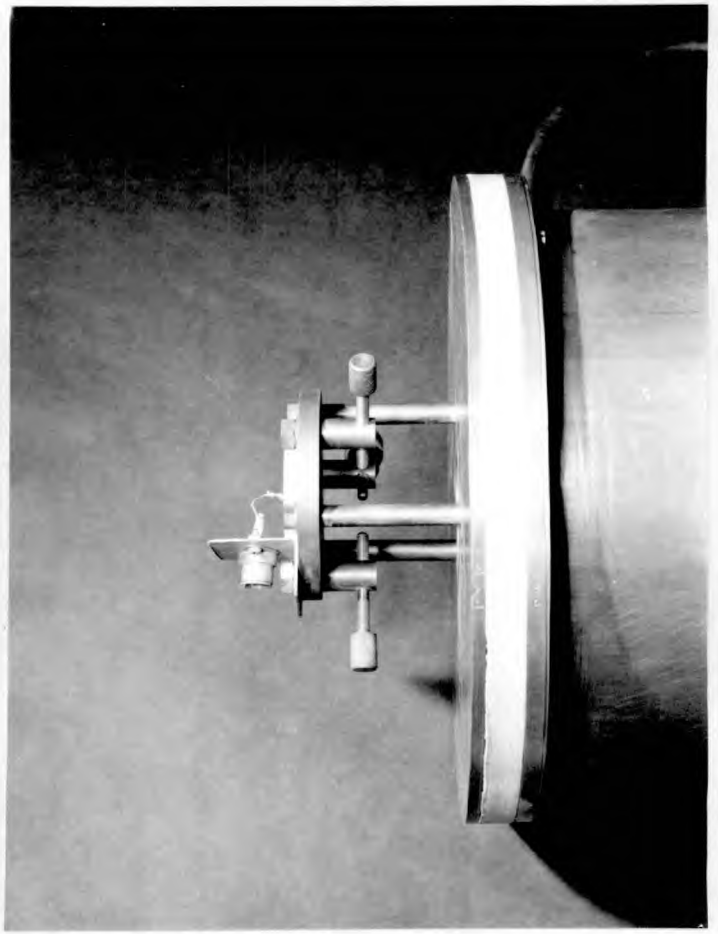

Plate 2. Transducer mounting.

At 20 MHz L is about 16 cm. The length of the delay rod was chosen to be 16 cm so that for frequencies as low as 20 MHz the sound pulse could be considered as a plane wave in the liquid. The frequency for which the plane wave condition applied for the total acoustic path length was 39 MHz.

The end faces of the delay rod were polished optically flat to within a wavelength of light. It was also necessary to consider the parallelism of these two faces. The problem of the resultant amplitude of the signal from the quartz transducer when a plane wave is incident at an angle θ to the normal is analogous to that of diffraction due to a circular aperture (Fraunhofer) and a minimum will occur when

$$J_1(z) = 0$$

$$\text{and} \quad z = \frac{2\,R\,\sin\theta}{\lambda} = 3.83 \quad . \tag{2.7}$$

For a transducer of radius 0.7 cm. and sound wavelength of 8.5×10^{-3} cm, the first minimum occurs when θ is about 25 minutes of arc. The end faces of the delay rod were polished parallel to within 1 minute of arc so that the ratio of the actual amplitude A to the amplitude A_o corresponding to $\theta = 0$ gave A/A_o of about 0.996.

The silica apparatus was fabricated by Thermal Syndicate Ltd., and fused silica type DL103 was used for the delay rod. One end of the delay

rod was ground with a 1:10 taper so as to take a B.24 socket. This allowed the silica container and delay rod to be disconnected and enabled the polished surface to be accessible to thorough cleaning. The container consisted of a 31 mm bore transparent silica tube with a B.24 socket at its lower end and a B.50 cone at its upper end. A silica B.50 socket fitted on to the container and had a central entry for the reflector rod and side entries for a thermocouple and inert gas. Further entries allowed for the container to be evacuated and for mercury to be filtered directly into the container. The reflector rod entry was sealed by a cylindrical piece of rubber which was cut from the thumb of a glove. Copper wire was used to tighten the rubber against the reflector rod and the rubber was pulled over the entry tube. The entries for evacuation, gas and thermocouple were sealed by rubber tubing.

The diameter of the reflector rod was chosen to be 18 mm so that its area was larger than that of the transducer and allowed for slight movements off the axis of the system. One face was polished optically flat and perpendicular to the axis of the rod whilst the other end of the rod was unpolished and was clamped to the slide.

2.5 Transducer Mounting

A chromium film was vacuum deposited on the end of the delay rod

and made contact with the brass base (the earth terminal) on which the delay rod rested. A copper electrode was pressed lightly against the transducer by means of a spring. The surface of the copper electrode was polished and the electrode insulated from the metal base by means of a disc of P.T.F.E. Three screws, one spring loaded, held the delay rod in position, see Plate 2, and an initial pressing of the rod on to the brass base was sufficient for electrical contact to be maintained.

Great care was taken in cleaning surfaces before vacuum deposition in an Edwards coating plant. The delay rod was first cleaned in hot concentrated hydrochloric acid and then left in warm chromic acid for several hours. The rod was afterwards washed with distilled water, carbon tetrachloride and absolute alcohol. The metal for deposition consisted of small pieces of chromium pellet containing 1% carbon which were held in a tungsten spiral and outgassed at red heat for a few minutes. The delay rod was then mounted vertically above the tungsten spiral in the vacuum chamber and the silica surfaces were cleaned by ionic bombardment. A 15 amp current was passed through the tungsten to get it to white heat and it was found that the chromium evaporated within a few minutes. A semi-transparent film was obtained which, however, was not sufficiently tenacious if it was too thick.

A chromium film was chosen since the film had to be very tenacious to withstand the prolonged "wringing" on of the transducer. Both faces

of the transducer were polished. The transducer was bonded to the delay rod by a thin film of silicone oil (the viscosity of the oil was 20 centipoise). A small drop of silicone oil was put on the silica surface and the transducer pressed firmly on to the surface. The transducer was moved to and fro, under slight pressure, across the surface and excess silicone oil was wiped off with a piece of chamois leather. It was essential to avoid dust particles getting beneath the transducer as then the film was scratched off. The wringing process was continued until, on looking through the transducer, no coloured interference fringes could be seen. The coupling film was then uniform and less than one optical wavelength thick.

2.6 Mechanical Construction and Alignment Mechanisms

The complete mechanical arrangement is seen in Plates 3 and 4. A $\frac{3}{8}$ in. aluminium platform of 12 in. diameter is supported by three $1\frac{3}{16}$ in. diameter steel rods. Three steel rods are mounted on the aluminium platform and are rigidly connected to one another by means of a $\frac{3}{8}$ in. aluminium cross-piece. A one inch aluminium bar, which is adjustable in height on the two steel rods, carries a kinematic slide and micrometer, see Fig. 2.3. The slide consists of two accurately machined $\frac{1}{4}$ in. steel rods which carry the holder for the reflector rod. These two rods are held in position on the aluminium bar by means of seven

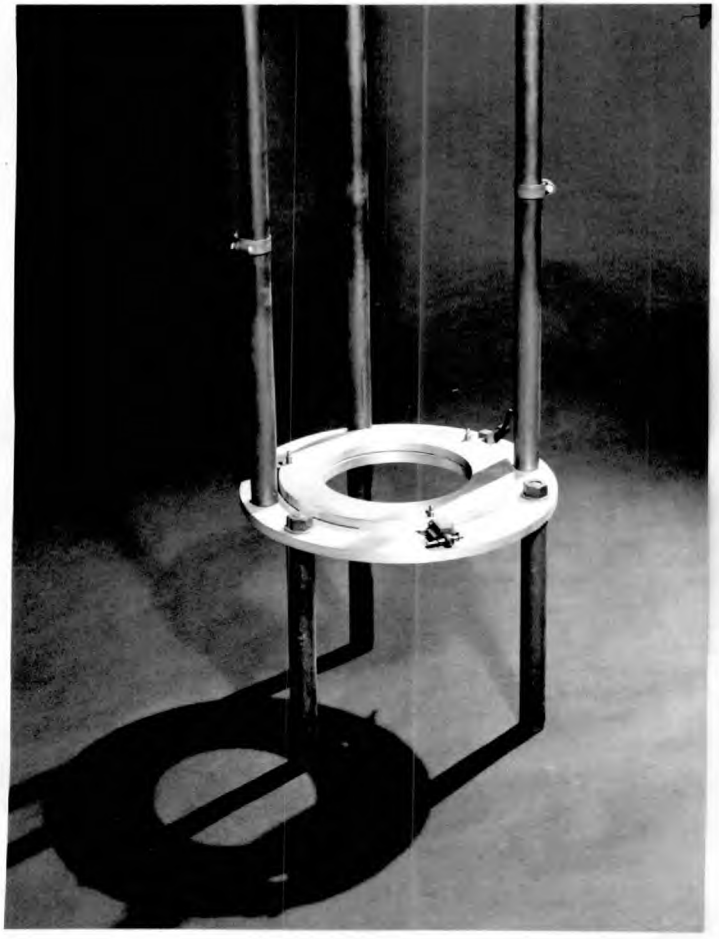

Plate 3. Framework

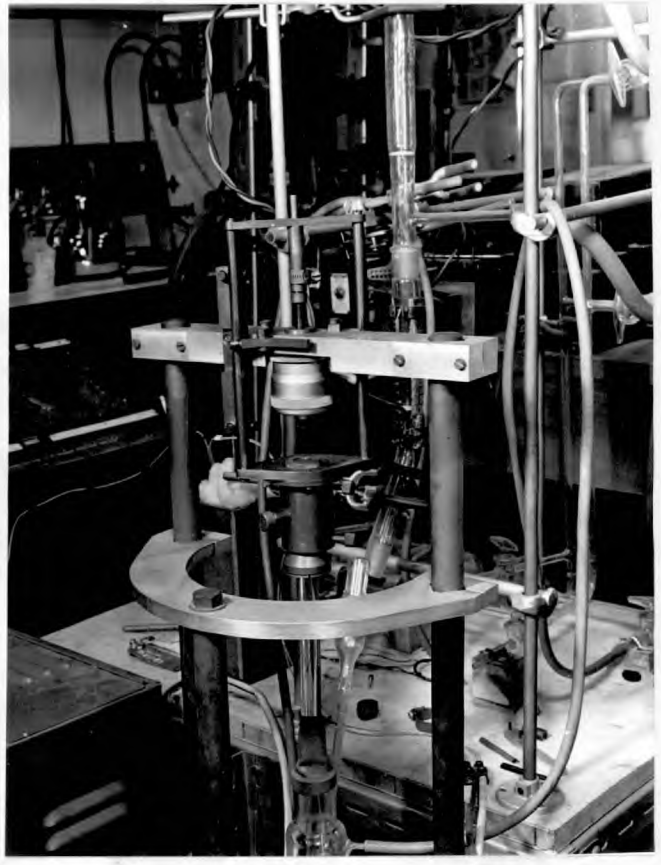

Plate 4. Framework

rollers, two of which are spring loaded against the rods. Vertical movement of the slide is controlled by rotation of the barrel micrometer (graduated in 0.002 cm divisions). The normal one inch movement of the micrometer is increased by insertion of a one inch slip rod between the micrometer spindle and the slide. When operating without the slip piece the two central spindles of the slide are held together by a jubilee clip in order to prevent rotation of the slide spindle when the micrometer is rotated.

A diagram of the holder for the reflector rod is shown in Fig. 2.4. The reflector rod is held in the split steel collar when the latter is pulled into the shaped brass cylinder. The cylinder is held in position within the brass holder by means of five screws, one of which is spring loaded. Adjustment of the four screws causes the reflector rod to change the inclination of its axis to the vertical.

The furnace rests on three levelling screws ($\frac{1}{4}$ in. B.S.F.) mounted in a $\frac{3}{8}$ in. aluminium ring. The screws fit into three radial grooves in the brass base plate of the furnace. Three screws, one of which is spring loaded, are in contact with the edge of the aluminium ring and can be adjusted so as to correctly position the furnace with respect to the reflector rod.

2.7 Furnace

A $8\frac{3}{8}$ in. brass tube of 8 in. diameter, 10 s.w.g. wall thickness,

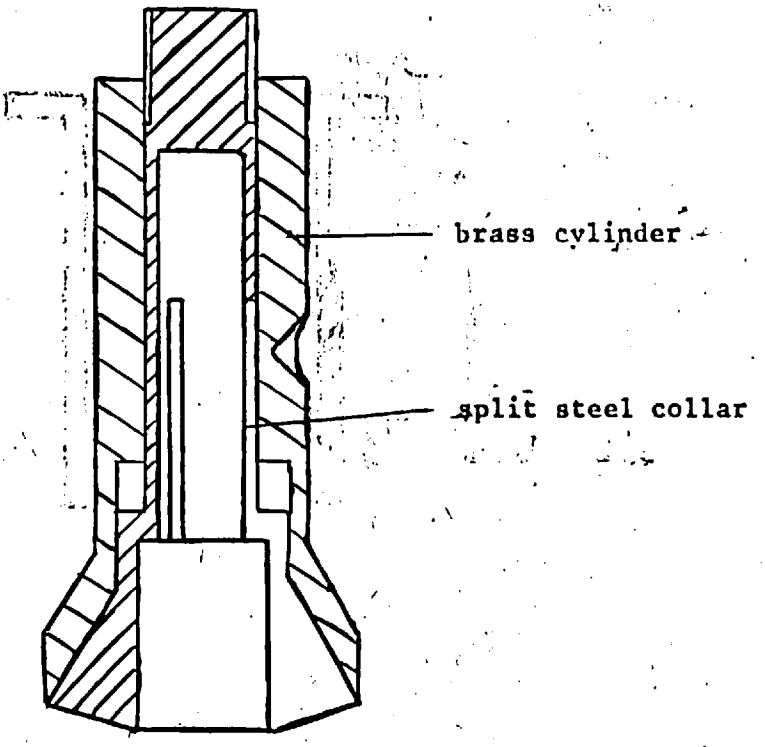

Fig. 2.4. Holder for reflector rod.

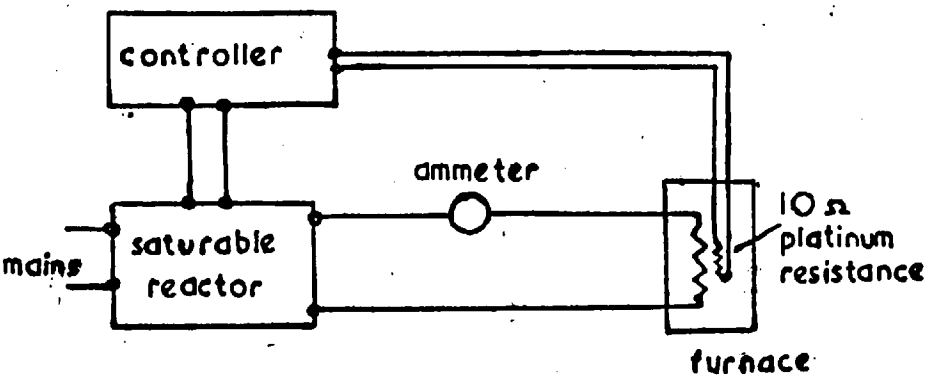

Fig. 2.5. Temperature control circuit.

forms the outer shell of the furnace. Syndanyo plates of $\frac{1}{4}$ and $\frac{1}{2}$ in. thickness respectively are bolted to brass flanges at the top and bottom of the furnace. A $\frac{1}{4}$ in. brass plate forms the base of the furnace. Central holes in the top and bottom of the furnace allow entry for the silica container and delay rod respectively. Three brass rods fixed to the base plate support the transducer mounting.

The silica container was surrounded by a close fitting steel tube in order to reduce any longitudinal temperature gradient in the central region of the furnace. Thermal insulation at both ends of the steel tube was provided by shaped rings of purimachos fire cement. The 8 in. steel tube was wrapped in several layers of asbestos paper, over which the heater tape was wound, the windings being closer at the ends. The ends of the heater tape were clamped in molybdenum collars at the top and bottom of the furnace. Electrical connections were made from the two insulated lead throughs in the furnace casing to the heater tape by thick copper wire enclosed in insulating beads. The heater tape in turn was covered with layers of asbestos paper and for thermal insulation asbestos wool was packed around the heater element and glass wool inserted in the interspace with the furnace casing.

Nichrome tape of $\frac{1}{16}$ in. width, 25 s.w.g. was used as the heater element. The total length of tape was 450 cm. and its resistance was 33 ohms, so that the density of windings at the centre was about 2

turns/cm , which increased at the ends.

2.8 Temperature Control and Measurement

Temperature control of the furnace was provided by a proportional temperature controller which used a saturable reactor (type S.R.1. manufactured by C.N.S. Instruments Ltd.), see Fig. 2.5. A 10 ohm platinum resistance was placed in the central region of the furnace and was strapped directly against the asbestos paper which covered the heater tape. The platinum resistance forms one arm of an A.C. bridge. Changes in resistance of the platunum are proportional to temperature and the output voltage from the A.C. bridge is amplified and rectified to give a D.C. output voltage, proportional to temperature, which is applied to the control windings of the saturable reactor. When the D.C. voltage is small the saturable reactor behaves like a high inductance in series with the furnace windings and results in a small furnace current. Increase in the D.C. voltage drives the iron circuit of the reactor towards saturation and therefore decreases the effective inductance and results in an increase of furnace current. Thus the furnace current is controlled continuously.

The equilibrium temperature reached by the furnace was altered by means of a variable resistance in one arm of the A.C. bridge. An ammeter indicated the furnace current and as a precaution against

breakdown of the furnace windings, the variable resistance was increased slowly so that the furnace current did not suddenly exceed 2 amps. A type SR60A saturable reactor rated at 240 volt, 6 amps, into a 30 ohm load was used. The sensitivity of the controller was adjusted according to the temperature range: setting on 5 for temperatures below about 300°C and on 4 for temperatures above 300°C. Since there was a minimum controllable current to the heater it was found that the time for reaching temperature equilibrium between 20 and 50°C was several hours. Above 50°C the temperature reached equilibrium after about ½ to 1 hr. A sound velocity measurement took about 20 minutes and in that time the temperature typically varied by less than 0.3°C.

The temperature of the liquid metal was measured with a sheathed chromel-alumel thermocouple for which a calibration was available. The thermocouple was protected by a sheath of twin bore silica tubing (see Plate 1) and the cold junctions contained inside Pyrex tubes immersed in water in a Dewar. A Tinsley potentiometer was used to measure the thermal e.m.f.

2.9 Evacuation and Cleaning of Materials

A Pyrex system was constructed so that a molten metal could be cleaned by being forced under pressure through two sintered glass filters. Simple heating elements were wrapped round the Pyrex tubes.

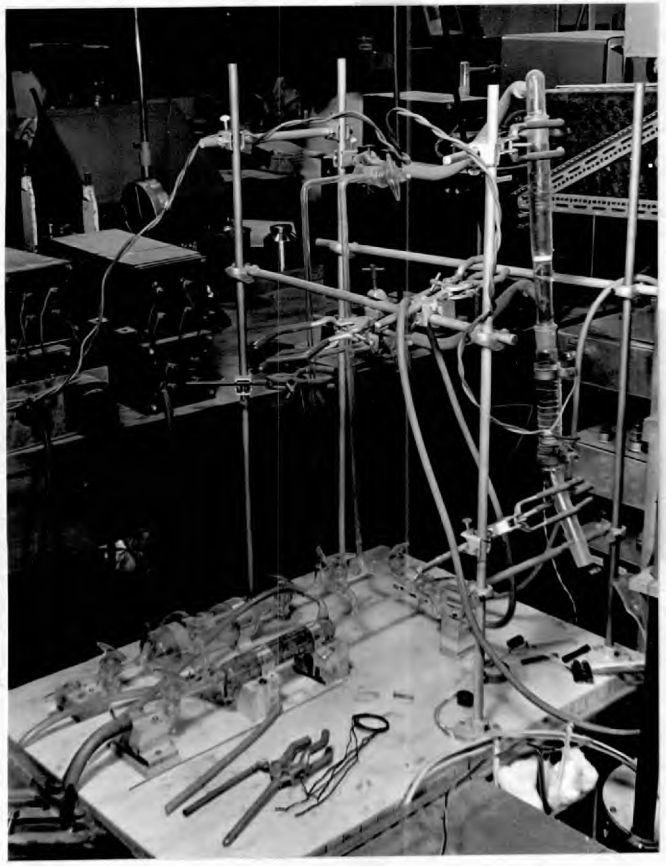

Plate 5. Pyrex system.

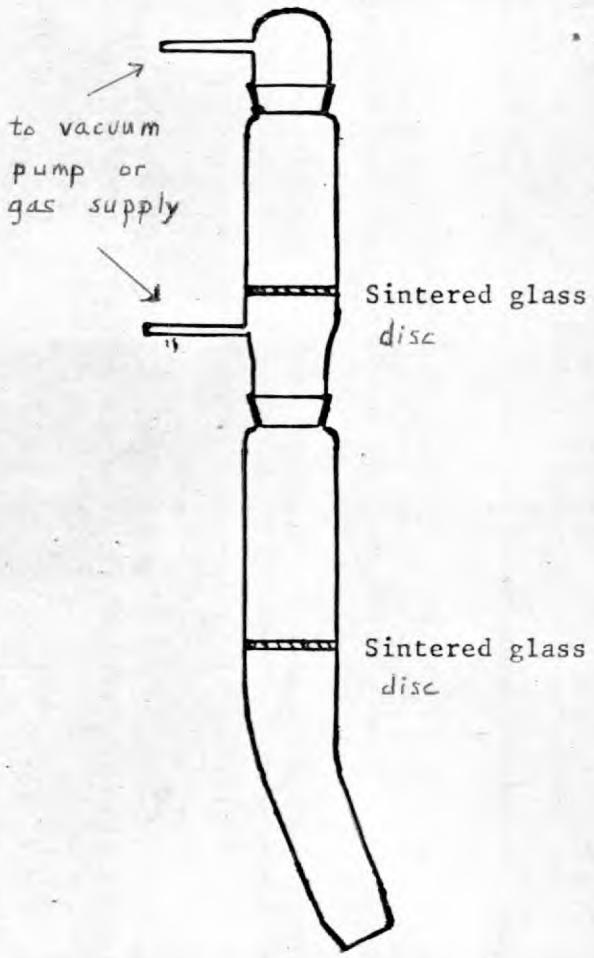

Fig. 2.6. Pyrex system.

The filter system could be attached directly to the silica container by means of a ground joint and a silica-Pyrex seal. A diagram of the Pyrex system is shown in Fig. 2.6 and the system is seen in Plate 5. The container was evacuated by means of a rotary pump and a water-cooled vapour trap was used to condense any metallic vapour present. A nitrogen gas cylinder was connected to a 2 litre chamber, from which the gas was released slowly. The system was used to filter a sample of mercury into the silica container and to maintain a nitrogen atmosphere above the mercury. Sound velocity measurements made on this sample of mercury were found to be in agreement, within experimental error, with measurements on samples of mercury which were filtered in a simpler Pyrex system constructed by Jarzynski (1961). In the latter system mercury was filtered through a sintered glass disc and collected in a beaker, and was then poured into the silica container after having been exposed to the air. It was not found necessary to use the Pyrex system to filter the other molten metals directly into the container.

In order to ensure a satisfactory transfer of acoustic signal into the liquid metal and to maintain the purity of the specimen, it was necessary to thoroughly clean the silica rods and container. Metallic deposits were dissolved away in concentrated nitric and hydrochloric acids. The container and rods were then washed with distilled water and cleaned with glass fibre soaked in cleaning powder (care was taken

not to scratch the polished surfaces of the rods). The silica was then left in warm chromic acid for about an hour, rinsed with distilled water and trichlorethylene and dried using absolute alcohol.

2.10 Experimental Procedure

The cleaned silica container and delay rod are connected and are then placed carefully in the furnace, the delay rod being held in position by tightening the three screws on the transducer mounting. The thermocouple and silica cap are then assembled and placed in position. The relevant transmitter coil and receiver unit are connected so as to operate at the selected frequency, usually 68 MHz. After making the electrical connection to the transducer, the transmitter, receiver and matching unit are alternately tuned to give maximum signal amplitude of those acoustic pulses which are reflected within the delay rod. Next the reflector rod is lowered carefully into the silica container and is allowed to rest freely within its holder. The micrometer is lowered so that the slide is free and the reflector rod is pushed against the delay rod under its own weight and that of the slide. This procedure helps to prevent a layer of oxide collecting on the polished surfaces when the metal specimen melts. The procedures which are then adopted for mercury, pure metals and alloys are described separately below.

A. Mercury

A known weight of mercury which had previously been filtered is poured carefully into the silica container. The weight was usually about 150 gm so as to give a volume of about 11 cm^3. The micrometer is now raised and the reflector rod is clamped in its holder. Then the reflector rod is raised until its polished surface is a few millimetres above the delay rod. When the rod is moved away from the surface of the delay rod the amplitude of the acoustic pulses decreases showing that some acoustic signal is being transmitted into the liquid. The four reflector rod screws and three levelling screws are adjusted until an acoustic pulse, returned from the reflector, appears. Care has to be taken not to force the reflector rod against the walls of the container or delay rod at any stage of the manipulations. The screw adjustments are critical to within a turn of the levelling screws. The reflector surface is accurately aligned parallel to the delay rod surface by adjusting the levelling screws so that the amplitude of the reflected pulse is a maximum. The furnace platform is moved laterally so that the reflector rod lies centrally above the delay rod. It was found that the screws did not require further adjustment during the period of the experiment and alignment was still maintained when the furnace was operated up to 520°C.

The platinum resistance leads are connected to the temperature

controller and the thermocouple to the potentiometer. The temperature controller is set to the temperature which is required and when the thermocouple indicates that the temperature of the liquid metal is varying by less than 0.3°C over a period of 20 minutes the wavelength of sound is measured. The positions of the first 10 minima are recorded and the micrometer is raised by 50 to 100 minima and the next ten positions are recorded. This usually corresponds to a vertical movement of about 1 mm. The micrometer is raised again and the procedure is repeated for the next few millimetres. The reflector rod is then lowered to the initial position and the above procedure is repeated three or more times. The sound wavelength is determined by averaging the differences between the micrometer positions for a known number of wavelengths, see Section 3.1A. The temperature and transmitter frequency are measured several times during the period of the measurements.

B. Pure Metals

Indium was the first metal investigated after mercury and it was found that the amplitude of the reflected pulses were small and it was difficult to align the system. The indium was melted in air at a pressure of a few mm of mercury. The measurements were carried out in the same manner as with mercury. An attempt was made to measure the sound velocity in liquid thallium in a similar manner but the acoustic

signal was too small. A hard crust of oxide formed on cooling and after cleaning the polished surfaces of the silica it was found that the surfaces had been pitted and required repolishing. To avoid the difficulty in finding the position of alignment the procedure that was followed for zinc, cadmium, tin, lead and bismuth gave improvement and was as follows.

After the cleaned silica had been assembled in the furnace the reflector rod was placed in contact with the delay rod, as described previously in the case of mercury, and about 15 cm^3 of absolute alcohol poured into the container. The same alignment procedure is carried out as for mercury, and once the system is aligned the reflector rod is again lowered on to the surface of the delay rod. Then the furnace is switched on so that the alcohol boils off and when the temperature has reached about 100^{o}C pellets of the metal are dropped into the container. The system is sealed and when the container is pumped to a low pressure (about 3 mm Hg) the surfaces of the reflector and delay rods are forced together. The furnace temperature is raised to about 10^{o}C above the melting point of the metal and while still molten the vacuum pump is switched off and atmospheric air is introduced. When the reflector rod is raised the reflected pulse is displayed on the oscilloscope showing that the system remains correctly aligned. After agitating the melt for a few minutes by raising and lowering the

reflector rod (care being taken not to raise it out of the melt so preventing oxide being collected on its polished surface) it is found that the system is set up for the sound velocity measurements.

C. Mercury Alloy Systems

The reflector rod is placed in contact with the delay rod and a known weight m_o of mercury is poured carefully into the container. The system is aligned by the procedure described previously. For an alloy of fractional atomic concentration b the fraction by weight of solute Y is given by

$$Y = \frac{b}{(1-b)\frac{M_0}{M_1} + b} \quad , \tag{2.8}$$

where M_0 and M_1 are the atomic masses of mercury and solute respectively. The weight m_1 of metal which is required is simply calculated from

$$m_1 = m_0 \frac{Y}{1-Y} \quad . \tag{2.9}$$

The metals are cut into small pieces (about 10 mm^3) so as to fit into the space between reflector rod and container. Zinc, indium, tin and lead are easily cut with stainless steel side-cutters (previously cleaned), whilst cadmium and bismuth are firstly sawn into pieces ready

for cutting. The temperature of the mercury or mercury alloy system is raised to about 50°C above the liquidus temperature, the rubber seal is removed and the metal pellets poured into the container and the seal is remade. In order to increase the rate of mixing the reflector rod is raised and lowered for a period of several minutes to agitate the liquid. The temperature is also varied rapidly over a range of about 100°C for at least three hours and at the same time the melt is periodically agitated. Contact between reflector and delay rods is avoided to prevent their surfaces becoming dirty. When the velocity measurements of a particular alloy concentration are completed a further weight of metal is added in order to make up the next composition. At high concentrations of solute (b of about 0.8 to 0.9) a known weight of mercury is added to the pure metal.

The procedure for removing the melt from the container is as follows. The furnace temperature is maintained at about 40°C above the melting point of the pure metal or liquidus temperature for the alloy composition. The reflector rod is unclamped and removed; the thermocouple leads are disconnected and the silica cap removed. Next the furnace current is switched off and the platinum resistance and furnace leads are disconnected. The furnace is then lifted from its stand with the aid of asbestos gloves and is tilted so that the melt pours into a pyroceramic dish, standing on asbestos, placed at a convenient height. The furnace is placed back in its stand and allowed to

cool. When the silica is cool it is carefully lifted out of the furnace and the cleaning procedure is commenced.

2.11 Sound Absorption Apparatus and Experimental Procedure

The electronic apparatus used for the measurement of sound absorption in mercury is shown in Fig. 2.7. In principle a delayed pulse triggers the comparison oscillator and a R.F. pulse passes through a precision attenuator. By adjustment of the delay the comparison pulse is displayed beside the "ultrasonic" pulse on the oscilloscope. The frequency of the comparison oscillator is made equal to the transmitter pulse by superimposing the two signals and adjusting for the absence of beats. Movement of the reflector rod in the mercury alters the acoustic path length and results in a change in amplitude of the reflected pulse. The absorption is measured by adjusting the attenuator for various acoustic path lengths so that the comparison pulse is exactly the same amplitude as the ultrasonic pulse. The sound absorption coefficient is calculated from the plot of amplitude (db) versus path length.

Either of the I.F. or video outputs can be displayed on the oscilloscope. In order to prevent overloading of the detector circuits by the transmitter pulse a blanking pulse is used to cut-off the first valve of the R.F. receiver for the duration of the transmitter pulse.

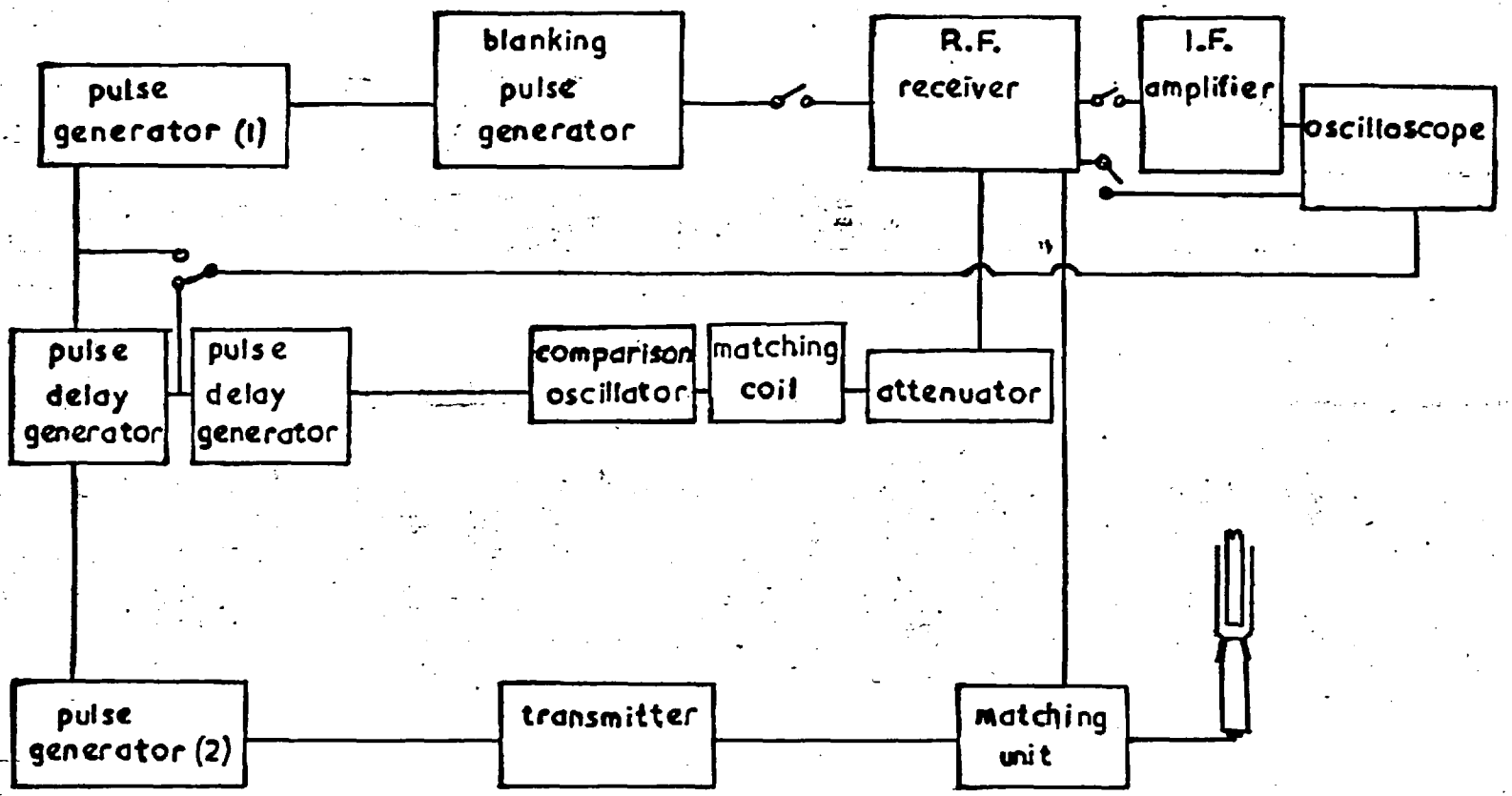

Fig. 2.7. Block diagram of sound absorption apparatus.

The circuit for the blanking pulse generator is due to Williams (1958) and is shown in the Appendix. The circuit generates a 200 volt negative pulse of variable pulse width up to 30 sec and this is applied to the grid of the first detector valve in the R.F. receiver unit.

The comparison oscillator is a British Communications type CT53 covering the frequency range from 8 to 300 MHz which has provision for external pulse modulation. The piston attenuator used is an Advance type A.57 with an attenuation range of 126 db and its scale is calibrated in units of 0.85 db. A tuned transformer is used at the input of the attenuator. A 75 ohm resistor (non-inductive) is inserted in the output of the attenuator and a single turn of wire is loosely coupled to the input coil of the R.F. receiver.

The experimental procedure is as follows. The apparatus is assembled and aligned as has been previously described for mercury in Section 2.10A. The slide is raised and a roller bearing is inserted over the micrometer spindle so as to reduce wear of the surfaces. The frequency of the comparison oscillator is adjusted to the frequency of the transmitter and the attenuator matching unit is adjusted for maximum signal amplitude. The carrier current of the comparison oscillator is kept below a value which produces a strong coupling with the receiver circuits and causes the ultrasonic pulses to jitter. The piston attenuator settings for equal pulse amplitudes are recorded for various acoustic path lengths.

Usually the path length is increased in intervals of 2 mm and a one inch slip gauge is inserted before the micrometer so as to increase the total range of movement. The attenuator settings (db) are plotted against the micrometer settings and the absorption coefficient α is calculated from the slope. A least square fit of the data according to the method given by Topping (1955) is used to compute the sound absorption coefficient. The experimental results and difficulties are discussed in Section 3.11.

3. Experimental Results and Discussions

3.1 Sound Velocity in Mercury

A. Typical Measurement and Results

The measurements were performed on triply distilled mercury (Grade 1, Johnson, Matthey and Co. Ltd.). The experimental procedure has been described in Section 2.10A. A typical set of micrometer readings for the positions of minima is shown in Table 3.1. In order to prevent error due to possible irregularity of the surfaces of the

Table 3.1 Typical Measurement (temperature 134.5°C)

Minima No.	Micrometer settings (mm) for shifts of 99 minima			
0	12.516	11.509	10.504	9.498
1	12.506	11.499	10.493	9.488
2	12.495	11.489	10.482	9.478
3	12.484	11.478	10.472	9.468
4	12.475	11.468	10.462	9.457
5	12.464	11.458	10.452	9.447
6	12.454	11.448	10.442	9.436
7	12.444	11.438	10.432	9.426
8	12.434	11.428	10.422	9.416
9	12.424	11.418	10.412	9.406

micrometer spindle and slide the number of minima were chosen so that the micrometer rotated almost exactly one complete rotation. All the measurements were taken when the reflector rod was being raised. Two further sets of micrometer readings were taken along with the above set and it was found that the settings were reproducible to within 0.002 mm. The average for 99λ was obtained by averaging the differences between the first and third, and second and fourth columns. The above set of results gave 2.0125 ± 0.001 mm for 99λ and the transmitter frequency was 60.845 ± 0.015 MHz. Thus the sound velocity was found to be 1399.5 ± 0.7 m/sec at 134.5 ± 0.5°C.

The variation of sound velocity with temperature is shown in Fig. 3.1, and it is seen that the sound velocity decreases linearly with temperature in the temperature range up to 156°C. A linear fit to the sound velocity data is obtained by the method of least squares from the Atlas Computer Laboratory program VB01A and is expressed in the form

$$c = c_m + d(t - t_m). \qquad (3.1)$$

Here c_m is the sound velocity at the melting point t_m and d is a constant, that is, the value of $(\partial c/\partial t)_p$. The best values and estimated errors for c_m and $(\partial c/\partial t)_p$ are given in Table 3.2. Evaluation of the experimental error is discussed in the following section.

B. Error in Velocity Results

The sources of possible error in sound velocity are due to the uncertainties in wavelength, frequency and to diffraction effects and non-uniform temperature in the specimen. These factors are discussed below.

(a) The measurement of the wavelength depended upon the accuracy of determining the positions of the successive minima and the stability of the transmitter frequency. It was found that the rigidity of the framework and the use of the kinematic slide resulted in excellent reproducibility of the measurements. Also the reproducibility of the micrometer settings indicated the absence of large fluctuations in temperature. The linear expansion coefficient for fused silica is about 0.5×10^{-6} deg C^{-1}. Thus the correction due to changes in length of the reflector rod as the rod was moved a few millimetres in the liquid was negligible. The position of a particular minima was maintained for several minutes. The standard deviation on the mean value of λ was usually about 0.05%.

(b) It was found that the frequency could be determined to within 0.02%. The transmitter frequency remained constant, within the error of frequency measurement, throughout the period of velocity measurement.

(c) The effect of diffraction on measured wave velocities has been investigated by McSkimin (1964). It was found that the excess

velocity Δc (over the plane wave velocity c) is given by the dimensionless parameter

$$\frac{\Delta c}{c} = \frac{\lambda^{3/2}}{4\pi^2 R\ell} , \qquad (3.2)$$

where λ is the sound wavelength, R the transducer radius and ℓ the distance from the transducer. For the present study the percentage excess velocity at 70 MHz was less than 1×10^{-3}. Measurements at 20.59 and 12.18 MHz gave 1450.5 ± 0.7 m/sec at 23.4°C and 1451.4 ± 0.4 m/sec at 22°C. respectively for the sound velocity. It was seen that although the sound pulse could no longer be considered as radiating as a plane wave at 12 MHz the measured velocity was larger than the value at 68.8 MHz by only 0.03%, whilst at 20 MHz the values agreed within the experimental error.

(d) Non-uniform temperature did not appear to affect the velocity measurements visibly and its effect was difficult to estimate. The vertical temperature gradient over the central region of the liquid was about 0.5 deg C/cm and this would result in an error of about 0.1 m/sec in the sound velocity. The chromel-alumel thermocouple was checked at the boiling point of water and was found to agree with the melting points of the various metals to within 0.5°C. The temperature of the mercury was therefore probably correct to 0.5°C.

In conclusion, it was estimated that the total error in sound velocity was about 0.05% due to the experimental errors in sound wavelength and frequency. The estimated errors in $-(\partial c/\partial t)_p$ and c_m were calculated from the computed deviations from the line of regression and the experimental error respectively.

C. Comparison with Other Investigations

The reported results for sound velocity in mercury are recorded in Table 3.4, and are seen to agree within a few m/sec. The values for c and $-(\partial c/\partial t)_p$ obtained in the present study are seen to agree closely, within experimental error, with the recent measurements of Hill and Ruoff (1965b), Seemann and Klein (1965), and Coppens et al. (1967). The techniques employed are indicated in Table 3.4, where the notation is as follows:-

A - Direct Pulse Methods

B - Pulse Comparison Method

C - Repetition Rate Method

D - Phase Comparison Methods

These techniques have already been described in Section 2.1. Abowitz and Gordon (1963), Hill and Ruoff (1965b) and Davis and Gordon (1967) used mercury maintained at a fixed temperature as the reference liquid, whilst Seemann and Klein (1965) used distilled water. The sound velocity data for mercury and distilled water were taken from Hubbard

and Loomis (1928) and Greenspan and Tschiegg (1957). It would appear that Abowitz and Gordon (1963) have underestimated their experimental error in sound velocity since they quote an accuracy of 0.1 m/sec in spite of the fact that Hubbard and Loomis give an error of 0.3 m/sec on their values for mercury. Also of interest is the fact that the results due to Hubbard and Loomis (1928) for distilled water are about 1 m/sec higher than recent values for the sound velocity [see McSkimin (1965)]. The data of Greenspan and Tschiegg (1957) has likewise been seen to be high by 0.35 m/sec and would result in the sound velocity for mercury determined by Seemann and Klein (1965) being systematically high by about 0.3 m/sec. The author's preliminary results for mercury have been reported [Webber (1965)] in which the highest temperature reached was 75°C. In contrast to the pulse comparison technique the methods used by Coppens et al. (1967) and in the present study measure directly the absolute sound velocity. The excellent agreement with the recent investigations show that the present apparatus and technique give consistent results for the sound velocity. It is also apparent that direct pulse methods are unreliable for measurements of $-(\partial c/\partial t)_p$.

3.2 Sound Velocities in Various Liquid Metals

The zinc, cadmium, indium, tin, lead and bismuth were 99.99, 99.95, 99.97, 99.9, 99.99 and 99.98% pure respectively. These materials

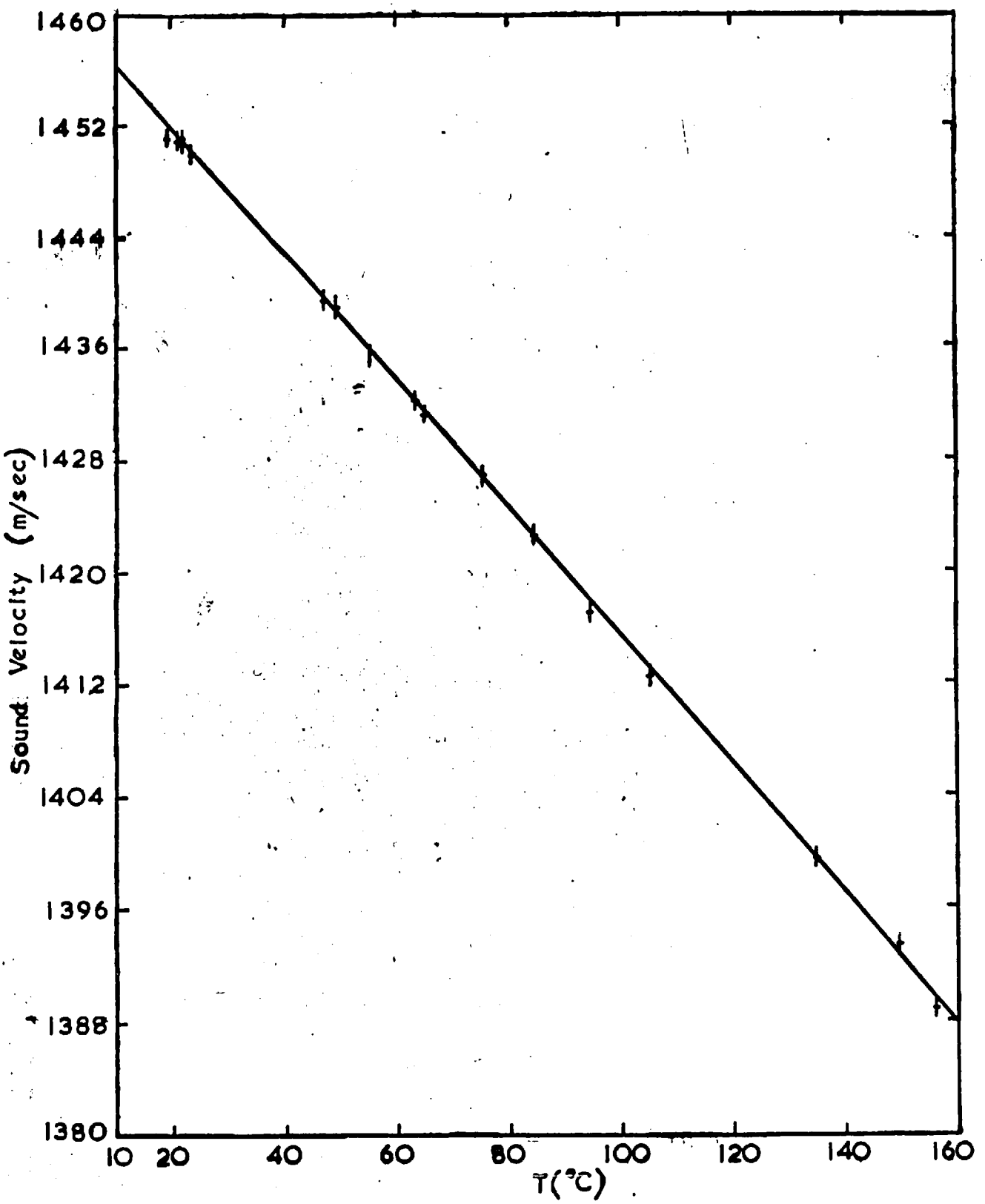

Fig. 3.1. Velocity of sound as a function of temperature in mercury.

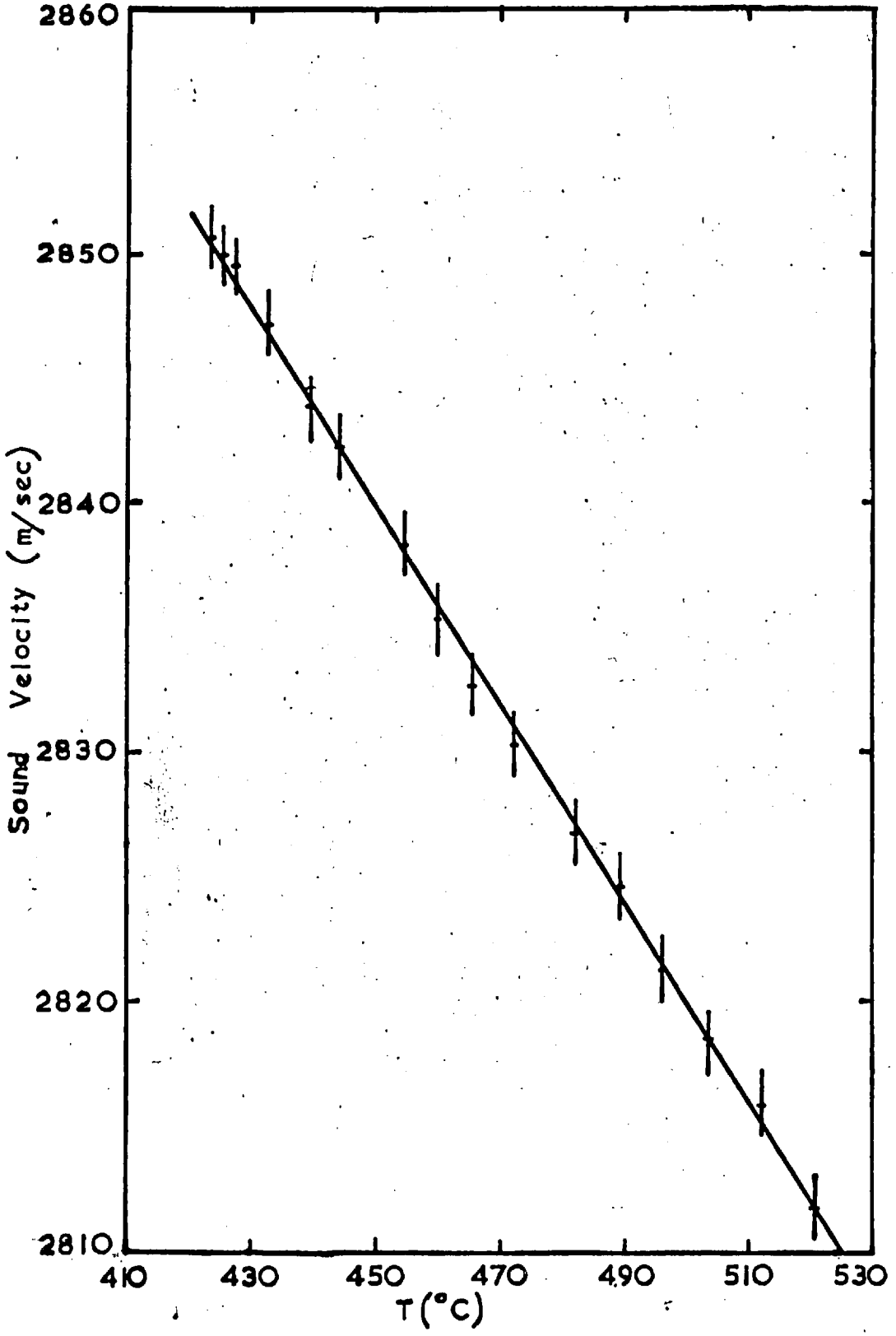

Fig. 3.2. Velocity of sound as a function of temperature in zinc.

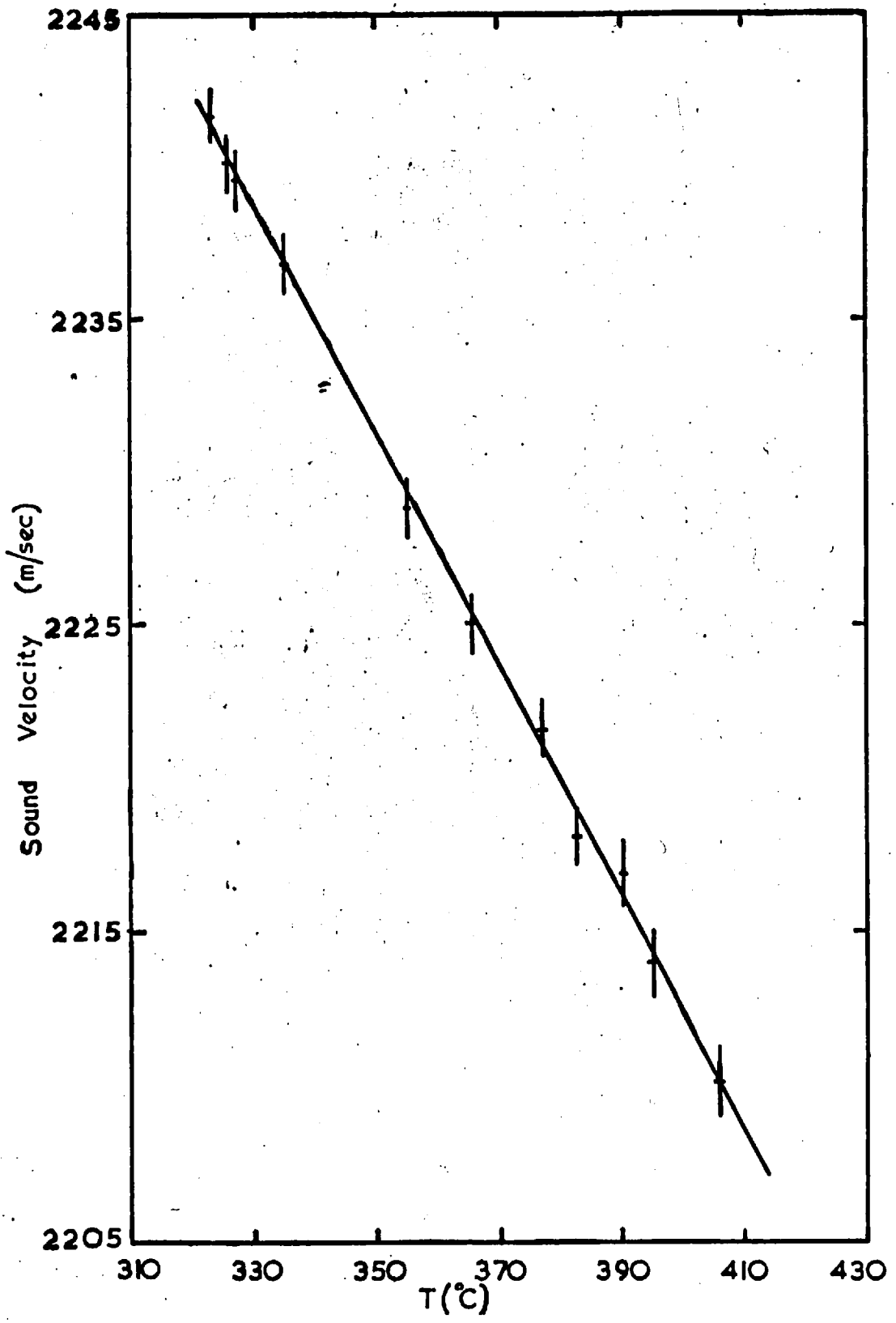

Fig. 3.3. Velocity of sound as a function of temperature in cadmium.

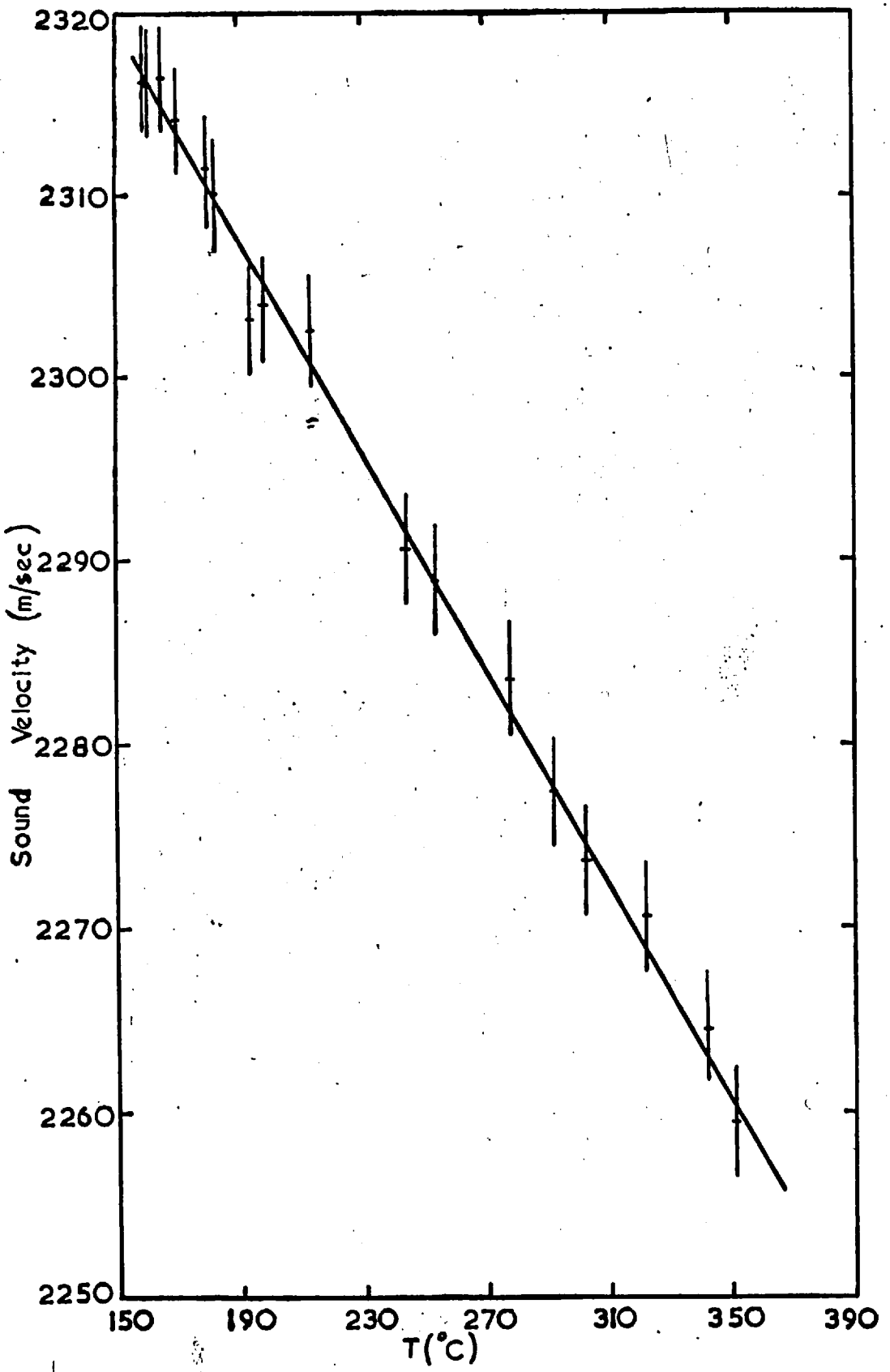

Fig.3.4. Velocity of sound as a function of temperature in indium.

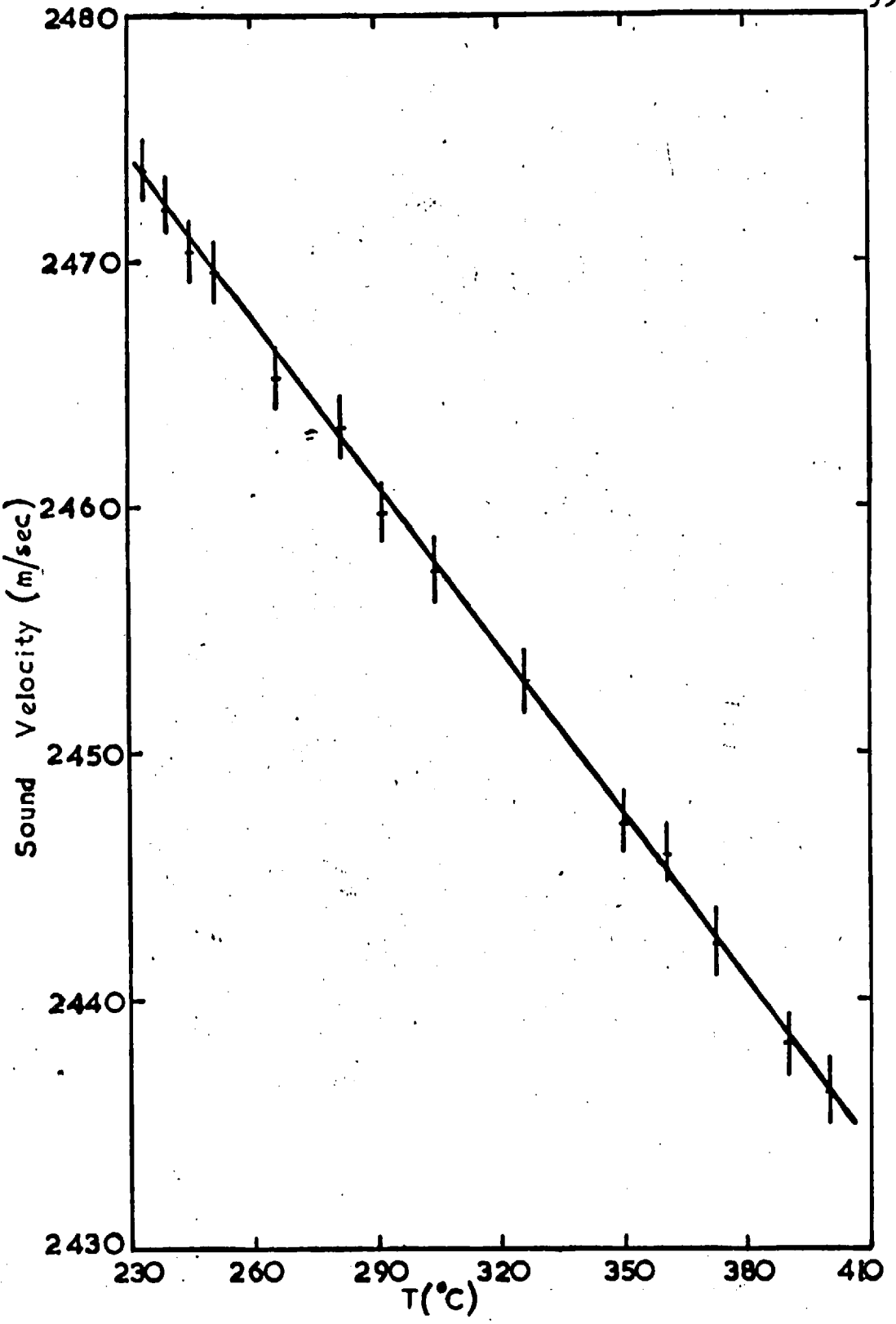

Fig.3.5. Velocity of sound as a function of temperature in tin.

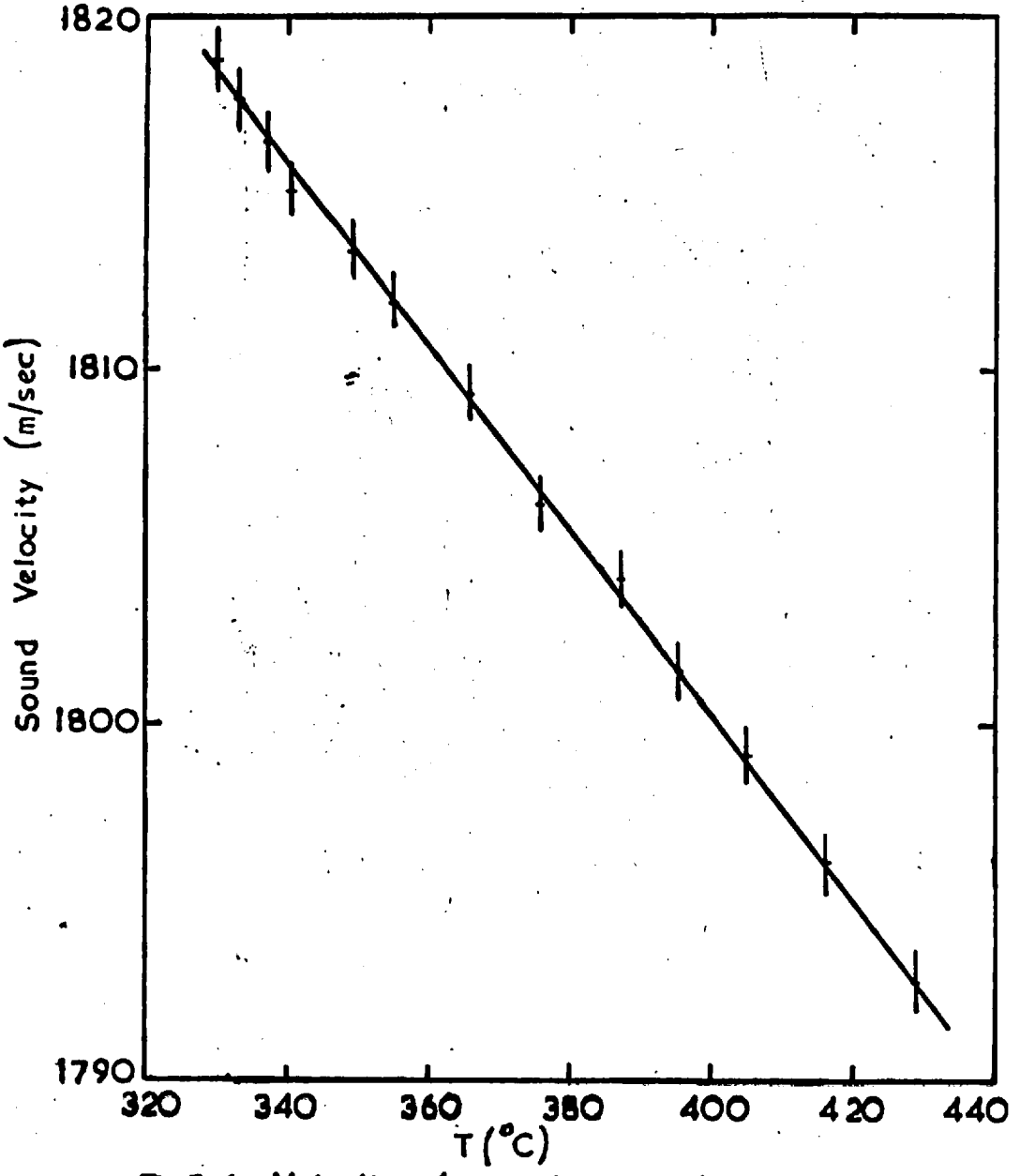

Fig.3.6. Velocity of sound as a function of temperature in lead.

Table 3.2 Results for Velocity of Sound in Pure Metals

Metal	t_m (°C)	c_m (m/sec)	$-(\partial c/\partial t)_p$ (m/sec.deg C)
Zn	420	2851.8 ± 1.4	0.400 ± 0.004
Cd	321	2242.1 ± 1.0	0.376 ± 0.005
Hg	-38.9	1478.7 ± 0.7	0.457 ± 0.003
In	156	2317.7 ± 3	0.293 ± 0.005
Sn	232	2473.9 ± 1.3	0.223 ± 0.003
Pb	328	1818.9 ± 0.8	0.259 ± 0.003

were supplied by Johnson, Matthey and Co. Ltd. The experimental procedure has been described in Section 2.10B. In the case of zinc, a draught of air from a fan was used to cool the outer casing of the furnace and air at a few lb/in^2 pressure blown over the transducer mounting so as to prevent a deterioration of the transducer bond. The poor transmission of ultrasound into the indium resulted in a slightly greater error in the measurement of λ as compared with the other pure metals.

It is seen from Figs. 3.2, 3.3, 3.4, 3.5, and 3.6 that within experimental error the sound velocity decreases linearly with increasing temperature in liquid zinc, cadmium, indium, tin and lead. A linear fit to the sound velocity data is used and the best values and estimated errors for c_m and $(\partial c/\partial t)_p$ for these liquid metals are shown in Table 3.2. The present results are compared with other investigations in Table 3.5 and discussed in Section 3.3.

Since Hill and Ruoff (1965b) had found that the sound velocity in liquid bismuth decreased non-linearly with temperature, the sound velocity in liquid bismuth was measured in greater detail, particularly below $300^{\circ}C$. The present results are recorded in Table 3.3 and plotted as a function of temperature in Fig. 3.7. A second and third degree polynomial were fitted to the data by the method of least squares from the Atlas Computer Laboratory program VC01A and it was found that the

Table 3.3 Sound Velocity in Liquid Bismuth

t (°C)	c (m/sec)	t (°C)	c (m/sec)
273	1648.8	309	1645.7
274.5	1649.1	310.5	1645.3
274.5	1648.4	317	1644.5
275.5	1648.8	321.5	1644.3
276	1648.3	325.5	1644.3
276.5	1648.5	333.5	1643.1
277	1648.4	334	1643.0
277.5	1648.7	340.5	1642.6
279	1648.7	341.5	1642.5
279	1648.4	343	1641.9
279.5	1648.5	346	1642.0
282	1647.8	349	1641.9
284.5	1648.1	349.5	1641.1
284.5	1647.9	354.5	1640.8
285	1647.8	360.5	1640.3
287	1647.8	368.5	1639.1
287.5	1647.6	377.5	1638.1
290.5	1647.5	381	1637.7
293.5	1646.9	392	1636.1
295.5	1646.8	401.5	1635.1
298.5	1647.1	408	1634.1
306	1646.2		

Estimated error in c = 0.7 m/sec

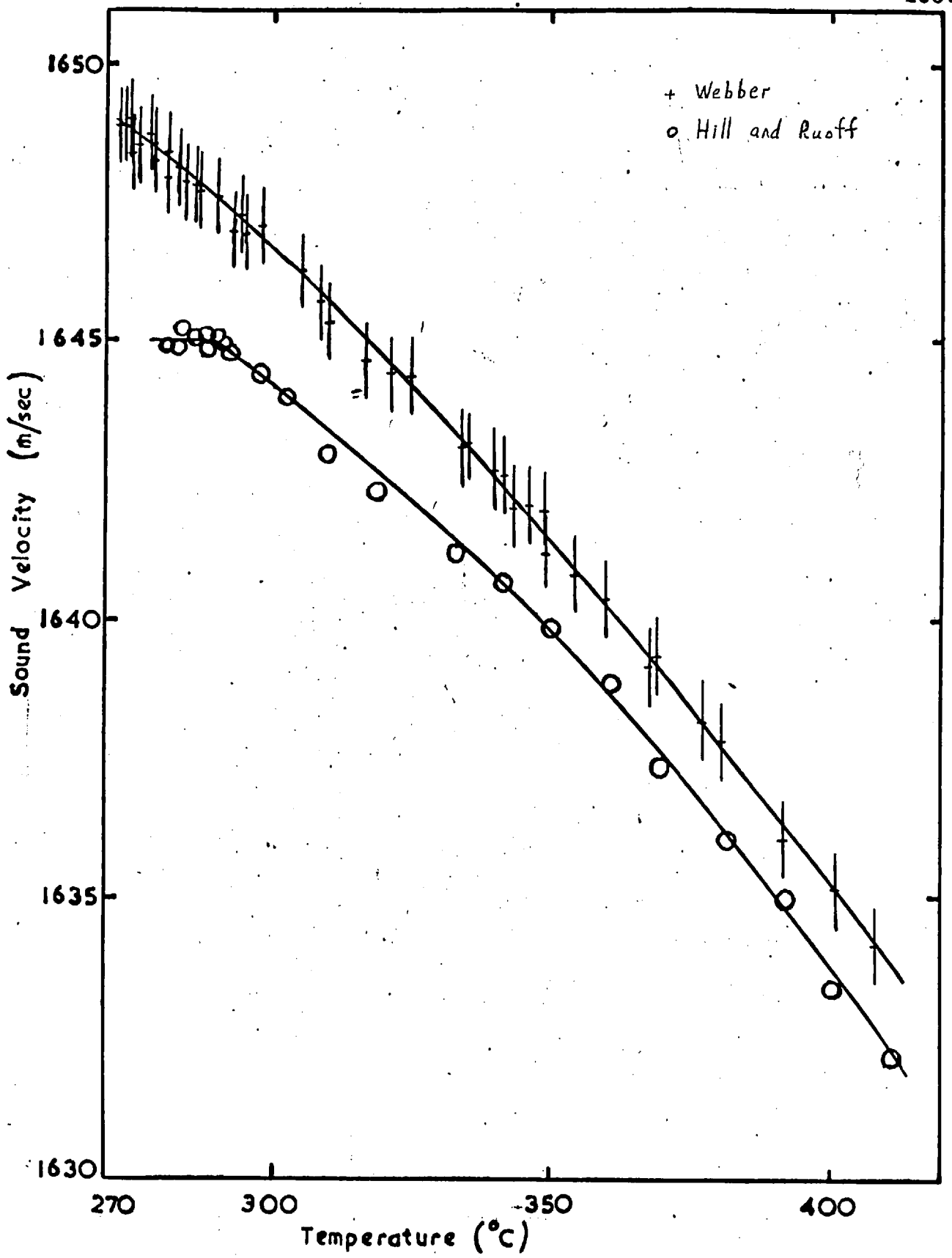

Fig.3.7. Velocity of sound as a function of temperature in bismuth.

best curve fit within experimental error was given by

$$c = 1653.4 + 4.52 \times 10^{-2}t - 2.27 \times 10^{-4}t^2, \qquad (3.3)$$

valid for $t \geq 271^{\circ}C$.

Estimated error in zeroth coefficient = 0.7 m/sec.

Estimated error in first coefficient = 0.12×10^{-2} m/sec.deg C.

Estimated error in second coefficient = 0.33×10^{-4} m/sec.deg C^2.

The present result is compared with other investigations in Table 3.5 and discussed more fully in Section 3.3F.

3.3 Discussion of Results for Pure Metals

A compilation of sound velocity measurements is recorded in Table 3.5. The present results for pure metals are discussed below.

A. Zinc

The present result for sound velocity is in excellent agreement with that of Gitis and Mikhailov (1966b). The inaccuracy of direct pulse methods is readily apparent. It is seen from Fig. 3.2 that the present results show that the sound velocity decreases linearly with temperature within the temperature range of the experiment, whilst Gitis and Mikhailov (1966b) report that the sound velocity falls off more rapidly as the temperature increases. Murthy and Rao (1967)

Table 3.4 Comparison of Published Values for Velocity of Sound in Mercury

t (°C)	c (m/sec)	$-(\partial c/\partial t)_p$ (m/sec deg C)	Technique	Temperature range (°C)	Investigator
30	1446.2 ± 0.3	0.464 ± 0.003	D	0 - 70	Hubbard and Loomis (1928)
23.8	1449 ± 2		D	20 - 28	Ringo et al (1947)
50	1440 ± 10	0.7	A	50 - 150	Kleppa (1950)
20	1452 ± 4	0.312	D	20 - 100	Polotskii and Khodov (1955)
20	1452 ± 3	0.37	D	20 - 100	Golik et al (1961)
30	1446.4 ± 0.1	0.46 ± 0.002	B		Abowitz and Gordon (1963)
30	1448 ± 2	0.60	B	25 - 130	Hunter et al (1963)
25	1450 ± 6	0.45	D	25 - 204	Jarzynski (1963)
30	1446		C		Beyer and Coppens (1965)
30	1447.4	0.473 ± 0.002	B	30 - 197	Hill and Ruoff (1965b)
20	1451.6 ± 0.4	0.458 ± 0.004	B	-36 - 60	Seemann and Klein (1965)
20	1451.5 ± 0.7	0.45 ± 0.01	D	20 - 75	Webber (1965)
30	1446.4 ± 0.2	0.462	C	30 - 199	Coppens et al (1967)
21.9	1450.1 ± 0.3	0.464 ± 0.003	C	22 - 53	Davis and Gordon (1967)
30	1447.2 ± 0.7	0.457 ± 0.003	D	20 - 156	Webber

Table 3.5 Comparison of Published Values for Velocity of Sound in Pure Metals

Metal	t (°C)	c (m/sec)	$-(\partial c/\partial t)_p$ (m/sec deg C)	Technique	Temperature range (°C)	Investigator
Zn	420	2790 ± 60		A	420 - 480	Kleppa (1950)
	450	2700		A		Plass (1963)
	440	2840 ± 40	0.268	A	440 - 850	Kazakov et al (1964)
	420	2850 ± 6	0.305	D	420 - 850	Gitis and Mikhailov (1966b)
	428	2816		D	428 - 670	Murthy and Rao (1967)
	420	2851.8 ± 1.4	0.400 ± 0.004	D	424 - 521	Webber
Cd	321	2200 ± 20	0.5	A	321 - 360	Kleppa (1950)
	335	2215 ± 7		A		Polotskii et al (1959)
	331	2223 ± 7		A		Khodov (1960)
	360	2150		A		Plass (1963)
	321	2220 ± 34	0.618	A	330 - 750	Pronin and Filippov (1963a)
	321	2256 ± 5	0.29	D	321 - 700	Gitis and Mikhailov (1966b)
	422	2225	0.58	D	420 - 650	Murthy and Rao (1967)
	321	2242.1 ± 1.0	0.376 ± 0.005	D	323 - 406	Webber
In	156	2215 ± 20	0.5	A	156 - 260	Kleppa (1950)
	160	2313		C		Beyer and Coppens (1965)
	167	2310.7	0.296 ± 0.001	B	167 - 345	Hill and Ruoff (1965b)

Table 3.5 continued

Metal	t (°C)	c (m/sec)	$-(\partial c/\partial t)_p$ (m/sec.deg C)	Technique	Temperature range (°C)	Investigator
In	156	2315 ± 5	0.27	D	156 - 950	Gitis and Mikhailov (1966b)
	156	2314.2 ± 0.6	0.29	C	159 - 230	Coppens et al (1967)
	156	2317.7 ± 3	0.293 ± 0.005	D	159 - 351	Webber
Sn	232	2270 ± 20	0.7	A	232 - 380	Kleppa (1950)
	232	2464 ± 4	0.236 ± 0.001	B	230 - 335	Gordon (1969)
	232	2473 ± 12	0.247	D	240 - 500	McSkimin (1959)
	247	2454 ± 8		A		Polotskii et al (1959)
	243	2466 ± 8	0.2	A		Khodov (1960)
	240	2470		A		Plass (1963)
	232	2420 ± 50	0.211	A	232 - 620	Pronin and Filippov (1963a)
	240	2470		C		Beyer and Coppens (1965)
	242	2470 ± 5		D		Litovitz and Jarzynski (1965)
	232	2480 ± 6	0.3	D	232 - 800	Gitis and Mikhailov (1966a)
	232	2481	0.284	B		Nagel (1966)
	232	2472 ± 3		C	239 - 262	Coppens et al (1967)
	232	2473.9 ± 1.3	0.223 ± 0.003	D	235 - 401	Webber
Pb	328	1790 ± 15	0.5	A	328 - 380	Kleppa (1950)
	328	1776 ± 4	0.277 ± 0.006	B	328 - 370	Gordon (1959)
	340	1834 ± 6		A		Polotskii et al (1959)
	344	1826 ± 6	0.3	A		Khodov (1960)

Table 3.5 continued

Metal	t (°C)	c (m/sec)	$-(\partial c/\partial t)_p$ (m/sec .deg C)	Technique	Temperature range (°C)	Investigator
Pb	340	1760		A		Plass (1963)
	328	1810 ± 27	0.381	A	328 - 930	Pronin and Filippov (1963a)
	330	1820 ± 4	0.3	D	328 - 800	Gitis and Mikhailov (1966a)
	328	1816	0.273	B		Nagel (1966)
	328	1818.9 ± 0.8	0.259 ± 0.003	D	330 - 428	Webber
Bi	271	1635 ± 15	0.5	A	271 - 380	Kleppa (1950)
	287	1663 ± 5		A		Polotskii et al (1959)
	289	1666 ± 5		A	289 - 356	Khodov (1960)
	305	1650 ± 8	0.8	D	305 - 442	Jarzynski (1963)
	280	1650		A		Plass (1963)
	271	1620 ± 24	0.209	A	271 - 930	Pronin and Filippov (1963a)
	318	1639		C		Beyer and Coppens (1965)
	280	1645		B	280 - 410	Hill and Ruoff (1965b)
	271	1674 ± 4	0.18	D	271 - 850	Gitis and Mikhailov (1966a)
	271	1650	0.13	B		Nagel (1966)
	318	1639.4 ± 2		C	318 - 357	Coppens et al (1967)
	271	1649.0 ± 0.7		D	273 - 408	Webber

report that the sound velocity increases in the temperature interval between the melting point and 500°C and then falls linearly with increasing temperature. The latter measurements would appear to be erroneous. The excellent agreement with other investigations of the present values for $-(\partial c/\partial t)_p$ in other pure metals suggests that the value for $-(\partial c/\partial t)_p$ determined by Gitis and Mikhailov is slightly in error.

B. Cadmium

The present result for sound velocity differs from that of Gitis and Mikhailov (1966b) by 14 m/sec and the direct pulse methods give values which are lower by about 20 m/sec. Gitis and Mikhailov observed that the sound velocity decreased linearly with temperature until about 600°C and then decreased more rapidly with temperature. It is seen from Fig. 3.3 that the present result shows that the sound velocity decreases linearly with temperature within the temperature range of the experiment. There is a large variation in the reported values for $-(\partial c/\partial t)_p$, the values due to Pronin and Filippov (1963a) and Murthy and Rao (1967) being exceptionally high.

C. Indium

Apart from the result obtained by Kleppa (1950) the sound velocities determined by various investigators agree to within 3 m/sec. The values for $-(\partial c/\partial t)_p$ obtained by Hill and Ruoff (1966b), Coppens et al.

(1967) and in the present study agree within the estimated experimental errors. The value determined by Gitis and Mikhailov (1966b) is about 7% lower and they report that the sound velocity decreases linearly with temperature up to about 875°C and then decreases more rapidly with temperature.

D. Tin

There is fairly good agreement between the literature values for sound velocity. Nine investigations agree to within 10 m/sec with the present determination, and five investigations to within 2 m/sec. The sound velocity determined by Kleppa (1950) is seen to be erroneous. The values for $-(\partial c/\partial t)_p$ are seen to be in fair agreement. In the temperature range from the melting point to 400°C the present results show that the sound velocity decreases linearly with temperature (see Fig. 3.5) whereas Gitis and Mikhailov (1966a) report that the velocity decreases non-linearly and less rapidly as the temperature increases.

E. Lead

The present result for sound velocity at the melting point agrees to within 5 m/sec with the values obtained by Gitis and Mikhailov (1966a) and Nagel (1966). These three investigations give values for $-(\partial c/\partial t)_p$ which are in fairly close agreement. The value of c determined by Gordon (1959) is seen to be low by 43 m/sec whereas $-(\partial c/\partial t)_p$ is close to the present result. The measurements of Kleppa (1950) and

Plass (1963) are again seen to be fairly inaccurate. Gitis and Mikhailov (1966a) report that the sound velocity decreases non-linearly with temperature in the temperature interval 328 to 400°C, contrary to the present result (see Fig. 3.6).

F. Bismuth

At the melting point the present result agrees to within 4 m/sec with the results of Hill and Ruoff (1965b) and Nagel (1966). The result due to Gitis and Mikhailov (1966a) is seen to be higher by 25 m/sec. It is seen from Fig. 3.7 that in the present study the sound velocity does not remain constant in the temperature interval between the melting point and 290°C as reported by Hill and Ruoff (1965b) but decreases with increasing temperature. Above 320°C the results of Hill and Ruoff, Nagel (1966), Coppens et al (1967) and the present investigation for the variation of velocity with temperature are very similar. The values for $-(\partial c/\partial t)_p$ obtained by Kleppa (1950) and Jarzynski (1963) are seen to be exceptionally high.

G. Summary of Sound Velocity Results in Pure Metals

It has been seen that the present apparatus and measuring technique is capable of giving results for sound velocity which are in close agreement with other investigations. Measurements obtained by direct pulse methods are seen to be inaccurate and unreliable, particularly the original results of Kleppa (1950). Pulse comparison, repetition rate

and phase comparison techniques are seen to be more accurate and consistent with one another. Although there is a large scatter in values of $-(\partial c/\partial t)_p$ reported in the literature, the present values are in fairly close agreement with other investigations on mercury, indium, tin, lead and bismuth where the values are more consistent. This suggests that for zinc and cadmium the present values for $-(\partial c/\partial t)_p$ can be considered as more reliable.

3.4 Sound Velocity in Mercury-Zinc Alloys

The experimental procedure is described in Section 2.10C. The results for the mercury alloy systems are presented in order of increasing valency and atomic weight of the solute whereas the experimental order is Hg-In, Hg-Bi, Hg-Cd, Hg-Pb, Hg-Sn and Hg-Zn. Each alloy system is maintained at a temperature above the liquidus temperature given by Hultgren et al. (1963) for the alloy composition. If the liquid alloy is taken below the liquidus temperature the sound velocity decreases rapidly as is expected since the solute becomes a suspension in mercury and the sound velocity tends towards the value for pure mercury. If this occurs accidentally the temperature is raised above the liquidus temperature and the liquid is agitated until the sound velocity measurements are consistent within themselves, showing that the alloy is thoroughly mixed.

All the mercury-zinc alloys are prepared by adding a known weight of zinc to mercury. Within the temperature range of the experiment the sound velocity is found to decrease linearly with temperature for each alloy. A linear fit to the velocity data is obtained from the Atlas Computer Laboratory program VB01A and the results are recorded in Table 3.6 for each composition. The error in the fractional atomic concentration a varies from about 0.1 to 0.3%.

The sound velocities are calculated for each composition at 158 and 350°C (see Table A.1) and are plotted in Fig. 3.8. Solid and dashed lines on the graph correspond to concentrations for which the alloy composition is above or below, respectively, the liquidus temperature. It is seen from Fig. 3.8 that the addition of zinc to mercury causes the sound velocity to increase, which confirms the measurements of Golik et al. (1961) and Abowitz and Gordon (1963). Contrary to the variation of sound velocity with composition in mercury-thallium alloys reported by Abowitz and Gordon (1963), (see Fig. 1.1), the graphical curvature between the pure component values is concave rather than convex. A theoretical approach to the variation of sound velocity with composition is discussed in Section 4.6.

The variation of $-(\partial c/\partial t)_p$ with alloy composition is shown in Fig. 3.14. The value of $-(\partial c/\partial t)_p$ is seen to decrease rapidly with increase in atomic concentration of zinc; Golik et al. (1961) and

Abowitz and Gordon (1963) report a more rapid decrease with composition than is found in the present investigation.

3.5 Sound Velocity in Mercury-Cadmium Alloys

Difficulty in measurement of sound velocity was experienced due to poor sound transmission into the molten alloys. As a result new alloy compositions were made up at 20 and 30 at. % Cd and additional cadmium was added to these to vary the composition.

The sound velocity results are recorded in Table 3.7 and are plotted as a function of composition at 158 and 350°C in Fig. 3.9; the calculated data are shown in Table A.2. The liquidus temperature of 158°C corresponds to the alloy composition 54 at. % Cd [Hultgren et al. (1963)]. At 350°C all the mercury-cadmium alloys are above their liquidus temperatures. It is seen from Fig. 3.9 that the sound velocity increases smoothly with concentration of Cd and shows a graphical convex curvature between the two pure component values. The variation of $-(\partial c/\partial t)_p$ with composition is shown in Fig. 3.15, from which it is seen that the value of $-(\partial c/\partial t)_p$ decreases fairly rapidly in the composition range up to 30 at. % Cd and then remains fairly constant. Golik et al. (1961) and Abowitz and Gordon (1963) report a more rapid decrease of $-(\partial c/\partial t)_p$ with concentration of Cd than is found in the present investigation.

3.6 Sound Velocity in Mercury-Indium Alloys

Mercury-indium was the first alloy system investigated. An alloy composition of 2 at. % In was prepared in a beaker and was poured into the silica container. At the end of the measurements the alloy was removed and the container cleaned. A second alloy composition of 2 at. % In was prepared in the usual manner, as described in Section 2.10C, and it was found that the two sets of measurements agreed within the experimental error. Several initial compositions were prepared and the composition varied, the different series of compositions over-lapping one another. The sound velocity was found to decrease linearly with temperature for all the alloy compositions.

The results are recorded in Table 3.8 and the calculated values for the sound velocity at 160°C for various compositions are shown in Table A.3. From Fig. 3.10 it is seen that the sound velocity increases smoothly with increasing at. % In. The values of $-(\partial c/\partial t)_p$ are plotted as a function of composition in Fig. 3.16 and it is seen that $-(\partial c/\partial t)_p$ decreases rapidly in the composition range up to about 30 at. % In and then remains fairly constant.

3.7 Sound Velocity in Mercury-Tin Alloys

The usual experimental procedure was carried out for compositions up to 40 at. % Sn, whilst in the composition range between 50 and 90 at. % Sn mercury was added successively to tin or mercury-tin alloys.

It was found that the mercury-tin alloys needed to be agitated for about a day before the sound velocity measurements became consistent within themselves. The sound velocity was found to decrease linearly with temperature for all the compositions.

The results are recorded in Table 3.9 and the calculated sound velocities at 240 and 350°C are plotted as a function of composition in Fig. 3.11, the data for which are shown in Table A.4. It is seen that the sound velocity increases smoothly with at.% Sn. The value of $-(\partial c/\partial t)_p$ is plotted as function of composition in Fig. 3.17 and it is found that $-(\partial c/\partial t)_p$ decreases rapidly to a minimum at about 20 at.% Sn and then increases to a value which is greater than that for pure tin.

3.8 Sound Velocity in Mercury-Lead Alloys

Poor sound transmission occurred in the composition range up to 20 at.% Pb and several of the compositions had to be repeated. The acoustic signal improved at higher concentrations of lead and it was possible to vary the composition as usual. It was found that the sound velocity decreased linearly with temperature in all the alloy compositions.

The sound velocity results are recorded in Table 3.10. Sound velocity is plotted as a function of composition at 158 and 350°C in Fig. 3.12 and it is found to vary smoothly across the alloy system.

Calculated data for Fig. 3.12 are shown in Table A.5. The value of $-(\partial c/\partial t)_p$ is plotted as a function of composition in Fig. 3.18, from which it is seen that $-(\partial c/\partial t)_p$ decreases rapidly to a minimum at about 15 at.% Pb and then increases to a value which is greater than that for pure lead. It is noted that the variation of $-(\partial c/\partial t)_p$ with composition is similar to that found in the mercury-tin system.

3.9 Sound Velocity in Mercury-Bismuth Alloys

The usual experimental procedure for mercury alloys was carried out. The composition 15 at.% Bi was repeated and it was found that the two sets of measurements agreed to within 1 m/sec. No experimental difficulty was experienced in obtaining consistent measurements once the usual agitation processes had been carried out. The 50 at.% Bi composition was taken below its liquidus temperature and the expected drop in sound velocity was observed. 90 at.% Bi was obtained by adding mercury to liquid bismuth.

The sound velocity results are recorded in Table 3.11 and Fig. 3.13 shows that at 158 and 350°C the sound velocity increases smoothly with concentration of bismuth. Liquidus temperature of 158°C corresponds to the alloy 48 at.% Bi. The velocity data for Fig. 3.13 are recorded in Table A.6. From Fig. 3.19 it is seen that $-(\partial c/\partial t)_p$ decreases rapidly in the composition range between 0 and 10 at.% Bi and then decreases approximately linearly with increasing at.% Bi.

Table 3.6 Sound Velocity in Mercury- Zinc Alloys

Fractional atomic concentration b of Zn	Temperature (°C)	c (m/sec)	$-(\partial c/\partial t)_p$ (m/sec·deg C)	Temperature range (°C)
0.0201	40	1472.9 ± 0.7	0.438 ± 0.008	40 - 110
0.0503	81	1500.0 ± 0.8	0.421 ± 0.006	81 - 164.5
0.100	72	1565.7 ± 0.8	0.362 ± 0.006	71.5 - 178
0.150	87	1623.0 ± 0.8	0.350 ± 0.006	87 - 201
0.200	115	1669.1 ± 0.8	0.326 ± 0.006	114.5 - 221
0.250	143	1716.7 ± 0.9	0.312 ± 0.006	143 - 245
0.300	161	1769.2 ± 0.9	0.317 ± 0.006	160.5 - 270
0.350	178	1822.7 ± 0.9	0.304 ± 0.006	178 - 277.5
0.400	208	1872.0 ± 0.9	0.295 ± 0.006	207.5 - 298
0.500	228	1988.3 ± 1.0	0.276 ± 0.006	227.5 - 321.5

Table 3.7 Sound Velocity in Mercury-Cadmium Alloys

Fractional atomic concentration b of Cd	Temperature (°C)	c (m/sec)	$-(\partial c/\partial t)_p$ (m/sec.deg C)	Temperature range (°C)
0.0200	54	1463.1 ± 0.7	0.451 ± 0.005	53 - 121
0.0500	72	1491.0 ± 0.7	0.429 ± 0.008	71.5 - 161
0.100	85	1543.1 ± 0.8	0.414 ± 0.006	84 - 164
0.150	103	1587.4 ± 0.9	0.389 ± 0.011	103 - 160
0.200	104	1638.6 ± 0.8	0.395 ± 0.009	103 - 184
0.250	113	1682.9 ± 0.8	0.378 ± 0.008	113 - 202.5
0.300	133	1721.2 ± 1.0	0.348 ± 0.012	132.5 - 196.5
0.350	148	1760.7 ± 0.9	0.359 ± 0.010	147.5 - 236
0.400	169	1797.3 ± 1.0	0.347 ± 0.014	169 - 260.5
0.500	176	1876.6 ± 1.0	0.354 ± 0.011	176 - 265.5
0.600	227	1939.5 ± 1.0	0.346 ± 0.010	226 - 286
0.700	264	2002.3 ± 1.0	0.359 ± 0.014	263 - 303.5

Table 3.8 Sound Velocity in Mercury-Indium Alloys

Fractional atomic concentration b of In	Temperature (°C)	c (m/sec)	$-(\partial c/\partial t)_p$ (m/sec deg C)	Temperature range (°C)
0.0060	22	1459.4 ± 0.7	0.439 ± 0.005	22 - 103
0.0100	35	1459.7 ± 0.7	0.441 ± 0.005	35 - 109
0.0150	23	1471.3 ± 0.7	0.439 ± 0.005	22 - 113
0.0200	33	1474.4 ± 0.7	0.436 ± 0.005	32.5 - 107
0.0200	23	1478.3 ± 0.7	0.431 ± 0.008	22.5 - 117
0.0500	24	1517.6 ± 0.8	0.394 ± 0.006	23 - 111.5
0.0800	31	1553.6 ± 0.8	0.383 ± 0.006	30 - 110.5
0.0946	24	1573.1 ± 0.8	0.364 ± 0.006	23 - 124
0.140	24	1624.3 ± 0.8	0.344 ± 0.006	23 - 104.5
0.181	24	1667.5 ± 0.8	0.334 ± 0.006	23 - 138
0.250	41	1727.6 ± 0.9	0.299 ± 0.006	40.5 - 129
0.300	23	1777.9 ± 0.9	0.281 ± 0.010	23 - 117.5
0.350	24	1820.4 ± 0.9	0.289 ± 0.006	23.5 - 110.5
0.400	22	1863.4 ± 1.0	0.299 ± 0.010	21.5 - 123.5
0.500	23	1942.4 ± 1.0	0.283 ± 0.006	22 - 126
0.600	21	2020.2 ± 1.0	0.282 ± 0.004	20.5 - 206
0.725	63	2108.0 ± 1.1	0.288 ± 0.004	62.5 - 165.5

Table 3.9 Sound Velocity in Mercury-Tin Alloys

Fractional atomic concentration b of Sn	Temperature (°C)	c (m/sec)	$-(\partial c/\partial t)_p$ (m/sec·deg C)	Temperature range (°C)
0.0200	67	1475.2 ± 0.7	0.405 ± 0.006	66.5 - 134.5
0.0500	92	1509.1 ± 0.8	0.311 ± 0.011	91.5 - 153
0.100	115	1564.8 ± 0.8	0.275 ± 0.008	114.5 - 190.5
0.142	126	1611.5 ± 0.8	0.215 ± 0.006	125.5 - 224
0.200	118	1676.0 ± 0.8	0.195 ± 0.006	117.5 - 226
0.250	124	1732.8 ± 0.9	0.200 ± 0.006	123.5 - 233.5
0.300	130	1787.3 ± 0.9	0.208 ± 0.006	129.5 - 258.5
0.400	145	1890.2 ± 0.9	0.215 ± 0.006	145 - 259
0.499	166	1985.1 ± 1.0	0.226 ± 0.006	165.5 - 299.5
0.598	162	2084.4 ± 1.0	0.232 ± 0.006	161.5 - 326
0.748	201	2223.3 ± 1.1	0.264 ± 0.009	200.5 - 326
0.899	224	2373.8 ± 1.2	0.276 ± 0.007	224 - 332.5

Table 3.10 Sound Velocity in Mercury-Lead Alloys

Fractional atomic concentration b of Pb	Temperature (°C)	c (m/sec)	$-(\partial c/\partial t)_p$ (m/sec.deg C)	Temperature range (°C)
0.0200	62	1469.1 ± 0.7	0.389 ± 0.008	61.5 - 104.5
0.0400	82	1484.6 ± 0.7	0.362 ± 0.008	82 - 127.5
0.0500	82	1492.3 ± 0.7	0.301 ± 0.008	81 - 137.5
0.0527	77	1494.8 ± 0.9	0.264 ± 0.012	76.5 - 120
0.0800	100	1511.3 ± 0.8	0.264 ± 0.008	99 - 150.5
0.0971	104	1520.5 ± 0.8	0.236 ± 0.008	104 - 166.5
0.050	118	1558.5 ± 0.8	0.215 ± 0.008	117 - 194.5
0.200	124	1592.8 ± 0.8	0.222 ± 0.008	123.5 - 216
0.250	132	1625.9 ± 0.8	0.239 ± 0.008	132 - 230.5
0.300	136	1658.3 ± 0.8	0.255 ± 0.008	136 - 240.5
0.350	148	1685.6 ± 0.8	0.275 ± 0.008	148 - 257
0.400	163	1709.2 ± 0.9	0.307 ± 0.008	162.5 - 268.5
0.450	168	1734.1 ± 0.9	0.305 ± 0.008	167.3 - 287
0.500	182	1751.7 ± 0.9	0.331 ± 0.008	181.5 - 275
0.600	204	1782.7 ± 0.9	0.325 ± 0.008	203.5 - 308
0.700	242	1801.2 ± 0.9	0.333 ± 0.008	241 - 309
0.796	270	1814.6 ± 0.9	0.327 ± 0.008	269.5 - 332.5

Table 3.11 Sound Velocity in Mercury-Bismuth Alloys

Fractional atomic concentration b of Bi	Temperature (°C)	c (m/sec)	$-(\partial c/\partial t)_p$ (m/sec.deg C)	Temperature range (°C)
0.0200	73	1456.9 ± 0.7	0.393 ± 0.012	73 - 105.5
0.0500	74	1482.8 ± 0.7	0.331 ± 0.010	74 - 140.5
0.100	88	1511.6 ± 0.8	0.309 ± 0.010	87.5 - 167
0.150	104	1535.1 ± 0.8	0.251 ± 0.010	103.5 - 170.5
0.200	120	1556.3 ± 0.9	0.253 ± 0.013	119 - 215.5
0.250	126	1577.6 ± 0.8	0.243 ± 0.010	126 - 226
0.300	129	1595.2 ± 0.9	0.241 ± 0.012	128.5 - 234.5
0.350	140	1606.4 ± 0.8	0.215 ± 0.008	139.5 - 249
0.400	144	1617.3 ± 0.8	0.199 ± 0.008	143.5 - 253
0.450	161	1625.1 ± 1.0	0.200 ± 0.014	160 - 261.5
0.500	165	1630.4 ± 0.9	0.164 ± 0.012	164.5 - 261
0.600	196	1638.6 ± 0.8	0.167 ± 0.008	196 - 305.5
0.700	216	1642.5 ± 0.8	0.136 ± 0.008	215.5 - 304
0.893	271	1644.9 ± 0.8	0.101 ± 0.008	270.5 - 310.5

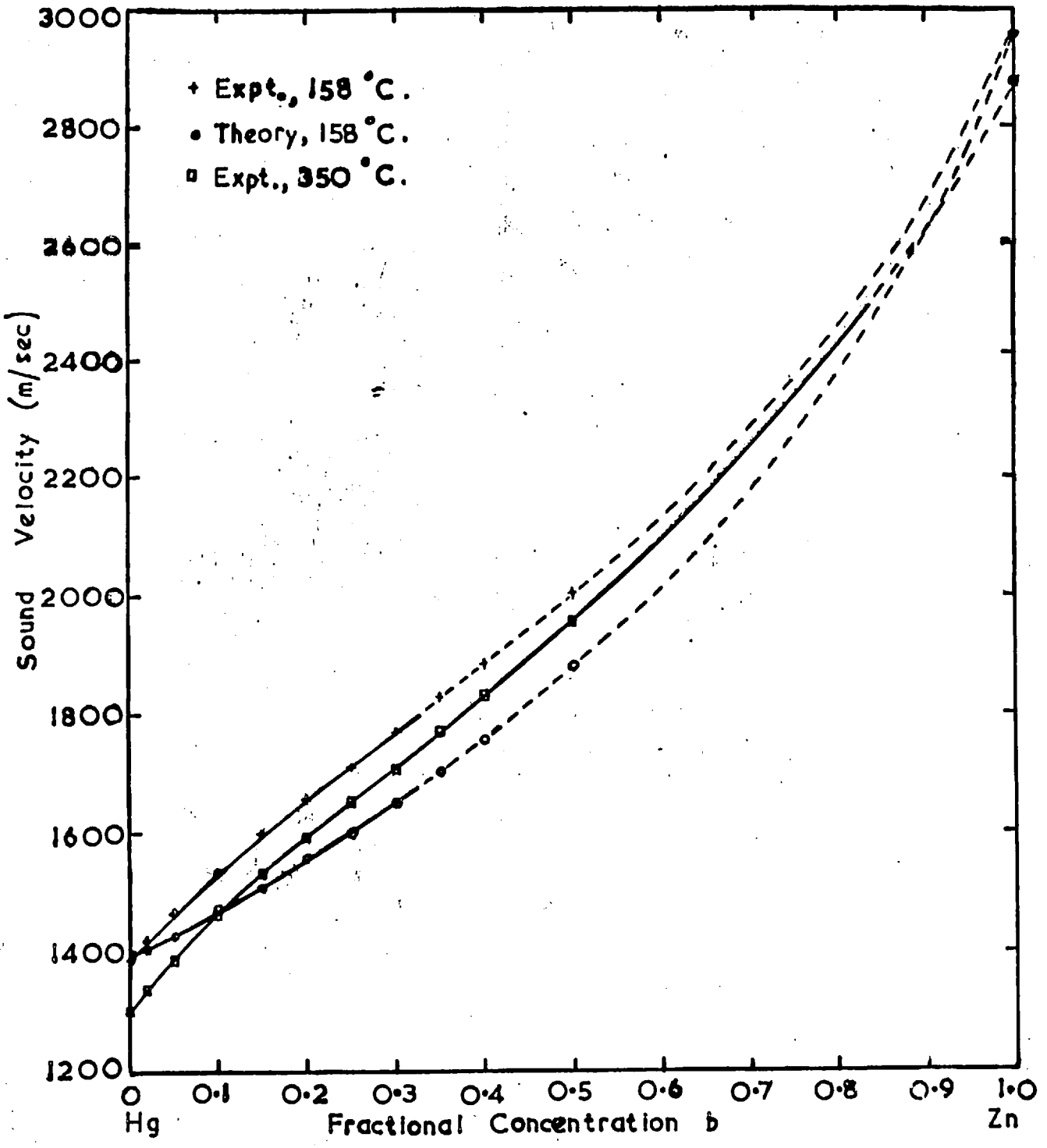

Fig.3.8. Sound velocity as a function of concentration b in the Hg–Zn alloy system. Sound velocity data shown in Table A.1.

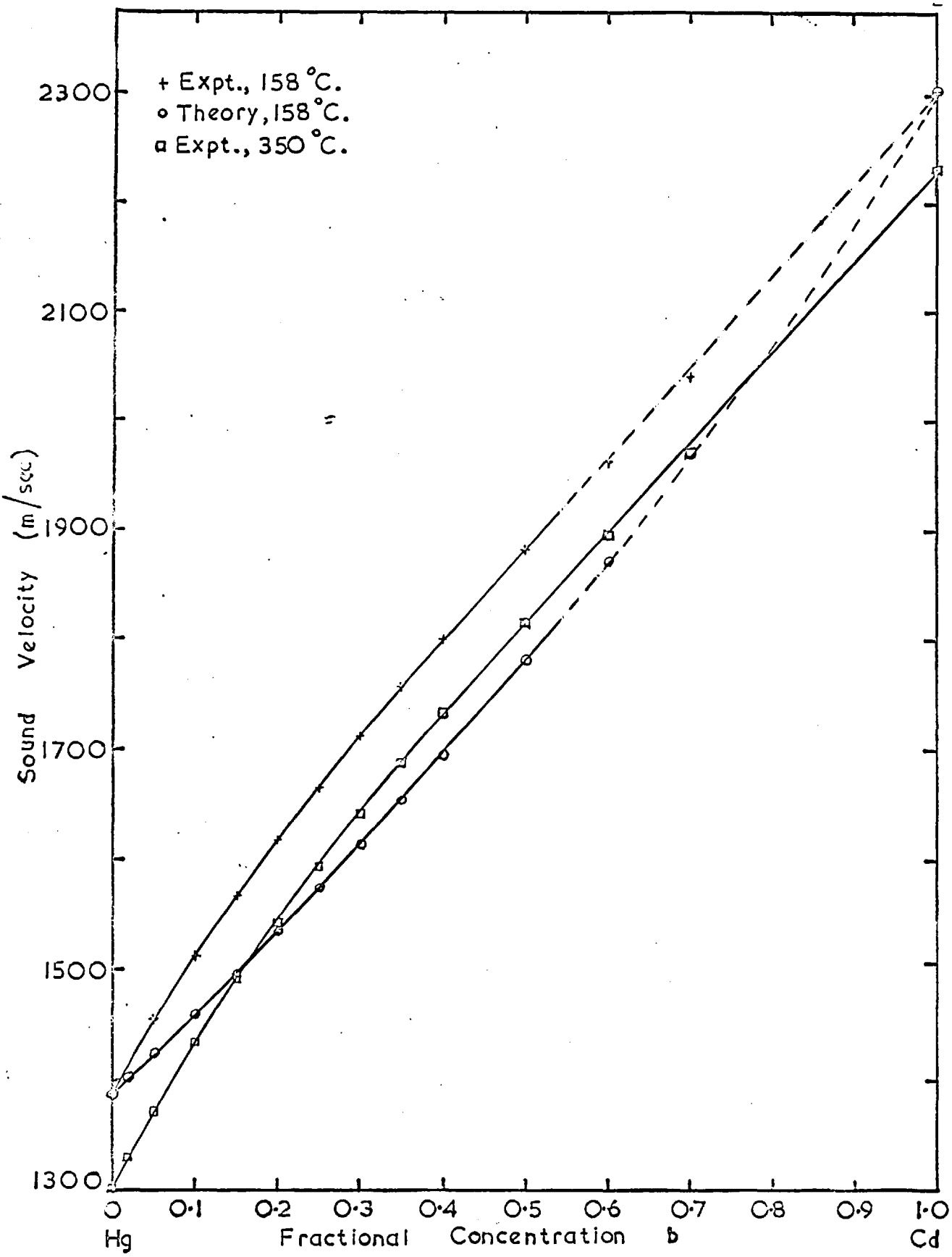

Fig. 3.9. Sound velocity as a function of concentration b in the Hg-Cd alloy system. Sound velocity data shown in Table A.2.

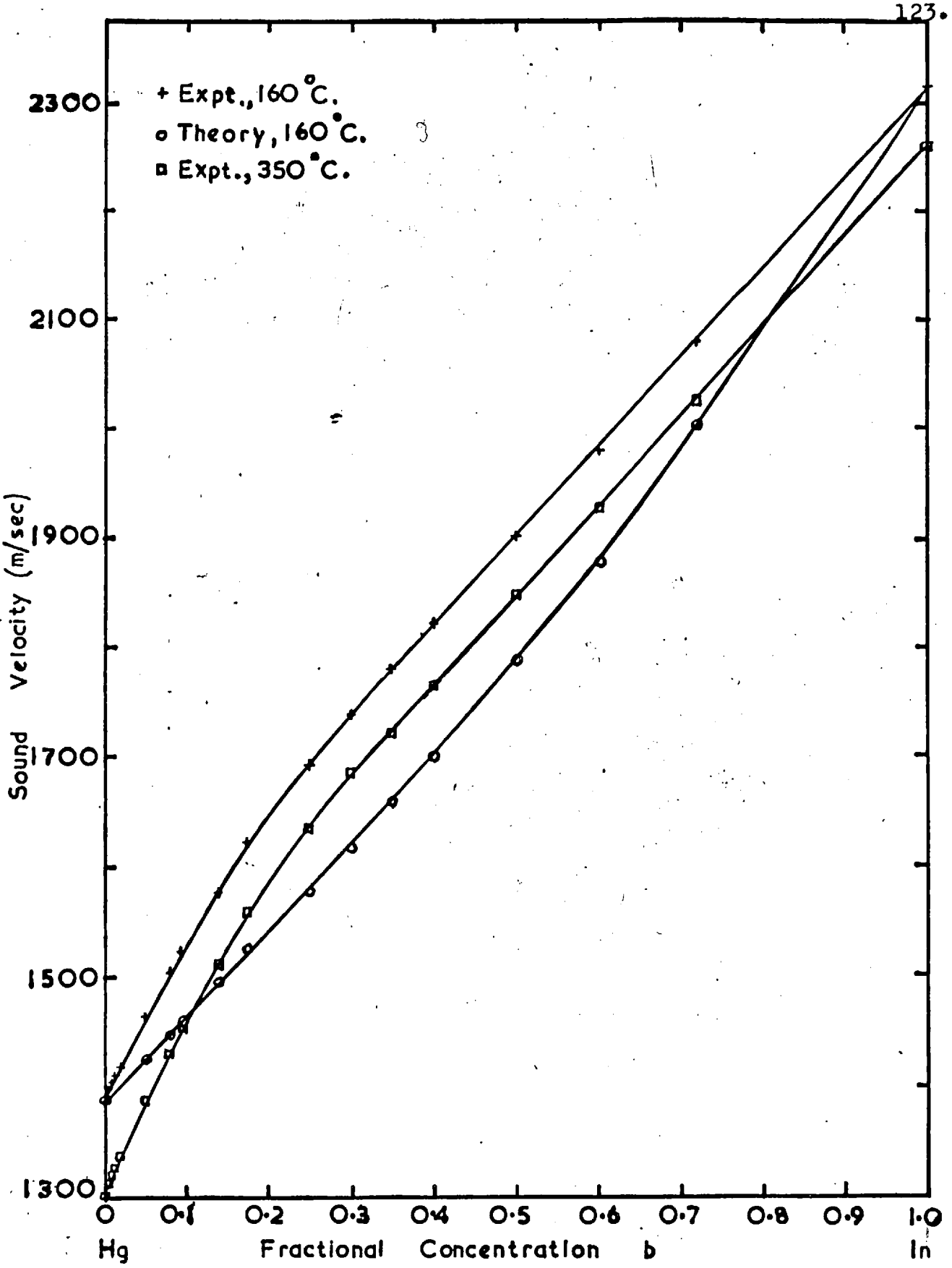

Fig.3.10. Sound velocity as a function of concentration b in the Hg-In alloy system. Sound velocity data shown in Table A.3.

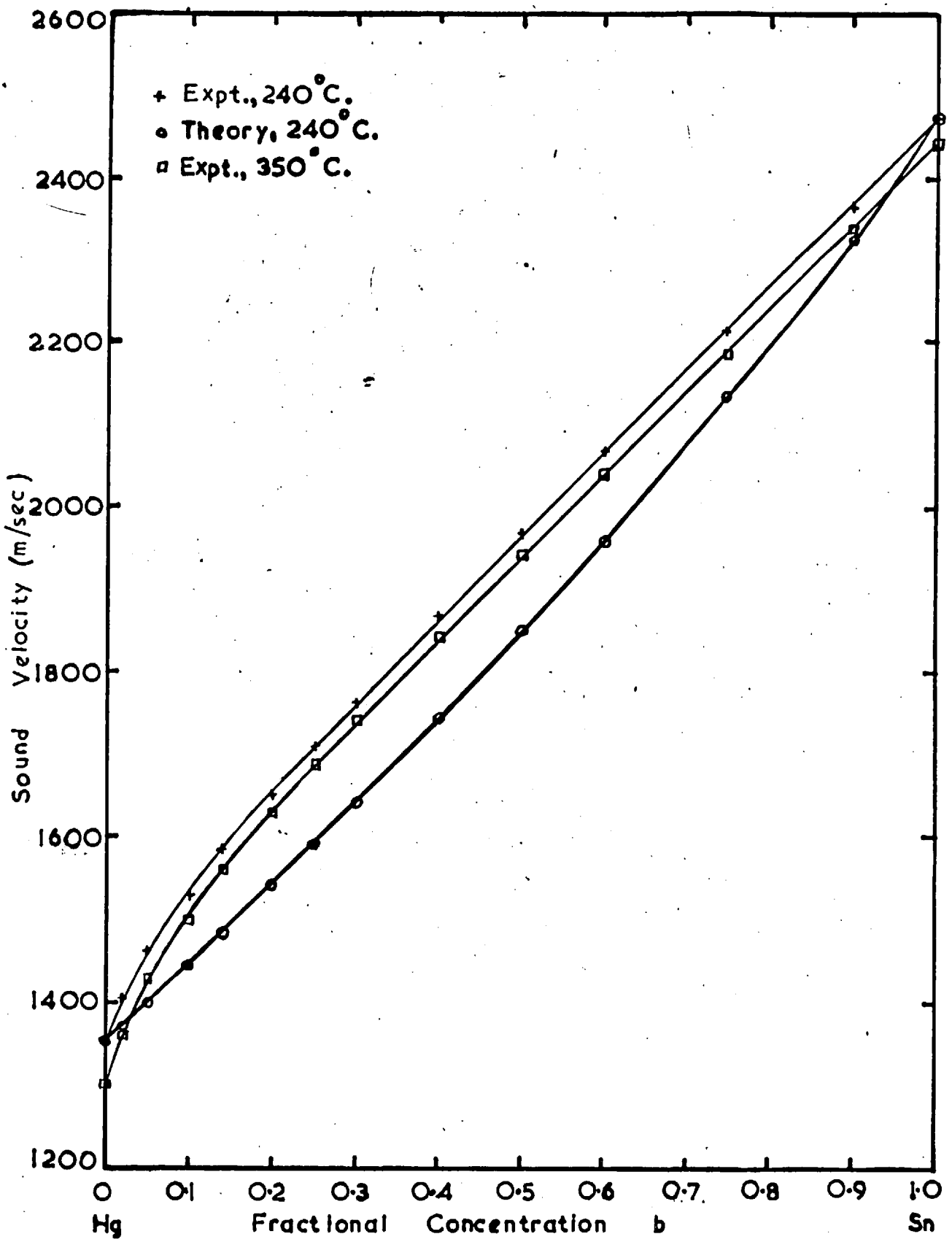

Fig.3.11. Sound velocity as a function of concentration b in the Hg-Sn alloy system. Sound velocity data shown in Table A.4.

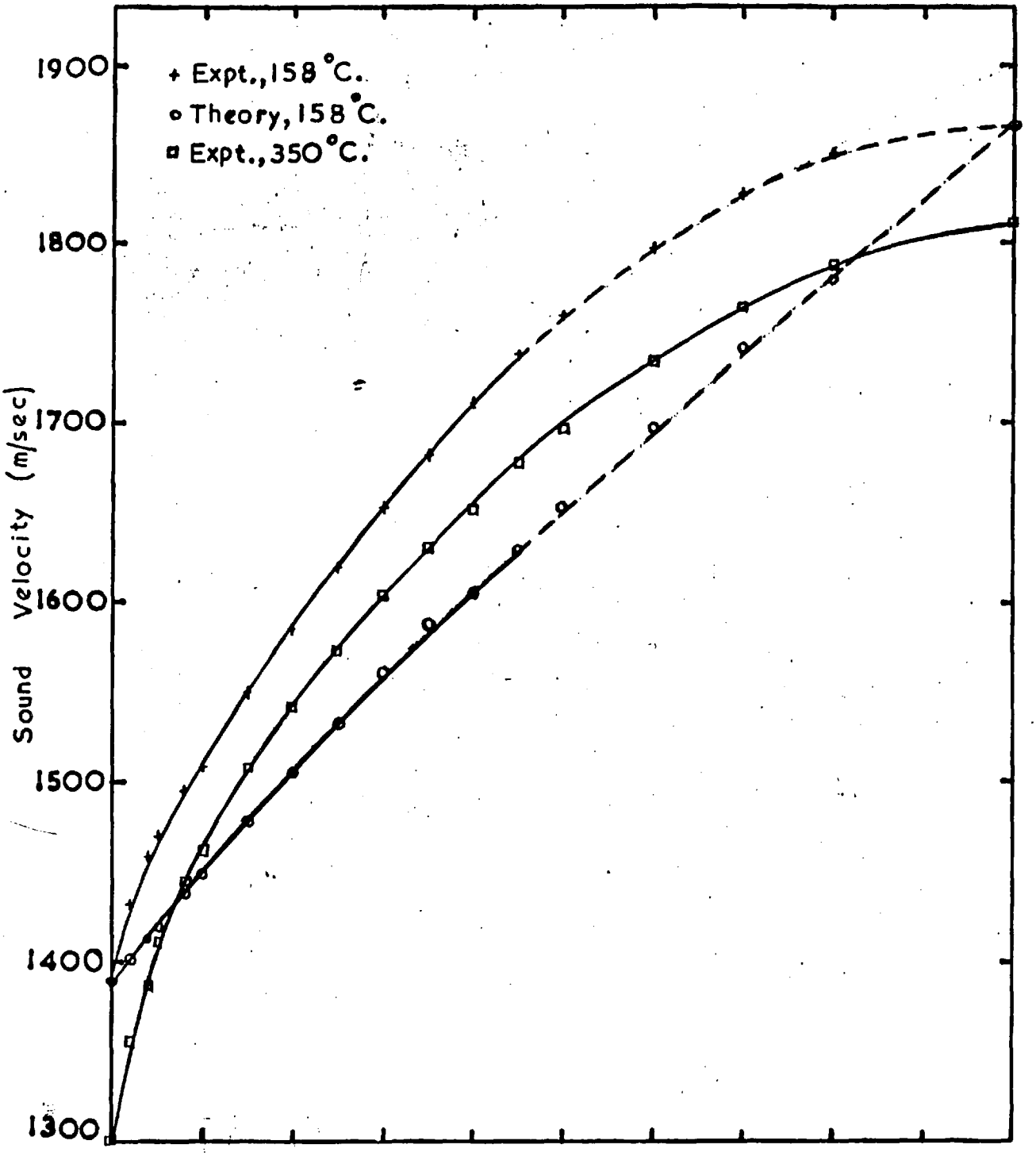

Fig.3.12. Sound velocity as a function of concentration b in the Hg-Pb alloy system. Sound velocity data shown in Table A.5.

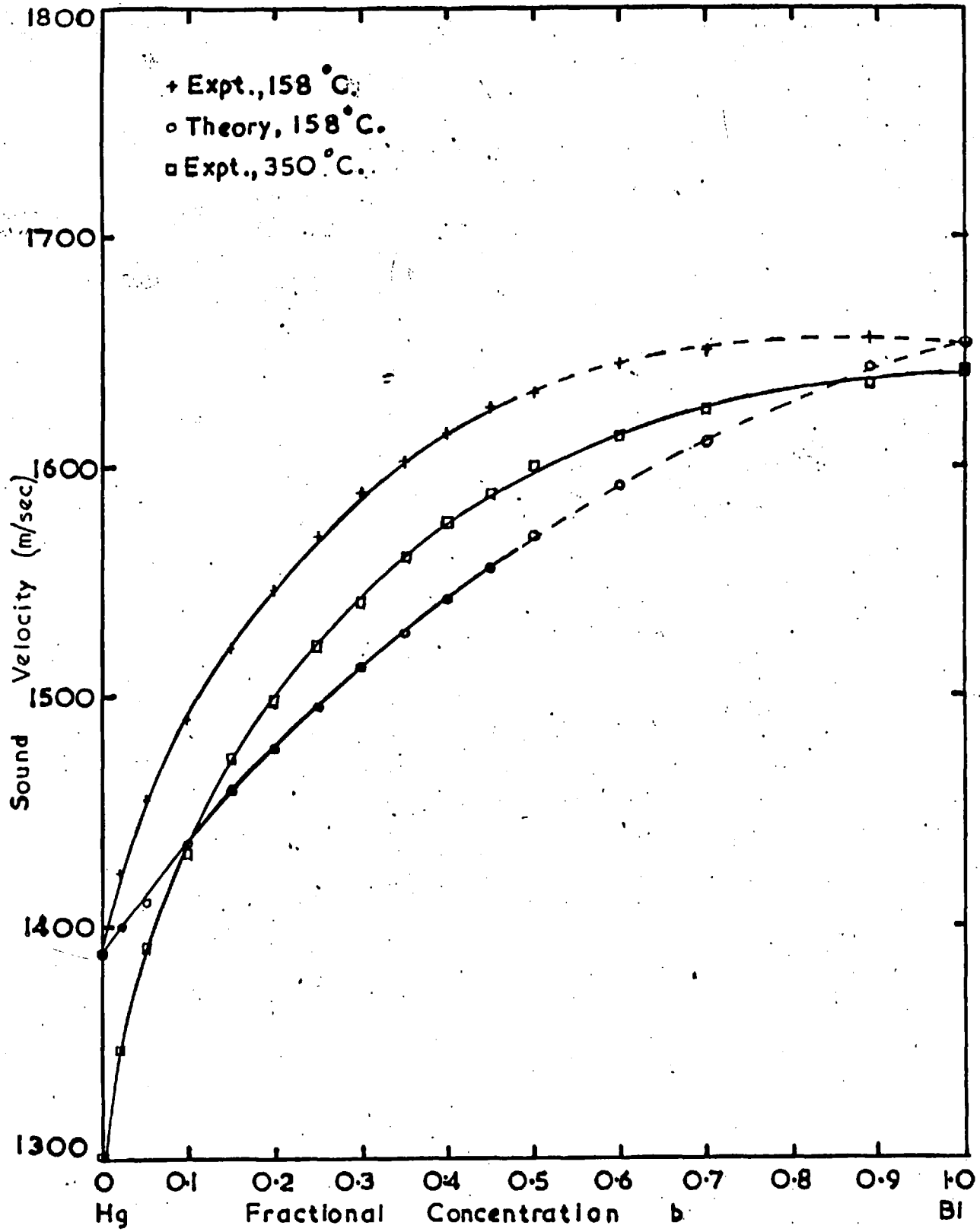

Fig.3.13. Sound velocity as a function of concentration b in the Hg-Bi alloy system. Sound velocity data shown in Table A.6.

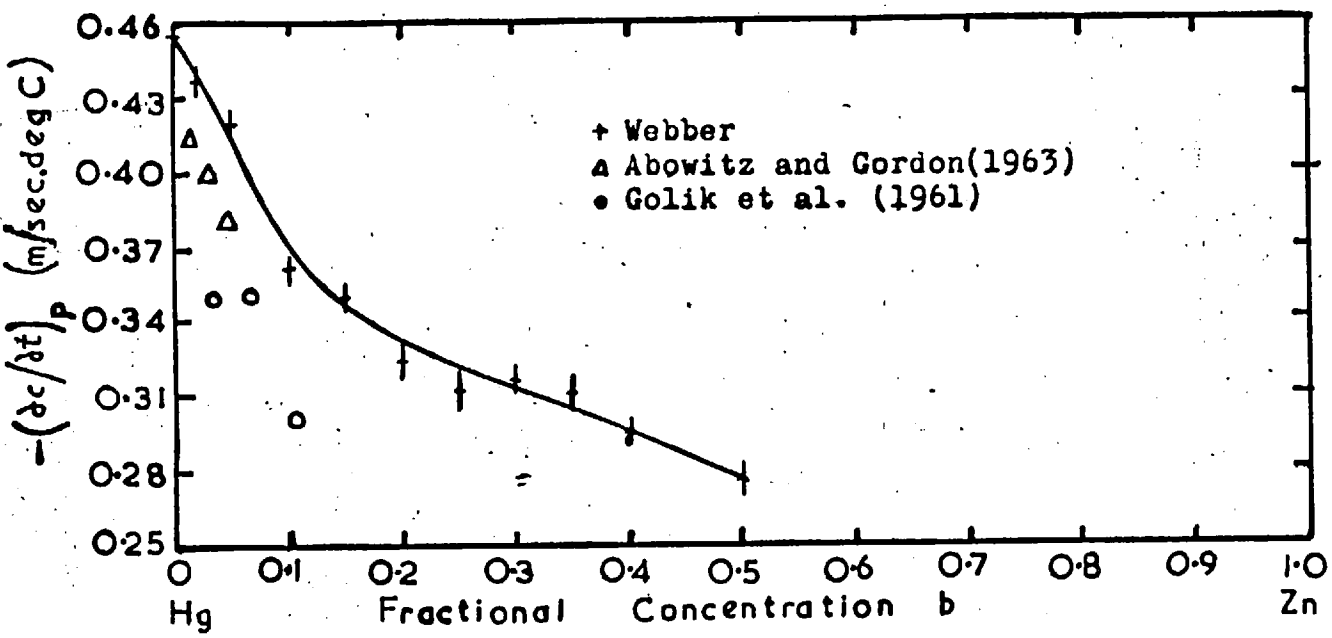

Fig.3.14. Variation of $-(\partial c/\partial t)_p$ with composition in the Hg- Zn alloy system .

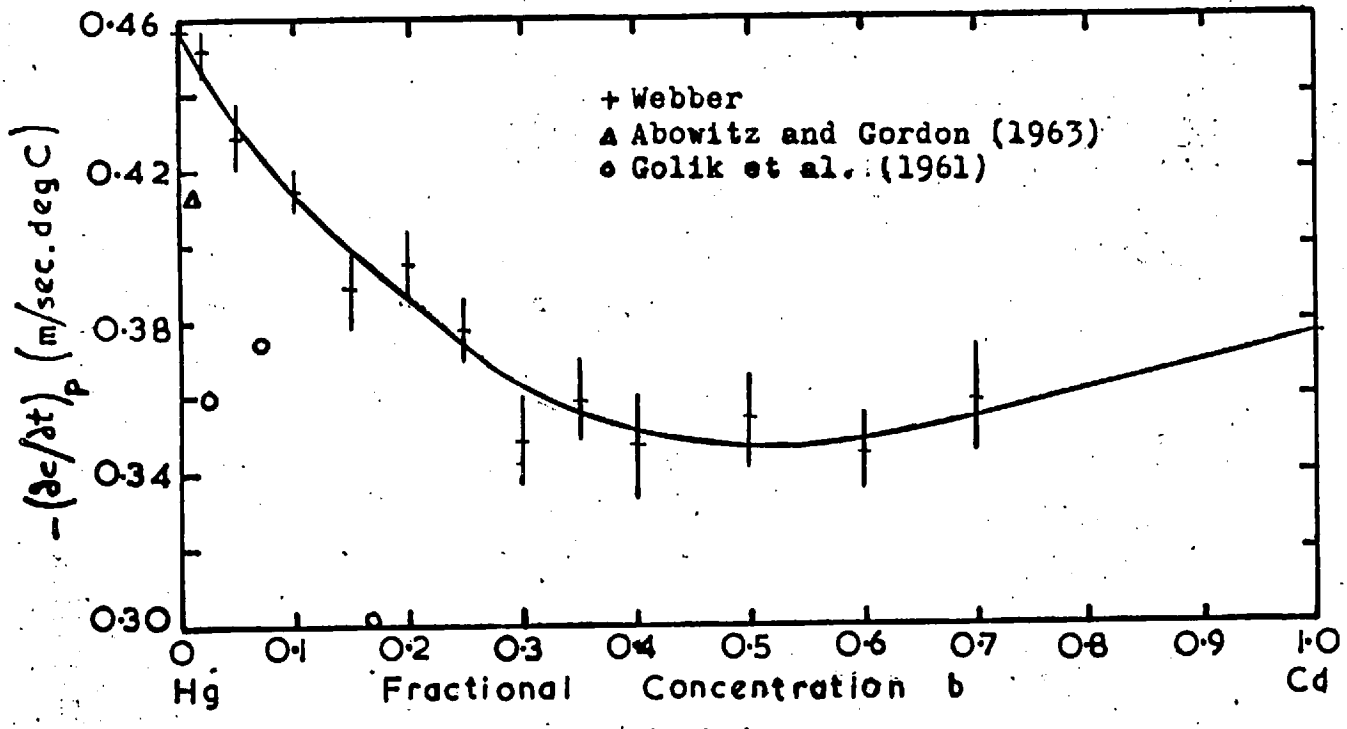

Fig.3.15. Variation of $-(\partial c/\partial t)_p$ with composition in the Hg-Cd alloy system .

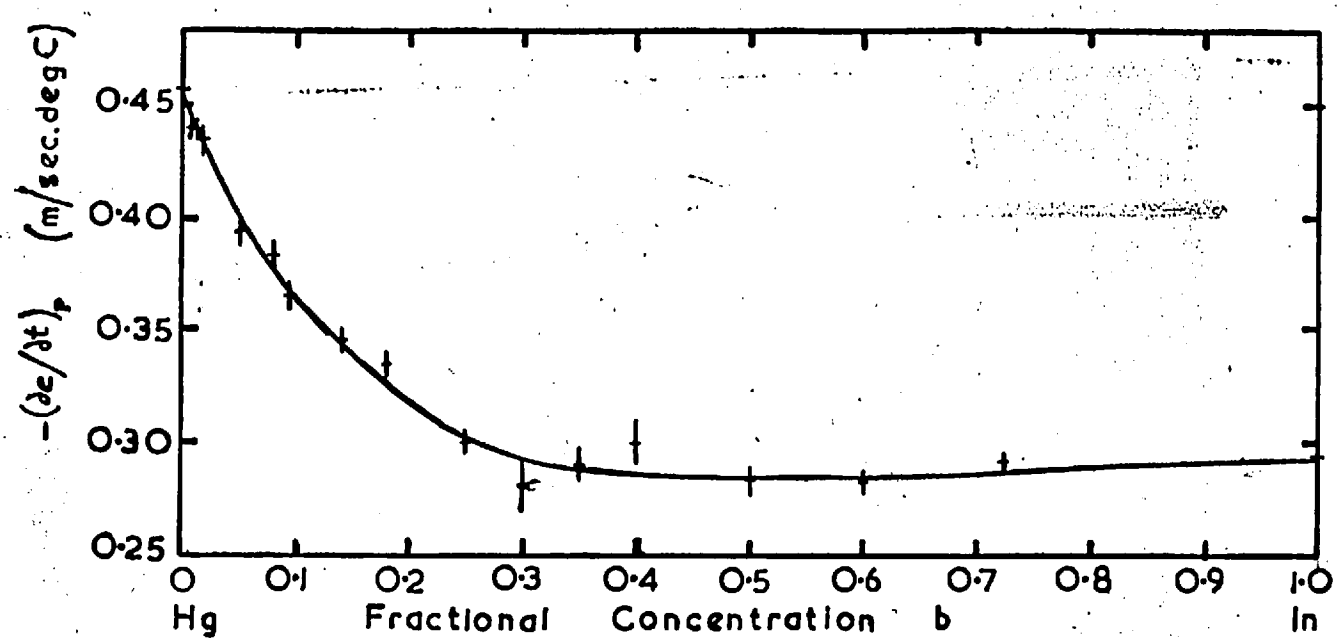

Fig. 3.16. Variation of $-(\partial c/\partial t)_p$ with composition in the Hg-In alloy system .

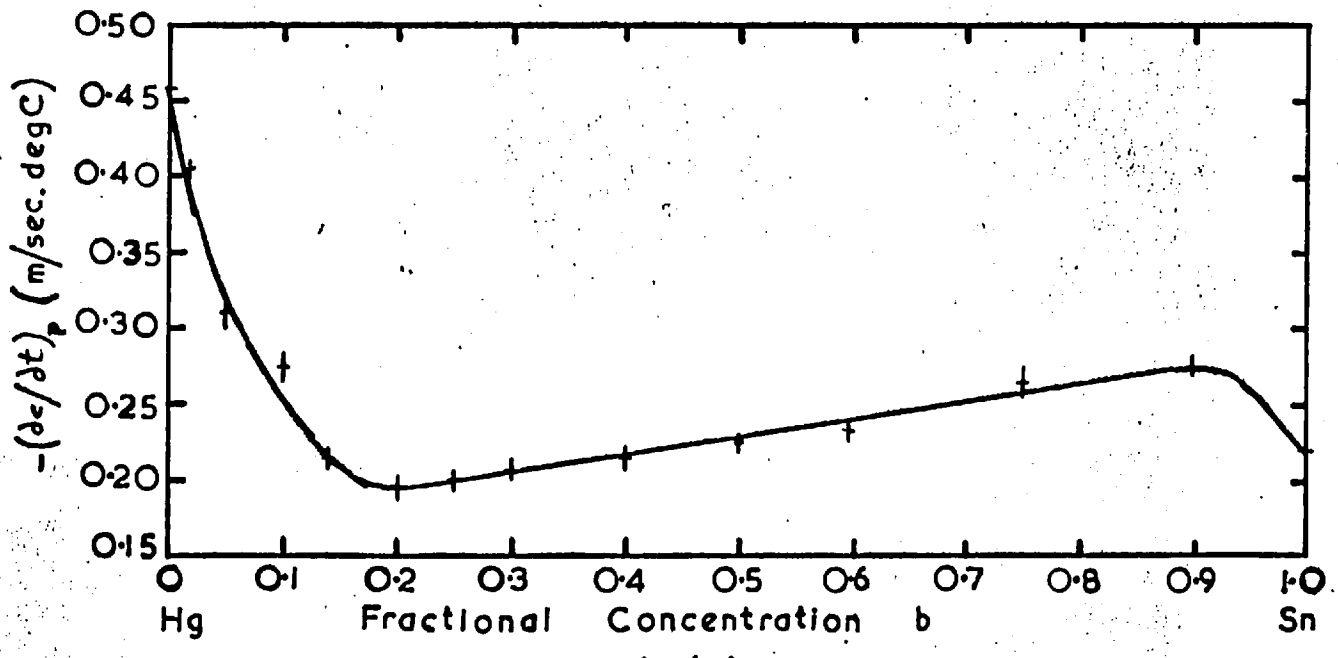

Fig.3.17. Variation of $-(\partial c/\partial t)_p$ with composition in the Hg-Sn alloy system .

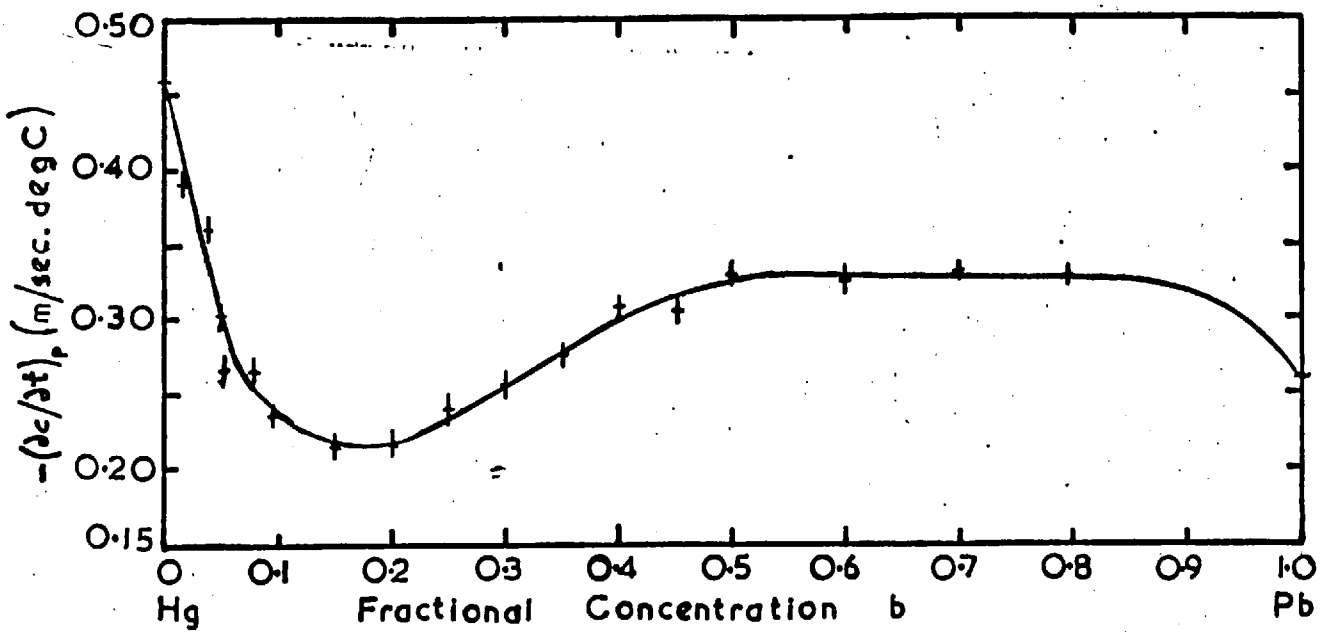

Fig.3.18. Variation of $-(\partial c/\partial t)_p$ with composition in the Hg-Pb alloy system .

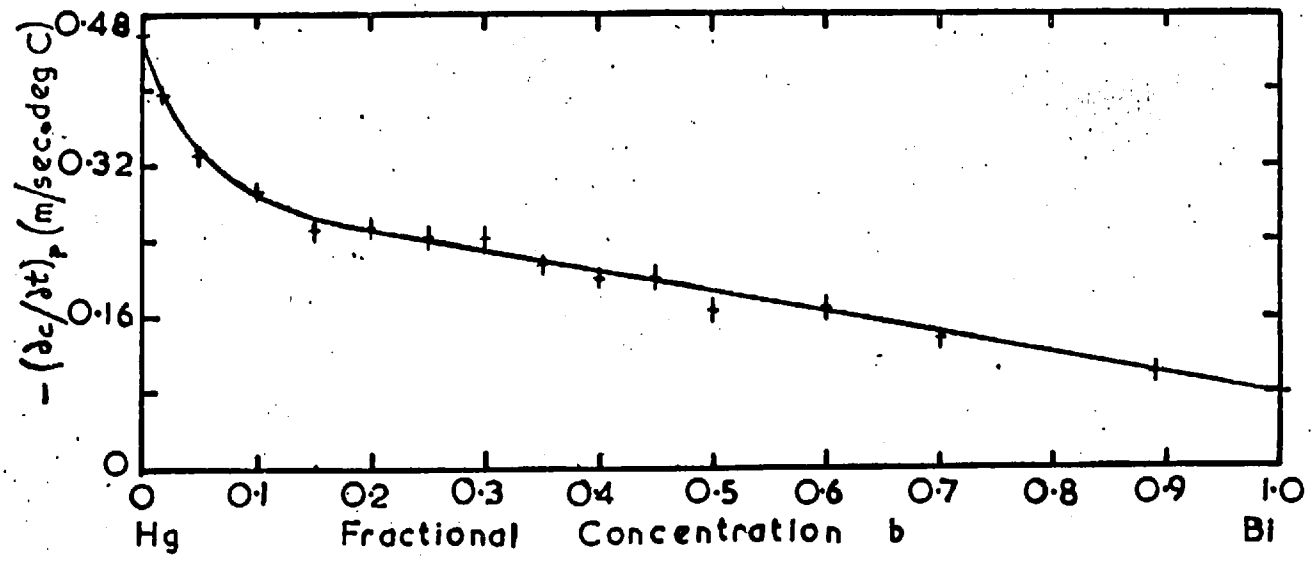

Fig.3.19 Variation of $-\left(\frac{\partial c}{\partial t}\right)_p$ with composition in the Hg-Bi alloy system .

3.10 Discussion of Sound Velocity Results for Mercury Alloys

The results for dilute mercury alloys can be compared with the measurements of Golik et al.(1961) and Abowitz and Gordon (1963). Comparison of results for mercury-zinc and mercury- cadmium alloys are shown in Figs. 3.20 and 3.21. At 158°C the sound velocity extrapolated from the measurements due to Abowitz and Gordon is 1387.5 m/sec for mercury, in excellent agreement with the present result, whilst the measurements due to Golik et al. give 1400 m/sec. It is seen from Fig. 3.20 that the present results for dilute Hg-Zn alloys are in good agreement with the other investigations. However, for dilute Hg-Cd alloys, the results due to Golik et al. agree fairly closely with the present results, whilst Abowitz and Gordon find that the sound velocity increases more rapidly with at.% Cd (see Fig. 3.21). The results due to the latter are in good agreement with the present results for dilute Hg-Sn, Hg-Pb and Hg-Bi alloys (see Fig. 3.23, 3.24, and 3.25 respectively) but are about 1% higher for dilute Hg-In alloys (see Fig. 3.22). This difference is outside experimental error and the reason is not readily apparent.

When the variations of sound velocity with composition at low atomic concentrations for each mercury alloy system are compared, it is found that the addition of tin produces the largest increase of sound velocity. The measurements on Hg-K due to Abowitz and Gordon (1963)

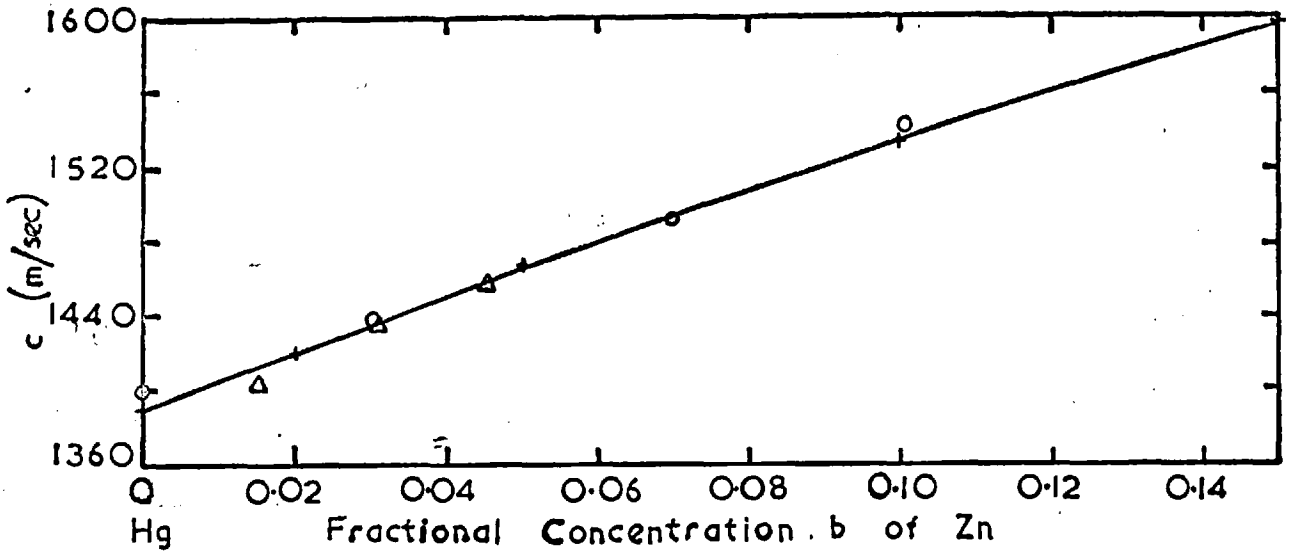

Fig. 3.20. Variation of sound velocity with composition in the Hg-Zn alloy system at 15 °C. Webber +, Abowitz and Gordon Δ, Golik et al. o.

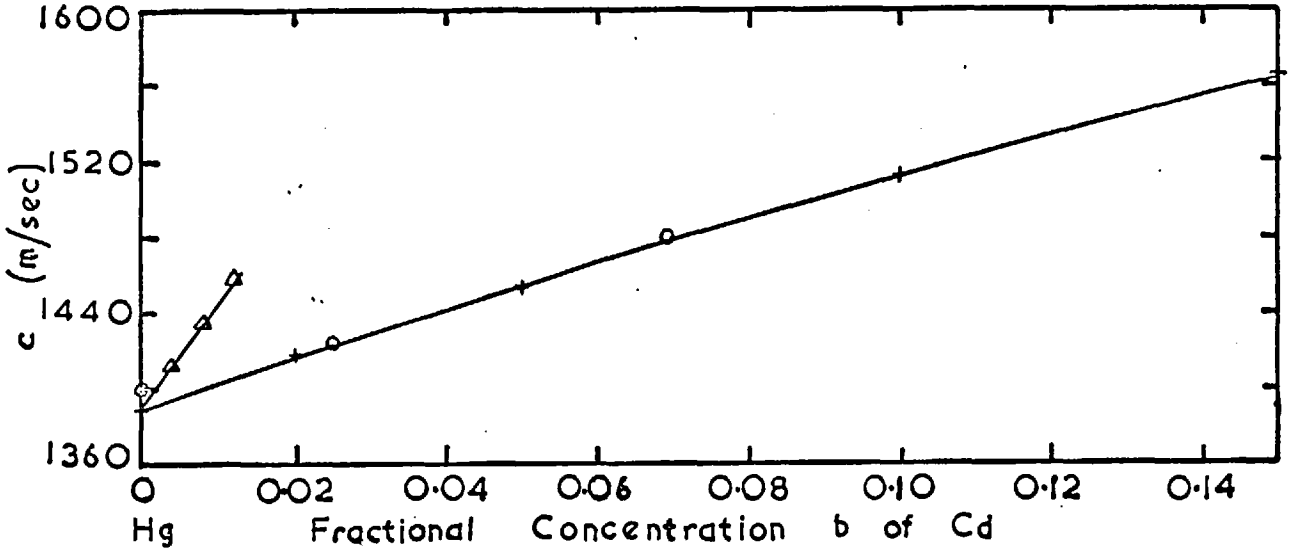

Fig. 3.21. Variation of sound velocity with composition in the Hg-Cd alloy system at 15 °C. Webber +, Abowitz and Gordon Δ, Golik et al. o.

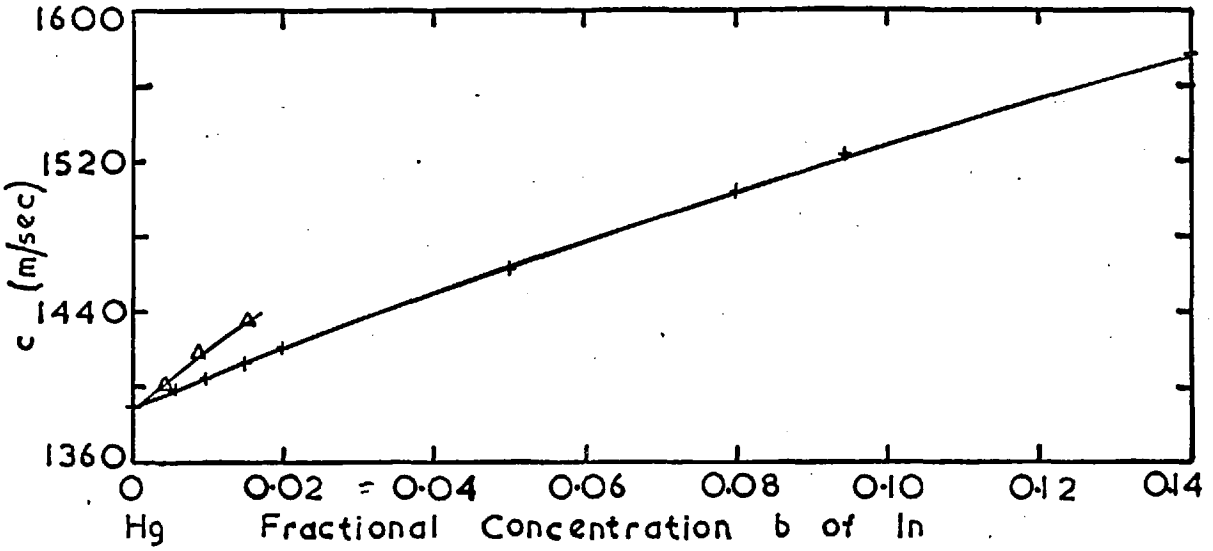

Fig. 3.22. Variation of sound velocity with composition in the Hg-In alloy system at 158°C. Webber +, Abowitz and Gordon Δ.

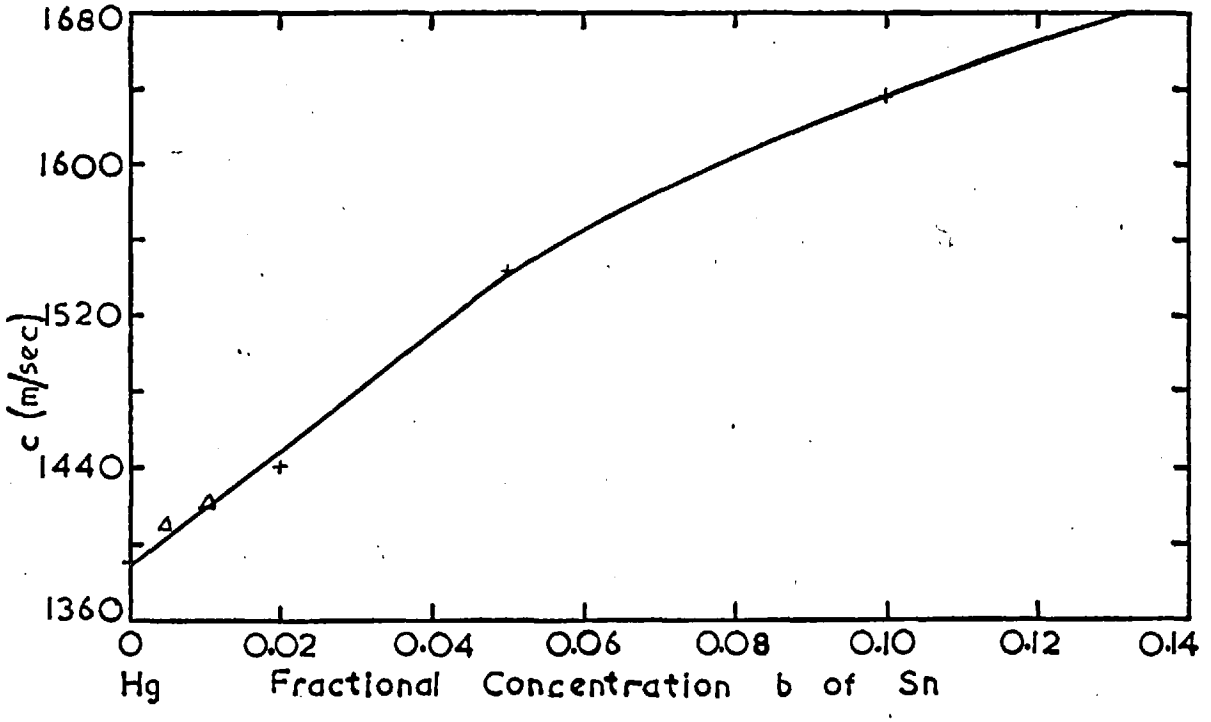

Fig. 3.24. Variation of sound velocity with composition in the Hg-Sn alloy system at 158°C. Webber +, Abowitz and Gordon Δ.

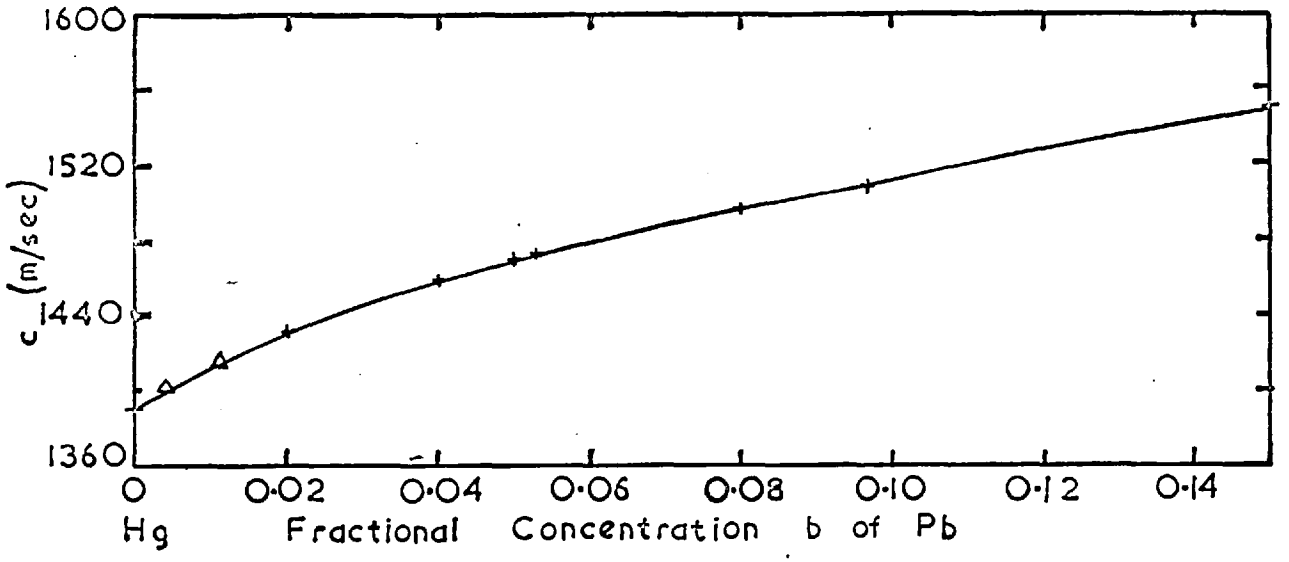

Fig. 3.24. Variation of sound velocity with composition in the Hg-Pb alloy system at 15° C. Webber +, Abowitz and Gordon Δ.

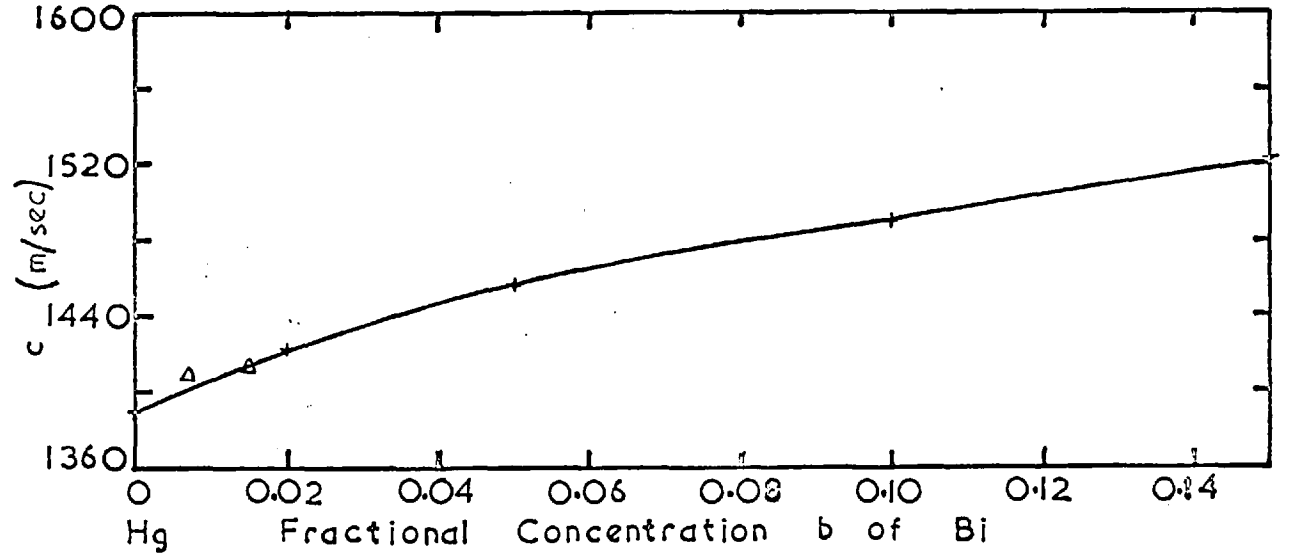

Fig. 3.25. Variation of sound velocity with composition in the Hg-Bi alloy system at 15°C. Webber +, Abowitz and Gordon Δ.

show that the addition of potassium causes a slight decrease of sound velocity, opposite in direction to the other mercury alloys. Study of the variation of sound velocity across the entire composition range for each alloy system, at a fixed temperature, shows that with the exceptions of Hg-K and Hg-Zn, the sound velocity at a given composition is greater than the weighted mean of the sound velocities of the pure components. The variation of sound velocity with composition of alloy is discussed from a theoretical viewpoint in Section 4.6.

3.11 Sound Absorption in Mercury

A. Sound Absorption Results

The sound absorption in distilled water at room temperature was measured in order to test the apparatus and experimental procedure. It was found that the value for α/f^2 of $(24.6 \pm 0.5) \times 10^{-17}$ cm^{-1} sec^2 at 22.3°C was in fair agreement with the value of $(24.3 \pm 0.3) \times 10^{-17}$ cm^{-1} sec^2 at the same temperature reported by Pinkerton (1947). However, greater difficulty was experienced in obtaining consistent sound absorption measurements in mercury, for which α/f^2 is about 5.7×10^{-17} cm^{-1} sec^2 at room temperature. One of the difficulties was due to the depression of the base line of the oscilloscope caused by overloading of the electronic circuits, leading to uncertainty in the signal amplitudes. In order to eliminate this effect measurements were made with both the I.F. and video outputs, together with the use of a blanking pulse. The results obtained with these two techniques were found to be the same within experimental error. It was also found preferable to keep the comparison pulse in a fixed position, usually before the first reflected pulse. All the measurements were made at 68 MHz; the ultrasonic pulse was too small for a measurement to be made at 92 MHz.

The present results for sound absorption in mercury are shown in Table 3.12 and α/f^2 is plotted as a function of temperature in Fig. 3.26. It is seen from Fig. 3.26 that α/f^2 increases approximately linearly with

temperature and the present results agree within experimental error with the measurements of Jarzynski (1963) and Hunter et al. (1963).

Table 3.12 Sound Absorption Results for Mercury

t (^{o}C)	$\alpha/f^2 \times 10^{17}$ (cm^{-1} sec^2)
22.5	5.6 ± 0.3
23.5	5.6 ± 0.3
52.5	6.7 ± 0.3
66	7.1 ± 0.4
76.5	7.4 ± 0.4
137.5	9.4 ± 0.4
141	9.5 ± 0.4
156	9.8 ± 0.4

B. Error in Sound Absorption Results

The sources of possible error in α/f^2 are due to uncertainties in the absorption coefficient α and in the frequency, and to diffraction effects and non-uniform temperature in the specimen. These contributions are discussed below.

a) A typical decrease in pulse amplitude for 2 cm. increase in

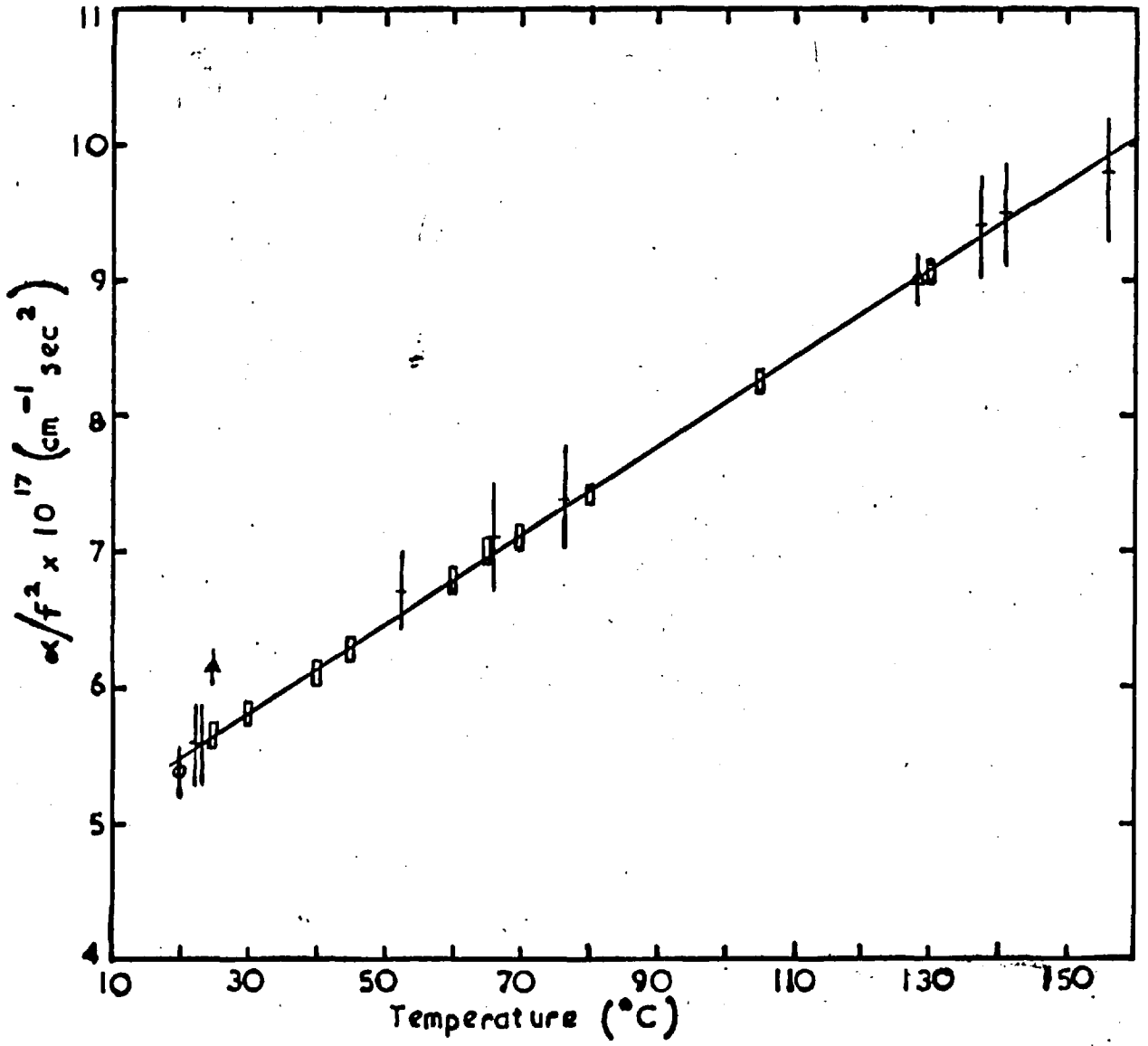

Fig. 3.26. Sound absorption as a function of temperature in mercury. Webber +, Hunter et'd □, Jarzynski ▲, Abowitz and Gordon ϕ.

acoustic path length was about 7 db. Attenuator settings could be read to ± 0.1 db. and the pulse heights aadjusted to equality to within ± 0.2 db. A plot of attenuator setting (db) against acoustic path length gave the absorption D in db/cm, from which the sound absorption coefficient $\alpha(cm^{-1})$ was calculated according to the relation

$$\alpha = D/8.68 \quad . \tag{3.10}$$

The measurements were taken with the reflector rod being raised and lowered and at least six absorption measurements were made at a given temperature. It was found that measurements of D were only reproducible to within 3 to 5%, accuracy of measurement improving at higher temperature since the total change in amplitude was greater.

b) The measurement of frequency has already been discussed in Section 3.1B and was accurate to within 0.02%. Thus the possible error in attenuation due to this cause was 0.04% and was negligible.

c) When the present apparatus was operated at 68 MHz the sound pulse could be considered to be propagating as a plane wave in the liquid (see Section 2.4e). Even within the Fresnel zone correction of the apparent absorption, which includes a diffraction loss, must be considered since the total sound absorption of the sample was small. This diffraction loss which is geometrical in nature due to the gradual spreading out of the ultrasonic beam has been studied by Seki et al. (1956).

They consider the case when the transducer vibrates as a piston and the source radiates into a semi-infinite medium. They assume that the amplitude of the received pulse is proportional to the maximum value of the pressure averaged over the surface of the receiving transducer at a given time. The decrease in amplitude of the pulse, due to diffraction, is a function of distance and is given approximately by 1.7 db per unit of distance R^2/λ, where R is the transducer radius and λ the sound wavelength. In addition, when the liquid is confined laterally by the walls of a container, as in the present apparatus, the diffraction pattern is influenced by reflection at the walls and depends upon the ratio R'/R of the radii of the transducer and container (R'), and on the acoustic impedances of the liquid and wall material [see Carome and Witting (1961) and Carome et al. (1961)]. These authors find that for R'/R = 2, as is the case for the present apparatus, the diffraction loss is approximately 2 db per unit of distance R^2/λ.

In the present measurements it was assumed that, at a particular temperature, the fractional decrease in amplitude due to diffraction in the delay rod remained constant. The possible error was considered to be that due to the additional diffraction which occurred when the acoustic path length was altered. For a change in path length of 3 cm the decrease in pulse amplitude due to diffraction was estimated from Carome and Witting (1961) to be about 0.02 db. The error in the measurement of α/f^2, due to diffraction, is therefore less than 0.2%.

d) It was also necessary to consider the errors which arose from thermal fluctuations and gradients within the mercury. The maximum variation in the thermocouple reading during the absorption measurements was 0.5°C. Since the change of α/f^2 with temperature was about 0.03 cm^{-1} sec^2 deg C^{-1} the error due to a variation of 0.5°C in the temperature of the mercury was less than 0.3% at room temperature. A temperature gradient of 0.5 deg C/cm in the direction of sound propagation would result in an error of about 0.1% in the measured sound absorption. Error due to thermal expansion of the silica reflector rod was also negligible. Error in absorption measurements due to temperature gradients in the plane perpendicular to the direction of propagation was difficult to estimate. A temperature difference between the centre and outer edge of the ultrasonic beam would distort the plane wavefront but the resultant effect on pulse amplitude could not be large since at all temperatures the pulse amplitude was found to decrease exponentially with path length.

In conclusion it was found that accuracy in the measurements of the sound absorption in mercury was limited by the reproducibility of the measurements for α, which was between 3 to 5% and improved transmitter detector circuits are required if greater accuracy is to be achieved and would necessarily require temperature control to within 0.1°C. The amplitude of the reflected pulse was too small for attenuation measurements to be carried out on the other pure metals and alloys.

Table 3.13 Sound Attenuation Measurements in Mercury at 25°C

Investigator and technique	f MHz	Observed attenuation $\alpha/f^2 \times 10^{17}$ cm^{-1} sec^2
Bär (1937), light diffraction:	54	6.6
Reickmann (1939), radiation pressure:	21.5	6.3
	54.0	6.4
Ringo et al (1947), continuous wave:	152	5.8 ± 0.5
	291	5.5 ± 0.5
	390	5.7 ± 0.5
	774	4.7 ± 1.0
	996	6.0 ± 1.0
Jarzynski (1963), pulse:	68	6.2 ± 0.3
	92	6.2 ± 0.3
Abowitz and Gordon (1962b), pulse:	45	5.4 ± 0.5
	65	5.4 ± 0.3
	75	5.5 ± 0.2
	115	5.3 ± 0.1
Hunter et al (1962), pulse:	130	5.6
	270	5.4
Hunter et al (1963), pulse:	90	5.71± 0.1
	150	5.72± 0.1
	270	5.67± 0.1
Webber (1965), pulse:	68	5.6 ± 0.3

C. Comparison with Other Investigations

It has been seen from Fig. 3.26 that the present results for sound absorption are in fairly good agreement with the measurements of Jarzynski (1963) and Hunter et al. (1963). The ultrasonic attenuation in mercury has been measured by a variety of techniques over a large frequency range, as shown in Table 3.13. It is only recently that agreement has been found in the experimental values obtained from the use of pulse techniques. The present result at room temperature is in close agreement with that obtained by Hunter et al (1963) and it would appear that the value obtained by Jarzynski (1963) is slightly high. The results obtained by Abowitz and Gordon (1962b) are fairly close to the value of the classical sound absorption. Sound absorption measurements and the calculation of the ratio of bulk to shear viscosities for mercury and other liquid metals are discussed in Sections 4.1 and 4.2.

4. DISCUSSION OF SOUND ABSORPTION AND VELOCITY IN LIQUID METALS AND ALLOYS

4.1 Structural Viscosity of Liquid Metals

A. η_B/η_s for Mercury

Measurements of sound absorption in several types of liquid have shown the existence of a volume viscosity. Litovitz and Davis (1965) observe that the volume or bulk viscosity is usually of about the same magnitude as the shear viscosity. Molten metals are monatomic in character, and ultrasonic absorption measurements have shown that vibrational or rotational isomeric relaxation does not occur but that a structural relaxation similar to that in nonmetallic liquids does [Stephens (1963)].

The Stokes-Kirchhoff classical attenuation coefficient α_o is given by the addition of the viscous α_s and thermal-conduction α_T attenuation coefficients, such that

$$\alpha_o = \alpha_s + \alpha_T$$

$$= \frac{2\pi^2}{\rho c^3}\left(\frac{4}{3}\eta_s + \frac{\gamma^2\alpha_p^2 k_T T}{C_p^2 J}\right) f^2, \quad \text{for } \alpha c/f \ll 1 \qquad (4.1)$$

where η_s is the shear viscosity, k_T the thermal conductivity, C_p the specific heat at constant pressure, J the mechanical equivalent of heat and f the frequency of the sound wave. The excess absorption coefficient

is formally attributed to a volume viscosity η_B, defined by

$$\alpha_B = \alpha - \alpha_o = \frac{2\pi^2 \eta_B f^2}{\rho c^3} \quad , \tag{4.2}$$

where α is the experimental attenuation coefficient. The bulk viscosity η_B can therefore be calculated from

$$\eta_B = \frac{4}{3} \eta_s \left(\frac{\alpha - \alpha_o}{\alpha_s}\right) \quad . \tag{4.3}$$

The values of the classical sound absorption for mercury at various temperatures are shown in Table 4.1, together with the values of η_B/η_s. The physical data used are shown in Table A.7. The estimated error in α_s/f^2 is about 1%, mainly due to error in η_s, and the error in α_T/f^2 is about 2%, mainly due to the uncertainty in k_T. It is seen that η_B/η_s is constant within experimental error. The probable value of η_B/η_s is 0.86 ± 0.3, which is slightly higher than the value of 0.45 ± 0.1 estimated by Hunter et al. (1963). Unfortunately Hunter et al. incorrectly use the thermal expansion equation due to Beattie et al. (1940) which resulted in their using higher values for α_p, also their values of sound velocity c are low. Correction of the data used by Hunter et al. results in their sound absorption measurements yielding

Table 4.1 Sound Absorption and Ratio of Bulk to Shear Viscosity for Mercury

t (^{o}C)	$\alpha_s/f^2 \times 10^{17}$ (cm^{-1} sec^2)	$\alpha_T/f^2 \times 10^{17}$ (cm^{-1} sec^2)	$\alpha/f \times 10^{17}$ (cm^{-1} sec^2)	η_B/η_s
22.5	0.99	4.26	5.6	0.48 $\pm$ 0.4
23.5	0.98	4.28	5.6	0.45 $\pm$ 0.4
52.5	0.91	5.17	6.7	0.93 $\pm$ 0.4
66	0.89	5.61	7.1	0.90 $\pm$ 0.6
76.5	0.87	5.97	7.4	0.86 $\pm$ 0.6
137.5	0.84	7.82	9.4	1.19 $\pm$ 0.6
141	0.84	7.93	9.5	1.17 $\pm$ 0.6
156	0.83	8.42	9.8	0.88 $\pm$ 0.6

a value for η_B/η_s of 0.62 ± 0.1. The sound absorption measurements of Jarzynski (1963) and Abowitz and Gordon (1962b) yield values for η_B/η_s of 1.3 ± 0.3 and 0.17 ± 0.2 respectively. The experimental values for η_B/η_s in mercury are compared with theoretical values derived from a dense-gas formulation applied to liquid metals in Section 4.2.

B. η_B/η_s for Various Liquid Metals

The reported experimental sound absorption α/f^2 for various liquid metals are shown in Table 4.2, taken from Webber and Stephens (1968), together with the calculated classical absorption and η_B/η_s. The required physical data are recorded in Table A.8. The thermal conductivities of zinc, cadmium, gallium and indium are calculated from the modified Wiedermann-Franz law, evaluated by Ewing and associates (1957), which is reliable to within 12%. Errors shown for η_B/η_s are calculated from the experimental errors alone. Letcher and Beyer (1963) take a higher value for the expansion coefficient to calculate $\eta_B/\eta_s < 1$ for sodium, whilst Jarzynski and Litovitz (1964) calculate the ratio of bulk to shear viscosity as 2.6. For potassium Letcher and Beyer (1963) and Jarzynski and Litovitz (1964) calculate η_B/η_s to be 1.7 and <1.9 respectively. Less emphasis must be placed on the exceptional values of η_B/η_s for zinc and cadmium since Plass (1963) reported greater experimental difficulties with these two metals. At the same temperatures, Gitis et al. (1968) recently report values for α/f^2 of 4.6×10^{-17}

Table 4.2 Sound Absorption and Ratio of Bulk to Shear Viscosities in Liquid Metals

Metal	t (^{o}C)	$\alpha_s/f^2 \times 10^{17}$ (cm^{-1} sec^2)	$\alpha_T/f^2 \times 10^{17}$ (cm^{-1} sec^2)	$\alpha/f^2 \times 10^{17}$ (cm^{-1} sec^2)	η_B/η_s
Na	100	1.24	8.31	11.5 $\pm$ 0.3[a]	2.0 $\pm$ 0.5
K	75	2.41	26.9	29.9 $\pm$ 0.9[a]	0.4 $\pm$ 1
Zn	450	0.75	3.48	3.7 $\pm$ 0.6[b]	0.9 $\pm$ 2
Cd	360	0.48	10.8	14.5 $\pm$ 2.9[b]	9.0 $\pm$ 9
Hg	25	0.98	4.29	5.71 $\pm$ 0.1[c]	0.6 $\pm$ 0.8
Ga	30	0.37	1.04	1.58 $\pm$ 0.03[d]	0.6 $\pm$ 0.2
In	200	0.51	3.60	5.9 $\pm$ 0.6[e]	4.7 $\pm$ 1.6
Sn	240	0.49	3.84	5.63 $\pm$ 0.3[b]	3.5 $\pm$ 1
Pb	340	1.13	6.44	8.4 $\pm$ 0.3[b]	2.1 $\pm$ 0.5
Bi	280	1.07	4.66	8.05 $\pm$ 0.3[b]	2.9 $\pm$ 0.5

[a] Jarzynski and Litovitz (1964)

[b] Plass (1963)

[c] Hunter et al (1963)

[d] Hunter and Hovan (1964a,b)

[e] Gitis et al (1968)

and 12.0 x 10^{-17} cm^{-1} sec^2 for zinc and cadmium respectively, from which we calculate the corresponding values of η_B/η_s to be 0.7 and 2.0. Using the experimental value of 4.7 x 10^{-17} cm^{-1} sec^2 for α/f^2 measured in tin by Litovitz and Jarzynski (1965) gives a value of 1.9 for η_B/η_s. For tin these investigators take smaller values for the expansion coefficient and the thermal conductivity to estimate 2.3 x 10^{-17} cm^{-1} sec^2 for α_T/f^2, which results in the value of 5.1 for η_B/η_s. Jarzynski and Litovitz [see Litovitz and Davis (1965)] estimate a value of $\eta_B/\eta_s < 0.4$ for lead because of their higher estimation of α_T/f^2 and their smaller observed value for α/f^2 of 8.9 x 10^{-17} cm^{-1} sec^2 at 357°C. Gitis et al. (1968) measured α/f^2 in lead to 340°C to be 10.0 x 10^{-17} cm^{-1} sec^2, from which we calculate the value of η_B/η_s as 2.9. For bismuth, Jarzynski (1963) calculated η_B/η_s to be 4.2. Recently, Smirnow and Jarzynski (1967) have reported the value of η_B/η_s for antimony to be 4.2.

It is seen that the excess sound absorption is less than 10% of the total observed absorption in potassium, mercury, gallium and is between 20 and 40% in indium, tin and bismuth. In general, η_B/η_s is of the order of unity, sodium, cadmium, indium, tin, lead and antimony having higher values, between 2 and 5. The structural rearrangements in bismuth and antimony close to their melting points which results in a non-linear variation of sound velocity with temperature suggests the existence of a large bulk viscosity in these metals. Study of the temperature dependence of the sound absorption in sodium, potassium,

mercury, gallium and bismuth has shown that the bulk viscosity decreases with increasing temperature and that η_B/η_s is independent of temperature within the small temperature ranges of the experiments. This indicates that the excitation enthalpies for shear and for structural viscosity mechanisms are closely related. However, the recent sound absorption measurements by Gitis et al. (1968) on zinc, cadmium, indium and lead over a wider temperature range up to 850°C would appear to give conflicting evidence for the temperature variation of bulk viscosity. According to their experimental observations of α/f^2 and estimations of α_o/f^2, their results show that $\alpha - \alpha_o$ increases with temperature, rather than decreasing, and this would give η_B increasing with temperature, contrary to the expected physical behaviour. Their experimental results and calculations of classical absorption require further examination.

Jarzynski and Litovitz (1964) considered the possibility of a relaxation of the electronic specific heat, giving rise to the excess sound absorption in sodium. They found that this effect is several orders of magnitude smaller than the excess absorption, which cannot be attributed to a slow transfer of thermal energy from the liquid lattice to the free electrons. It appears that the excess ultrasonic absorption in liquid metals is due to a structural relaxation, in which there is a slow structural rearrangement of the liquid lattice following the temperature and pressure fluctuations produced in the liquid by

by the ultrasonic wave. Litovitz and Jarzynski (1965) suggest that a correlation exists between η_B/η_s and the co-ordination number of the liquid metal. The liquid metals with low co-ordination numbers, such as tin and bismuth, generally have a larger value of η_B/η_s and the relatively more closely packed metals with a number of nearest neighbours of about 12 have the smallest values for the ratio, see Table 4.3.

4.2 Dense-Gas Formulation for Ultrasonic Absorption in Liquid Metals

Sharma (1968) discussed the excess ultrasonic absorption from a viewpoint in terms of a dense-gas formulation when the behaviour of the system is dominated by collisions. Ascarelli and Paskin (1968) use a dense-gas formulation to calculate the values of the self-diffusion coefficient in liquid metals and obtain good agreement with experimental data. These authors use the van der Waals concept in the Enskog theory for dense gases. The van der Waals concept of a fluid considers the particles as having a potential made up of a hard-core plus a weak long-range attractive force. Particles are assumed to move in straight lines between core collisions. The attractive potential energy or cohesive energy term is thrcugh of as a uniform negative potential which does not affect the basically hard-sphere collisions.

From the Enskog theory the expression for the bulk viscosity η_B derived in Hirschfelder et al. (1964) may be written as

$$\eta_B = \chi\ 16z^2\ (Mk_BT)^{\frac{1}{2}}/\pi^{3/2}\sigma^2, \qquad (4.4)$$

where M is the atomic mass, z the packing factor, σ the hard-sphere diameter and χ the Enskog high-density correction. In terms of the hard-sphere pressure p_h, the factor χ can be expressed by

$$\chi = \frac{1}{4z}\left(\frac{p_h \Omega}{Nk_B T} - 1\right). \tag{4.5}$$

Hence the bulk viscosity (c.g.s. units) is given by

$$\eta_B = \frac{4z}{\pi^{3/2}\sigma^2}\left(\frac{p_h \Omega}{Nk_B T} - 1\right)(Mk_B T)^{\frac{1}{2}} . \tag{4.6}$$

Guggenheim (1965) proposes that the equation of state for non-interacting rigid-spheres is given by

$$\frac{p\Omega}{Nk_B T} = \frac{-a}{Nk_B T\Omega} + \frac{1}{(1 - z)^4} . \tag{4.7}$$

At atmospheric pressure the hard-sphere pressure has to be balanced almost completely by an attractive van der Waals term, such that at the melting point

$$a = \frac{Nk_B T_m \Omega_m}{(1-z_m)^4} . \tag{4.8}$$

If a is assumed to be independent of temperature and pressure, then

$$\frac{p_h \Omega}{Nk_B T} = \frac{T_m \Omega_m}{T\Omega(1 - z_m)^4} . \tag{4.9}$$

Hence from equation (4.6), the bulk viscosity at any temperature is given by

$$\eta_B = \frac{4z}{\pi^{2/3}\sigma^2}\left[\frac{T_m\Omega_m}{T\Omega(1 - z_m)^4} - 1\right](Mk_BT)^{\frac{1}{2}}. \qquad (4.10)$$

The value of the packing fraction z_m is taken to be 0.45 for all simple metals. The variation of z with temperature is derived from equation (4.8) and Guggenheims' equation of state for hard-spheres and is simply

$$z = 1 - (1 - z_m)\left(\frac{T\Omega}{T_m\Omega_m}\right)^{\frac{1}{4}}. \qquad (4.11)$$

The Enskog theory for dense hard-sphere systems includes consideration of collisional transfer of momentum and energy and of an increased number of collisions over that in dilute gases, but does not include the effect of correlating the successive hard-sphere collisions. The principal correlation effect can be ascribed to the backscattering caused by the high probability of the reversal of the velocity of a particle upon collision with the nearest neighbours. Alder and Wainwright (1967) find from molecular dynamics calculations of hard-spheres that the effect of this backscattering correction is to divide χ by a factor of $0.73z_m/z$. The bulk viscosity η_B' corrected for the effect of backscattering is thus given by

$$\eta_B' = \frac{5.48z^2}{\pi^{2/3}\sigma^2 z_m}\left[\frac{T_m\Omega_m}{T\Omega(1 - z_m)^4} - 1\right](Mk_BT)^{\frac{1}{2}}. \qquad (4.12)$$

Sharma (1968) uses equation (4.10) to calculate values of η_B for several liquid metals and those values are compared with experimental values in Table 4.3. The experimental values for η_B/η_s are taken from Section 4.1. Although there are considerable variations in the estimates of η_B/η_s from experiment, it is seen that the dense-gas formulation gives reasonable estimates for η_B/η_s. Inclusion of the correction for the effect of backscattering would have increased the estimate for η_B by about 30%.

Hirschfelder et al. (1964) show that the ratio η_B/η_s derived from the dense-gas formulation can be written as

$$\frac{\eta_B}{\eta_s} = \frac{H^2}{1 + 0.8H + 0.761H^2}, \qquad (4.13)$$

where

$$H = \frac{p_h\Omega}{Nk_BT} - 1. \qquad (4.14)$$

The theoretical value of η_B'/η_s corrected for the effect of backscattering is simply given by

$$\frac{\eta_B'}{\eta_s} = \frac{1.88H^2z^2}{z_m^2 + 1.10Hzz_m + 1.43H^2z^2}. \qquad (4.15)$$

Table 4.3 Comparison of Theoretical and Experimental Bulk Viscosities near the Melting Points of Various Liquid Metals

Metal	Theory	Experiment		
	η_B (cP)	η_B (cP)	η_B/η_s	Co-ordination Number [a]
Na	0.52	1.4	2.0	9.5
K	0.42	0.20	0.4	9.5
Zn	2.27	2.6	0.7	10.8
Cd	2.29	2.9	2.0	8.3
Hg	1.72	0.95	0.6	10.0
Ga		1.2	0.6	11.0
In		7.8	4.7	8.0
Sn	1.76	3.6	1.9	8.5
Pb	2.34	7.4	2.9	8.0
Sb			4.2	6.1[b]
Bi			2.9	7-8

[a] Waghorne et al (1967) [b] Wilson (1965)

and

Table 4.4 Comparison of Theoretical/Experimental Bulk Viscosities as a Function of Temperature for Mercury

t (°C)	Theory		Experiment
	η_B/η_s	η_B'/η_s	η_B/η_s
-39	1.17	1.21	∿0.62
25	1.11	1.15	0.62
128	1.02	1.04	0.62
204	0.95	0.94	∿0.62

Sharma (1968) assumes that H can be evaluated from equation (4.9) with $z_m = 0.45$. In Table 4.4 the theoretical values for η_B/η_s and η_B'/η_s for mercury calculated by Sharma are compared with experimental values taken from our correction of the data due to Hunter et al. (1963). It is seen that the theoretical values of η_B/η_s and η_B'/η_s are about twice the experimental values and decrease more rapidly with temperature than values obtained by experiment. The correction to the ratio of bulk to shear viscosity for the effect of backscattering is found not to be too important.

From equations (4.13) and (4.15) we find that at the melting points of simple liquid metals η_B/η_s and η_B'/η_s are 1.17 and 1.21 respectively. If H is calculated by using the Percus and Yevick hard-sphere equation of state given by equation (1.11) we find that the values for η_B/η_s and η_B'/η_s at the melting point are 1.16 and 1.20 respectively, showing that the choice of equation of state for hard-spheres is not critical. Modification of the dense-gas formulation as applied to liquid metals would appear to be necessary to account for experimental values of η_B/η_s which differ significantly from unity, see Table 4.3. In conclusion it is seen that the dense-gas formulation provides reasonable estimates for η_B/η_s, but further accurate sound absorption measurements over a wide range of temperature are required to evaluate η_B/η_s from experiment.

4.3 Compressibilities of Pure Liquid Metals

A. Mercury

Knowledge of density, expansion coefficient and specific heat as a function of temperature enables the isothermal compressibility β_T to be calculated from the present acoustic measurements by the use of the following thermodynamic relationship

$$\beta_T = \gamma/\rho c^2$$

$$= (1 + \frac{c^2\alpha_p^2 T}{C_p J}) \frac{1}{\rho c^2} , \qquad (4.16)$$

where γ is the ratio of the principal specific heats. The most reliable data have been used for the computations of β_s and β_T shown in Table 4.5. The values of C_p are taken from Douglas et al. (1951) who used an ice calorimeter to measure the heat evolved in cooling samples of mercury from a given temperature to $0^\circ C$. They estimate the probable error in C_p as 0.3%. The values of α_p are those of Beattie et al. (1940). Cook (1956) considers that Beatties' expansion formula is correct to 1 part in 10^6. Density values are taken from Bigg (1964), who used the most recent determination of the density of mercury at $20^\circ C$, in conjunction with Beatties' expansion formula to determine ρ as a function of temperature to within 4 parts in 10^6. The estimated

Table 4.5 Adiabatic and Isothermal Compressibilities as a Function of Temperature for Mercury

t (^{o}C)	ρ (gm/cm^3)	$\alpha_p \times 10^4$ (deg C^{-1})	C_p (cal/g-atom.deg C)	c (m/sec)	γ	$\beta_s \times 10^{12}$ (cm^2/dyne)	$\beta_T \times 10^{12}$ (cm^2/dyne)
-39	13.6910	1.824168	6.7578	1478.7	1.1208	3.341	3.744
-20	13.64456	1.819121	6.7272	1470.0	1.1289	3.391	3.829
-10	13.61978	1.816779	6.7120	1465.5	1.1331	3.419	3.874
0	13.59508	1.814643	6.6967	1460.9	1.1373	3.447	3.920
10	13.57045	1.812714	6.6825	1456.3	1.1415	3.474	3.966
20	13.54588	1.810999	6.6683	1451.7	1.1456	3.503	4.013
30	13.52139	1.809492	6.6551	1447.2	1.1496	3.531	4.060
40	13.49695	1.808200	6.6419	1442.6	1.1537	3.560	4.107
50	13.47257	1.807121	6.6298	1438.0	1.1577	3.589	4.155
60	13.44825	1.806259	6.6176	1433.5	1.1617	3.619	4.204
70	13.42398	1.805616	6.6065	1428.9	1.1656	3.649	4.253
80	13.39977	1.805190	6.5954	1424.3	1.1696	3.679	4.303
90	13.37560	1.804987	6.5853	1419.7	1.1735	3.709	4.353
100	13.35148	1.805006	6.5752	1415.2	1.1774	3.740	4.403
110	13.3274	1.805249	6.5662	1410.6	1.1813	3.771	4.455
120	13.3034	1.805711	6.5571	1406.0	1.1852	3.802	4.507
130	13.2793	1.806420	6.5491	1401.5	1.1890	3.834	4.559
140	13.2554	1.807336	6.5410	1396.9	1.1929	3.866	4.612

Table 4.5 continued

t (^{o}C)	ρ (gm/cm^3)	$\alpha_p \times 10^4$ (deg C^{-1})	C_p (cal/g-atom.deg C)	c (m/sec)	γ	$\beta_s \times 10^{12}$ (cm^2/dyne)	$\beta_T \times 10^{12}$ (cm^2/dyne)
150	13.2314	1.808499	6.5340	1392.3	1.1967	3.899	4.666
160	13.2075	1.809885	6.5270	1 387.7	1.2006	3.932	4.720
170	13.1836	1.811509	6.5210	1383.2	1.2044	3.965	4.775
180	13.1597	1.813371	6.5150	1378.6	1.2083	3.998	4.831
190	13.1359	1.815459	6.5100	1374.0	1.2121	4.032	4.888
200	13.1120	1.817802	6.5050	1369.4	1.2160	4.067	4.945

standard errors in γ, β_s and β_T are 0.04, 0.07 and 0.08% respectively.

The compressibilities β_s and β_T are plotted as a function of temperature in Fig. 4.1. These estimates of compressibilities are in very close agreement with Davis and Gordon (1967) who used the same physical data together with their sound velocity measurements. Seemann and Klein (1965) used different physical data and their estimates of β_s and β_T differ from the present estimates by about 0.05%. Since Seemann and Klein (1965) found that the sound velocity decreased linearly with temperature in the interval between -35 and 48°C, and Hill and Ruoff (1965b) found that this was also true between 30° and 197°C, then it is reasonable to extrapolate the present acoustic measurements to cover the interval -39 to 200°C.

Several investigations have been made on the isothermal compressibility of mercury. The measurements of Carnazzi (1903) on the change of volume with pressure yield isothermal compressibilities which are low by between 3 to 8%. Bridgman (1911) used a piezometer method to measure the compression of mercury in terms of the compressibility of water. Bett et al. (1954) analysed Bridgmans' results and, using the Hudleston relationship for liquid compression, calculated the isothermal compressibilities to be 3.926×10^{-12} and 4.036×10^{-12} cm^2/dyne at 0 and 22°C respectively. It is seen from Fig. 4.1 that these measurements are about 0.2% higher than β_T calculated from sound velocity measurements. Richards and Bartlett (1915) used a piezometer method

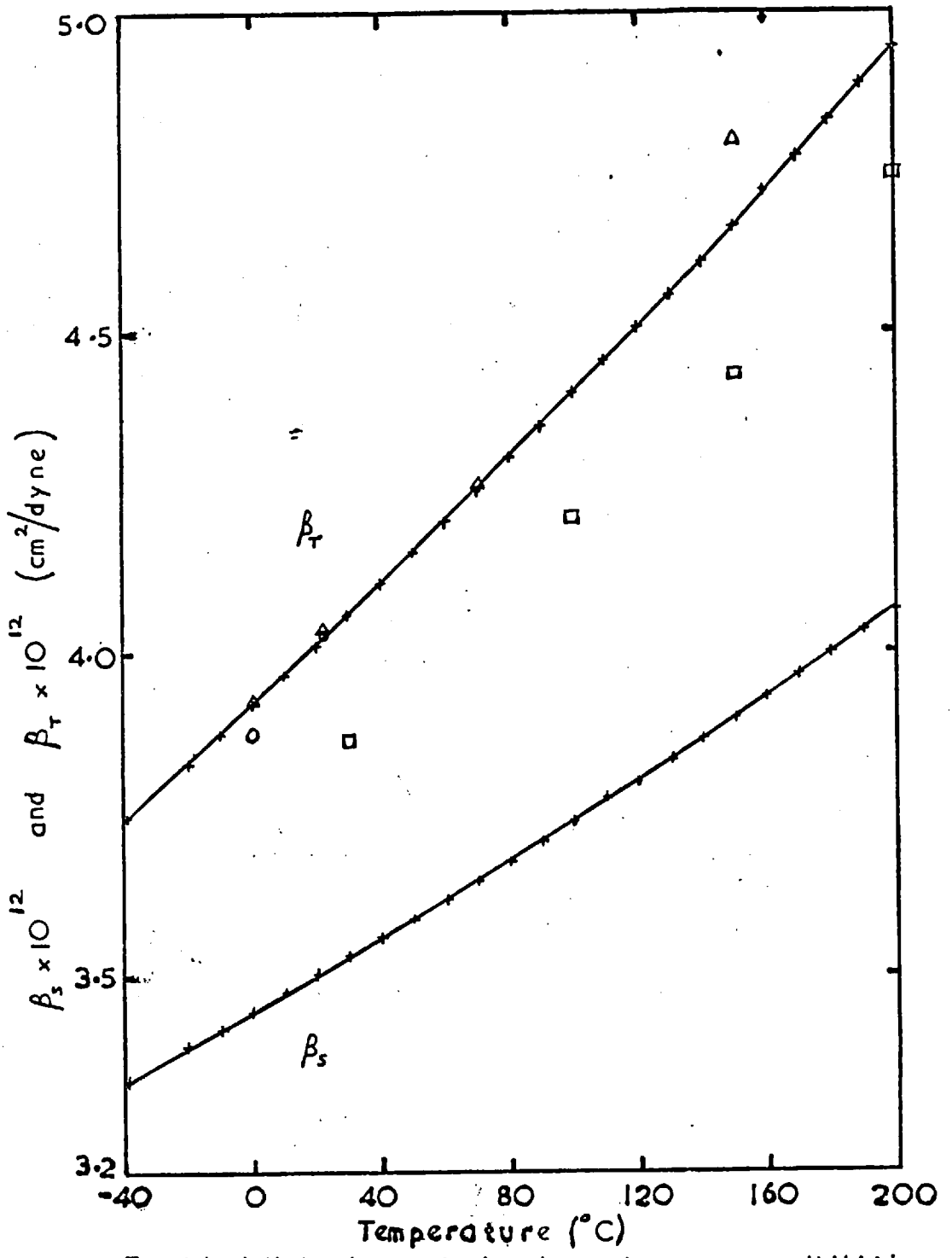

Fig.4.1. Adiabatic and isothermal compressibilities as a function of temperature for mercury. Webber + , Bett et al. Δ , Bridgman o , Smith and Keyes □ .

in which the level of mercury in a capilliary tube was determined by a pointed platinum wire which completed an electrical circuit. When the steel piezometer was compressed a known weight of mercury was added in order to remake the electrical contact and thus the difference between the compressibility of mercury and the soft steel was determined. The authors took Bridgmans' value for the compressibility of steel and found the isothermal compressibility of mercury at 20°C to be 3.96 x 10^{-12} cm^2/dyne.

Smith and Keyes (1934b) used a nickel dilatometer to measure the mean compressibility $\overline{\beta}_T$ of mercury up to 300°C, where $\overline{\beta}_T$ is given by

$$\overline{\beta}_T = -\frac{1}{\Omega_o}\frac{\Delta\Omega}{\Delta p} \quad , \tag{4.17}$$

and Ω_o is the volume at 0°C. The isothermal compressibilities calculated from their results are seen from Fig. 4.1 to be high, particularly at 200°C. Measurements above 200°C were considered as less reliable due to amalgamation of nickel with mercury. It is also of further interest that Rowlinson (1959) pointed out that the direct measurements of β_T for water made by Smith and Keyes (1934a) were about 8% lower than values calculated from β_s for water. Diaz Peña and McGlashan (1959) used a piezometer method to measure the compressibilities of water and mercury and verified Rowlinsons' statement. Their compressibilities for mercury are in fairly close agreement with the present

evaluation. Recent accurate density measurements on mercury as a function of temperature and pressure by Postill et al. (1968) using an Archimedes method enables β_T to be calculated from equations of isochores, such that

$$\beta_T = \alpha_p \left(\frac{\partial T}{\partial p}\right)_\Omega . \qquad (4.18)$$

Their values agree within experimental error with those of Beatt et al. (1954).

B. Pure Metals

There have been no published work on the direct measurement of the isothermal compressibility of liquid metals other than mercury. The compressibilities β_s and β_T have been calculated as a function of temperature from the present sound velocity measurements for zinc, cadmium, indium, tin, lead and bismuth and are shown in Figs. 4.2 to 4.7 respectively. The relevant physical data are compiled in Tables A.9 to A.14. Different values for the expansion coefficients taken from various density investigations give estimated errors of a few percent in β_T. It is seen that both β_s and β_T increase smoothly with temperature, in a similar manner to the alkali metals. Other acoustic measurements on these metals by Gitis and Mikhailov (1966a,b,c), Pronin and Filippov (1963a) and Kazakov et al. (1964) show that β_s continues to increase smoothly with increasing temperature.

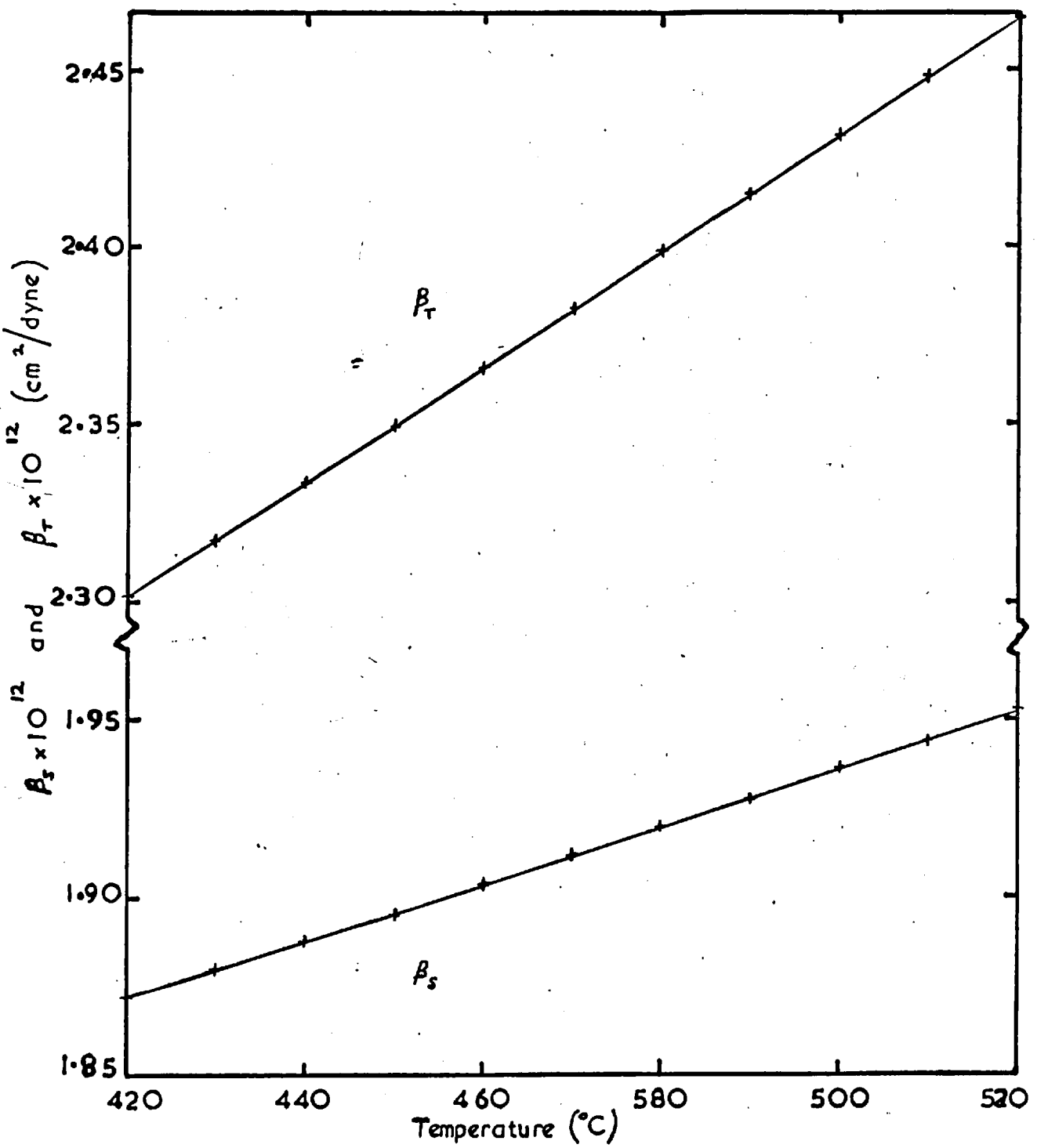

Fig.4.2. Adiabatic and isothermal compressibilities as a function of temperature for zinc.

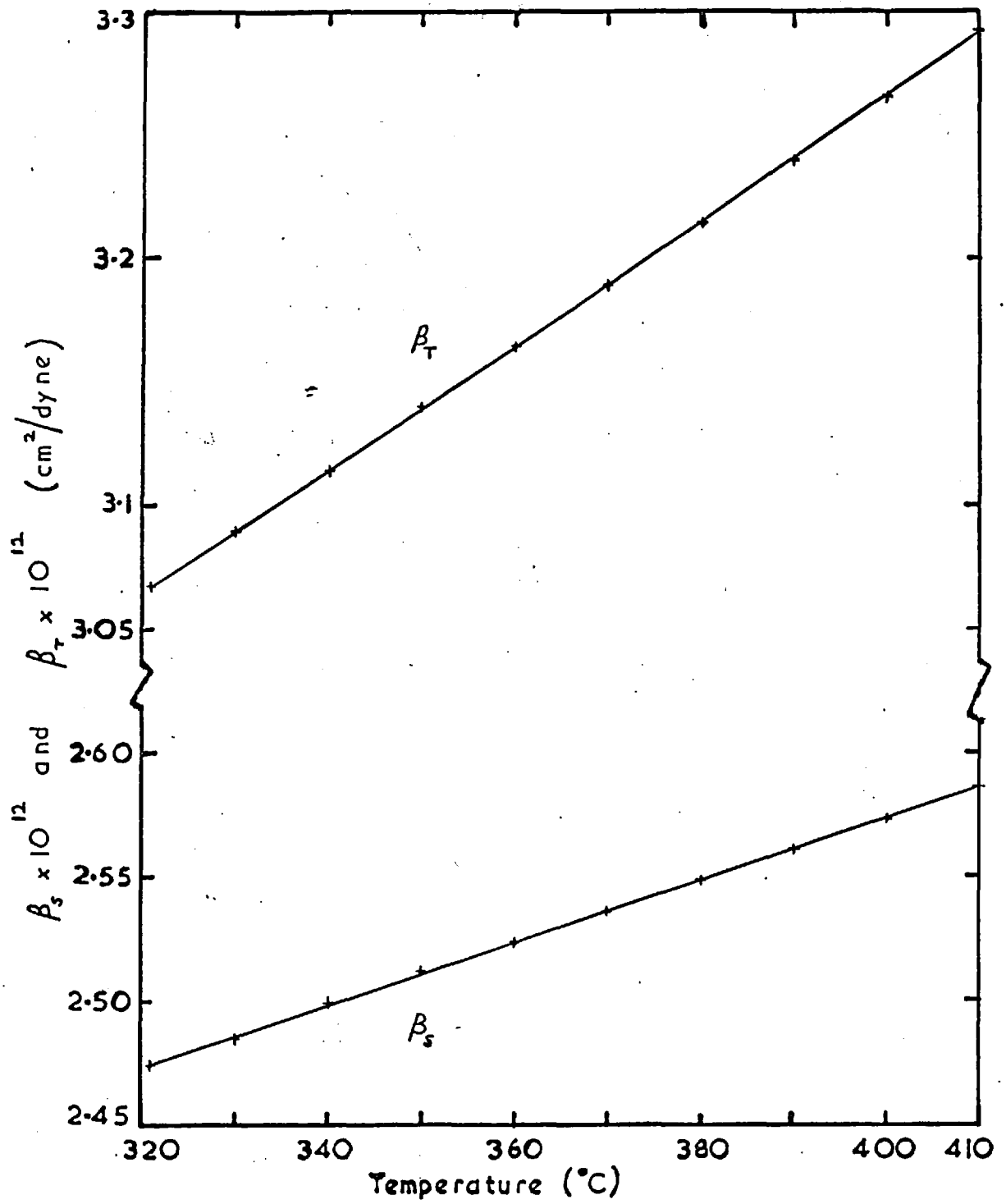

Fig. 4.3. Adiabatic and isothermal compressibilities as a function of temperature for cadmium.

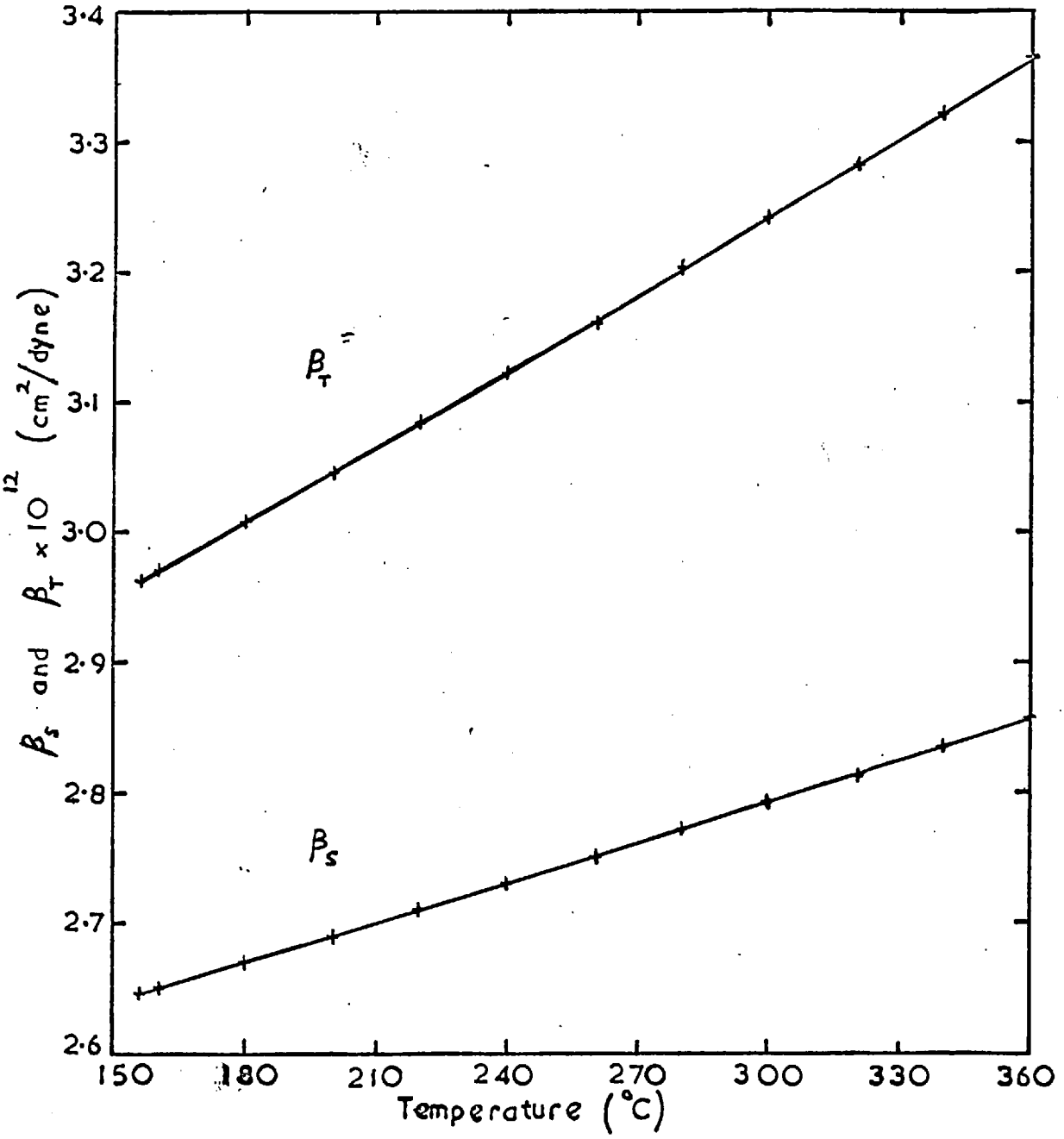

Fig. 4.4. Adiabatic and isothermal compressibilities as a function of temperature for indium.

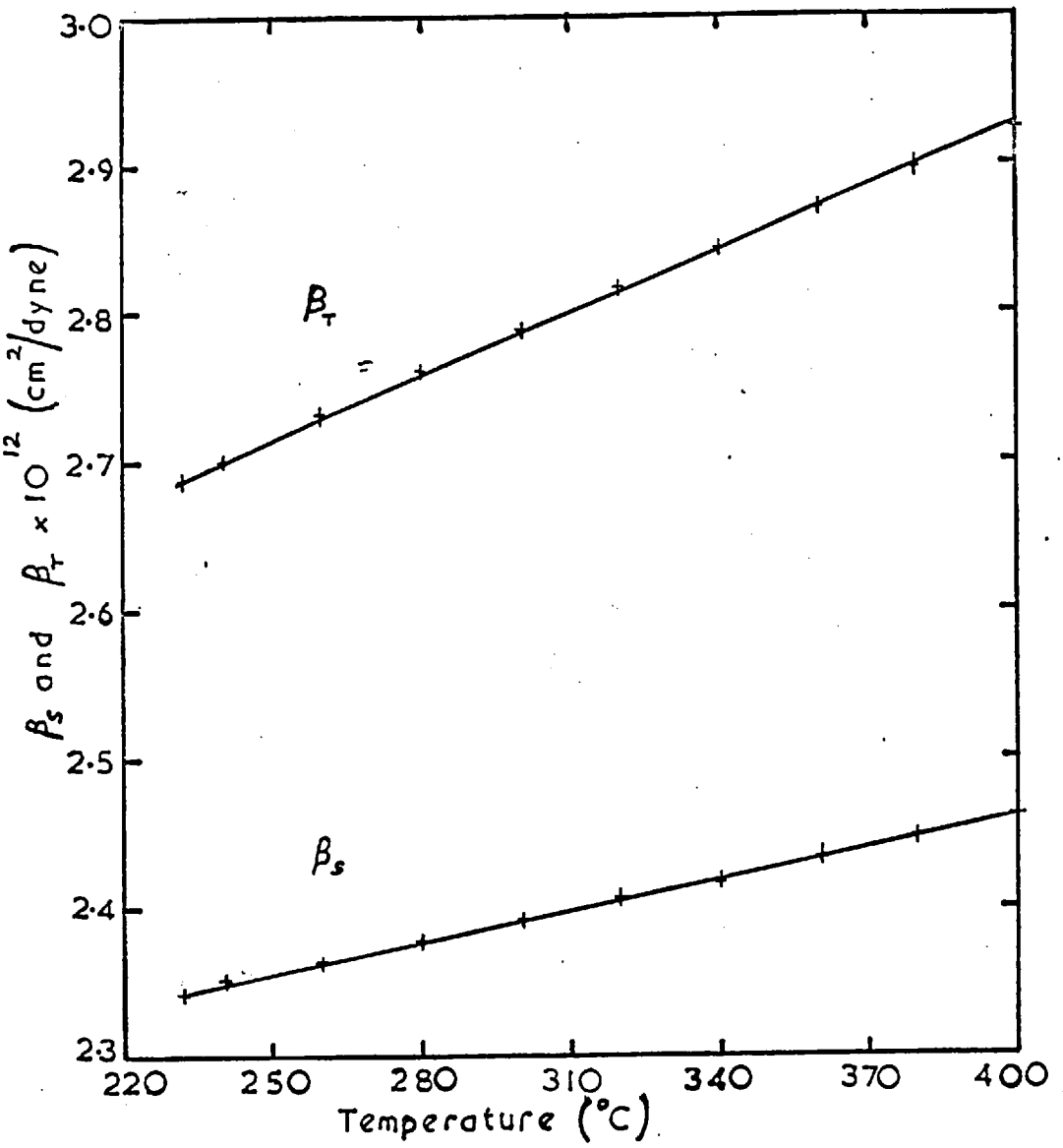

Fig. 4.5. Adiabatic and isothermal compressibilities as a function of temperature for tin.

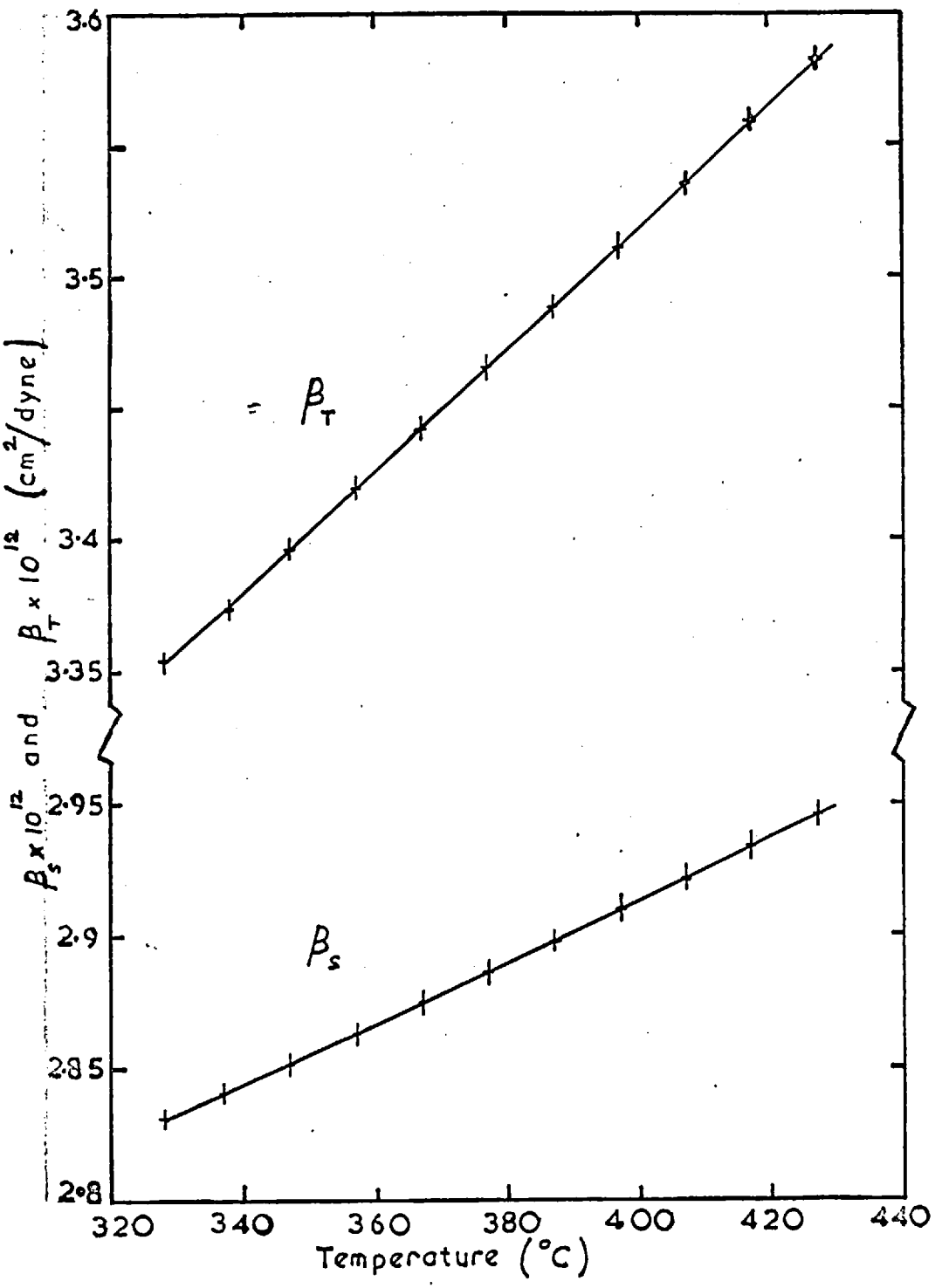

Fig. 4.6. Adiabatic and isothermal compressibilities as a function of temperature for lead.

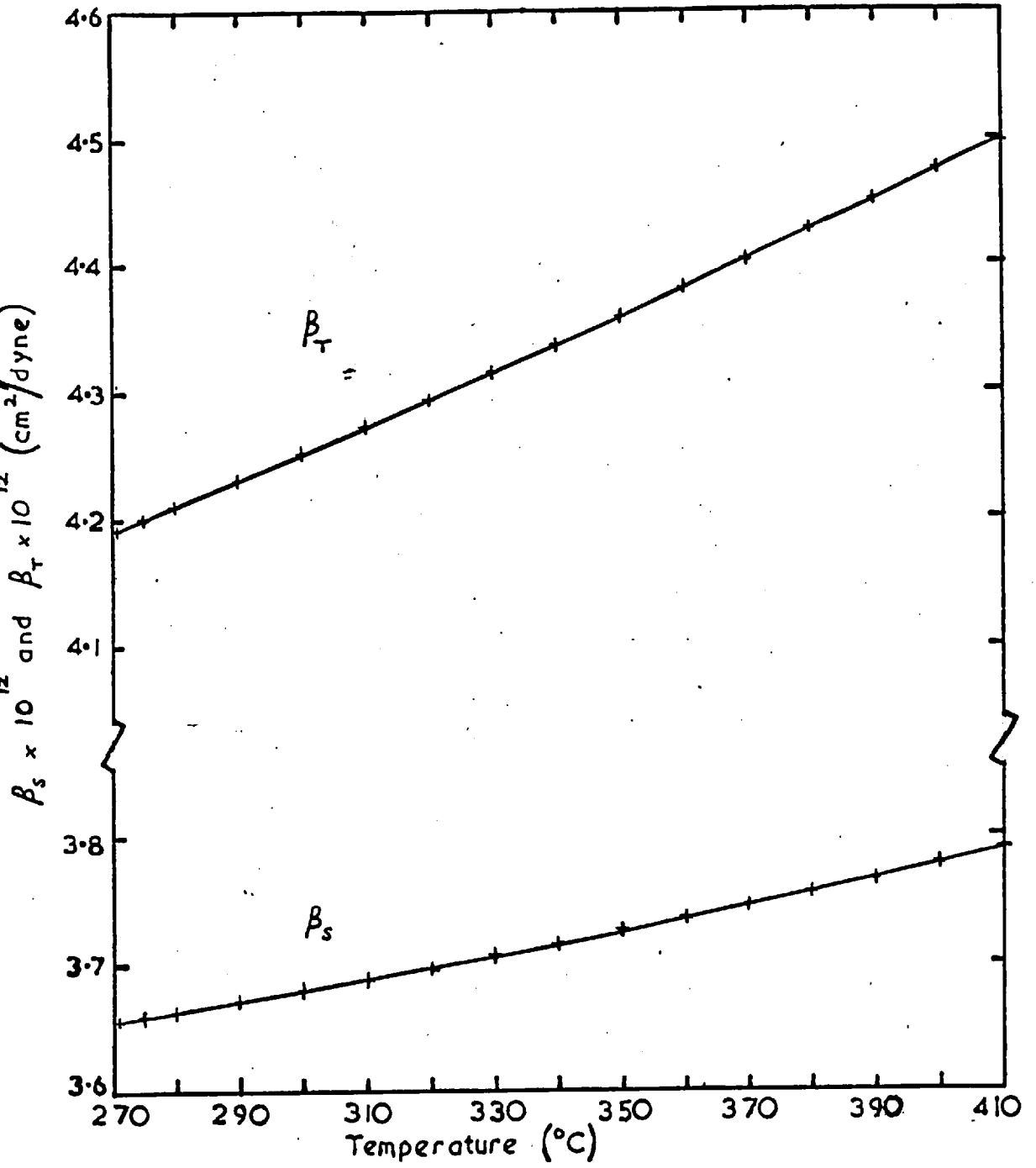

Fig. 4.7. Adiabatic and isothermal compressibilities as a function of temperature for bismuth.

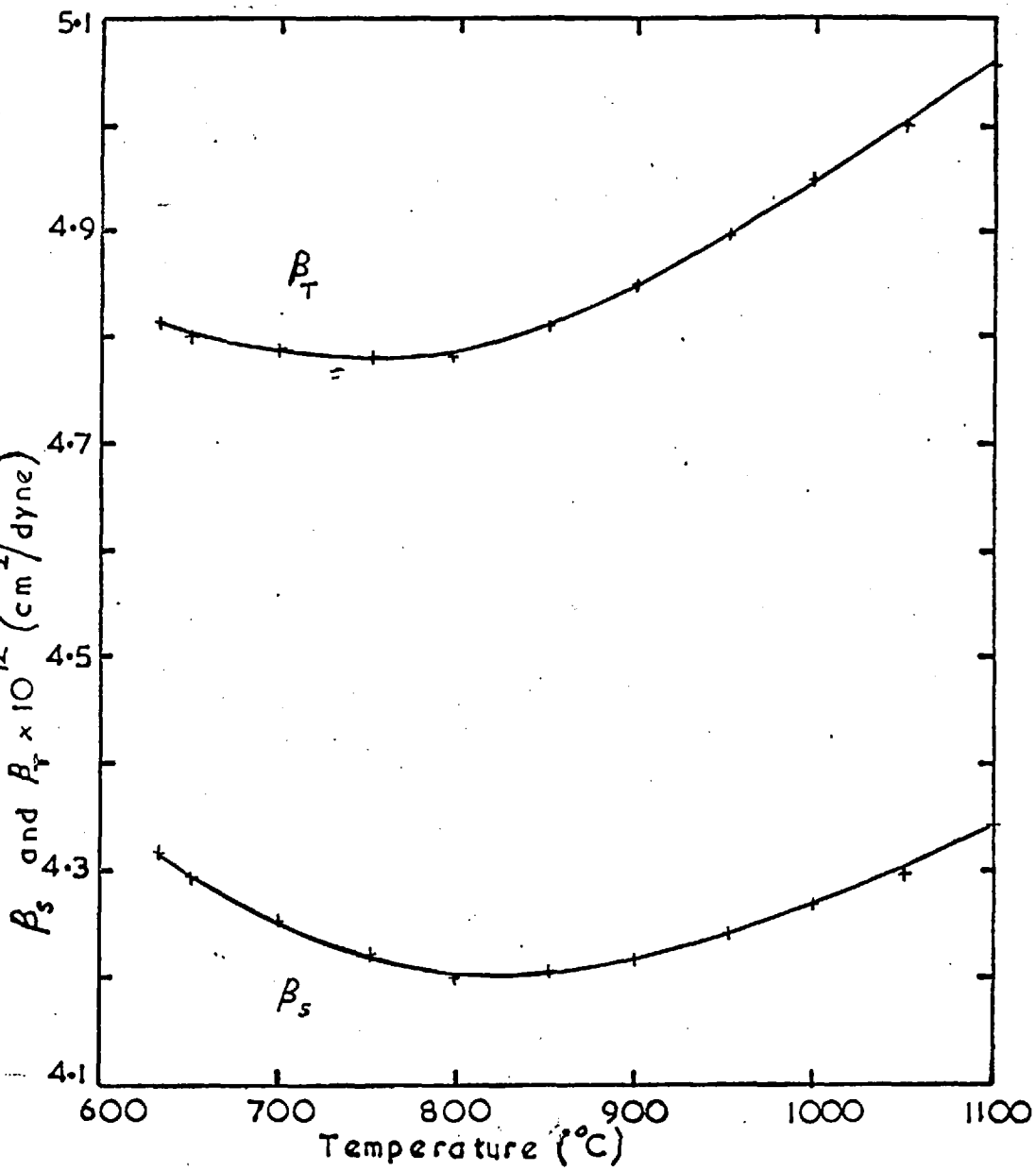

Fig.4.8 Adiabatic and isothermal compressibilities as a function of temperature for antimony.

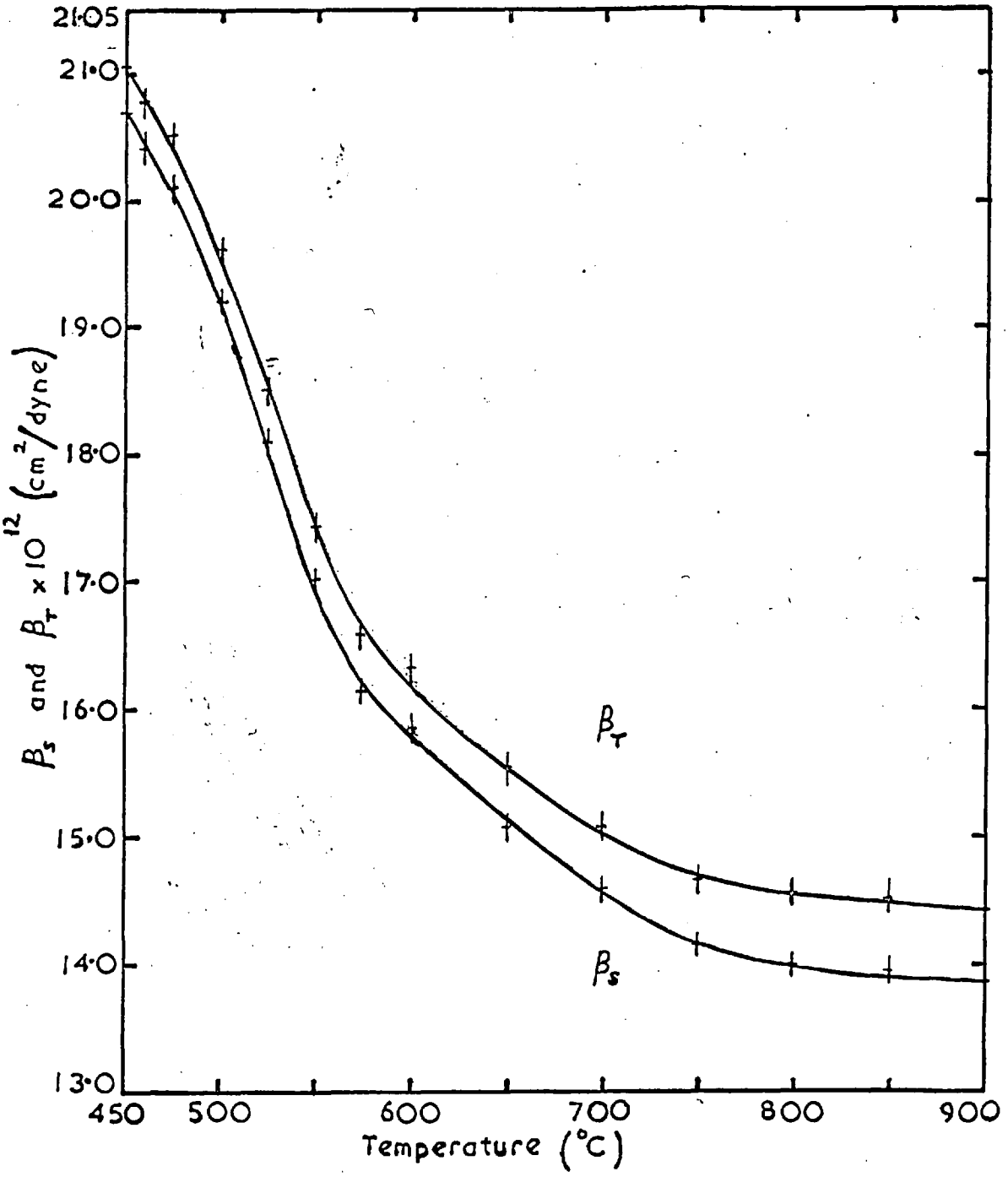

Fig. 4.9. Adiabatic and isothermal compressibilities as a function of temperature for tellurium.

It is of interest to contrast the above behaviour of β_S and β_T for the metals discussed with the variation of the compressibilities with temperature in antimony and in tellurium, shown in Figs. 4.8 and 4.9 respectively. The relevant physical data are collected in Tables A.15 and A.16. In antimony both β_S and β_T exhibit a minimum at about 800°C. This behaviour has been suggested by Gitis and Mikhailov (1966c) as being due to the presence of two structures of different co-ordination number. One structure corresponds to the structure of antimony in the solid state and the other to a close-packed structure. As the temperature increases the increase in volume is expected to lead to an increase in compressibility, whilst an increase in the relative number of atoms in the close-packed structure would lead to a decrease of β_T with increasing temperature, which may be sufficient to account for the observed behaviour. In tellurium the adiabatic and isothermal compressibilities decrease rapidly with temperature at first and then decrease more slowly above 800°C. Tellurium is reported to be a semiconductor in the liquid state which becomes more metallic as the temperature is increased. The compressibility of tellurium does not seem to show a typical metallic behaviour below 700°C.

In order to calculate the adiabatic and isothermal compressibilities for further metals it is necessary to review the sound velocity data available for them. The various published measurements are collected

in Table 4.6, and are discussed briefly below.

a) Sodium. Six investigations agree to within 1 m/sec for the sound velocity and are in fairly close agreement for $-(\partial c/\partial t)_p$. The measurements due to Kleppa and Trelin et al. are seen to be inconsistent with a preferred value for sound velocity of 2527 m/sec at the melting point.

b) Potassium. There is fairly close agreement between three of the investigations. The measurements due to Kleppa and Trelin et al. differ considerably from those due to Abowitz and Gordon, which are taken for the calculation of compressibilities.

c) Rubidium. The recent measurements due to Jarzynski et al. are in fairly close agreement with those due to Kleppa, and are used in further calculations.

d) Caesium. This has only been investigated by Kleppa so far and the sound velocity may be somewhat in error.

e) Copper. The measurements of Gitis and Mikhailov have been seen in Section 3.3 to be generally more reliable than those due to Pronin and Filippov.

f) Silver. The measurements of Gitis and Mikhailov, and Nagel are in fairly close agreement, Nagel's measurements have been shown in Section 3.3 to be generally in better agreement with results in other metals.

Table 4.6 Comparison of Published Values for Velocity of Sound in Pure Metals

Metal	t (°C)	c (m/sec)	$-(\partial c/\partial t)_p$ (m/sec.deg C)	Technique	Temperature range (°C)	Investigator
Na	98	2395 ± 25	0.3	A	98 - 235	Kleppa (1950)
	98	2526 ± 5	0.524 ± 0.003	B	98 - 272	Pochapski (1951)
	100	2533	0.66	D	100 - 180	Ilgūnas & Yaronis (1958)
	98	2653 ± 27	0.577	D		Trelin & Vasil'ev (1961)
	100	2526 ± 5	0.524 ± 0.003	B		Abowitz & Gordon (1962a)
	104	2523 ± 13	0.50	D	104 - 154	Jarzynski & Litovitz (1964)
	110	2521		C		Beyer & Coppens (1965)
	98	2526	0.523		98 - 315	Ying & Scott (1965)
	98	2631 ± 27	0.542	D	100 - 800	Trelin et al. (1966)
	98	2527 ± 1	0.530	C	109 - 140	Coppens et al. (1967)
K	64	1820 ± 20	0.5	A	64 - 160	Kleppa (1950)
	64	1880	0.52	D	64 - 140	Ilgūnas & Yaronis (1958)
	100	1869 ± 5	0.53 ± 0.03	B		Abowitz & Gordon (1962a)
	74	1887 ± 10	0.58	D	74 - 150	Jarzynski & Litovitz (1964)
	100	1922 ± 20	0.539	D	100 - 800	Trelin et al. (1966)
Rb	39	1260 ± 10	∿0.4	A	39 - 160	Kleppa (1950)
	56	1253 ± 2	0.399	D	56 - 260	Jarzynski et al. (1969)
Cs	29	967 ± 10	∿0.3	A	29 - 130	Kleppa (1950)

Table 4.6 continued

Metal	t (°C)	c (m/sec)	$-(\partial c/\partial t)_p$ (m/sec.deg C)	Technique	Temperature range (°C)	Investigator
Cu	1083	3270 ± 49	0.978	A	1083 - 1400	Pronin & Filippov (1963b)
	1100	3450 ± 7	0.46	D	1100 - 1490	Gitis & Mikhailov (1966a)
Ag	961	2770 ± 32	0.466	A	961 - 1540	Pronin & Filippov (1963b)
	970	2710 ± 6	0.41	D	961 - 1220	Gitis & Mikhailov (1966a)
	961	2693	0.293	B		Nagel (1966)
Al	660	4673 ± 15	0.468 ± 0.022	B	660 - 1000	Seemann and Klein (1965)
	660	4730 ± 25	0.16	D	700 - 1000	V'yugov & Gumenyuk (1966)
Ga	30	2740 ± 50		A	30 - 50	Kleppa (1950)
	30	2880 ± 14	0.18	D	57 - 438	Jarzynski (1961)
	29.8	2871 ± 1	0.3	D	20 - 41	Proffit & Carome (1962)
	30	2873	0.3		30 - 80	Hunter & Hovan (1964b)
	75	2770 ± 40	0.25	A	750 - 950	Kazakov et al. (1965)
	30	2872 ± 6	0.225	D	30 - 850	Gitis & Mikhailov (1966b)
	40	2760 ± 60			~40	Shapira (1967)
Tl	302	1625 ± 15		A	302 - 310	Kleppa (1950)
	305	1660 ± 4	0.231	D	302 - 850	Gitis & Mikhailov (1966b)
Sb	650	1980 ± 30	0	A	650 - 1000	Kazakov et al. (1964)
	650	1900 ± 4	-0.25	D	640 - 1100	Gitis & Mikhailov (1966a)
Te	451	913 ± 5	-1.0	D	451 - 900	Gitis & Mikhailov (1966b)
	451	980	-0.75	D	451 - 710	Murphy et al. (1967)

g) Aluminium. The investigation due to Seemann and Klein is considered to be more accurate than that due to V'yugov and Gumenyuk.

h) Gallium. The sound velocity results due to Proffit and Carome, Hunter and Hovan, and Gitis and Mikhailov agree to within a few m/sec.

i) Thallium, Antimony and Tellurium. The investigations due to Gitis and Mikhailov are considered the mose reliable for these metals.

The preferred values for sound velocity and $-(\partial c/\partial t)_p$ for pure liquid metals, at their melting point t_m, are shown in Table 4.7. It should be noted that within each valency group, the sound velocities decrease with increasing atomic weight. This point will be discussed later in Section 4.4. Also the values of $-(\partial c/\partial t)_p$ become smaller for higher valency metals.

The computed compressibilities and ratio of principal specific heats, at the melting point of various liquid metals, are shown in Table 4.8, and the required physical data are collected in Table A.17. Different values for the expansion coefficients taken from various density investigations give estimated errors of a few percent in the isothermal compressibilities. The following points revealed by Table 4.8 are significant:

1) With the exceptions of aluminium and the pentavalent metals, the compressibilities within each valency group increase with increasing atomic volume. The variation of β_T with r_s for each valency group

Table 4.7 Sound Velocities at the Melting Points of Various Liquid Metals

Metal	t_m (°C)	c (m/sec)	$-(\partial c/\partial t)_p$ (m/sec.deg C)
Na	98	2527	0.530
K	64	1888	0.53
Rb	39	1260	0.399
Cs	29	967	~0.3
Cu	1083	3458	0.46
Ag	961	2693	0.293
Zn	420	2852	0.400
Cd	321	2242	0.376
Hg	-39	1479	0.457
Al	660	4673	0.468
Ga	30	2873	0.30
In	156	2318	0.293
Tl	303	1660	0.231
Sn	232	2474	0.223
Pb	328	1819	0.259
Sb	631	1893	-0.23
Bi	271	1649	0.078
Te	451	913	-1.0

Table 4.8 Computed Compressibilities and Ratios of Principal Specific Heats at the Melting Points of Various Liquid Metals

Metal	t_m (^oC)	$\beta_s \times 10^{12}$ (cm^2/dyne)	$\beta_T \times 10^{12}$ (cm^2/dyne)	γ
Na	98	16.9	18.6	1.10
K	64	34.1	38.2	1.12
Rb	39	42.7	49.3	1.15
Cs	29	58.1	68.8	1.18
Cu	1083	1.03	1.50	1.45
Ag	961	1.47	2.14	1.45
Zn	420	1.87	2.30	1.23
Cd	321	2.48	3.07	1.24
Hg	-39	3.34	3.74	1.12
Al	660	1.93	2.42	1.25
Ga	30	1.99	2.19	1.10
In	156	2.65	2.96	1.12
Tl	303	3.10	3.67	1.18
Sn	232	2.34	2.69	1.15
Pb	328	2.83	3.35	1.19
Sb	631	4.32	4.81	1.12
Bi	271	3.66	4.19	1.15
Te	451	20.7	21.1	1.019

is shown in Fig. 4.10.

2) The compressibilities of the alkali metals and tellurium are an order of magnitude larger than those of the noble and polyvalent metals.

3) The compressibilities may be compared with values obtained from sound velocity measurements in the solid metals near their melting points [Schramm (1962a)]. The increase in isothermal compressibility through the melting point is generally about 5 to 20%. Schramm (1962b) used acoustic data and Birch (1942) used the hydrostatic data given by Bridgman (1931) to estimate the values 53.0 x $10^{-12}$and 71.0 x 10^{-12} cm^2/dyne for the isothermal compressibilities of rubidium and caesium respectively at room temperature. Jarzynski et al. (1969) found by taking different density data together with their sound velocity data on liquid rubidium that the calculated isothermal compressibility is between 46.2 and 49.4 x $10^{-12}cm^2$/dyne, which is smaller than Bridgman's value. Further hydrostatic and acoustic measurements are required to confirm the decrease in isothermal compressibility through the melting point for rubidium and caesium.

4) The ratios of the principal specific heats of the metals are not widely different when compared at the same temperature. The liquid semiconductor tellurium is seen to have a value for γ which is very close to unity.

4.4 Comparison of Theoretical and Experimental Compressibilities of Liquid Metals

A. Free-Electron Compressibility

The Bohm-Staver sound velocity and the free-electron compressibility were derived in Sections 1.3D and 1.3E, and the expression for the compressibility is given by equation (1.24.) A comparison between the theoretical and experimental compressibilities of various liquid metals at their melting points is shown in Table 4.9. The free-electron value of the Fermi energy is used. It is seen that the free-electron compressibilities $\beta_T^{(e\ell)}$ are in close agreement with experiment for the alkali metals. In the case of the two noble metals the comparison shows that the presence of a strong repulsive force between the ions drastically reduces their compressibility. As the valency in the polyvalent group of metals increases, then the theoretical compressibility $\beta_T^{(e\ell)}$ becomes progressively smaller than the experimental compressibility. Within each valency group, the theoretical and experimental compressibilities decrease with increasing atomic weight, aluminium and antimony being exceptions. It is seen from equation (1.28) that $\beta_T^{(e\ell)}$ is proportional to r_s^5 and β_T is plotted as a function of r_s in Fig. 4.10, in which a family of curves is produced according to valency; the behaviour of the pentavalent metals would appear to be exceptional.

It was mentioned in Section 1.3E that Harrison (1966) included a correction in the dielectric function, $\varepsilon(q)$, due to exchange interaction

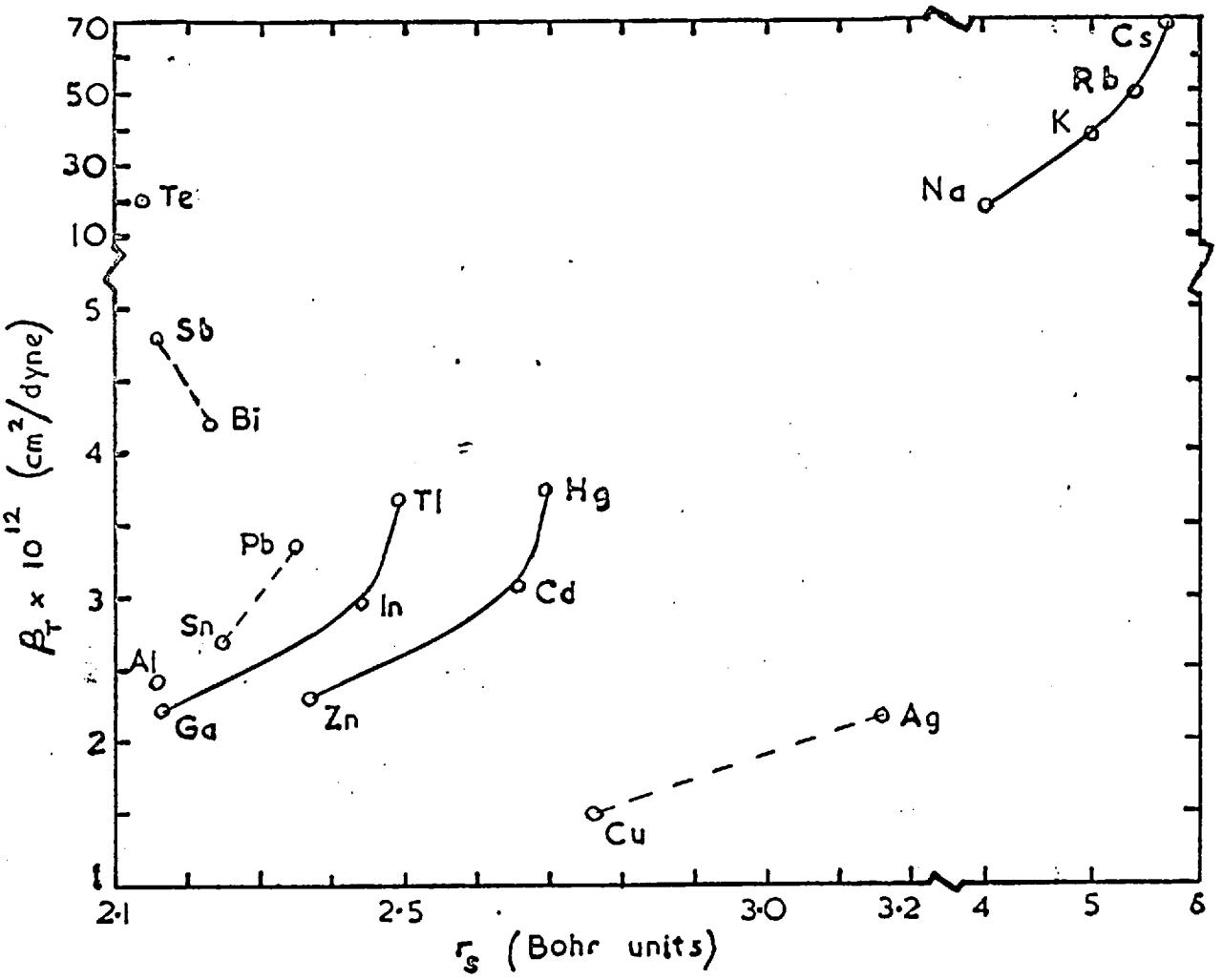

Fig. 4.10. Isothermal compressibilities versus r_s for various liquid metals.

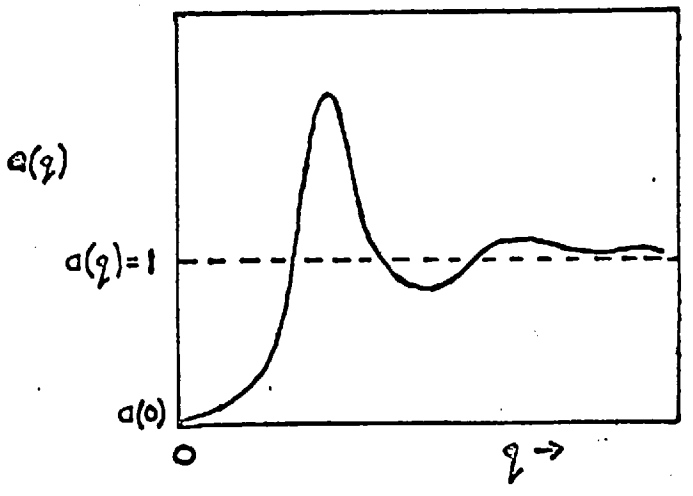

Fig. 4.11. Structure factor for liquid metal.

and he derived the expression for the isothermal sound velocity, $c^{(H)}$, as

$$[c^{(H)}]^2 = [c^{(BS)}]^2[1 - 0.249\ r_s], \qquad (4.19)$$

where $c^{(BS)}$ is the Bohm-Staver sound velocity. This correction reduces the sound velocity to 8 and 70% of the Bohm-Staver velocity in sodium and in aluminium respectively, showing that a correction for exchange alone is more drastic for the alkali metals. Thus the exchange interaction does not offer an explanation for the required correction to the theoretical sound velocity in the polyvalent metals.

We reported in Smith et al. (1967) and Webber and Stephens (1968) that a fairly good correlation appeared to exist between the experimental compressibility and the compressibility $\beta_T^{(W)}$ defined by the empirical relation

$$\beta_T^{(W)} = Z\ \beta_T^{(e\ell)}\ , \qquad (4.20)$$

where Z is the valency. It is seen from Table 4.9 that agreement is poorer for antimony, bismuth and tellurium. To account for this relation it would be necessary for $N(E_F)$ to be increased by a factor of Z, which has not been confirmed by any other physical measurement. Rice (1963) has calculated that the electron-electron Coulomb interaction and the virtual phonon interactions increase the density of states $N(E_F)$ in solids by up to 10 and 30% respectively. The inclusion of

Table 4.9 Isothermal Compressibilities at the Melting Points of Various Metals

Metal	Z	Theoretical		Ascarelli	Experimental
		$\beta_T^{(e\ell)} \times 10^{12}$ (cm^2/dyne)	$Z\,\beta_T^{(e\ell)} \times 10^{12}$ (cm^2/dyne)	$\beta_T^{(A)} \times 10^{12}$ (cm^2/dyne)	$\beta_T \times 10^{12}$ (cm^2/dyne)
Na	1	12.5	12.5	19.9	18.6
K	1	37.2	37.2	47.2	38.2
Rb	1	51.9	51.9	64.1	49.3
Cs	1	69.9	69.9	78.9	68.8
Cu	1	1.86	1.86	1.95	1.50
Ag	1	3.54	3.54	3.34	2.14
Zn	2	0.87	1.74	2.57	2.30
Cd	2	1.53	3.06	4.23	3.07
Hg	2	1.66	3.31	5.65	3.74
Al	3	0.55	1.65	2.02	2.42
Ga	3	0.56	1.67	2.32	2.19
In	3	1.01	3.02	3.93	2.96
Tl	3	1.13	3.38	3.94	3.67
Sn	4	0.67	2.68	2.77	2.69
Pb	4	0.83	3.33	2.98	3.35
Sb	5	0.54	2.70	1.78	4.81
Bi	5	0.64	3.21	2.64	4.19
Te	6	0.41	2.49	1.80	21.1

these factors would increase the compressibility $\beta_T^{(e\ell)}$ by several percent but not to the extent of the factor Z. It has been seen in Section 1.3F that the pseudo-potential approach to the calculation of compressibility can successfully account for the compressibility of solid metals, where the free-electron compressibility differs significantly, and therefore it may be that the factor Z is a fortuitous numerical factor and not physically significant. The application of the pseudo-potential approach to the calculation of compressibilities of liquid metals will be discussed in the next Section 4.4B.

B. Pseudo-Potential Approach

The pseudo-potential approach for the calculation of total energy and compressibility of simple solid metals has been discussed in Section 1.3F, where it was seen that Ashcroft and Langreth (1967a) obtained excellent agreement between theory and experiment. Since the structure factors $S(\underline{q})$ and $a(q)$ are no longer delta functions, but are continuous functions of q, see Fig. 4.11, it is necessary to develop expressions for the total energy and compressibility of simple liquid metals. We may start with the total energy expression for simple solid metals given in equation (1.67) and we must consider the Fuchs and band-structure energies which are both structure dependent and therefore different for liquid metals. It can be seen from equation (1.53) that the Fuchs

term E_{ii}/Z, in atomic units, is given by

$$\frac{E_{ii}}{Z} = \frac{1}{8\pi^3}\int_0^\infty \frac{4\pi Z}{q^2}\,[a(q) - 1]\,4\pi q^2 dq$$

$$= \frac{2Z}{\pi}\int_0^\infty [a(q) - 1]dq. \qquad (4.21)$$

Ashcroft and Langreth (1967a) numerically integrated this expression using the hard-sphere structure factor of Ashcroft and Lekner (1966) and found that for simple liquid metals the Fuchs term (ryd/electron) is given by

$$\frac{E_{ii}}{Z} = \frac{-1.73\ Z^{2/3}}{r_s} \quad . \qquad (4.22)$$

In order to calculate the band-structure contribution E_{BS}/Z to the total energy of the liquid metal we may start with the expression for E_{BS} given in equation (1.47). If we use the relationship between $S^*(\underline{q})S(\underline{q})$ and $a(q)$ given in equation (1.49) and replace the sum by an integral, then the band-structure energy (per electron), written in atomic units, is given by

$$\frac{E_{BS}}{Z} = \frac{\Omega}{8\pi^3 Z}\int_0^\infty \frac{\Omega q^2}{16\pi N^2}\,|w_q^o|^2\left(\frac{1}{\varepsilon_q} - 1\right)a(q)\,4\pi q^2 dq$$

$$= \frac{\Omega^2}{32\pi^3 Z N^2}\int_0^\infty q^4 |w_q^o|^2\left(\frac{1}{\varepsilon_q} - 1\right)a(q)dq. \qquad (4.23)$$

Using the definition of V_q given in equation (1.51), the above expression may be written as

$$\frac{E_{BS}}{Z} = \frac{1}{32\pi^3 Z}\int_0^\infty q^4 V_q^2 \left(\frac{1}{\varepsilon} - 1\right) a(q)dq. \qquad (4.24)$$

If we use the simple form for V_q proposed by Ashcroft (1966), given by equation (1.61), then equation (4.24) becomes

$$\frac{E_{BS}}{Z} = \frac{-2Z}{\pi}\int_0^\infty \cos^2(qr_c)\left[\frac{\varepsilon - 1}{\varepsilon}\right] a(q)dq. \qquad (4.25)$$

The total energy $E^{(AL,\ell)}$ of the simple liquid metal may therefore be written in the form

$$E^{(AL,\ell)} = \frac{2.21}{r_s^2} - \frac{0.916}{r_s} - (0.115 - 0.031\ell n r_s) + \frac{3A}{4\pi r_s^3}$$

$$- \frac{1.73Z^{2/3}}{r_s} - \frac{2Z}{\pi}\int_0^\infty \cos^2(qr_c)\left[\frac{\varepsilon - 1}{\varepsilon}\right] a(q)dq. \qquad (4.26)$$

We now proceed to the calculation of the band-structure contribution to the compressibility of liquid metals, for which it is necessary to know the volume dependence of E_{BS}. The volume dependence of a(q) is not known accurately from experiment. However, the hard-sphere structure factor due to Ashcroft and Lekner (1966) could be used for

the evaluation of E_{BS} and its volume dependence. If we put q in units of $2k_F$, see equation (1.59), then the structure factor a(q) may be written as $a(x, r_s)$. Using the definition of y given in equation (1.63), the band-structure energy given by equation (4.25) becomes

$$\frac{E_{BS}}{Z} = \frac{-7.68Z}{\pi} \int_0^\infty \cos^2 y \left[\frac{\epsilon(x, r_s) - 1}{\epsilon(x, r_s) r_s} \right] a(x, r_s) dx. \qquad (4.27)$$

The first derivative of the band-structure energy given in equation (4.27) with respect to r_s at constant x is found to be

$$\frac{\partial}{\partial r_s} \left(\frac{E_{BS}}{Z}\right) = \frac{-7.68Z}{\pi} \int_0^\infty \left\{ \frac{ay \sin 2y}{r_s} - \left(\frac{\epsilon-1}{\epsilon r_s}\right) a \cos^2 y + \frac{\partial a}{\partial r_s} \cos^2 y \right\} \left(\frac{\epsilon-1}{\epsilon r_s}\right) dx, \qquad (4.28)$$

where $\epsilon(x, r_s)$ is given by equation (1.56). The second derivative is found to be

$$\frac{\partial^2}{\partial r_s^2} \left(\frac{E_{BS}}{Z}\right) = \frac{7.68Z}{\pi} \int_0^\infty \left\{ \frac{2ay}{r_s^2} (\sin 2y + y \cos 2y) \right.$$

$$+ \frac{2y}{r_s} \left[\left(\frac{\epsilon-1}{\epsilon r_s}\right) a - \frac{\partial a}{\partial r_s} \right] \sin 2y$$

$$\left. - \left[2\left(\frac{\epsilon-1}{\epsilon r_s}\right)^2 a - 2\left(\frac{\epsilon-1}{\epsilon r_s}\right) \frac{\partial a}{\partial r_s} + \frac{\partial^2 a}{\partial r_s^2} \right] \cos^2 y \right\} \left(\frac{\epsilon-1}{\epsilon r_s}\right) dx. \qquad (4.29)$$

When we calculate the isothermal compressibility by the more accurate procedure of eliminating A from equation (4.26) by using the zero-pressure condition $\partial E/\partial r_s = 0$, then we require the expression for $\frac{4}{r_s}\frac{\partial}{\partial r_s}(\frac{E_{BS}}{Z}) + \frac{\partial^2}{\partial r_s^2}(\frac{E_{BS}}{Z})$. It follows from equations (4.28) and (4.29) that

$$\frac{4}{r_s}\frac{\partial}{\partial r_s}(\frac{E_{BS}}{Z}) + \frac{\partial^2}{\partial r_s^2}(\frac{E_{BS}}{Z}) = \frac{-2.44Z}{r_s^2}\int_0^\infty \{2ay(\sin 2y - y\cos 2y)$$

$$- 2r_s[(\frac{\varepsilon-1}{\varepsilon r_s})a - \frac{\partial a}{\partial r_s}][y\sin 2y + 2\cos^2 y]$$

$$+ r_s^2[2(\frac{\varepsilon-1}{\varepsilon r_s})^2 a - 2(\frac{\varepsilon-1}{\varepsilon r_s})\frac{\partial a}{\partial r_s} + \frac{\partial^2 a}{\partial r_s^2}]\cos^2 y\}(\frac{\varepsilon-1}{\varepsilon r_s})dx \qquad (4.30)$$

$$= \frac{-2.44Z}{r_s^2} G'(r_s) \quad , \qquad (4.31)$$

where $G'(r_s)$ is defined by the integral in equation (4.30). It is seen that the first term of $G'(r_s)$ corresponds to $G(r_s)\{2y(\sin 2y - y\cos 2y)\}$, obtained for a solid metal. The further terms in $G'(r_s)$ come from the consideration of the volume dependence of $a(x, r_s)$ and $(\frac{\varepsilon-1}{\varepsilon r_s})$, the contribution due to the latter being negligible in the case of the solid metal.

The isothermal compressibility $\beta_T^{(AL,\ell)}$ for a simple liquid metal

can be calculated in the manner outlined in Section 1.3F and is found to be given by

$$\frac{\beta_T^{(AL,\ell)}}{\beta_T^{(e\ell)}} = \frac{22.1}{[0.093r_s^2 + 2(0.916 + 1.73Z^{2/3})r_s - 4.42 - 2.44Zr_s^2G'(r_s)]} \quad (4.32)$$

The evaluation of this expression for isothermal compressibility requires the knowledge of $G'(r_s)$, which could be evaluated numerically. Since the increase is isothermal compressibility through the melting point is generally about 5 to 20% it is expected that the band-structure contribution to the compressibility does not change significantly. In conclusion it is seen that the pseudo-potential approach to the calculation of compressibility of liquid metals requires further knowledge of the volume dependences of pseudo-potentials and structure factors.

C. Semi-Phenomenological Model due to Ascarelli

The theoretical approach to the calculation of the sound velocity in liquid metals proposed by Ascarelli (1968) has been described in Section 1.3G. Ascarelli calculated the theoretical sound velocity $[c^{(A)}]_m$ from equation (1.87) and those values are compared with the Bohm-Staver and experimental sound velocities for various liquid metals, at their melting points, in Table 4.10. Slightly different values of $[c^{(A)}]_m$ would be obtained if experimental values of γ for each metal

Table 4.10 Comparison of Theoretical and Experimental Sound Velocities at the Melting Points of Various Metals

Metal	t_m (^oC)	Theoretical		Experimental
		Bohm-Staver $c^{(BS)}$ (m/sec)	Ascarelli $[c^{(A)}]_m$ (m/sec)	c (m/sec)
Na	98	2940	2500	2527
K	64	1810	1720	1888
Rb	39	1140	1103	1260
Cs	29	880	890	967
Cu	1083	2580	2700	3458
Ag	961	1740	1920	2693
Zn	420	4180	2610	2852
Cd	321	2850	1840	2242
Hg	-39	2100	1220	1479
Al	660	8750	4900	4673
Ga	30	5430	2850	2873
In	156	3760	2041	2318
Tl	303	2750	1580	1660
Sn	232	4630	2440	2474
Pb	328	3350	1900	1819
Sb	631	5340	3150	1893
Bi	271	2940	2080	1649
Te	451	6450	3320	913

were used rather than the common value of 1.15 chosen by Ascarelli. There is a fairly close agreement between $[c^{(A)}]_m$ and experimental values, and the decrease of sound velocity with increasing atomic mass within each valency group is obtained. This approach is a significant improvement over the Bohm-Staver result for the polyvalent metals. With the exceptions of copper, silver, antimony, bismuth and tellurium the calculated $[c^{(A)}]_m$ agree generally to better than 20% of the experimental value. For copper and silver an extra contribution to the energy due to overlap between electron shells of neighbouring atoms is probably needed. For antimony and bismuth $[c^{(A)}]_m$ is 40 and 20% respectively smaller than the experimental value and modification of this theory would appear to be necessary to account for the discrepancy. Gitis and Mikhailov (1966c), previously mentioned in Section 4.4B, suggest that structural changes occur in these two metals near their melting points since their temperature dependence of sound velocity differ considerably from the other liquid metals.

This simple model of hard-spheres in a uniform background potential yields values for sound velocity which are in close agreement with experiment and is a noticeable improvement over the free-electron approach to compressibility. In order to improve the agreement between calculated and measured sound velocity a better understanding of the interatomic forces and their volume dependence in liquid metals is probably needed. In this connection, it is of interest to note that

Ashcroft (private communication) has found that the Born-Mayer interaction is important in mercury.

4.5 Adiabatic Compressibility of Mercury Alloys

It is of interest to calculate the adiabatic compressibility of the mercury alloys studied here and to compare the variations of compressibility with concentration for these alloys with the behaviour for mercury-thallium alloys. The density data at fixed temperatures were calculated from the volume contraction measurements due to Kleppa et al. (1961) and Davies (1966). Density, sound velocity and adiabatic compressibility data are given as a function of composition for the Hg-Zn, Hg-Cd, Hg-In, Hg-Sn, Hg-Pb and Hg-Bi alloy systems, at a fixed temperature in Tables A.1 to A.6. Adiabatic compressibility at a fixed temperature is plotted as a function of concentration for six mercury alloy systems in Figs. 4.12 to 4.14, from which it is seen that the addition of zinc, cadmium, indium, tin, lead, or bismuth produce a rapid decrease in the compressibility. This behaviour is in agreement with the dilute alloy measurements due to Abowitz and Gordon (1963). For concentrations up to 40 at.% the variation of adiabatic compressibility with concentration for these six mercury alloy systems is similar to the behaviour of the mercury-thallium system. In the mercury-lead and mercury-bismuth systems the adiabatic compressibilities exhibit minima at about 70 at.% Pb and 40 at.% Bi respectively.

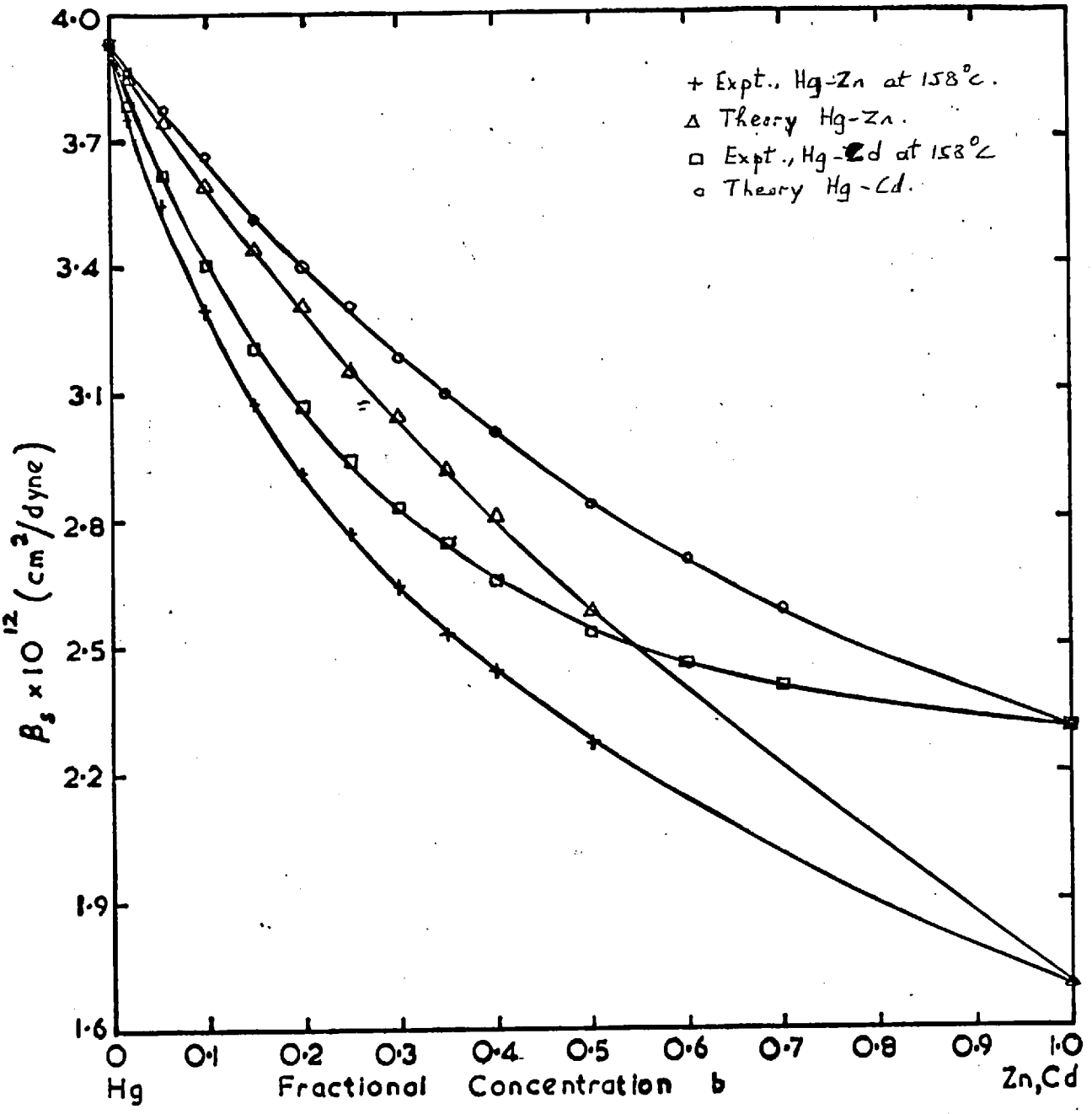

Fig. 4.12. Variation of adiabatic compressibilities with composition in the Hg-Zn and Hg-Cd alloy systems. Data shown in Tables A1 and A2.

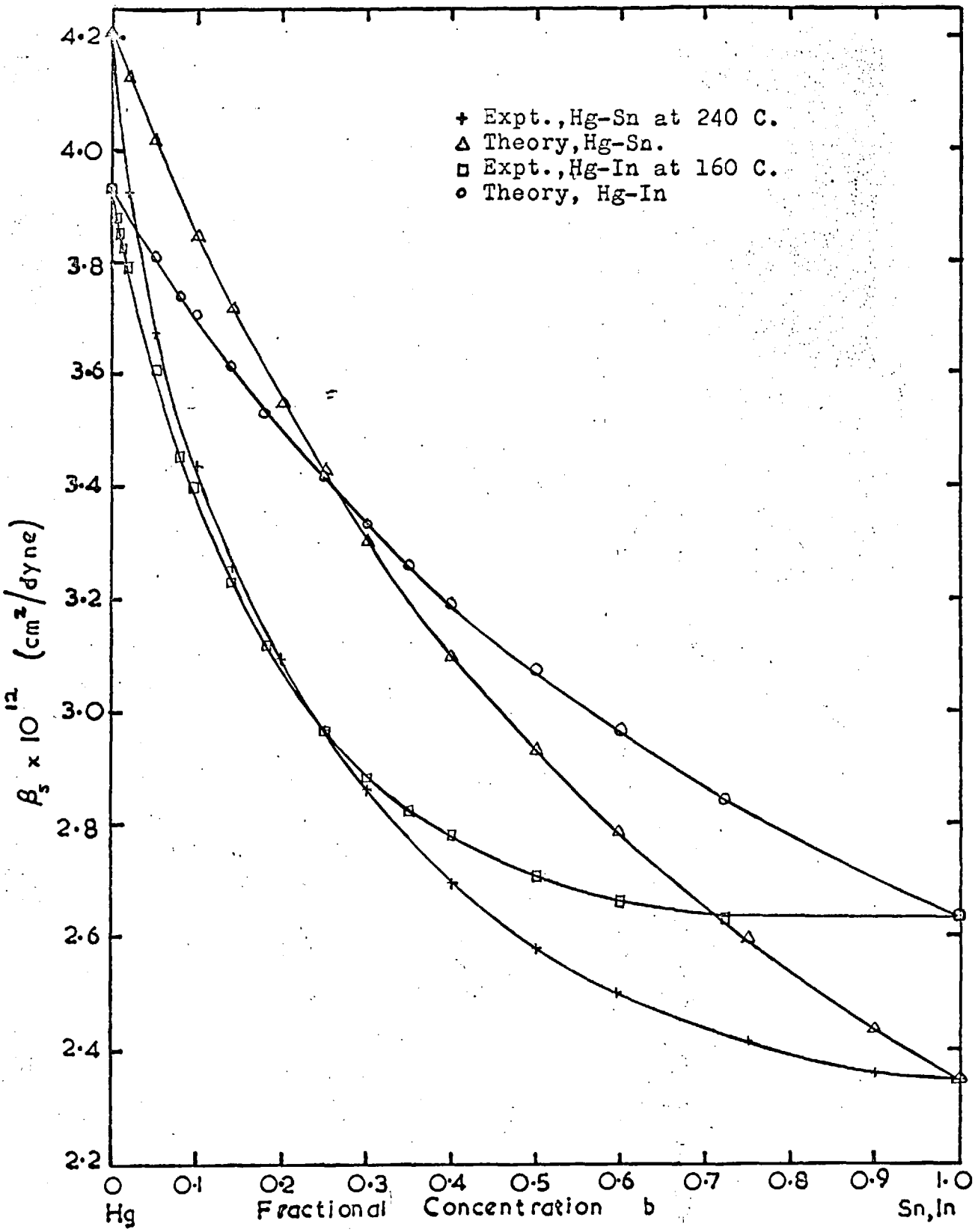

Fig.4.13. Adiabatic compressibilities as a function of concentration b in the Hg-Sn and Hg-In alloy systems. Data shown in Tables A.4 and A.3 .

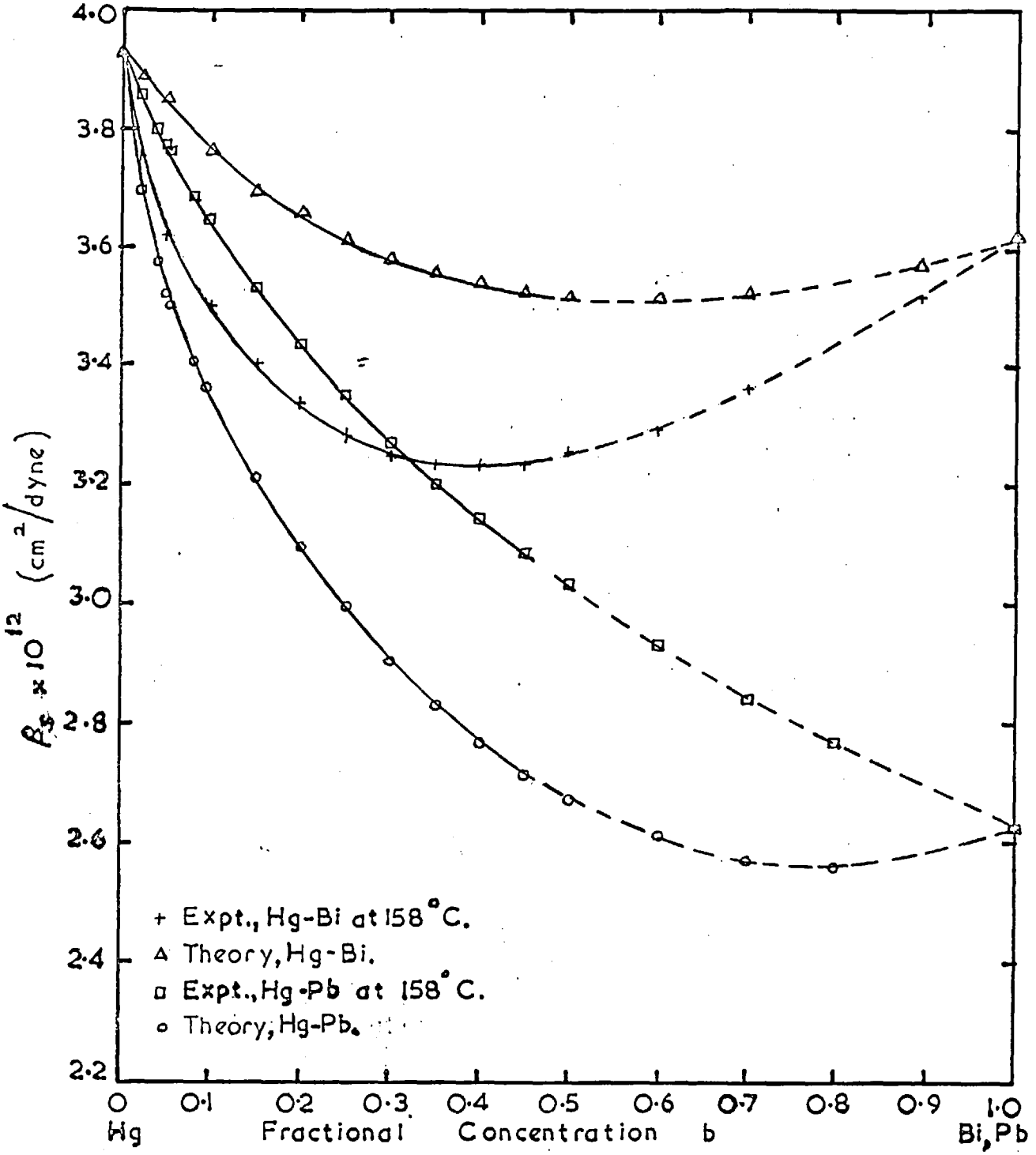

Fig.4.14. Adiabatic compressibilities as a function of concentration b in the Hg-Bi and Hg-Pb alloy systems. Data shown in Tables A.6 and A.5.

The measurements of isothermal compressibility on mercury-tin alloys by Lussana [see Bridgman (1958), page 147] indicated also that a minimum occurred in compressibility. Since specific heat data are not available for this alloy system it is not possible to calculate isothermal compressibility from these sound velocity measurements. However, the specific heat C_p has been determined for mercury-thallium alloys and therefore the ratio of principal specific heats γ and isothermal compressibility can be calculated from the sound velocity measurements due to Abowitz and Gordon (1963). The data for ρ, α_p, ϵ_p, c and calculated values of γ, β_s and β_T for mercury-thallium alloys are given in Table A.18. The ratio of specific heats is found to increase between 0 and 5 at.% Tl and then decreases towards the extrapolated value of γ for pure Tl (see Fig. 4.15). Using these values for γ it is found that the specific heat at constant volume C_Ω increases smoothly with increase in concentration of thallium. The physical reason for the peak in γ is not readily apparent. Isothermal compressibility is seen from Fig. 4.16 to decrease smoothly with increasing concentration of thallium and deviates from linearity with concentration by up to 9%. A comparison between the theoretical and experimental variation of compressibility with alloy composition is discussed in the following Section 4.6.

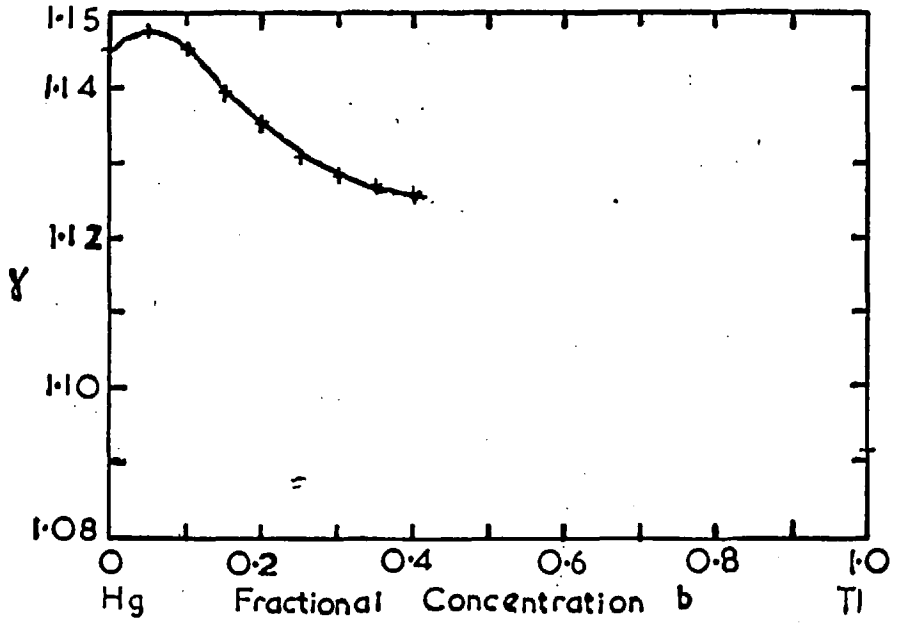

Fig. 4.15. Variation of γ with composition in the Hg-Tl alloy system.

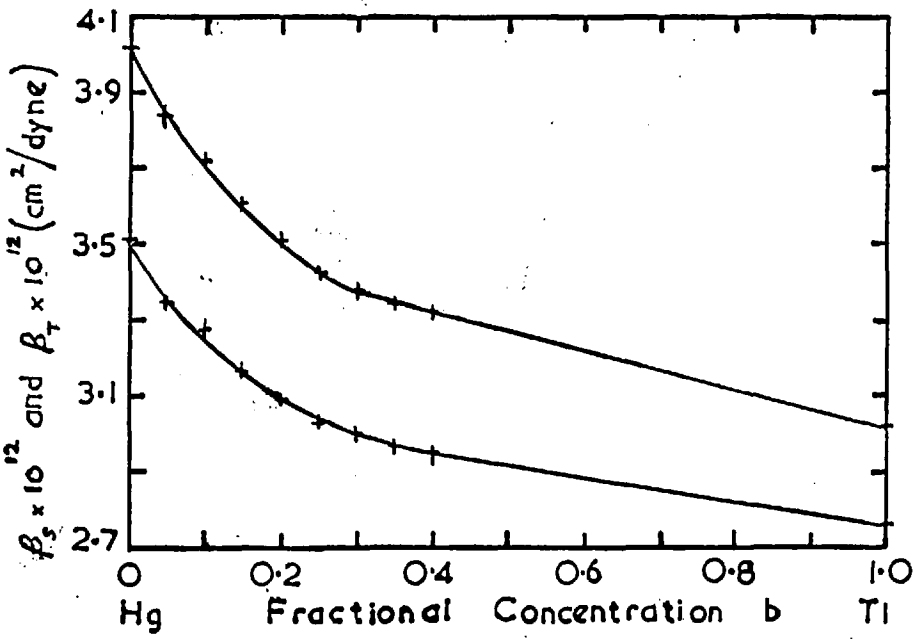

Fig. 4.16. Variation of isothermal compressibilities with composition in the Hg-Tl alloy system.

4.6 Comparison of Theoretical and Experimental Compressibilities for Mercury Alloys

A. Bohm-Staver Sound Velocity

The author decided to formulate the Bohm-Staver sound velocity for alloys and to compare it with the present alloy results. The derivation of the Bohm-Staver sound velocity for pure metals has been given in Sections 1.3D and 1.3E, and can be simply extended to include alloy systems. For an alloy of metals of ionic masses M_o, M_1 and valencies Z_0, Z_1 respectively, the number of electrons/unit volume for an alloy of atomic fraction b is simply given by

$$\left[\frac{NZ}{\Omega}\right]_b = \frac{\rho_b[Z_1\, b + Z_0(1 - b)]}{[M_1\, b + M_0(1 - b)]} \quad , \tag{4.33}$$

where ρ_b is the density of the alloy. Hence the pressure p_b of the electron gas at T = 0 is found to be

$$p_b = \frac{2\hbar^2}{5m}(3\pi^2)^{2/3}\left\{\frac{\rho_b[Z_1 b + Z_0(1 - b)]}{M_1 b + M_0(1 - b)}\right\}^{5/3} \quad . \tag{4.34}$$

From the differentiation of p_b with respect to density it is found that the isothermal compressibility $[\beta_T^{(e\ell)}]_b$ for atomic fraction b is given by

$$[\beta_T^{(e\ell)}]_b = \frac{3[M_1 b + M_0(1 - b)]}{2[E_F]_b[Z_1 b + Z_0(1 - b)]\rho_b} \quad , \tag{4.35}$$

where $[E_F]_b$ is the free-electron Fermi energy for an alloy of atomic fraction b.

The theoretical isothermal compressibilities of the pure components, which are obtained by putting b equal to zero or unity in equation (4.35), have been seen in Section 4.4A to be much smaller than experiment for the polyvalent metals. In a similar manner to the empirical relation for the compressibilities of pure metals defined by $Z\beta_T$, which was discussed in Section 4.4A, it is possible to define an empirical compressibility $[\beta_T^{(W)}]_b$ for alloys of atomic fraction b by $[Z_1 b + Z_0(1 - b)]$ $[\beta_T^{(el)}]_b$, so that

$$[\beta_T^{(W)}]_b = \frac{3[M_1 b + M_0(1 - b)]}{2[E_F]_b \rho_b} . \qquad (4.36)$$

Equation (4.36) gives fair agreement with experiment for the pure metal compressibilities $[\beta_T]_0$ and $[\beta_T]_1$. This expression for the variation of compressibility with alloy composition at a fixed temperature was first derived in Webber and Stephens (1968). Later, Enderby and March (private communication) pointed out that equation (4.35) can be rewritten by substituting for Z_0 and Z_1 from the Bohm-Staver relation. At a fixed temperature, the variation of isothermal compressibility $[\beta_T^{(EM)}]_b$ with alloy composition is then given by

$$[\beta_T^{(EM)}]_b = \frac{M_1 b + M_0(1 - b)}{\left[\dfrac{M_1 b}{[\beta_T]_1 [E_F]_1 \rho_1} + \dfrac{M_0(1 - b)}{[\beta_T]_0 [E_F]_0 \rho_0}\right] [E_F]_b \rho_b} . \qquad (4.37)$$

This approach has the advantage over equation (4.36) of fixing the end points to the known pure component compressibilities and then it is possible to readily compare the theoretical compressibility with experiment for the alloys.

The corresponding sound velocity $[c^{(EM)}]_b$ for the alloy of atomic fraction b, at a fixed temperature, found from equation (4.37) is

$$[c^{(EM)}]_b^2 = \frac{[E_F]_b\left[\frac{M_1 b c_1^2}{[E_F]_1} + \frac{M_0(1-b)c_0^2}{[E_F]_0}\right]}{[M_1 b + M_0(1-b)]} , \qquad (4.38)$$

with the assumption that $\gamma_b' \approx \gamma_1' \approx \gamma'$. This theoretical sound velocity is compared with the experimental sound velocity for mercury alloys in Figs. 3.8 to 3.13, where it is seen that this approach gives the correct graphical curvature for the variation of sound velocity with composition for mercury-zinc, mercury-lead and mercury-bismuth. For mercury-cadmium, mercury-indium and mercury-tin alloys theory gives the oppostie graphical curvature for the variation of sound velocity with composition to that found experimentally.

It was decided to apply this theoretical approach for sound velocity to alloy systems of the same valency and experimental data were available for sodium-potassium [Abowitz and Gordon (1962a)] and tin-lead alloys [Gordon (1961)]. The theoretical variations of sound velocity with composition for these two alloy systems are shown in Figs. 4.17 and 4.18 respectively, and are seen to be in fairly close

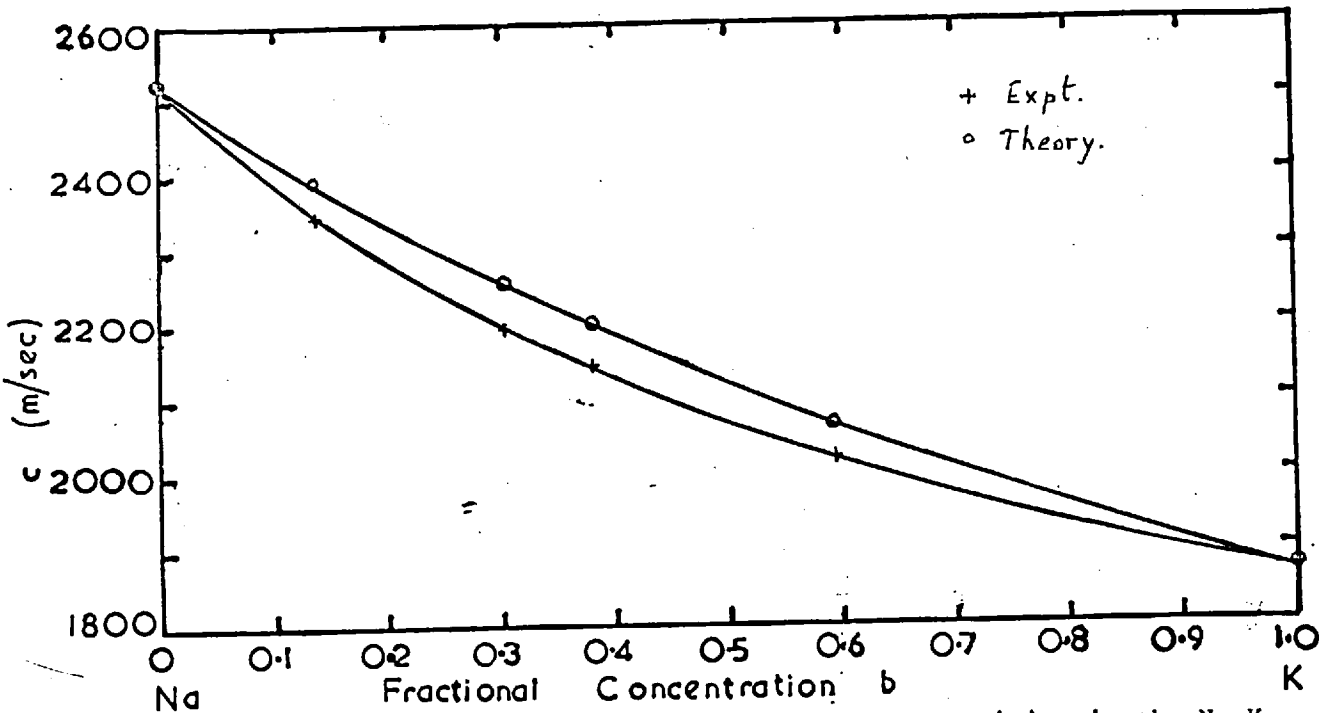

Fig. 4.17. Variation of sound velocity with composition in the Na-K alloy system. Density data taken from "Liquid Metals Handbook, Na-K Supplement".

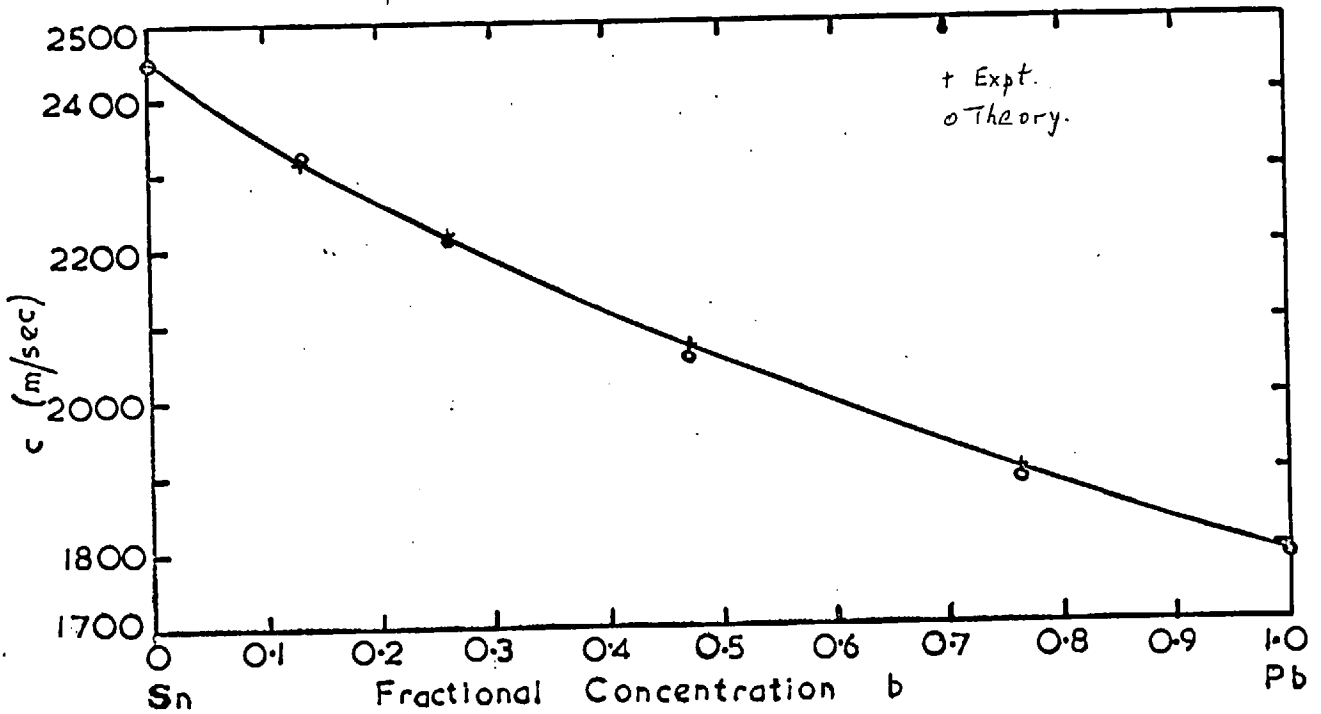

Fig. 4.18. Variation of sound velocity with composition in the Sn-Pb alloy system. Density data obtained from linear interpolation between the two pure component values.

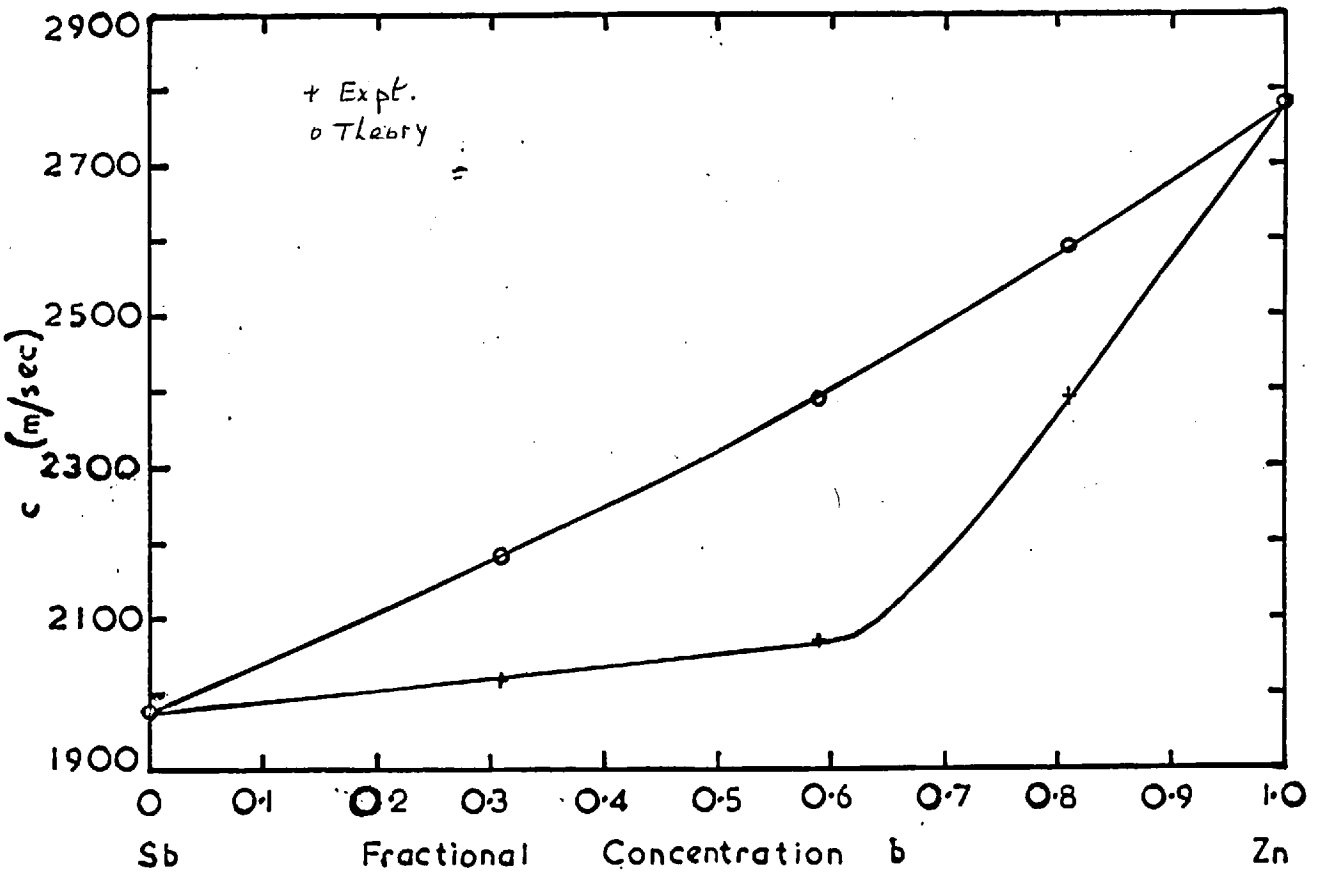

Fig. 4.19. Variation of sound velocity with composition in the Sb-Zn alloy system. Density data taken from Matuyama (1129).

agreement with experiment, particularly for tin-lead. A further system antimony-zinc was examined [see Fig. 4.19]. Although theory gives the correct graphical shape for the variation of sound velocity with composition, the deviation from linearity is not as great as that found experimentally by Kazakov et al. (1964). We conclude that the Bohm-Staver sound velocity for alloys generally agrees fairly well with experiment but exceptions occur amongst mercury alloys.

The theoretical variations of adiabatic compressibility with composition calculated from equation (4.37) for six mercury alloy systems are compared with experiment in Figs. 4.12 to 4.14, where it is seen that the theory gives the correct graphical shape for the variation of compressibility across the whole alloy system for these mercury alloys. The deviations from linearity with composition of experimental values for adiabatic compressibilities are greater than predicted theoretically. It is of interest that for the mercury-bismuth alloy system theory predicts a minimum in compressibility, but the minimum occurs at about 60 at.% Bi rather than at 40 at.% Bi found experimentally.

Abowitz and Gordon (1963) attempt to explain the rapid decrease of compressibility on alloying mercury as being due to the presence of more effective electrons than given by the valence electrons. Although this idea has some support from one interpretation of Hall coefficient data for mercury alloys by Matthews (1966), which indicates an increase

in the effective number of electrons, a strict theoretical account for Hall coefficient values in liquid alloys has not been carried out.

It has been seen that for mercury alloys the free-electron compressibility for alloys does not successfully account for the large decrease of compressibility on alloying. In the following Section 4.6B we shall examine the pseudo-potential approach, which includes energies due to electron-electron, electron-ion and ion-ion interactions, to the calculation of compressibility for alloys.

B. Pseudo-Potential Approach for Alloys

Ashcroft and Langreth (1967a) showed that the pseudo-potential approach to the calculation of compressibility agreed satisfactorily with experiment for simple solid metals. In Section 4.4B the pseudo-potential approach to compressibility for liquid metals was discussed and we shall extend that approach to alloys. We need to consider the Fuchs and band-structure energies which are structure dependent. The partial structure factor $a_{\alpha\beta}$, see Faber and Ziman (1964), is defined by

$$a_{\alpha\beta}(q) = 1 + \frac{4\pi N}{\Omega} \int_0^\infty [g_{\alpha\beta}(r) - 1]\, r^2 \frac{\sin qr}{qr}\, dr, \qquad (4.39)$$

where $g_{\alpha\beta}(r)$ represents the average distribution of type β atoms observed from an α atom at the origin. Here α and β are dummy suffices which may take the values 0 or 1 for a binary alloy. There are therefore

three independent structure factors involved; $a_{11}(q)$, $a_{00}(q)$, and $a_{10}(q)$; it is easily seen that $a_{10}(q)$ and $a_{01}(q)$ are identical. Then Faber and Ziman (1964) show that

$$\sum_{\underline{r}_\alpha}\sum_{\underline{r}_\beta} \exp i\underline{q}.(\underline{r}_\alpha - \underline{r}_\beta) = \sum_{\underline{r}_\alpha}\sum_{\underline{r}_\beta} \delta(\underline{r}_\alpha - \underline{r}_\beta) + \sum_{\underline{r}_\alpha}\sum_{\underline{r}_\beta \neq \underline{r}_\alpha} \exp i\underline{q}.(\underline{r}_\alpha - \underline{r}_\beta)$$

$$= Nc_\alpha\delta_{\alpha\beta} + 4\pi c_\alpha c_\beta \frac{N^2}{\Omega}\int_0^\infty [g_{\alpha\beta} - 1]r^2 \frac{\sin qr}{qr}\,dr$$

$$= Nc_\alpha\delta_{\alpha\beta} + Nc_\alpha c_\beta(a_{\alpha\beta} - 1), \qquad (4.40)$$

where c_α and c_β are the concentrations of the two species. The initial δ-function is needed to cover the case where α and β happen to describe the same species, so that $\underline{r}_\alpha$ and $\underline{r}_\beta$ can refer to the same ion.

The expression for the ion-ion interaction (per ion) in a pure metal of valency Z is given in equation (1.53), which may be rewritten in the form (atomic units)

$$E_{ii} = \frac{4\pi}{N}{\sum_q}' \sum_{i\neq j} Z(q)^2 \exp i\underline{q}.(\underline{r}_i - \underline{r}_j), \qquad (4.41)$$

where $Z(q) = Z/q$. (4.42)

If we multiply Z(q) by its complex conjugate and define the functions

$$Z_\alpha(q) = Z_\alpha/q$$

and $$Z_\beta(q) = Z_\beta/q, \qquad (4.43)$$

where Z_α and Z_β are the valencies of species α and β respectively, then the ion-ion interaction for an alloy is given by

$$[E_{ii}]_{alloy} = \frac{4\pi}{N} \sum_{q}{}' \sum_{\alpha} \sum_{\beta} Z_\alpha(q) Z_\beta(q) \sum_{\underline{r}_\alpha} \sum_{\underline{r}_\alpha \neq \underline{r}_\beta} \exp i\underline{q}.(\underline{r}_\alpha - \underline{r}_\beta)$$

$$= \frac{4\pi}{N} \sum_{q}{}' \sum_{\alpha} \sum_{\beta} Z_\alpha(q) Z_\beta(q)\, N c_\alpha c_\beta (a_{\alpha\beta} - 1)$$

$$= 4\pi \sum_{q}{}' [Z_\alpha(q)^2 c_\alpha^2 (a_{\alpha\alpha} - 1) + Z_\beta(q)^2 c_\beta^2 (a_{\beta\beta} - 1) + 2 Z_\alpha(q) Z_\beta(q) c_\alpha c_\beta (a_{\alpha\beta} - 1)]$$

$$= 4\pi \sum_{q}{}' \frac{1}{q^2} [Z_0^2 (1 - b)^2 (a_{00} - 1) + Z_1^2 b^2 (a_{11} - 1) + 2 Z_1 Z_0 b (1 - b)(a_{10} - 1)]. \qquad (4.44)$$

Here b is the atomic fraction of species β or 1, Z_0 and Z_1 are the valencies of the two species. If Z^* is an effective valency determined from the ratio of the electron density to the ion density, the Fuchs term (per electron) becomes on replacing the sum by an integral

$$\frac{E_{ii}}{Z^*} = \frac{2}{\pi Z^*} \int_0^\infty [Z_0^2 (1 - b)^2 (a_{00} - 1) + Z_1^2 b^2 (a_{11} - 1) + 2 Z_0 Z_1 b (1 - b)(a_{10} - 1)] dq. \qquad (4.45)$$

The Fuchs terms for the pure components of the alloy are obtained when b equals 0 or 1. As expected, the evaluation of the Fuchs term depends

upon knowledge of the partial structure factors $a_{00}(q)$, $a_{11}(q)$ and $a_{10}(q)$, which are not available experimentally for mercury alloys. However, Ashcroft and Langreth (1967b, 1968) have extended the Percus-Yevick equation for a system of hard-spheres to binary systems and their partial structure factors could be used to evaluate the Fuchs term.

The band-structure energy E_{BS} (per ion) for a pure metal has been discussed in Section 1.3F and is given in equation (1.54), which may be written in the form

$$E_{BS} = \frac{1}{16\pi\Omega N} \sum_{q}{}' \sum_{i} \sum_{j} q^2 \, V(q)^2 \left(\frac{1}{\varepsilon} - 1\right) \exp i\underline{q}(\underline{r}_i - \underline{r}_j), \qquad (4.46)$$

where $V(q)$ is the qth Fourier component of the bare interaction of an electron with a single ion. If we multiply $V(q)$ by its complex conjugate and label $V_\alpha(q)$ and $V_\beta(q)$ as the qth Fourier components of the bare interactions of an electron with ions of species α and β, then the band-structure energy for an alloy becomes

$$\begin{aligned}
[E_{BS}]_{alloy} &= \frac{1}{16\pi\Omega N} \sum_{q}{}' \sum_{\alpha} \sum_{\beta} q^2 \left(\frac{1}{\varepsilon} - 1\right) V_\alpha(q) V_\beta(q) \sum_{\underline{r}_\alpha} \sum_{\underline{r}_\beta} \exp i\underline{q}(\underline{r}_\alpha - \underline{r}_\beta) \\
&= \frac{1}{16\pi\Omega N} \sum_{q}{}' q^2 \left(\frac{1}{\varepsilon} - 1\right) \sum_{\alpha} \sum_{\beta} V_\alpha(q) V_\beta(q) \left[N c_\alpha \delta_{\alpha\beta} + N c_\alpha c_\beta (a_{\alpha\beta} - 1)\right] \\
= &= \frac{1}{16\pi\Omega} \sum_{q}{}' q^2 \left(\frac{1}{\varepsilon} - 1\right) \left[V_\alpha(q)^2 c_\alpha + V_\beta(q)^2 c_\beta + V_\alpha(q)^2 c_\alpha^2 (a_{\alpha\alpha} - 1)\right. \\
&\qquad \left. + V_\beta(q)^2 c_\beta^2 (a_{\beta\beta} - 1) + 2 V_\alpha(q) V_\beta(q) c_\alpha c_\beta (a_{\alpha\beta} - 1)\right]
\end{aligned}$$

$$= \frac{1}{16\pi\Omega} \sum_{q}{}' q^2\left(\frac{1}{\varepsilon} - 1\right)\left[V_0(q)^2(1 - b) + V_1(q)^2 b + V_0(q)^2(1 - b)^2\right.$$

$$(a_{00} - 1) + V_1(q)^2 b^2 (a_{11} - 1) + 2V_0(q)V_1(q)b$$

$$\left.(1 - b)(a_{10} - 1)\right]. \qquad (4.47)$$

Here $V_0(q)$ and $V_1(q)$ are the Fourier transforms of the bare electron-ion interactions for species 0 and 1, respectively, immersed in the same screening cloud of electrons. Replacing the sum by an integral, the band-structure energy E_{BS}/Z^* (per electron) becomes

$$\frac{E_{BS}}{Z^*} = \frac{1}{32\pi^3 Z^*} \int_0^\infty q^4\left(\frac{1}{\varepsilon} - 1\right)\left[V_0(q)^2(1 - b) + V_1(q)^2 b + V_0(q)^2(1 - b)^2\right.$$

$$(a_{00} - 1) + V_1(q)^2 b^2 (a_{11} - 1) + 2V_0(q)V_1(q)b$$

$$\left.(1 - b)(a_{10} - 1)\right]dq \ . \qquad (4.48)$$

This expression reduces to the pure component values for the band-structure energies when b equals 0 or 1. Evaluation of the band-structure energy depends upon knowledge of $V_0(q)$, $V_1(q)$, $a_{00}(q)$, $a_{11}(q)$ and $a_{10}(q)$, which are not available experimentally for mercury alloys.

The total energy E_b for the alloy of atomic fraction b may therefore be written in the form

$$E_b = \frac{2.21}{r_s^2} - \frac{0.916}{r_s} - (0.115 - 0.031\ell nr_s) + \frac{3A}{4\pi r_s^3}$$

$$+ \frac{2}{\pi Z^*}\int_0^\infty [Z_0^2(1-b)^2(a_{00}-1) + Z_1^2 b^2(a_{11}-1) + 2Z_0Z_1 b(1-b)$$

$$(a_{10}-1)]dq + \frac{1}{32\pi^3 Z^*}\int_0^\infty q^4(\frac{1}{\epsilon}-1)[V_0(q)^2(1-b) + V_1(q)^2 b$$

$$+ V_0(q)^2(1-b)^2(a_{00}-1) + V_1(q)^2 b^2(a_{11}-1) + 2V_0(q)V_1(q)b$$

$$(1-b)(a_{10}-1)]dq. \qquad (4.49)$$

Here the value of r_s is calculated from the electron density of the alloy. In order to calculate the isothermal compressibility in the usual manner it is necessary to know the volume dependences of the pseudo-potentials and partial structure factors, which are not known experimentally or theoretically for alloys.

C. Hard-Sphere Model

Ashcroft and Langreth (1967b) have derived the isothermal compressibility for a binary mixture of hard-spheres of atomic fraction b, $[\beta_T^{(h)}]_b$. For binary systems equation (1.13) must be modified in the following manner:-

$$\left[\beta_T^{(h)}\right]_b = \frac{\Omega_b\,(1 - z_b)^4}{N_b k_B T\left[(1 + 2z_b)^2 - \Delta_b\right]} \quad , \tag{4.50}$$

where Δ_b is given by the expression

$$\Delta_b = \frac{3b(1 - b)z_b(1 - f)^2}{b + f^3(1 - b)}\left\{(2 + z_b)(1 + f) + \frac{3z_b f}{b + f^3(1 - b)}\left[f^2(1 - b) + b\right]\right\}. \tag{4.51}$$

Here b is the atomic fraction of species 1 with the largest hard-sphere diameter, and f is the ratio of the hard-sphere diameter of species 0 to that of species 1. The value of f is therefore

$$f = \sigma_o/\sigma_1 \quad , (0 \leq f \leq 1). \tag{4.52}$$

It is usual to calculate the value of the packing fraction z_b for atomic fraction b, at a fixed temperature, by using a linear interpolation between the two pure component values, z_0 and z_1, such that

$$z_b = z_1 b + z_0(1 - b). \tag{4.53}$$

Jarzynski et al. (1969) use this approach to calculate the isothermal compressibilities of sodium-potassium alloys. They find that the hard-sphere compressibilities are in good agreement with experiment when the value of f is taken to be 0.72. For polyvalent metals, however,

the hard-sphere compressibilities are considerably smaller than experimental compressibilities and therefore this approach is not readily applicable to polyvalent alloys.

D. Semi-Phenomenological Hard-Sphere Model

The isothermal compressibilities for liquid metals calculated on the basis of the semi-phenomenological model proposed by Ascarelli (1968) are in good agreement with experiment (see Sections 1.3F and 4.4C) and we decided to extend this model to alloys. For liquid metals, Ascarelli proposed that the total pressure is due to the sum of the pressure derived from the total energy of the system, expressed by equation (1.82), and the pressure of a hard-sphere fluid. In a similar manner, we propose that the total pressure for an alloy system is due to the sum of the pressure derived from the total energy of the alloy system and the pressure for a mixture of hard-spheres of atomic fraction b, $[p_h]_b$. We must first calculate $[p_h]_b$ and this may be derived from equations (4.50) and (4.51). Ashcroft and Langreth (1967b) define the total packing fraction for the mixture by

$$z_b = \frac{\pi}{6\Omega_b}\left[N_0\sigma_0^3 + N_1\sigma_1^3\right], \qquad (4.54)$$

$$= D_b/\Omega_b \quad ,$$

where there are N_0 hard-spheres of diameter σ_0 and N_1 with diameter σ_1 (in the volume Ω_b). For simplicity, D_b is defined from equation (4.54). From equations (4.50) and (4.54) it can readily be shown that the variation of the hard-sphere pressure with packing fraction, at constant temperature, $(\partial p_h/\partial z)_T$, is given by

$$\left(\frac{\partial p_h}{\partial z}\right)_T = \frac{N_b k_B T}{D_b}\left[\frac{(1 + 2z_b)^2 - \Delta_b}{(1 - z_b)^4}\right] \quad . \tag{4.55}$$

We may rewrite Δ_b given by equation (4.51) in the form

$$\Delta_b = H_b z_b + F_b z_b^2 \quad , \tag{4.56}$$

where

$$H_b = \frac{6b(1 - b)(1 - f)^2(1 + f)}{b + f^3(1 - b)} \tag{4.57}$$

and

$$F_b = \frac{3b(1 - b)(1 - f)^2[(1 + 4f)b + (4f^3 + f^4)(1 - b)]}{[b + f^3(1 - b)]^2} \quad . \tag{4.58}$$

Integration of equation (4.55) with respect to packing fraction gives the pressure $[p_h]_b$ due to a mixture of hard-spheres of atomic fraction b, at a fixed temperature T, in the following manner:-

$$[p_h]_b = \frac{N_b k_B T}{D_b}\int\left\{\frac{9}{(1 - z_b)^4} - \frac{12}{(1 - z_b)^3} + \frac{4}{(1 - z_b)^2} - \frac{(H_b + F_b)}{(1 - z_b)^4} + \frac{(H_b + 2F_b)}{(1 - z_b)^3} - \frac{F_b}{(1 - z_b)^2}\right\}dz_b$$

$$= \frac{N_b k_B T}{D_b}$$

$$\left[\frac{1 - 2z_b + 4z_b^2 + G_b(1-z_b)^3 + (\{(H_b - 2F_b) + (6F_b - 3H_b)z_b - 6F_b z_b\}/6)}{(1 - z_b)^3}\right] \tag{4.59}$$

Here G_b is a constant of integration. For a single component system of hard-spheres $\Delta_b = H_b = F_b = 0$ and equation (4.59) reduces to the usual hard-sphere pressure, see equation (1.11), when G_b takes the value -1. The equation of state for a mixture of hard-spheres of atomic fraction b is therefore expressed by

$$\left[\frac{P_h \Omega}{N k_B T}\right]_b = \frac{1 + z_b + z_b^2 + (\{(H_b - 2F_b) + (6F_b - 3H_b)z_b - 6F_b z_b^2\}/6z_b)}{(1 - z_b)^3} \tag{4.60}$$

This expression for the pressure due to a mixture of hard-spheres reduces to the usual hard-sphere pressure when b equals 0 or 1.

The volume dependences of the interactions which contribute to the total energy of the alloy system are the same as those discussed in Section 1.3G for pure metals. With the same approximations as assumed by Ascarelli (1968) for pure metals, the total energy $[E^{(A)}]_b$ of the alloy system at temperature T_o may be written in the form [c.f. Eq. (1.82)]

$$\frac{N_b[E^{(A)}]_b}{k_B T_o} = \frac{3N_b Z_b^* [E_F]_b}{5k_B T_o} - 3C_b N_b \left(\frac{\Omega_o}{\Omega}\right)^{1/3}, \tag{4.61}$$

where $[E_F]_b$ is the free-electron Fermi energy for an alloy of atomic

fraction b, at temperature T_o, Ω_o the volume of the system at temperature T_o and zero pressure, Z_b^* the effective valency and C_b a dimensionless constant. The subscripts b indicate that the physical quantities are evaluated for atomic fraction b. On the free-electron model, if Z_o and Z_1 are the valencies of species 0 and 1 respectively, then the effective valency is simply

$$Z_b^* = Z_1 b + Z_0(1 - b) \ . \tag{4.62}$$

In this semi-phenomenological model, the total pressure for the alloy of atomic fraction b, at a fixed temperature T_o, is assumed to be given by

$$\left[\frac{p\Omega}{Nk_BT_o}\right]_b = \frac{2Z_b^*[E_F]_b}{5k_BT_o} - C_b\left(\frac{\Omega_o}{\Omega}\right)^{1/3} + \frac{1 + z_b + z_b^2 + (\{(H_b - 2F_b) + (6F_b - 3H_b)z_b - 6F_b z_b^2\}/6z_b)}{(1 - z_b)^3} \ . \tag{4.63}$$

When the alloy system is under an ambient pressure of one atmosphere and at a fixed temperature T_o, we may approximate the pressure to zero and hence determine C_b from equation (4.63). Thus

$$C_b = \frac{2Z_b^*[E_F]_b}{5k_BT_o} + \frac{1 + z_b + z_b^2 + (\{(H_b - 2F_b) + (6F_b - 3H_b)z_b - 6F_b z_b^2\}/6z_b)}{(1 - z_b)^3} \ . \tag{4.64}$$

The isothermal compressibility $[\beta_T^{(A)}]_b$ for the alloy of atomic fraction b, at a fixed temperature T_o, may be calculated from equation (4.63) in the usual manner and is given by

$$\frac{1}{[\beta_T^{(A)}]_b} = \frac{N_b k_B T_o}{\Omega_b}\left[\frac{(1+2z_b)^2 - \Delta_b}{(1-z_b)^4} + \frac{2Z_b^*[E_F]_b}{3k_B T_o} - \frac{4C_b}{3}\right]. \quad (4.65)$$

Substitution of the value of C_b given by equation (4.64) into equation (4.65) gives

$$\frac{1}{[\beta_T^{(A)}]_b} = \frac{N_b k_B T_o}{\Omega_b}$$

$$\left[\left\{4z_b^3 + 12z_b^2 + 12z_b - 1 + (\{(4F_b - 2H_b) - (16F_b - 8H_b)z_b + (24F_b - 15H_b)z_b^2 - 21F_b z_b^3\}/3z_b)\right\}/3(1-z_b)^4 + \frac{2Z_b^*[E_F]_b}{15k_B T_o}\right]. \quad (4.66)$$

Therefore in this semi-phenomenological model the isothermal compressibility for the alloy of atomic fraction b, at temperature T_o, may be written in the form

$$\frac{1}{[\beta_T^{(A)}]_b} = \frac{N_b k_B T_o}{\Omega_b}\left[\frac{4z_b^3 + 12z_b^2 + 12z_b - 1 + \delta_b}{3(1-z_b)^4} + \frac{2Z_b^*[E_F]_b}{15k_B T_o}\right], \quad (4.67)$$

where

$$\delta_b = \{\{(4F_b - 2H_b) - (16F_b - 8H_b)z_b + (24F_b - 15H_b)z_b^2 - 21F_b z_b^3\}/3z_b\}. \tag{4.68}$$

This expression reduces to the expression for the isothermal compressibility of a pure metal given by equation (1.87) when $\delta_b = 0$ and $z_b = 0.45$. This theoretical variation of isothermal compressibility with alloy composition would be useful to compare with experiment for alloys since the pure component isothermal compressibilities are reproduced fairly well. The sound velocity $[c^{(A)}]_b$ for the alloy of atomic fraction b, at temperature T_o, can be obtained from equations (4.67) and (4.68), and is given by

$$[c^{(A)}]_b^2 = \frac{\gamma_b' k_B T_o}{[M_1 b + M_0(1-b)]} \left[\frac{4z_b^3 + 12z_b^2 + 12z_b - 1 + \delta_b}{3(1 - z_b)^4} + \frac{2Z_b^* [E_F]_b}{15 k_B T_o} \right]. \tag{4.69}$$

Here γ_b' is the theoretical ratio of principal specific heats for the alloy, M_0 and M_1 the atomic masses of species 0 and 1 respectively. Numerical calculations of the theoretical sound velocity $[c^{(A)}]_b$ for alloys are not yet available to compare with experimental values of sound velocity.

4.7 Conclusion

The ratio of bulk to shear viscosity for mercury has been measured

to be 0.86 ± 0.3 and within experimental error is independent of temperature in the temperature range of the experiment. Correction of the data due to Hunter et al. (1963) gives the most reliable value for η_B/η_s as 0.62 ± 0.1. A review of the values of η_B/η_s for various liquid metals shows that mercury has a comparatively low value for this ratio. Potassium, zinc, mercury and gallium appear to have values of η_B/η_s less than unity, whilst indium and antimony have values greater than four for this ratio. The dense-gas formulation for ultrasonic absorption in liquid metals is found to give reasonable estimates for bulk viscosity and η_B/η_s. Modification of the theory would appear to be necessary to account for experimental values of η_B/η_s which differ significantly from unity. It should be possible to extend this theory to alloys, where comparison can be made with sound absorption measurements which are already available for sodium-potassium, tin-lead, silver-tin, and mercury-thallium alloys. Abowitz and Gordon (1962b) have found that relaxation phenomena occur in mercury-thallium alloys and therefore it would be of interest to perform sound absorption measurements on other mercury alloy systems.

The present investigation of the sound velocity and adiabatic compressibility of six mercury alloy systems has shown that the adiabatic compressibility decreases rapidly with increasing concentration of solute. These measurements confirm the decrease of adiabatic compressibility in dilute mercury alloys found by Golik et al. (1961)

and Abowitz and Gordon (1963). The present study of these alloys over the whole range of concentration shows that for concentrations up to 40 at.% solute the variation of adiabatic compressibility with concentration is similar to the behaviour of the mercury-thallium system. In the mercury-lead and mercury-bismuth systems the adiabatic compressibilities exhibit minima at about 70 at.% Pb and 40 at.% Bi respectively, whereas theory predicts a minimum at about 60 at.% Bi. The free-electron compressibility for alloys gives the correct graphical shape for the variation of compressibility across the whole alloy system for these six mercury alloy systems but the deviations from linearity with composition of experimental values for adiabatic compressibility are greater than predicted theoretically.

When applied to the six mercury alloy systems the Bohm-Staver sound velocity for alloys gives the correct graphical curvature for the variation of sound velocity with composition only for mercury-zinc, mercury-lead and mercury-bismuth alloys. For sodium-potassium and tin-lead alloys the theoretical variation of sound velocity with composition is in fairly close agreement with experiment. The theoretical deviation of sound velocity from linearity with composition in antimony-zinc alloys is not as great as that found experimentally.

The pseudo-potential approach to the compressibility of simple solid metals and the semi-phenomenological model for liquid metals due to Ascarelli have been seen to give fairly good agreement with experiment.

These two theoretical approaches to compressibility have been extended to liquid alloy systems and further numerical calculations are required before comparison can be made with experiment. Calculation of isothermal compressibility using a pseudo-potential approach requires more theoretical and experimental knowledge of the volume dependences of pseudo-potentials and partial structure factors. The isothermal compressibility derived by considering a mixture of hard-spheres in a uniform background potential is simpler to evaluate and further work is being carried out in this direction by the author.

It has been seen that sound velocity measurements provide a means of calculating the adiabatic and isothermal compressibilities of high melting point metals where direct measurements of isothermal compressibility are difficult to perform. Fused silica can be used as the material for the acoustic delay rod and container up to temperatures of about 1050^{o}C and therefore it would be possible to investigate the propagation of sound in liquid gold and germanium. It is also of interest to investigate the propagation of sound in liquid metals and alloys subject to applied pressure in order to gain further knowledge of the equation of state of these materials. Further investigations of the effect on sound velocity and compressibility of the addition of solutes, with different valencies, to a particular metal are required in order to make comparison with theory.

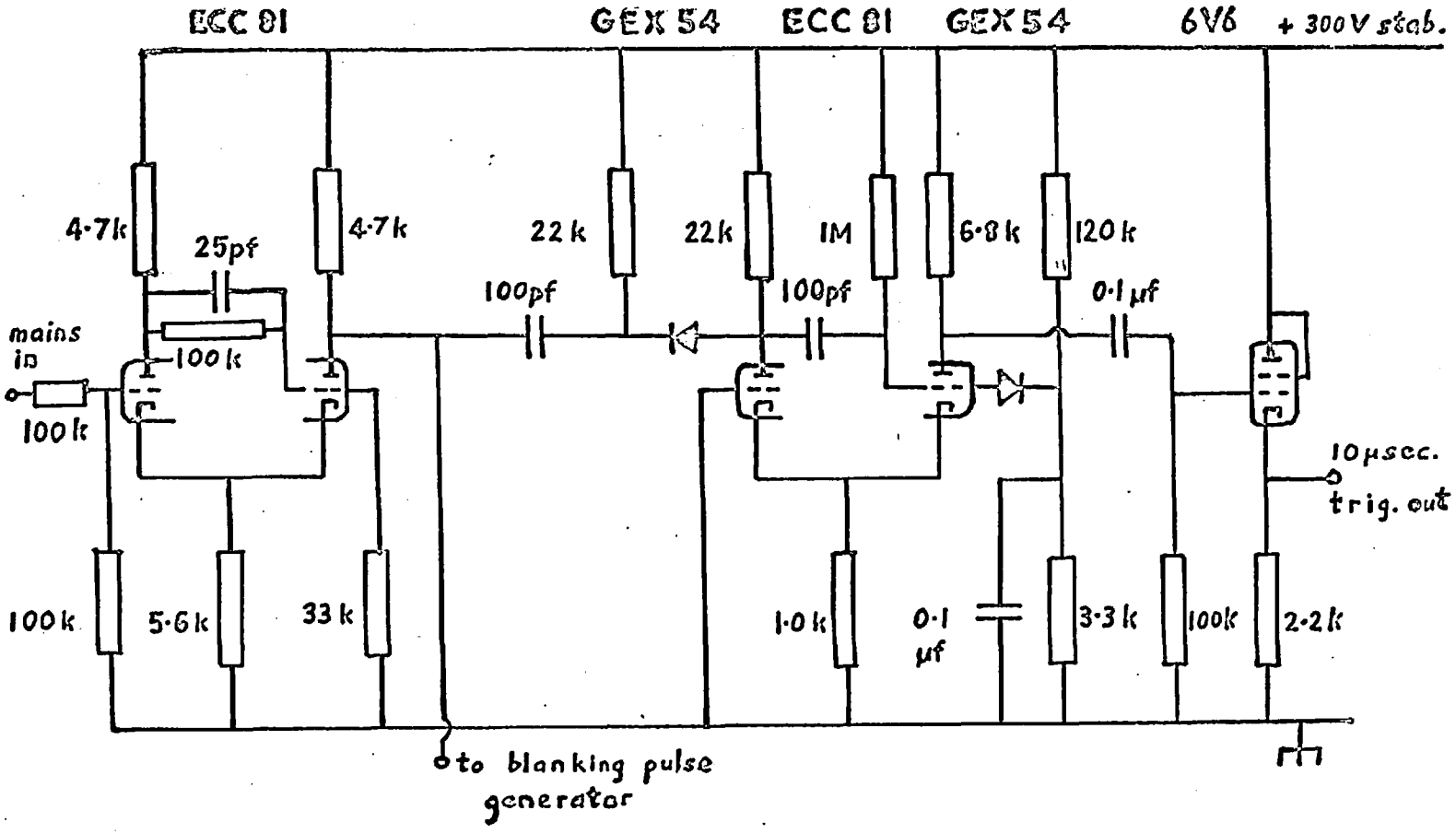

Fig. A. I. Pulse Generator (I)

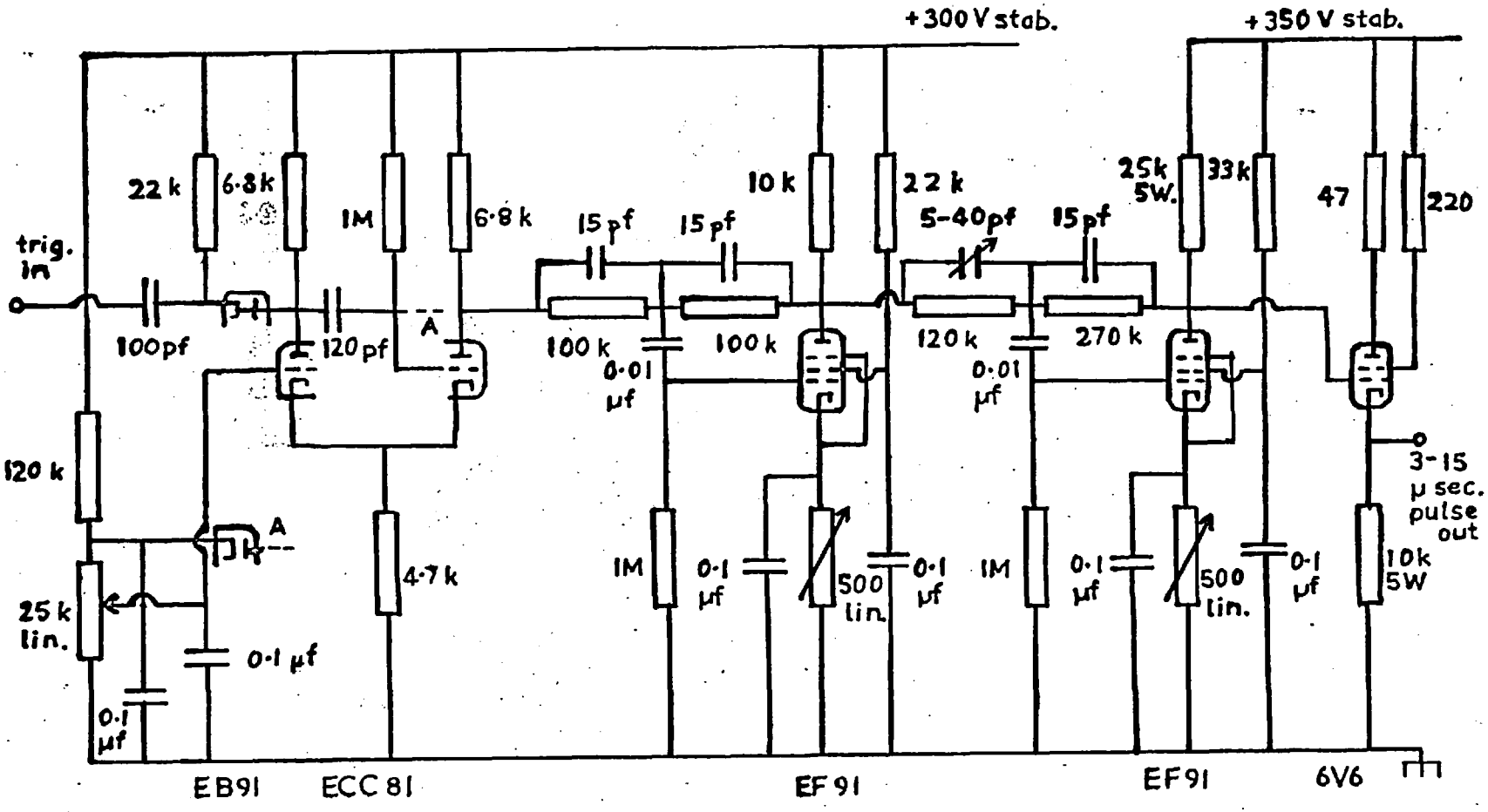

Fig.A.2. Pulse Generator (2)

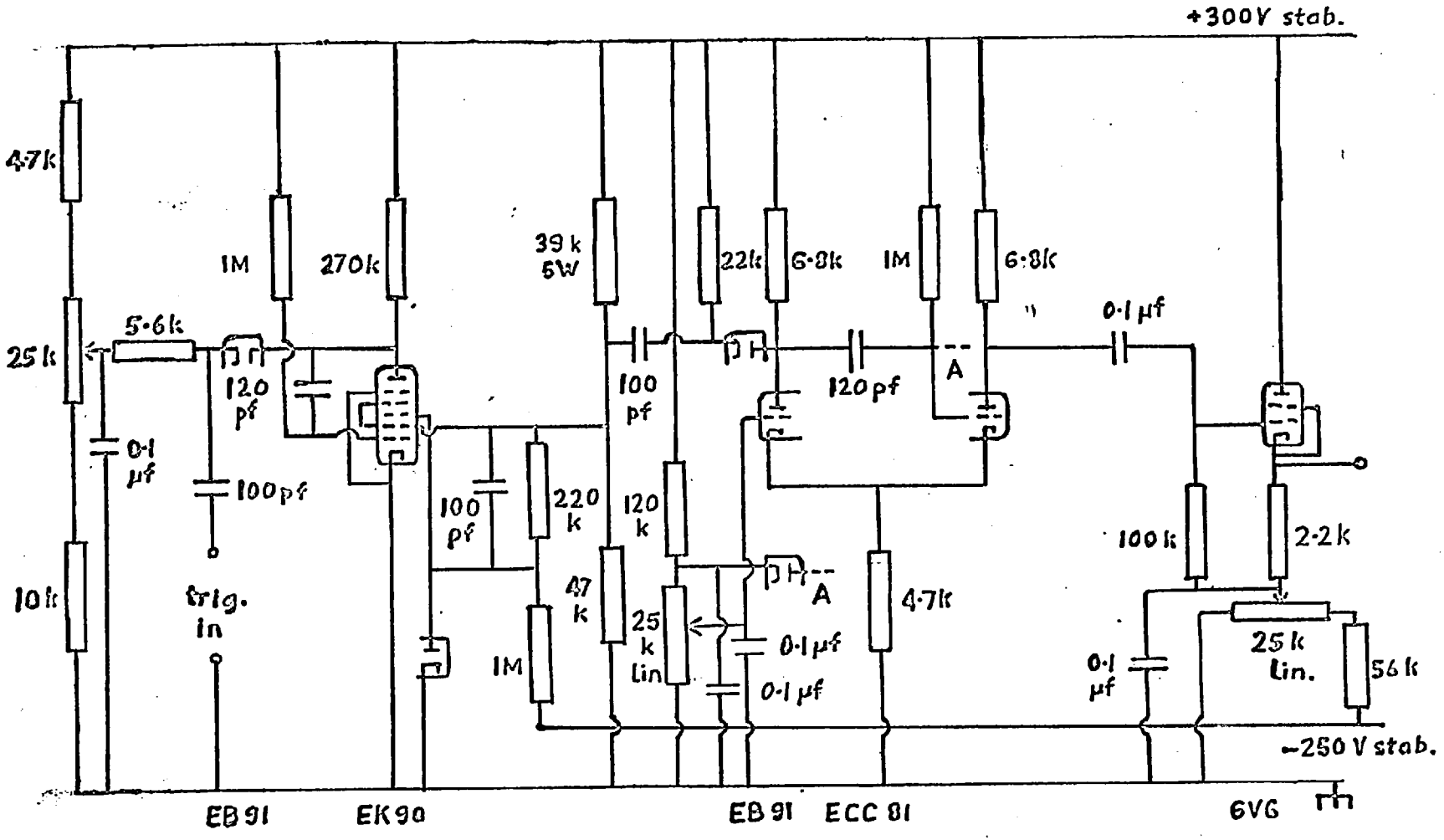

Fig. A.3. Pulse delay generator.

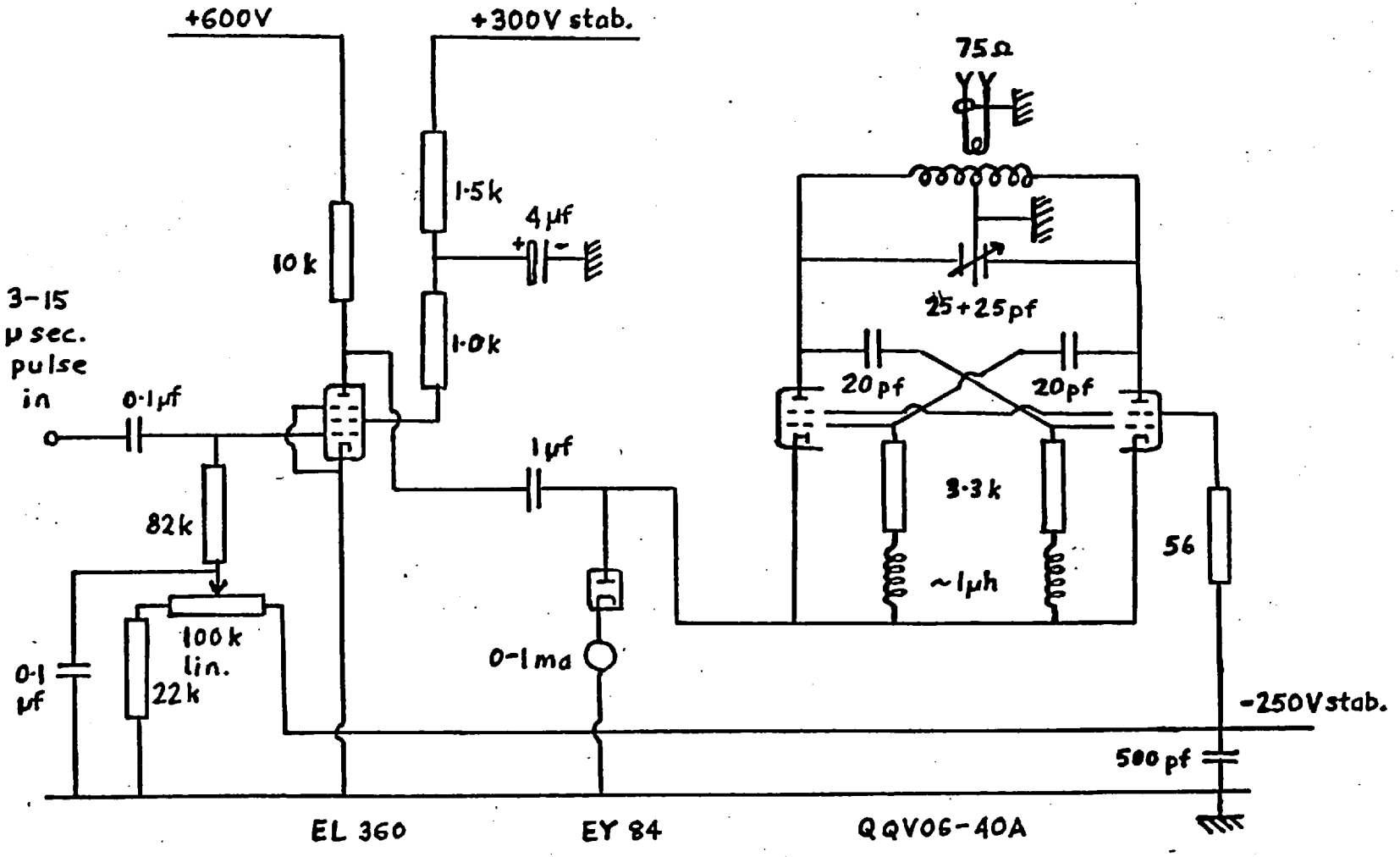

Fig. A.4. Transmitter.

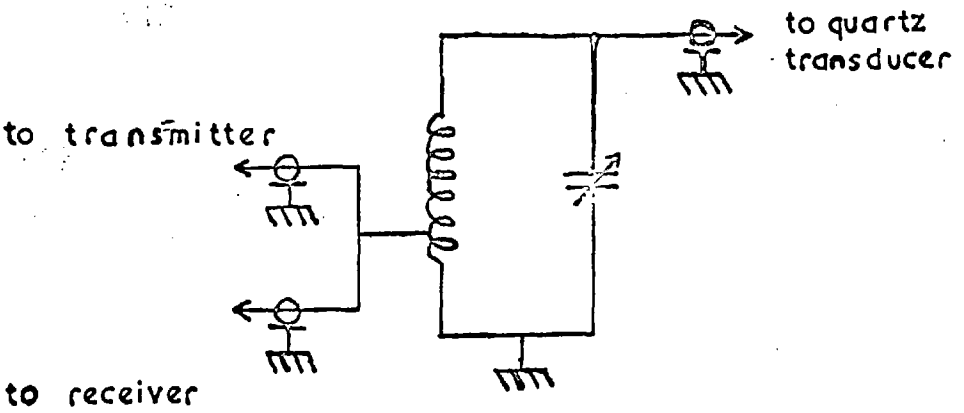

Fig. A.5. Matching Unit.

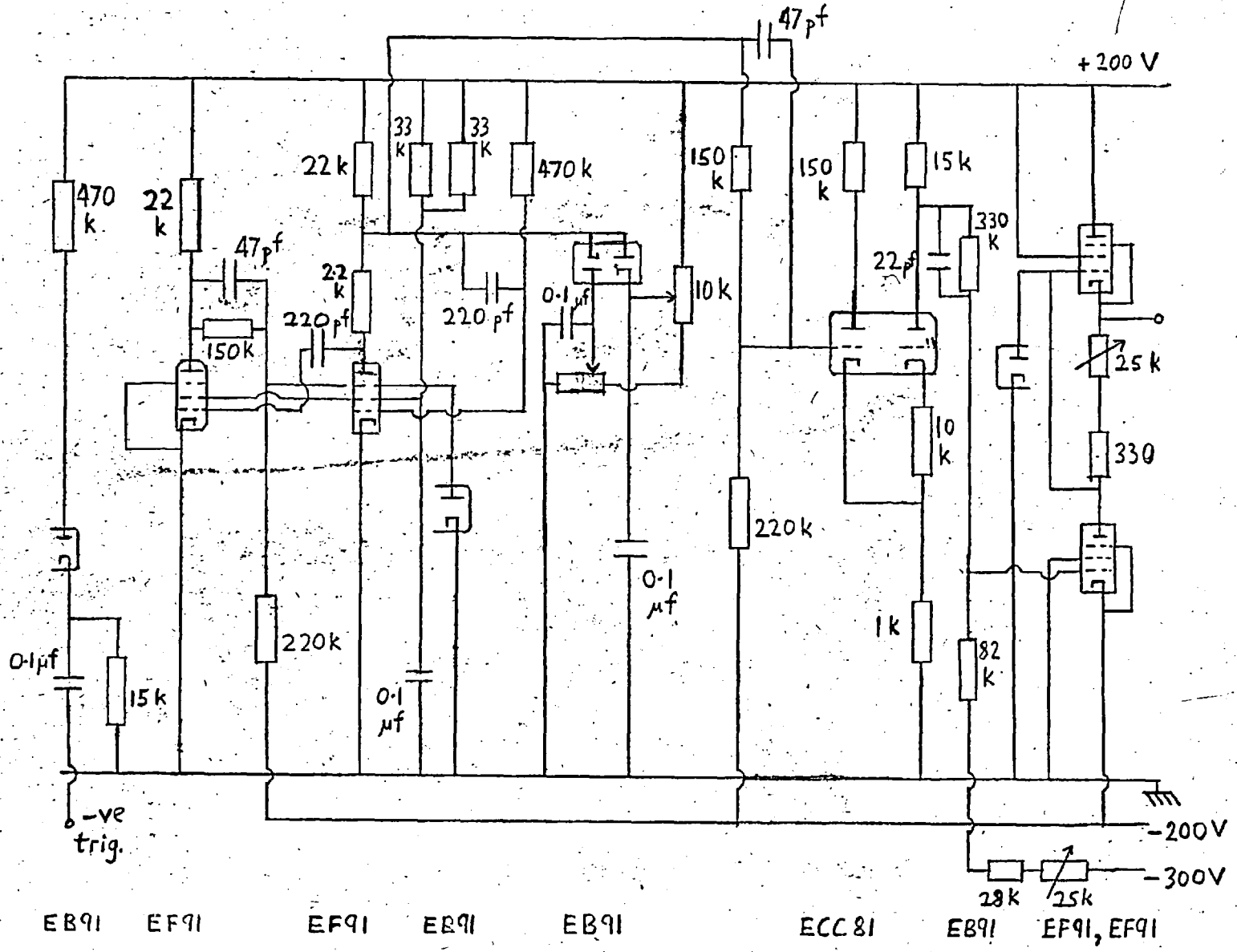

Fig. A.6. Blanking pulse generator.

Table A.1 Comparison of Theoretical and Experimental Values for Sound Velocity and Adiabatic Compressibility at 158°C for the Mercury-Zinc Alloy System

Atomic fraction of Zn b	ρ[a] (gm/cm^3)	Expt. c (m/sec)	Theory $[c^{(EM)}]_b$ (m/sec)	Expt. $\beta_s \times 10^{12}$ (cm^2/dyne)	Theory $[\beta_s^{(EM)}]_b \times 10^{12}$ (cm^2/dyne)
0	13.21	1389	1389	3.92	3.92
0.0201	13.17	1421	1404	3.76	3.85
0.0503	13.08	1468	1428	3.55	3.75
0.100	12.92	1535	1470	3.29	3.58
0.150	12.74	1498	1510	3.07	3.44
0.200	12.54	1655	1554	2.91	3.30
0.250	12.33	1712	1601	2.77	3.16
0.300	12.07	1770	1650	2.64	3.04
0.350	11.81	1829	1702	2.53	2.92
0.400	11.53	1887	1757	2.44	2.81
0.500	10.94	2008	1880	2.27	2.59
1	6.740	2957	2957	1.70	1.70

[a] Kleppa et al. (1961).

Table A.2 Comparison of Theoretical and Experimental Values for Sound Velocity and Adiabatic Compressibility at 158°C for the Mercury-Cadmium Alloy System

Atomic fraction of Cd b	ρ[a] (gm/cm^3)	Expt. c (m/sec)	Theory $[c^{(EM)}]_b$ (m/sec)	Expt. $\beta_s \times 10^{12}$ (cm^2/dyne)	Theory $[\beta_s^{(EM)}] \times 10^{12}$ (cm^2/dyne)
0	13.21	1389	1389	3.92	3.92
0.0200	13.15	1416	1403	3.79	3.86
0.0500	13.05	1454	1424	3.63	3.78
0.100	12.82	1513	1459	3.41	3.67
0.150	12.68	1566	1496	3.22	3.52
0.200	12.47	1617	1535	3.07	3.40
0.250	12.26	1666	1574	2.94	3.29
0.300	12.04	1713	1613	2.83	3.19
0.350	11.82	1757	1654	2.74	3.09
0.400	11.59	1801	1696	2.66	3.00
0.500	11.09	1883	1782	2.54	2.84
0.600	10.55	1963	1873	2.46	2.70
0.700	9.977	2040	1969	2.41	2.58
1	8.134	2303	2303	2.32	2.32

[a]Kleppa et al. (1961).

Table A.3 Comparison of Theoretical and Experimental Values for Sound Velocity and Adiabatic Compressibility at 160°C for the Mercury-Indium Alloy System

Atomic fraction of In b	ρ[a] (gm/cm^3)	Expt. c (m/sec)	Theory $[c^{(EM)}]_b$ (m/sec)	Expt. $\beta_s \times 10^{12}$ (cm^2/dyne)	Theory $[\beta_s^{(EM)}]_b \times 10^{12}$ (cm^2/dyne)
0	13.21	1388	1388	3.93	3.93
0.0060	13.18	1399	1392	3.88	3.92
0.0100	13.15	1405	1395	3.85	3.91
0.0150	13.13	1411	1399	3.83	3.89
0.0200	13.10	1419	1403	3.79	3.88
0.0200	13.10	1419	1403	3.79	3.88
0.0500	12.94	1464	1424	3.61	3.81
0.0800	12.78	1504	1447	3.46	3.74
0.0946	12.70	1524	1458	3.39	3.70
0.140	12.44	1578	1492	3.23	3.61
0.181	12.19	1622	1524	3.12	3.53
0.250	11.78	1692	1577	2.97	3.42
0.300	11.47	1739	1617	2.88	3.33
0.350	11.16	1781	1659	2.83	3.26
0.400	10.84	1822	1700	2.78	3.19
0.500	10.20	1904	1787	2.71	3.07
0.600	9.564	1981	1877	2.66	2.97
0.725	8.781	2080	2002	2.63	2.84
1	7.062	2317	2317	2.64	2.64

[a] Davies (1966).

Table A.4 Comparison of Theoretical and Experimental Values for Sound Velocity and Adiabatic Compressibility at 240°C for the Mercury-Tin Alloy System

Atomic fraction of Sn b	ρ[a] (gm/cm^3)	Expt. c (m/sec)	Theory $[c^{(EM)}]_b$ (m/sec)	Expt. $\beta_s \times 10^{12}$ (cm^2/dyne)	Theory $[\beta_s^{(EM)}]_b \times 10^{12}$ (cm^2/dyne)
0	13.02	1351	1351	4.21	4.21
0.0200	12.90	1405	1370	3.93	4.13
0.0500	12.73	1463	1398	3.67	4.02
0.100	12.44	1531	1446	3.43	3.85
0.142	12.19	1587	1486	3.26	3.72
0.200	11.85	1652	1543	3.09	3.55
0.250	11.54	1710	1592	2.97	3.42
0.300	11.23	1764	1642	2.86	3.30
0.400	10.62	1870	1744	2.69	3.10
0.499	9.989	1968	1848	2.58	2.93
0.598	9.372	2066	1957	2.50	2.79
0.748	8.455	2213	2134	2.42	2.60
0.899	7.562	2369	2329	2.36	2.44
1	6.982	2472	2472	2.34	2.34

[a] Davies (1966).

Table A.5 Comparison of Theoretical and Experimental Values for Sound Velocity and Adiabatic Compressibility at 158°C for the Mercury-Lead Alloy System

Atomic fraction of Pb	ρ[a] (gm/cm^3)	expt. c (m/sec)	Theory $\lvert c^{(EM)} \rvert_b$ (m/sec)	Expt. $\beta_s \times 10^{12}$ (cm^2/dyne)	Theory $\lvert \beta_s^{(EM)} \rvert_b \times 10^{12}$ (cm^2/dyne)
0	13.21	1389	1389	3.92	3.92
0.0200	13.20	1432	1401	3.70	3.86
0.0400	13.17	1457	1414	3.58	3.80
0.0500	13.15	1469	1419	3.52	3.78
0.0527	13.15	1473	1420	3.50	3.77
0.0800	13.11	1496	1436	3.41	3.69
0.0971	13.08	1508	1448	3.36	3.65
0.150	12.97	1550	1478	3.21	3.53
0.200	12.86	1585	1505	3.10	3.43
0.250	12.74	1620	1531	2.99	3.35
0.300	12.61	1653	1557	2.90	3.27
0.350	12.48	1683	1581	2.83	3.20
0.400	12.34	1711	1605	2.77	3.14
0.450	12.21	1737	1629	2.71	3.09
0.500	12.09	1760	1652	2.67	3.03
0.600	11.84	1798	1697	2.61	2.93
0.700	11.61	1829	1741	2.57	2.84
0.796	11.39	1851	1780	2.56	2.77
1	10.97	1863	1863	2.63	2.63

[a] Kleppa et al. (1961)

Table A.6 Comparison of Theoretical and Experimental Values for Sound Velocity and Adiabatic Compressibility at 158°C for the Mercury-Bismuth Alloy System

Atomic fraction of Bi	ρ^a (gm/cm^3)	Expt. c (m/sec)	Theory $\lvert c^{(EM)} \rvert_b$ (m/sec)	Expt. $\beta_s \times 10^{12}$ (cm^2/dyne)	Theory $\lvert \beta_s^{(EM)} \rvert_b \times 10^{12}$ (cm^2/dyne)
0	13.21	1389	1389	3.92	3.92
0.0200	13.15	1424	1399	3.75	3.89
0.0500	13.05	1455	1411	3.62	3.85
0.100	12.87	1490	1437	3.50	3.76
0.150	12.70	1522	1460	3.40	3.70
0.200	12.53	1547	1477	3.34	3.66
0.250	12.36	1570	1496	3.28	3.62
0.300	12.20	1588	1513	3.25	3.58
0.350	12.03	1602	1528	3.24	3.56
0.400	11.86	1615	1543	3.23	3.54
0.450	11.71	1626	1557	3.23	3.53
0.500	11.54	1632	1570	3.25	3.52
0.600	11.23	1645	1592	3.29	3.51
0.700	10.92	1650	1611	3.36	3.53
0.893	10.37	1656	1643	3.52	3.57
1	10.07	1655	1655	3.62	3.62

[a] Kleppa et al. (1961).

Table A.7 Physical Data for Mercury used in Table 4.1

t (^{o}C)	ρ[a] (gm/cm^3)	α_p[a] x 10^4 (deg C^{-1})	C_p[b] (calgm^{-1}deg C^{-1})	η_s[c] (cp)	k_T[d] (calsec^{-1}deg C^{-1}cm^{-1})	c[e] (m/sec)
22.5	13.54	1.811	0.0332	1.55	0.0202	1450.6
23.5	13.54	1.810	0.0332	1.54	0.0202	1450.2
52.5	13.47	1.807	0.0330	1.38	0.0218	1436.9
66	13.43	1.806	0.0330	1.33	0.0225	1430.7
76.5	13.41	1.805	0.0329	1.29	0.0230	1425.9
137.5	13.26	1.807	0.0326	1.15	0.0244	1398.0
141	13.25	1.807	0.0326	1.15	0.0244	1396.4
156	13.22	1.809	0.0326	1.12	0.0247	1389.6

[a] Bigg (1964)

[b] Hultgren et al. (1963)

[c] Erk (1928)

[d] Powell and Tye (1961)

[e] Webber

Table A.8 Physical Data used in Table 4.2

Metal	t (^{o}C)	ρ^{a} (gm/cm^{3})	$\alpha_{p}^{a} \times 10^{4}$ (deg C^{-1})	C_{p}^{a} (calgm^{-1}deg C^{-1})	η_{s} (cP)	k_{T} (calsec^{-1}deg C^{-1}cm^{-1})	c^{n} (m/sec)
Na	100	0.927	2.43	0.331	0.705[b]	0.206[i]	2526
K	75	0.824	2.91	0.195	0.503[b]	0.114[i]	1882
Zn	450	6.54	1.40	0.115	3.78[c]	0.121[j]	2700
Cd	360	7.99	1.46	0.0632	1.44[d]	0.117[j]	2150
Hg	25	13.5	1.81	0.0334	1.53[e]	0.020[k]	1449
Ga	30	6.10	1.26	0.0954	2.06[f]	0.073[j]	2873
In	200	7.00	1.16	0.0613	1.66[g]	0.073[j]	2305
Sn	240	6.96	1.09	0.0595	1.92[h]	0.081[l]	2462
Pb	340	10.7	1.17	0.0352	2.56[h]	0.034[m]	1772
Bi	280	10.1	1.23	0.0364	1.83[c]	0.026[n]	1645

References for Table A.8

[a] Same references as in Tables A.7, A.9 to A.14 & A.17.

[b] Ewing et al. (1951).

[c] Ofte and Wittenberg (1963).

[d] "Liquid Metals Handbook" (1952).

[e] Erk (1928).

[f] Gutman and Simmons (1952).

[g] Culpin (1957).

[h] Rothwell (1962).

[i] Ewing et al. (1955).

[j] Ewing et al. (1957).

[k] Powell and Tye (1961).

[l] Powell (1949).

[m] Powell and Tye (1958).

[n] Webber and Stephens (1968).

Table A.9 Adiabatic and Isothermal Compressibilities as a Function of Temperature for Zinc

t (°C)	ρ[a] (gm/cm^3)	α_p[a] x 10^4 (deg C^{-1})	c_p[b] (cal/gm.deg C)	c[c] (m/sec)	γ	β_s x 10^{12} (cm^2/dyne)	β_T x 10^{12} (cm^2/dyne)
420	6.569	1.40	0.115	2851.8	1.23	1.87	2.30
430	6.560	1.40	0.115	2847.8	1.23	1.88	2.32
440	6.551	1.40	0.115	2843.8	1.24	1.89	2.33
450	6.542	1.40	0.115	2839.8	1.24	1.90	2.35
460	6.533	1.41	0.115	2835.8	1.24	1.90	2.37
470	6.523	1.41	0.115	2831.8	1.25	1.91	2.38
480	6.514	1.41	0.115	2827.8	1.25	1.92	2.40
490	6.505	1.41	0.115	2823.8	1.25	1.93	2.42
500	6.496	1.41	0.115	2819.8	1.26	1.94	2.43
510	6.487	1.42	0.115	2815.8	1.26	1.94	2.45
520	6.478	1.42	0.115	2811.8	1.26	1.95	2.47

[a] Thresh (1965).
[b] Hultgren et al. (1963).
[c] Webber.

Table A.10 Adiabatic and Isothermal Compressibilities as a Function of Temperature for Cadmium.

t (^{o}C)	ρ^{a} (gm/cm^3)	$\alpha_p^{a} \times 10^4$ (deg C^{-1})	c_p^{b} (cal/gm.deg C)	c^{c} (m/sec)	γ	$\beta_s \times 10^{12}$ (cm^2/dyne)	$\beta_T \times 10^{12}$ (cm^2/dyne)
321	8.031	1.45	0.0632	2242.1	1.24	2.48	3.07
330	8.021	1.46	0.0632	2238.7	1.24	2.49	3.09
340	8.009	1.46	0.0632	2234.9	1.25	2.50	3.11
350	7.998	1.46	0.0632	2231.2	1.25	2.51	3.14
360	7.986	1.46	0.0632	2227.4	1.25	2.52	3.16
370	7.974	1.46	0.0632	2223.7	1.26	2.54	3.19
380	7.963	1.47	0.0632	2219.9	1.26	2.55	3.22
390	7.951	1.47	0.0632	2216.0	1.27	2.56	3.24
400	7.939	1.47	0.0632	2212.4	1.27	2.57	3.27
410	7.928	1.47	0.0632	2208.6	1.27	2.59	3.29

[a] Greenaway (1948).

[b] Hultgren et al. (1963).

[c] Webber.

Table A.11 Adiabatic and Isothermal Compressibilities as a Function of Temperature for Indium

t (°C)	ρ[a] (gm/cm^3)	α_p[a] x 10^4 (deg C^{-1})	c_p[b] (cal/gm.deg C)	c[c] (m/sec)	γ	β_s x 10^{12} (cm^2/dyne)	β_T x 10^{12} (cm^2/dyne)
156	7.033	1.16	0.0614	2317.7	1.12	2.65	2.96
160	7.030	1.16	0.0614	2316.5	1.12	2.65	2.97
180	7.013	1.16	0.0614	2310.7	1.13	2.67	3.01
200	6.997	1.16	0.0613	2304.8	1.13	2.69	3.05
220	6.981	1.16	0.0613	2299.0	1.14	2.71	3.08
240	6.965	1.17	0.0612	2293.1	1.14	2.73	3.12
260	6.948	1.17	0.0611	2287.2	1.15	2.75	3.16
280	6.932	1.17	0.0611	2281.4	1.15	2.77	3.20
300	6.916	1.18	0.0610	2275.5	1.16	2.79	3.24
320	6.899	1.18	0.0609	2269.7	1.17	2.81	3.28
340	6.883	1.18	0.0609	2263.8	1.17	2.83	3.32
360	6.867	1.18	0.0608	2257.9	1.18	2.86	3.36

[a] "Liquid Metals Handbook" (1952)

[b] Hultgren et al. (1963)

[c] Webber

Table A.12 Adiabatic and Isothermal Compressibilities as a Function of Temperature for Tin

t (°C)	ρ[a] (gm/cm^3)	α_p[a] x 10^4 (deg C^{-1})	c_p[b] (cal/gm.deg C)	c[c] (m/sec)	γ	β_s x 10^{12} (cm^2/dyne)	β_T x 10^{12} (cm^2/dyne)
232	6.969	1.09	0.0598	2473.9	1.15	2.34	2.69
240	6.963	1.09	0.0595	2472.1	1.15	2.35	2.70
260	6.948	1.08	0.0588	2467.6	1.16	2.36	2.73
280	6.933	1.08	0.0583	2463.2	1.16	2.38	2.76
300	6.918	1.08	0.0581	2458.7	1.17	2.39	2.79
320	6.903	1.08	0.0579	2454.2	1.17	2.41	2.82
340	6.888	1.07	0.0578	2449.8	1.18	2.42	2.84
360	6.873	1.07	0.0578	2445.3	1.18	2.43	2.87
380	6.858	1.07	0.0577	2440.8	1.18	2.45	2.90
400	6.844	1.07	0.0577	2436.4	1.19	2.46	2.92

[a] Übelacker and Lucas (1962)

[b] Hultgren et al. (1963)

[c] Webber

Table A.13 Adiabatic and Isothermal compressibilities as a Function of Temperature for Lead

t (°C)	ρ[a] (gm/cm^3)	α_p[a] x 10^4 (deg C^{-1})	C_p[b] (cal/gm.deg C)	c[c] (m/sec)	γ	β_s x 10^{12} (cm^2/dyne)	β_T x 10^{12} (cm^2/dyne)
328	10.68	1.17	0.0353	1818.9	1.19	2.83	3.35
337	10.67	1.17	0.0353	1816.6	1.19	2.84	3.37
347	10.66	1.18	0.0353	1814.0	1.19	2.85	3.40
357	10.65	1.18	0.0352	1811.4	1.19	2.86	3.42
367	10.63	1.18	0.0352	1808.8	1.20	2.87	3.44
377	10.62	1.18	0.0352	1806.2	1.20	2.89	3.47
387	10.61	1.18	0.0351	1803.6	1.20	2.90	3.49
397	10.60	1.18	0.0351	1801.0	1.21	2.91	3.51
407	10.58	1.18	0.0351	1798.5	1.21	2.92	3.54
417	10.57	1.19	0.0350	1795.9	1.21	2.93	3.56
427	10.56	1.19	0.0350	1793.3	1.22	2.95	3.58

[a] Strauss et al. (1960)

[b] Hultgren et al. (1963)

[c] Webber

Table A.14 Adiabatic and Isothermal Compressibilities as a Function of Temperature for Bismuth

t (°C)	ρ[a] (gm/cm^3)	α_p[a] x 10^4 (deg C^{-1})	c_p[b] (cal/gm.deg C)	c[c] (m/sec)	γ	β_s x 10^{12} (cm^2/dyne)	β_T x 10^{12} (cm^2/dyne)
271	10.06	1.23	0.0364	1649.0	1.15	3.66	4.19
275	10.05	1.23	0.0364	1648.7	1.15	3.66	4.20
280	10.05	1.23	0.0364	1648.3	1.15	3.66	4.21
290	10.04	1.23	0.0364	1647.4	1.15	3.67	4.23
300	10.02	1.23	0.0364	1646.5	1.16	3.68	4.25
310	10.01	1.23	0.0364	1645.6	1.16	3.69	4.27
320	9.998	1.24	0.0364	1644.6	1.16	3.70	4.29
330	9.986	1.24	0.0364	1643.6	1.16	3.71	4.31
340	9.974	1.24	0.0364	1642.6	1.17	3.72	4.34
350	9.961	1.24	0.0364	1641.5	1.17	3.73	4.36
360	9.949	1.24	0.0364	1640.3	1.17	3.74	4.38
370	9.937	1.24	0.0364	1639.1	1.18	3.75	4.40
380	9.924	1.25	0.0364	1637.9	1.18	3.76	4.43
390	9.912	1.25	0.0364	1636.5	1.18	3.77	4.45
400	9.900	1.25	0.0364	1635.2	1.18	3.78	4.47
410	9.887	1.25	0.0364	1633.8	1.19	3.79	4.50

[a] Strauss and Richards (1962)

[b] Hultgren et al. (1963)

[c] Webber

Table A.15 Adiabatic and Isothermal Compressibilities as a Function of Temperature for Antimony

t (°C)	ρ^a (gm/cm^3)	$\alpha_p^a \times 10^4$ (deg C^{-1})	C_p^b (cal/gm.deg C)	c^c	γ	$\beta_s \times 10^{12}$ (cm^2/dyne)	$\beta_T \times 10^{12}$ (cm^2/dyne)
631	6.464	0.957	0.0616	1893	1.12	4.32	4.81
650	6.452	0.955	0.0616	1900	1.12	4.29	4.80
700	6.422	0.951	0.0616	1913	1.13	4.26	4.79
750	6.391	0.947	0.0616	1925	1.13	4.22	4.78
800	6.361	0.943	0.0616	1935	1.14	4.20	4.78
850	6.332	0.939	0.0616	1938	1.14	4.21	4.81
900	6.301	0.935	0.0616	1940	1.15	4.22	4.85
950	6.273	0.931	0.0616	1939	1.15	4.24	4.90
1000	6.244	0.926	0.0616	1937	1.16	4.27	4.95
1050	6.219	0.921	0.0616	1935	1.16	4.29	5.00
1100	6.187	0.917	0.0616	1931	1.17	4.33	5.06

[a] Lucas and Urbain (1962a)

[b] Hultgren et al. (1963)

[c] Gitis and Mikhailov (1966a)

Table A.16 Adiabatic and Isothermal Compressibilities as a Function of Temperature for Tellurium

t (^{o}C)	ρ^{a} (gm/cm^{3})	$\alpha_{p}^{a} \times 10^{4}$ (deg C^{-1})	C_{p}^{b} (cal/gm.deg C)	c^{c} (m/sec)	γ	$\beta_{s} \times 10^{12}$ (cm^{2}/dyne)	$\beta_{T} \times 10^{12}$ (cm^{2}/dyne)
451	5.797	0.957	0.0705	913	1.019	20.69	21.08
460	5.792	0.956	0.0705	920	1.019	20.40	20.79
475	5.784	0.954	0.0705	927	1.020	20.12	20.52
500	5.770	0.952	0.0705	950	1.021	19.20	19.61
525	5.757	0.950	0.0705	980	1.023	18.09	18.51
550	5.743	0.947	0.0705	1012	1.026	17.00	17.44
575	5.729	0.945	0.0705	1040	1.028	16.14	16.59
600	5.716	0.943	0.0705	1050	1.029	15.87	16.33
650	5.689	0.938	0.0705	1080	1.032	15.07	15.55
700	5.662	0.933	0.0705	1100	1.034	14.60	15.10
750	5.636	0.928	0.0705	1120	1.037	14.15	14.67
800	5.610	0.922	0.0705	1128	1.039	14.01	14.56
850	5.584	0.917	0.0705	1133	1.041	13.95	14.52
900	5.559	0.912	0.0705	1140	1.043	13.84	14.44

[a] Lucas and Urbain (1962b)

[b] Kubaschewski (1950)

[c] Gitis and Mikhailov (1966b)

Table A.17 Physical Data at the Melting Point used in Table 4.8

Metal	ρ (gm/cm^3)	$\alpha_p \times 10^4$ (deg C^{-1})	c_p (cal/gm.deg C)
Na	0.9269[a]	2.42[a]	0.331[i]
K	0.8237[b]	2.90[b]	0.196
Rb	1.475 [c]	3.38[i]	0.0877
Cs	1.84 [d]	3.95[j]	0.0573
Cu	8.090 [e]	1.17[e]	0.118
Ag	9.333 [f]	1.19[f]	0.0677
Al	2.374 [c]	1.16[c]	0.260
Ga	6.095[g]	1.26[g]	0.0954
Tl	11.70 [h]	1.30[h]	0.0352[i]

[a] Thomson and Garelis (1954)

[b] "Liquid Metals Handbook, Sodium-Potassium Supplement" (1955)

[c] "Liquid Metals Handbook" (1952)

[d] Gering and Sauerwald (1935)

[e] El-Mehairy and Ward (1963)

[f] Lucas (1961)

[g] Hoather (1936)

[h] Schneider et al. (1954)

[i] Hultgren et al. (1963)

Table A.13 Adiabatic and Isothermal Compressibilities at 20°C as a Function of Concentration b in the Mercury-Thallium Alloy System

Atomic fraction of Tl b	ρ^a (g/cm^3)	$\alpha_p^a \times 10^4$ (deg C^{-1})	c_p^b (cal/gm.deg C)	c^a (m/sec)	γ	$\beta_s \times 10^{12}$ (cm^2/dyne)	$\beta_T \times 10^{12}$ (cm^2/dyne)
0	13.546	1.82	0.0334	1450	1.145	3.511	4.02
0.05	13.319	1.80	0.0342	1492	1.148	3.348	3.84
0.1	13.314	1.77	0.0349	1521	1.145	3.247	3.72
0.15	13.208	1.72	0.0355	1547	1.140	3.164	3.61
0.2	13.115	1.68	0.0360	1570	1.135	3.093	3.51
0.25	13.022	1.64	0.0364	1592	1.131	3.030	3.43
0.3	12.881	1.62	0.0368	1610	1.129	2.995	3.38
0.35	12.807	1.60	0.0371	1622	1.127	2.968	3.35
0.4	12.703	1.59	0.0374	1633	1.126	2.952	3.32
1	12.157	1.25	0.0352	1726	1.093	2.762	3.02

[a] Abowitz and Gordon (1963)

[b] Richards and Daniels (1919)

Principal Symbols

For alloy systems, subscript b means that the physical quantity is evaluated at atomic fraction b.

A	defined in equation (1.52)
$a(q)$, $a(x,r_s)$	structure factors
$a_{\alpha\beta}$	partial structure factors
C	constant defined by equation (1.84)
C_b	constant defined by equation (4.64)
C_p	specific heat at constant pressure
c	sound velocity
$c^{(A)}$	theoretical sound velocity defined in equation (1.87)
$c^{(BS)}$	theoretical sound velocity defined in equation (1.23)
$[c^{(EM)}]_b$	theoretical sound velocity defined in equation (4.38)
c_α, c_β	atomic fractions of species α and β respectively
E_{BS}	band-structure energy
E_{bs}	band-structure energy
E_c	correlation energy
E_d	energy due to direct interaction between ions
E_e	potential energy of uniform electron cloud in Coulomb field of ions
E_{ec}	potential energy of uniform electron cloud in field w^o_{core} of ion.

E_{ee}	electron-electron interaction
E_{el-el}	electron-electron interaction
E_F	Fermi energy
E_g	binding energy
E_{ii}	Fuchs energy
$E(\underline{k})$	electron energy
E_{su}	Coulomb self energy of a uniform negative charge distribution
E_x	exchange energy
e	electronic charge
F_b	defined in equation (4.58)
F(q)	energy-wavenumber characteristic defined in equation (1.71)
f	frequency
f	ratio of hard-sphere diameters
f(x)	defined in equation (1.57)
$G(r_s)$	defined in equation (1.65)
$G'(r_s)$	defined in equation (4.31)
g(r)	radial distribution function
$g_{\alpha\beta}(r)$	radial distribution function for alloy of species α and β
H	defined in equation (4.14)
H_b	defined in equation (4.57)
$\hbar$	Planck's constant /2π
J	mechanical equivalent of heat
k_B	Boltzmann's constant

k_F	Fermi vector
k_T	thermal conductivity
M	atomic mass
m	electron mass
N	number of atoms in volume Ω
N_{av}	Avogadro's number
$N(E_F)$	density of states at the Fermi level
n	number of atoms per unit volume
n_q	Fourier components of $n'(r)$
$n'(r)$	oscillatory component of electron density
p	pressure
p_h	hard-sphere pressure
R	universal gas constant
R	defined in equation (1.74)
$\underline{r}$	position vector
r_c	radius defined in equation (1.60)
r_s	radius defined by equation (1.26)
$S(\underline{q})$	structure factor
$S^*(\underline{q})$	complex conjugate of $S(\underline{q})$
T	absolute temperature
t	temperature in deg. C
t_m	temperature of melting point in deg. C
U^o	bare potential

$u(r)$ pair potential

$V_d(r)$ direct interaction between ions

$V_{eff}(R)$ effective interaction between ions

$V_{ind}(R)$ indirect interaction between ions

V_q defined in equation (1.61)

$V_\alpha(q)$, $V_\beta(q)$ qth. Fourier components of the bare interaction of an electron with ions α and β

v_F Fermi velocity

$W(\underline{r})$ total pseudo-potential

$W^i(\underline{r})$ potential due to conduction electrons

$W^o(\underline{r})$ sum of potentials due to the ions

$W^i(q)$ Fourier components of $W^i(\underline{r})$

$W^o(q)$ Fourier components of $W^o(\underline{r})$

w ionic pseudo-potential

w^o local potential

x ratio of q to $2k_F$

y defined by equation (1.63)

Z valency

Z^* effective valency

$Z_\alpha(q)$, $Z_\beta(q)$ defined in equation (4.43)

z packing fraction

z_m value of packing fraction at the melting point

α $(4/9\pi)^{1/3}$

α	observed sound attenuation coefficient
α_o	classical attenuation coefficient
α_B	excess absorption coefficient
α_p	volume expansion coefficient
α_s	sound attenuation coefficient due to shear viscosity
α_T	sound attenuation coefficient due to thermal-conduction
β_s	adiabatic compressibility
$\beta_s^{(BS)}$	Bohm-Staver compressibility
$\beta_T^{(A)}$	theoretical compressibility defined in equation (1.85)
$\beta_T^{(e\ell)}$	free-electron compressibility
$[\beta_T^{(EM)}]_b$	compressibility of alloy system defined by equation (4.37)
$\beta_T^{(h)}$	hard-sphere compressibility
$\beta_T^{(W)}$	empirical compressibility defined by equation (4.20)
γ	ratio of principal specific heats
γ'	theoretical value for γ
Δ_b	defined by equation (4.51)
δ_b	defined by equation (4.68)
$\varepsilon(q)$	dielectric function
η_B	bulk viscosity
η_B'	theoretical value for η_B corrected for backscattering
η_s	shear viscosity
λ	sound wavelength
λ_L	defined in equation (1.57)

ρ	density
σ	hard-sphere diameter
χ	Enskog high-density correction
Ω	volume of system
Ω_A	gram-atomic volume
Ω_m	volume of system at the melting point

Glossary

The Born-Mayer interaction is due to the interaction between closed electron shells and is written in the form $V(r) = A \exp(-\frac{r}{\rho})$, in which A and ρ are constants.

A Canonical Ensemble consists of a large number of systems, each a replica of the system of interest, which can exchange energy but not particles, and whose total energy remains constant.

References

Abowitz, G., and Gordon, R. B. (1962a). J. Chem. Phys. 37, 125.

Abowitz, G., and Gordon, R. B. (1962b). Acta Met. 10, 671.

Abowitz, G., and Gordon, R. B. (1963). Trans. AIME 227, 51.

Alder, B. J., and Wainwright, T. E. (1967). Phys. Rev. Letters 18, 988.

Ascarelli, P. (1968). Phys. Rev. 173, 271.

Ascarelli, P., and Paskin, A. (1968). Phys. Rev. 165, 222.

Ashcroft, N. W. (1966). Phys. Letters 23, 48.

Ashcroft, N. W., and Langreth, D. C. (1967a). Phys. Rev. 155, 682.

Ashcroft, N. W., and Langreth, D. C. (1967b). Phys. Rev. 156, 685.

Ashcroft, N. W., and Langreth, D. C. (1967c). Phys. Rev. 159, 500.

Ashcroft, N. W., and Leckner, J. (1966). Phys. Rev. 145, 83.

Bär, R. (1937). Helv. Phys. Acta 10, 332.

Beattie, J. A., Blaisdell, B. E., Kaye, J., Gerry, H. T., and Johnson, C. A. (1940). Proc. Am. Acad. Arts Sci. 74, 371.

Bett, K. E., Weale, K. E., and Newitt, D. M. (1954). Brit. J. Appl. Phys. 5, 243.

Beyer, R. T., and Coppens, A. B. (1965). Proc. Intern. Comm. Acoustics Congr., 5th, Liege, 1965.

Bigg, P. H. (1964). Brit. J. Appl. Phys. 15, 1111.

Birch, F. (1942). "Handbook of Physical Constants" Geol. Soc. Am. Spec. Papers 36.

Bohm, D., and Staver, T. (1951). Phys. Rev. 84, 836.

Bridgman, P. W. (1911). Proc. Amer. Acad. Arts Sci. 47, 345.

Bridgman, P. W. (1931). "The Physics of High Pressure", 1st ed. Bell, London.

Bridgman, P. W. (1958). "The Physics of High Pressure", New Impression, Bell, London.

Carnazzi, P. (1903). Nuovo Cim. 5, 180.

Carome, E. F., and Witting, J. M. (1961). J. Acoust. Soc. Am. 33, 187.

Carome, E. F., Witting, J. M., and Fleury, P. A. (1961). J. Acoust. Soc. Am. 33, 1417.

Cook, A. H. (1956). Brit. J. Appl. Phys. 7, 285.

Coppens, A. B., Beyer, R. T., and Ballou, J. (1967). J. Acoust. Soc. Am. 41, 1443.

Culpin, M. F. (1957). Proc. Phys. Soc. 70B, 1069.

Davies, H. A. (1966). Ph.D. Thesis, University of London.

Davis, L. A., and Gordon, R. B. (1967). J. Chem. Phys. 46, 2650.

Diaz Peña, M., and McGlashan, M. L. (1959). Trans. Far. Soc. 55, 2018.

Douglas, T. B., Ball, A. F., and Ginnings, D. C. (1951). J. Res. Natl. Bur. Std., 46, 334.

Eckhardt, M., and Graefe, E. (1900). Z. Anorg. Chem. 23, 378.

Egelstaff, P. A. (1967). "An Introduction to Liquid State". Academic Press, London.

El-Mehairy, A. E., and Ward, R. G. (1963). Trans. AIME 227, 1226.

Erk, S. (1928). Z. Physik 47, 886.

Ewing, C. T., Grand, J. A., and Miller, R. R. (1951). J. Am. Chem. Soc. 73, 1168.

Ewing, C. T., Seebold, R. E., Grand, J. A., and Miller, R. R. (1955). J. Phys. Chem. 59, 524.

Ewing, C. T., Walker, B. E., Grand, J. A., and Miller, R. R. (1957). Chem. Eng. Progr. Symp. Ser. 53, 19.

Eyring, H., and Hirschfelder, J. O. (1937). J. Phys. Chem. 41, 249.

Faber, T. E., and Ziman, J. M. (1964). Phil. Mag. 11, 153.

Frenkel, J. (1956). "Kinetic Theory of Liquids". Oxford Univ. Press, London and New York.

Gering, K., and Sauerwald, F. (1935). Z. Anorg. Chem. 223, 204.

Gitis, M. B., and Mikhailov, I. G. (1966a). Soviet Phys. Acoust. 11, 372.

Gitis, M. B., and Mikhailov, I. G. (1966b). Soviet Phys. Acoust. 12, 14.

Gitis, M. B., and Mikhailov, I. G. (1966c). Soviet Phys. Acoust. 12, 131.

Gitis, M. B., Mikhailov, I. G., and Niyazov, S. (1968). Soviet Phys. Acoust. 14, 42.

Golik, A. Z., Kassen, I. F., and Kuchak, G. M. (1961). Soviet Phys. Acoust. 7, 202.

Gordon, R. B. (1959). Acta Met. 7, 1.

Gordon, R. B. (1961). "Physical Chemistry of Process Metallurgy," Part 1, 461. Wiley, (Interscience), New York.

Greenaway, H. T. (1948). J. Inst. Met. 74, 133.

Greenspan, M., and Tschiegg, C. E. (1957). J. Res. Natl. Bur. Std. 59, 249.

Guggenheim, E. A. (1965). Mol. Phys. 9, 199.

Gutman, F., and Simmons, L. M. (1952). J. Appl. Phys. 23, 977.

Hackspill, L. (1911). Compt. Rend. 152, 259.

Harrison, W. A. (1966). "Pseudo-potentials in the Theory of Metals," Benjamin, New York.

Helfand, E., Frisch, H. L., and Lebowitz, J. L. (1961). J. Chem. Phys. 34, 1037.

Heine, V., and Weaire, D. (1966). Phys. Rev. 152, 603.

Hill, J. E., and Ruoff, A. L. (1965a). Rev. Sci. Instr. 36, 1465.

Hill, J. E., and Ruoff, A. L. (1965b). J. Chem. Phys. 43, 2150.

Hirschfelder, J. O., Curtiss, C. F., and Bird, R. B. (1964). "Molecular Theory of Gases and Liquids." Wiley, New York.

Hoather, W. H. (1936). Proc. Phys. Soc. (London) 48, 699.

Hubbard, J. C., and Loomis, A. L. (1928). Phil. Mag. 5, 1177.

Hultgren, R., Orr, R. L., Anderson, P. D., and Kelley, K. K. (1963). "Selected values of Thermodynamic Properties of Metals and Alloys." Wiley, New York.

Hunter, J. L. and Hovan, K. S. (1964a). J. Acoust. Soc. Am. 36, 1040.

Hunter, J. L. and Hovan, K. S., (1964b). J. Chem. Phys. 41, 4013.

Hunter, J. L., Storey, W. T., and Lewis, T. B. (1962). J. Acoust. Soc. Am. 34, 1985.

Hunter, J. L., Welch, T. J., and Montrose, C. J. (1963). J. Acoust. Soc. Am. 35, 1568.

Ilgūnas, V. I., and Yaronis, É. P. (1958). Abstracts of Papers at the Fourth All-Union Conference (1958), 59.

Jarzynski, J. (1961). Ph.D. Thesis, University of London.

Jarzynski, J. (1963). Proc. Phys. Soc. (London) 81, 745.

Jarzynski, J., and Litovitz, T. A. (1964). J. Chem. Phys. 41, 1290.

Jarzynski, J., Smirnow, J. R., and Davis, C. M. (1969). Phys. Rev. 178, 288.

Kazakov, N. B., Pronin, L. A., and Filippov, S. I. (1964). Ivz. Vysshikh Uchebn. Zavedenni Chernaya Met. (11), 11.

Kazakov, N. B., Pronin, L. A., and Filippov, S. I. (1965). Ivz. Vysshikh Uchebn. Zavedenni Chernaya Met. (9), 5.

Khodov, Z. L. (1960). Phys. Metals Metallog. (USSR) 10, (5), 129.

Kleppa, O. J. (1950). J. Chem. Phys. 18, 1331.

Kleppa, O. J., Kaplan, M., and Thalmayer, C. E. (1961). J. Phys. Chem. 65, 843.

Kubaschewski, O. (1950). Z. Metallk. 41, 445.

Letcher, S. V., and Beyer, R. T. (1963). J. Acoust. Soc. Am. 35, 1571.

"Liquid Metals Handbook" (1952). (R. N. Lyon, Ed.). U.S. At. Energy Comm., U.S. Govt. Printing Office, Washington, D.C.

"Liquid Metals Handbook, Sodium-Potassium Supplement" (1955). U.S. At. Energy Comm. and Dept. of Navy, U.S. Govt. Printing Office, Washington, D.C.

Litovitz, T. A., and Davis, C. M. (1965). "Physical Acoustics" (W. P. Mason, Ed.), Vol. 2A, Chapter 5. Academic Press, New York.

Litovitz, T. A. and Jarzynski, J. (1965). Proc. Intern. Comm. Acoustics Congr., 5th., Liège, 1965.

Lucas, L.-D. (1961). Compt. Rend. 253, 2526.

Lucas, L-D., and Urbain, G. (1962a). Compt. Rend. 255,2414.

Lucas L-D., and Urbain, G. (1962b). Compt. Rend. 255, 3406.

Nagel, H. H. (1966). Diplomarbeit, University of Saarbrücken.

Matthews, J. M. (1966). Ph.D. Thesis, University of London.

Matuyama, Y. (1929). Sci. Rept. Tohoku University. First Ser. 18, 737.

McSkimin, H. J. (1959). J. Acoust. Soc. Am. 31, 287.

McSkimin, H. J. (1965). J. Acoust. Soc. Am. 37, 325.

Murphy, T. K., and Rao, K. S. (1967). Current Science 36, (12), 315.

Ofte, D., and Wittenberg, L. J. (1963), Trans. AIME 227, 706.

Pines, D. (1955). "Solid State Physics" (F. Seitz and D. Turnbull, eds.) Vol. 1, 367. Academic Press, New York.

Pines, D., and Nozières, P. (1966). "The Theory of Quantum Liquids." Benjamin, New York.

Pinkerton, J. M. M. (1947). Nature 160, 128.

Plass, K. G. (1963). Acustica 13, 240.

Pochapsky, T. E. (1951). Phys. Rev. 84, 553.

Polotskii, I. G., Taborov, V. F., and Khodov, Z. L. (1959). Soviet Phys. Acoust. 5, 202.

Postill, D. R., Ross, R. G. and Cusack, N. E. (1968). Phil. Mag. 18, 519.

Powell, R. W. (1949). J. Iron Steel Inst. (London) 162, 315.

Powell, R. W., and Tye, R. P. (1958). Proc. Joint Conf. Thermodynamics Transport Properties Fluids, 1958, p. 182. Inst. Mech. Engrs., London.

Powell, R. W., and Tye, R. P. (1961). International Development of Heat Transfer, p. 856.. Am. Soc. Mech. Engrs., New York.

Proffit, R. L., and Carome, E. F. (1962). ONR Tech. Rept. No. 5. John Carroll Univ., Cleveland, Ohio.

Pronin, L. A., and Filippov, S. I. (1963a). Izv. Vysshikh Uchebn. Zavedenni Chernaya Met. (5), 10.

Pronin, L. A., and Filippov, S. I. (1963b). Izv. Vysshikh Uchebn. Zavedenni Chernaya Met. (11), 11.

Rice, T. M. (1963). Ph.D. Thesis, University of Cambridge.

Richards, T. W., and Bartlett, E. P. (1915). J. Amer. Chem. Soc. 37, 470.

Richards, T. W., and Daniels, F. (1919). J. Amer. Chem. Soc. 41, 1732.

Rieckmann, P. (1939). Physik. Z. 40, 582.

Ringo, G. R., Fitzgerald, J. W., and Hurdle, B. G. (1947). Phys. Rev. 72, 87.

Rothwell, E. (1962). J. Inst. Metals 90, 389.

Rowlinson, J. S. (1959). "Liquids and Liquid Mixtures". Butterworth, London.

Schneider, A., Stauffer, A., and Heymer, G. (1954). Naturwissenschaften 41, 326.

Schramm, K. H. (1962a). Z. Metallk. 53, 316.

Schramm, K. H. (1962b). Z. Metallk. 53, 729.

Seemann, H. J., and Klein, F. K. (1965). Z. Angew. Phys. 19, 368.

Seki, H., Granato, A., and Truell, R. (1956). J. Acoust. Soc. Am. 28, 230.

Shapira, Y. (1967). J. Acoust. Soc. Am. 41, 584.

Sharma, K. C. (1968). Phys. Rev. 176, 319.

Smirnow, J. R., and Jarzynski, J. (1967). J. Acoust. Soc. Am. 42, 1161.

Smith, L. B. and Keyes, F. G. (1934a). Proc. Am. Acad. Arts Sci. 69, 285.

Smith, L. B. and Keyes, F. G. (1934b). Proc. Am. Acad. Arts Sci. 69, 313.

Smith, R. T., Webber, G. M. B., Young, F. R., and Stephens, R. W. B. (1967). Advan. Phys. 16, 515.

Stephens, R. W. B. (1963). "Dispersion and Absorption of Sound by Molecular Processes" (D. Sette, ed.). Academic Press, New York.

Strauss, S. W., and Richards, L. E. (1962). J. Nucl. Mater. 5, 12.

Strauss, S. W., Richards, L. E., and Brown, B. F. (1960). Nucl. Sci. Eng. 7, 442.

Thomson, G. W. and Garelis, E. (1954). Physical and Thermodynamic Properties of Sodium. Rept. 2. Ethyl Corp.

Thresh, H. R. (1965). Trans. AIME 233, 79.

Trelin, Y. S., and Vasil'ev, I. M. (1961). "Applications of Ultrasonics to the Investigation of Matter" (in Russian) MOPl, (13), 3.

Trelin, Y. S., and Vasil'ev, I. N. (1966). High Temperature 4, 352.

Übelacker, E., and Lucas, L-D. (1962). Compt. Rend. 254, 1622.

V'yugov, P. N., and Gumenyuk, V. S. (1966). Ukr. Fiz. Zh. 11, 440.

Waghorne, R. M., Rivlin, V. G. and Williams, G. I. (1967). Advan. Phys. 16, 215.

Webber, G. M. B. (1965). Proc. Intern. Comm. Acoustics Congr., 5th, Liège, 1965.

Webber, G. M. B., and Stephens, R. W. B. (1968). "Physical Acoustics" (W. P. Mason, ed.). Vol. 4B, Chapter 11. Academic Press, New York.

Williams, (1958). Ph.D. Thesis, University of London.

Wilson, J. R. (1965). Metallurgical Reviews 10, (40), 381.

Yao, T. P., and Kondic, V. J. (1952). J. Inst. Metals 81, 17.

Ying, S. P., and Scott, C. C. (1965). USAEC Report APDA 180.

Ziman, J. M. (1964). Advan. Phys. 13, 89.

ACKNOWLEDGEMENTS

The author wishes to thank Dr. R. W. B. Stephens for his help and guidance during the course of this work and is indebted to members of the Acoustics Group, Physics Department at Imperial College of Science and Technology for many helpful and stimulating discussions. He would wish to thank Professor N. E. Cusack and his colleagues of the School of Mathematics and Physics for advice and inspiration in the work. The author is grateful to the Science Research Council for financial assistance.